Development of LRFD Procedures for Bridge Pile Foundations in Iowa

Volume II: Field Testing of Steel Piles in Clay, Sand, and Mixed Soils and Data Analysis

BRIDGE ENGINEERING CENTER

Final Report
September 2011

IOWA STATE UNIVERSITY
Institute for Transportation

Sponsored by
Iowa Highway Research Board
(IHRB Project TR-583)
Iowa Department of Transportation
(InTrans Project 08-312)

About the Bridge Engineering Center

The mission of the Bridge Engineering Center (BEC) is to conduct research on bridge technologies to help bridge designers/owners design, build, and maintain long-lasting bridges.

About the Institute for Transportation

The mission of the Institute for Transportation (InTrans) at Iowa State University is to develop and implement innovative methods, materials, and technologies for improving transportation efficiency, safety, reliability, and sustainability while improving the learning environment of students, faculty, and staff in transportation-related fields.

Disclaimer Notice

The contents of this report reflect the views of the authors, who are responsible for the facts and the accuracy of the information presented herein. The opinions, findings and conclusions expressed in this publication are those of the authors and not necessarily those of the sponsors.

The sponsors assume no liability for the contents or use of the information contained in this document. This report does not constitute a standard, specification, or regulation.

The sponsors do not endorse products or manufacturers. Trademarks or manufacturers' names appear in this report only because they are considered essential to the objective of the document.

Non-Discrimination Statement

Iowa State University does not discriminate on the basis of race, color, age, religion, national origin, sexual orientation, gender identity, genetic information, sex, marital status, disability, or status as a U.S. veteran. Inquiries can be directed to the Director of Equal Opportunity and Compliance, 3280 Beardshear Hall, (515) 294-7612.

Iowa Department of Transportation Statements

Federal and state laws prohibit employment and/or public accommodation discrimination on the basis of age, color, creed, disability, gender identity, national origin, pregnancy, race, religion, sex, sexual orientation or veteran's status. If you believe you have been discriminated against, please contact the Iowa Civil Rights Commission at 800-457-4416 or Iowa Department of Transportation's affirmative action officer. If you need accommodations because of a disability to access the Iowa Department of Transportation's services, contact the agency's affirmative action officer at 800-262-0003.

The preparation of this (report, document, etc.) was financed in part through funds provided by the Iowa Department of Transportation through its "Agreement for the Management of Research Conducted by Iowa State University for the Iowa Department of Transportation," and its amendments.

The opinions, findings, and conclusions expressed in this publication are those of the authors and not necessarily those of the Iowa Department of Transportation.

Technical Report Documentation Page

1. Report No.	2. Government Accession No.	3. Recipient's Catalog No.
IHRB Project TR-583		

4. Title and Subtitle	5. Report Date
Development of LRFD Design Procedures for Bridge Piles in Iowa – Field Testing of Steel H-Piles in Clay, Sand, and Mixed Soils and Data Analysis (Volume II)	September 2011
	6. Performing Organization Code

7. Author(s)	8. Performing Organization Report No.
Kam Weng Ng, Muhannad T. Suleiman, Matthew Roling, Sherif S. AbdelSalam, and Sri Sritharan	InTrans Project 08-312

9. Performing Organization Name and Address	10. Work Unit No. (TRAIS)
Institute for Transportation Iowa State University 2711 South Loop Drive, Suite 4700 Ames, IA 50010-8664	**11. Contract or Grant No.**

12. Sponsoring Organization Name and Address	13. Type of Report and Period Covered
Iowa Highway Research Board Iowa Department of Transportation 800 Lincoln Way Ames, IA 50010	Final Report
	14. Sponsoring Agency Code

15. Supplementary Notes

Visit www.intrans.iastate.edu for color PDF files of this and other research reports.

16. Abstract

In response to the mandate on Load and Resistance Factor Design (LRFD) implementations by the Federal Highway Administration (FHWA) on all new bridge projects initiated after October 1, 2007, the Iowa Highway Research Board (IHRB) sponsored these research projects to develop regional LRFD recommendations.

The LRFD development was performed using the Iowa Department of Transportation (DOT) Pile Load Test database (PILOT). To increase the data points for LRFD development, develop LRFD recommendations for dynamic methods, and validate the results of LRFD calibration, 10 full-scale field tests on the most commonly used steel H-piles (e.g., HP 10 x 42) were conducted throughout Iowa.

Detailed in situ soil investigations were carried out, push-in pressure cells were installed, and laboratory soil tests were performed. Pile responses during driving, at the end of driving (EOD), and at re-strikes were monitored using the Pile Driving Analyzer (PDA), following with the CAse Pile Wave Analysis Program (CAPWAP) analysis. The hammer blow counts were recorded for Wave Equation Analysis Program (WEAP) and dynamic formulas.

Static load tests (SLTs) were performed and the pile capacities were determined based on the Davisson's criteria. The extensive experimental research studies generated important data for analytical and computational investigations. The SLT measured load-displacements were compared with the simulated results obtained using a model of the TZPILE program and using the modified borehole shear test method. Two analytical pile setup quantification methods, in terms of soil properties, were developed and validated. A new calibration procedure was developed to incorporate pile setup into LRFD.

17. Key Words	18. Distribution Statement
BST—CAPWAP—dynamic analysis—LRFD—mBST—PILOT—PDA—static load test—WEAP	No restrictions.

19. Security Classification (of this report)	20. Security Classification (of this page)	21. No. of Pages	22. Price
Unclassified.	Unclassified.	226	NA

Form DOT F 1700.7 (8-72) **Reproduction of completed page authorized**

Development of LRFD Design Procedures for Bridge Piles in Iowa – Field Testing of Steel H-Piles in Clay, Sand, and Mixed Soils and Data Analysis

Final Report-Volume II
September 2011

Principal Investigator
Sri Sritharan
Wilson Engineering Professor
Department of Civil, Construction, and Environmental Engineering, Iowa State University

Research Associate
Muhannad T. Suleiman
Assistant Professor
Department of Civil and Environmental Engineering, Lehigh University

Research Assistant
Kam Weng Ng
Matthew Roling
Sherif S. AbdelSalam

Authors
Kam Weng Ng, Muhannad T. Suleiman, Matthew Roling, Sherif S. AbdelSalam, and Sri Sritharan

Sponsored by
The Iowa Highway Research Board
(IHRB Project TR-583)

Preparation of this report was financed in part
through funds provided by the Iowa Department of Transportation
through its research management agreement with the
Institute for Transportation
(In Trans Project 08-312)

A report from
Institute for Transportation
Iowa State University
2711 South Loop Drive, Suite 4700
Ames, IA 50010-8664
Phone: 515-294-8103
Fax: 515-294-0467
www.intrans.iastate.edu

TABLE OF CONTENTS

LIST OF FIGURES

LIST OF TABLES

ACKNOWLEDGMENTS

The authors would like to thank the Iowa Highway Research Board (IHRB) for sponsoring the research project: TR-583. We would like to thank the Technical Advisory Committee of the research for their guidance and Kyle Frame of Iowa DOT for his assistance with the PDA tests. Particularly the following individuals served on the Technical Advisory Committee of this research project: Ahmad Abu-Hawash, Dean Bierwagen, Lyle Brehm, Ken Dunker, Kyle Frame, Steve Megivern, Curtis Monk, Michael Nop, Gary Novey, John Rasmussen and Bob Stanley. The members of this committee represent Office of Bridges and Structures, Office of Design, and Office of Construction of the Iowa DOT, FHWA Iowa Division, and Iowa County Engineers. Thanks are extended to Team Services of Des Moines, Iowa, for conducting the SPT tests and Geotechnical Services, Inc. (GSI) of Des Moines, Iowa, for conducting the CPT tests. A special thank you is due to Douglas Wood in setting up the DAS system and helping on static load tests. Also, special thanks are due to Donald Davidson and Erica Velasco for the assistance with laboratory soil tests. We would also like to thank the following contractors for their contribution to the field tests:

ISU1 at Mahaska County – Cramer & Associates
ISU2 at Mills County – Dixon Construction Co.
ISU3 at Polk County – Cramer & Associates
ISU4 at Jasper County – Peterson Contractors, Inc.
ISU5 at Clarke County – Herberger Construction
ISU6 at Buchanan County – Taylor Construction, Inc
ISU7 at Buchanan County – Taylor Construction, Inc
ISU8 at Poweshiek County – Peterson Contractors, Inc.
ISU9 at Des Moines County – Iowa Bridge and Culvert, LC
ISU10 at Cedar County – United Contractors, Inc

CHAPTER 1: OVERVIEW

1.1. Background

Since the mid-1980s, the Load and Resistance Factor Design (LRFD) method has been progressively developed to ensure a better and more uniform reliability of bridge design in the United States. The Federal Highway Administration (FHWA) has mandated that all new bridges initiated after October 1, 2007 will follow the LRFD design approach. Because of high variability in soil characteristics, complexity in soil-pile interaction, and difficulty in predicting a sensible pile resistance and driving stress, design in foundation elements pose more challenges than the superstructure elements. To improve the economy of foundation design, American Association of State Highway and Transportation Officials (AASHTO) has recommended that higher resistance factors be used in the LRFD design method at a specific region where research has been conducted and/or past foundation data is available for validating the changes.

1.2. Scope of Research Projects

In response to the above recommendation, the Iowa Highway Research Board (IHRB) sponsored a research project, TR-573, in July 2007 to develop resistance factors for pile design using the Pile Load Test database (PILOT) from past projects completed by the Iowa Department of Transportation (Iowa DOT) from 1966 to late 1980s. The details of the PILOT database are described in the LRFD Report Volume I. Although the PILOT database enables the development of the LRFD resistance factors for static methods, dynamic formulas and Wave Equation Analysis Program (WEAP) from the static load test data, it is not inclusive of all soil profiles in Iowa and provides only a limited amount of reliable data. Also, the PILOT database does not include Pile Driving Analyzer (PDA) driving data, which should be used for providing a reliable construction control method, predicting pile damage resulting from pile driving, determining the contribution of shaft friction and end bearing to pile resistance, and developing the LRFD resistance factors for PDA and CAse Pile Wave Analysis Program (CAPWAP).

Hence, two (2) add-on research projects (TR-583 and TR-584) were proposed and included to conduct ten (10) field tests and obtain a complete set of data. The commonly used steel H-piles in Iowa for bridge foundations were chosen in the ten (10) field tests that cover all five (5) geological regions in the State of Iowa. These field tests involved detailed site characterization using both in-situ subsurface investigations, which consisted of Standard Penetration Tests (SPTs), Piezocone Penetration Tests (CPTs) with pore water pressure dissipation measurements, Borehole Shear Tests (BSTs), and modified Borehole Shear Tests (mBSTs), as well as laboratory soil classification and consolidation tests. In addition, push-in pressure cells were installed within 24-in. (610-mm) from designated pile flanges to measure the changes in lateral earth pressure and pore water pressure during pile driving, re-strikes and static load tests (SLTs). Prior to pile driving, the test piles were instrumented with strain gauges along the embedded pile length for axial strain measurements. In addition, two PDA strain transducers and two accelerometers were installed 30-in. (750-mm) below the pile head to record the pile strains and accelerations during driving and re-strikes, which were converted into force and velocity records for CAPWAP analyses. During pile driving and re-strikes, pile driving resistances (hammer blow count) were recorded for WEAP analyses. After completing all the re-strikes on the test piles, vertical SLTs were performed on test piles following the “Quick Test” procedure of ASTM D1143.

The field tests provided the following data: (1) detailed soil profiles with appropriate soil parameters; (2) lateral earth and pore water pressure measurements from the push-in pressure cells; (3) strain and acceleration measurements using the PDA during driving, at end of driving (EOD) and at the beginning of re-strikes (BOR); and (4) vertical static load test data. Interpretation and analysis of data was performed using static analysis methods, dynamic analysis methods and dynamic formulas. The completion of these three (3) projects will: (1) lay the foundation for developing a comprehensive database that can be populated at a reduced cost; (2) establish LRFD specifications for designing steel H-piles using static methods, dynamic analysis methods and dynamic formulas; (3) develop a reliable construction control method using the dynamic analysis methods and dynamic formulas; and (4) quantify the increase in pile capacities as a function of time (pile setup).

1.3. Report Content

The purpose of this report is to clearly depict the site characterization work and the field tests of the ten (10) steel H-piles installed in different soil profiles in the State of Iowa. This report consists of five (5) chapters describing the experimental work and a summary of the results. Three (3) appendices include the information and results of the field tests and laboratory tests. The content of each chapter is as follows:

Chapter 1: OVERVIEW – A brief description of the background of the LRFD specifications development in the United States and the scope of the IHRB LRFD research projects.
Chapter 2: SELECTION OF TEST LOCATIONS – A brief description of the process and criteria of selecting the locations of the ten (10) field tests on steel H-piles and their corresponding geological regions in the State of Iowa.
Chapter 3: SITE CHARACTERIZATION – Site Characterization: Description of the geotechnical subsurface investigations of characterizing the soil profile at each test site using in-situ and laboratory soil tests.
Chapter 4:FULL-SCALE TESTS – Field Testing: A complete description of the steel H-piles and hammers used at the test sites, pile instrumentation, pile driving, PDA tests, dynamic analysis methods and vertical static load tests.
Chapter 5: INTERPRETATION AND ANALYSIS OF FIELD DATA – Performed concurrent analytical and computational investigations using the field test results combined with some data from the PILOT database.
Chapter 6: SUMMARY– Summary of the site characterizations and the field tests.
Chapter 7: CONCLUSIONS – A summary of the important conclusions made from the interpretation and analysis of field test results.

CHAPTER 2: SELECTION OF TEST LOCATIONS

2.1. Criteria of Selecting Test Locations

The Iowa DOT provided a list of possible sites for the 10 field tests from current and upcoming bridge construction projects. In order to select proper locations for the field tests, six criteria listed below were established:

1) The test locations covered all possible geological regions in the State of Iowa;
2) The test piles were installed at locations, which covered all soil profiles in Iowa;
3) The number of test piles was proportioned to increase the data set with a soil profile that is scarce in the PILOT database;
4) The test locations were selected at locations with relatively less dense soil;
5) The test locations avoided sites with shallow bedrock; and
6) Despite satisfying the above criteria, the selection of the test locations was eventually decided based upon the nature of bridge construction projects.

2.1.1. Geological Regions in the State of Iowa

Iowa has five geological regions as shown in Figure 2.1. The five geological regions are alluvium, loess, Wisconsin glacial, loamy glacial and loess on top of glacial. The test pile locations are selected and situated in all geological regions.

2.1.2. Soil Profiles

Following AASHTO, soil profiles are categorized into sand, clay and mixed soils. Sand profile is defined as having more than 70 percent of an embedded pile length surrounded with sandy soil. Similar to the sand profile, clay profile is defined as having more than 70 percent of an embedded pile length surrounded with clayey soil. If a profile matches neither the sand nor clay profile, it is classified as a mixed profile. A mixed profile usually consists of two or more soil layers, with a soil profile containing less than 70% sand or clay surrounding the embedded pile length. Prior to performing the detailed site characterization, preliminary soil profiles are identified from the available Iowa DOT boring logs, as briefly listed in Table 2.1. The soil profiles are confirmed afterward by the detailed soil tests described in Section 3. Hence, the selected test locations as shown in Figure 2.1 are seen to adequately cover all three soil profiles.

2.1.3. Increase Data Set

Figure 2.2 shows a comparison between the distribution of eighty (80) usable steel H-piles from the PILOT database and the distribution of the ten (10) selected test sites by soil profiles. As explicitly described in the LRFD report volume I (Roling et al., 2010), usable data were identified as those pile load tests possessing sufficient information for pile resistance estimations by means of either static or dynamic analysis methods. In recognizing a larger number of usable steel H-piles in the sand and mixed profiles and a relatively small number in clay profile, from the PILOT database, five preferable test pile locations with a clay profile are selected, as listed in Table 2.1 in order to increase the total datasets for clay profile.

2.1.4. Sites with Relatively Less Dense Soil

Bridge foundations, especially those constructed at riverbanks, are commonly located in

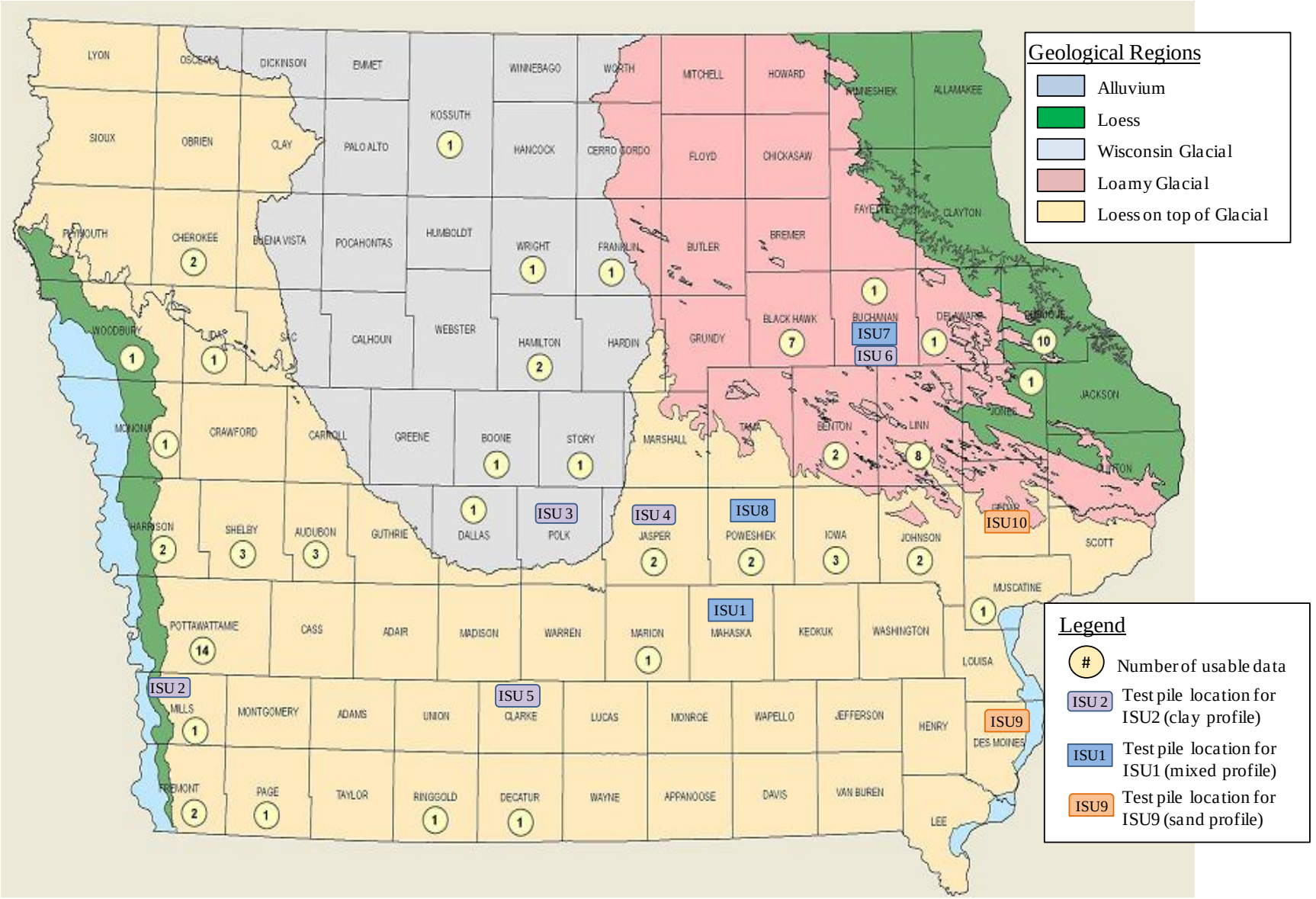

Figure 2.1. Iowa geological map and the test pile locations

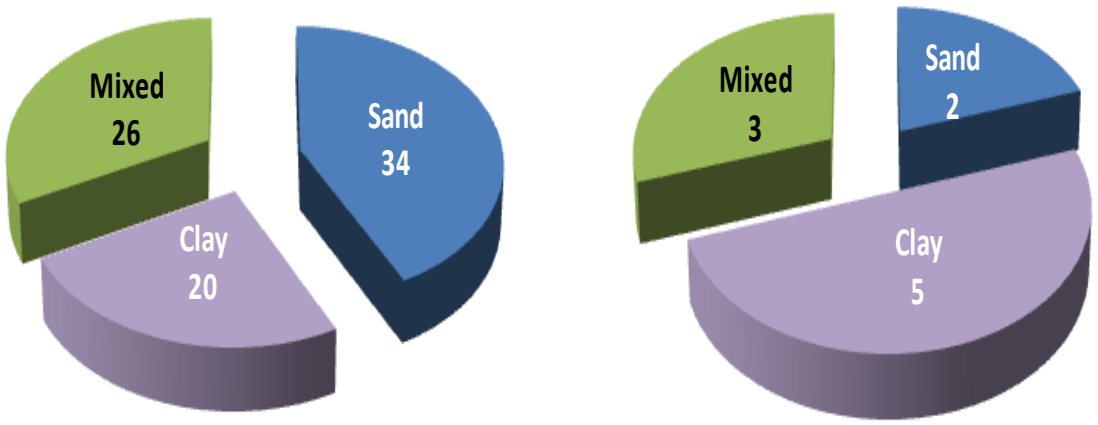

(a) Usable PILOT Database (b) Test Pile Locations

Figure 2.2. Distribution of steel H-piles by soil profiles

relatively less dense soils in the State of Iowa. Hence, these selected test locations are designed to most appropriately reflect the common less dense soil conditions and help in reducing any bias in the LRFD resistance factors calibration.

2.1.5. Sites with Shallow Bedrock

Shallow bedrock is not a common soil condition in Iowa for bridge foundations. In view of the fact that steel H-piles have relatively large perimeter and small cross sectional area, they are widely designed and used as frictional piles in the State of Iowa. Knowing standard steel H-piles are 60-ft (18.3-m) in length, any site with a bedrock layer less than 60-ft (18.3-m) is disregarded. Hence, all selected sites provided in Table 2.1 have bedrock layers more than 60-ft (18.3-m).

2.1.6. Nature of Bridge Construction Projects

Despite the selected site locations meeting the above criteria, the nature of the bridge construction projects could eventually govern the final selection. With the input from the project technical advisory committee, unfavorable project sites are identified with the following conditions: (1) projects have a short or constrained construction schedule; (2) projects located at critical and major highways, such as Interstates I-35 and I-80; and (3) projects have limited space for pile testing.

2.2. Selected Test Pile Locations

Based on the available bridge construction projects in Iowa, as designated by the Iowa DOT and following all criteria established above, ten (10) test sites were selected. Figure 2.1 and Table 2.1 show the locations of the test sites corresponding to the geological regions and the soil profiles. Project identifications (IDs) were assigned to the test sites, starting from ISU1 to ISU10, and these will be used throughout the report. Table 2.1 also provides the counties where the selected sites are situated, Iowa DOT bridge construction project numbers, closest Iowa DOT boring log to the test pile, soil layers, SPT N-values, and bedrock depth. Based on the Iowa DOT borehole soil information, the preliminary soil profiles were established. After completing all detailed soil characterization, the final soil profiles were established based on the final embedded pile lengths. The site layouts of the test pile locations are included in Appendix A.

Table 2.1. Information on selected steel H-pile test locations

Project ID	County	Iowa DOT Project Number	Geological Region	Closest Iowa DOT SPT Borehole	Description of Soil Layers according to Iowa DOT Boring Logs	SPT N-value (Soil Layer Thickness)	Bedrock Depth	Preliminary Soil Profile from Iowa DOT Boreholes	Final Embedded Test Pile Length (ft)	Confirmed Soil Profile from ISU Soil Tests
ISU 1	Mahaska	BRF-63-3(46)-38-62	Loess on Top Glacial	P-4010	ST:C, H:C	9 (10-ft), >50	> 60-ft	Clay	32.50	Mixed
ISU 2	Mills	BRF-978-1(15)-38-65	Loess	T-1420	SF:C to ST:C,F:SH, H:SH	4 (50-ft), 12 (20-ft), 22 (10-ft), >50	≈ 77-ft	Clay	55.83	Clay
ISU 3	Polk	BRFIM-0.35-3(182)87-05-77	Wisconsin Glacial	F-0957	F:C, F:SH, H:SH	13 (53-ft), 37 (12-ft), 55 (> 3-ft)	≈ 75-ft	Clay	51.00	Clay
ISU 4	Jasper	BRF-014-4(44)-38-50	Loess on Top Glacial	P-3666	ST:SL-C, F:C, GR, V.F:C	6 (5-ft), 7 (10-ft), 23 (20-ft), 10 (> 30-ft)	> 60-ft	Mixed	56.78	Clay
ISU 5	Clarke	BRFIMX-035-1(105)33-14-20	Loess on Top Glacial	T-1592	F:C, V.F:C	10 (30-ft), 23 (> 40-ft)	> 60-ft	Clay	56.67	Clay
ISU 6	Buchanan	BRF-150-3(58)-38-10	Loamy Glacial	F-1049	ST:SL-C, M:S, V.F:G-C	8 (11-ft), 5 (19-ft), 22 (> 30-ft)	> 60-ft	Mixed	57.2	Clay
ISU 7	Buchanan	BRF-150-3(58)-38-10	Loamy Glacial	F-1049	ST:SL-C, M:S, V.F:G-C	8 (11-ft), 5 (19-ft), 22 (> 30-ft)	> 60-ft	Mixed	26.90 (10-ft Prebore)	Mixed
ISU 8	Poweshiek	BRF-006-5(14)-38-79	Loess on Top Glacial	F-1027	F:SL-C, M:S, V.F:G-C	8 (14.4-ft), 9 (16-ft), 20 (30-ft)	> 60-ft	Mixed	57.21	Mixed
ISU 9	Des Moines	BROS-C029(56)-SF-29	Alluvium	1	F:SL-C, FN:S, F:SL-C, FN:S	11 (9-ft), 22 (45-ft), 19 (7-ft), 23 (> 25-ft)	> 86-ft	Sand	49.4	Sand
ISU 10	Cedar	n/a	Loamy Glacial	n/a	n/a	n/a	n/a	n/a	49.5	Sand

Notation for soil layer: B = Boulders, C = Clay, CR = Coarse, F = Firm, FN = Fine, G = Glacial, GR = Gravel, H = Hard, LS = Limestone, M = Medium, R = Rock, S = Sand, SF = Soft, SH = Shale, SL = Silt, SS = Sandstone, ST = Stiff, V = Very, and W = With

CHAPTER 3: SITE CHARACTERIZATION

The soil profiles at all test sites were characterized using both in-situ and laboratory soil tests. The in-situ soil investigations included Standard Penetration Tests (SPT), Cone Penetration Tests (CPT), conventional Borehole Shear Tests (BST), and modified Borehole Shear Tests (mBST). Five sites were selected for monitoring pore water pressure and lateral earth pressure before and after pile driving, during re-strikes and during static load tests. The layouts of the in-situ soil investigations are shown in Appendix A. The laboratory soil tests consisted of basic soil characterization (i.e., gradation, Atterberg's limits and moisture content) and consolidation tests. A general summary of both in-situ and laboratory soil investigations are shown in Table 3.1. Detailed descriptions of each test and the corresponding results are presented in the following sections. For additional measured soil results, refer to Appendix B.

Table 3.1. Summary of in-situ and laboratory soil investigations

Project ID	Standard Penetration Test (SPT)	Cone Penetration Test (CPT)	Borehole Shear Test (BST)	modified Borehole Shear Test (mBST)	Pore Water and Lateral Earth Pressure Measurement	Gradation and Atterberg's Limits Tests	Consolidation Test
ISU 1	Not Performed	2 Tests	1 Test (3 depths)	Not Performed	Not Performed	5 Tests	Not Performed
ISU 2	1 Test (9[a])	1 Test (2[b])	1 Test (2 depths)	Not Performed	Not Performed	6 Tests	3 Tests
ISU 3	1 Test (10[a])	1 Test (2[b])	1 Test (2 depths)	Not Performed	Not Performed	7 Tests	3 Tests
ISU 4	1 Test (9[a])	1 Test (4[b])	1 Test[c] (2 depths)	1 Test[c] (2 depths)	Not Performed	10 Tests	3 Tests
ISU 5	1 Test (8[a])	3 Tests (1[b] at Test 3)	1 Test[c] (3 depths)	1 Test[c] (3 depths)	2 Tests	9 Tests	3 Tests
ISU 6	1 Test (9[a])	1 Test (4[b])	1 Test[c] (3 depths)	1 Test[c] (3 depths)	2 Tests	8 Tests	3 Tests
ISU 7					1 Test		
ISU 8	1 Test (12[a])	1 Test (4[b])	1 Test[c] (3 depths)	1 Test[c] (3 depths)	1 Test	10 Tests	3 Tests
ISU 9	1 Test (12[a])	1 Test (2[b])	Not Performed	Not Performed	Not Performed	9 Tests	Not Performed
ISU 10	1 Test (10[a])	1 Test	Not Performed	Not Performed	1 Test	7 Tests	Not Performed

[a] - Number of SPT N-value recorded
[b] - Number of CPT pore water pressure dissipation tests
[c] - BST or mBST with shearing displacement measurement

3.1. Standard Penetration Tests (SPT)

Team Services of Des Moines, Iowa, conducted all Standard Penetration Tests (SPT) at locations shown in Appendix A. All SPT tests were performed in accordance with American Society for Testing and Materials (ASTM) standard D1586. SPT determines the standard penetration resistances, or the "N-values", that are used in the pile static and dynamic analyses presented in the IHRB TR-573, TR-583 and TR-584 Report Volume III. The N-value is computed by adding the number of 140-lb (63.5-kg) hammer blows, of a 2-in. (50-mm) diameter thick-walled split-spoon sampler, required for the second and third penetrations of 6-in. (150-mm) depth, as shown

in Figure 3.1. The results of the SPT N-values for ISU5 at Clarke County are presented in Figure 3.2, and similar SPT results for other sites are included in Appendix B. The N-values (N_F) obtained from the field SPT under different effective overburden pressures were corrected (N_{cor}) to correspond to a standard effective vertical stress (σ'_v), using Eq. 3-1 (Das 1990). The correction factor (C_N) used in this conversion, was determined using Eq. 3-2 (Liao and Whitman 1986).

$$N_{cor} = C_N N_F \tag{3-1}$$

$$C_N = \sqrt{\frac{1}{\sigma'_v(\text{ton/ft}^2)}} \tag{3-2}$$

As an example, the results from the ISU5's SPT are illustrated in Figure 3.2, where at a depth of 38-ft (10-m) the field SPT N-value was 22, effective stress is 2.45 tons/ft^2 (235 kPa), and a calculated C_N of 0.64, using Eq.3-2, was obtained, and the corrected SPT N-value (N_{cor}) is 14.

Disturbed soil samples were collected by the research team during the SPT tests for soil gradation tests, Atterberg's limits tests and soil classifications according to the Unified Soil Classification System (USCS) described in Section 3.5. In addition, undisturbed soil samples were collected using 3-in. (75-mm) Shelby tube thin-walled samplers for laboratory consolidation tests.

(a) SPT blow count (b) Split-spoon sampling

Figure 3.1. Typical Standard Penetration Test (SPT)

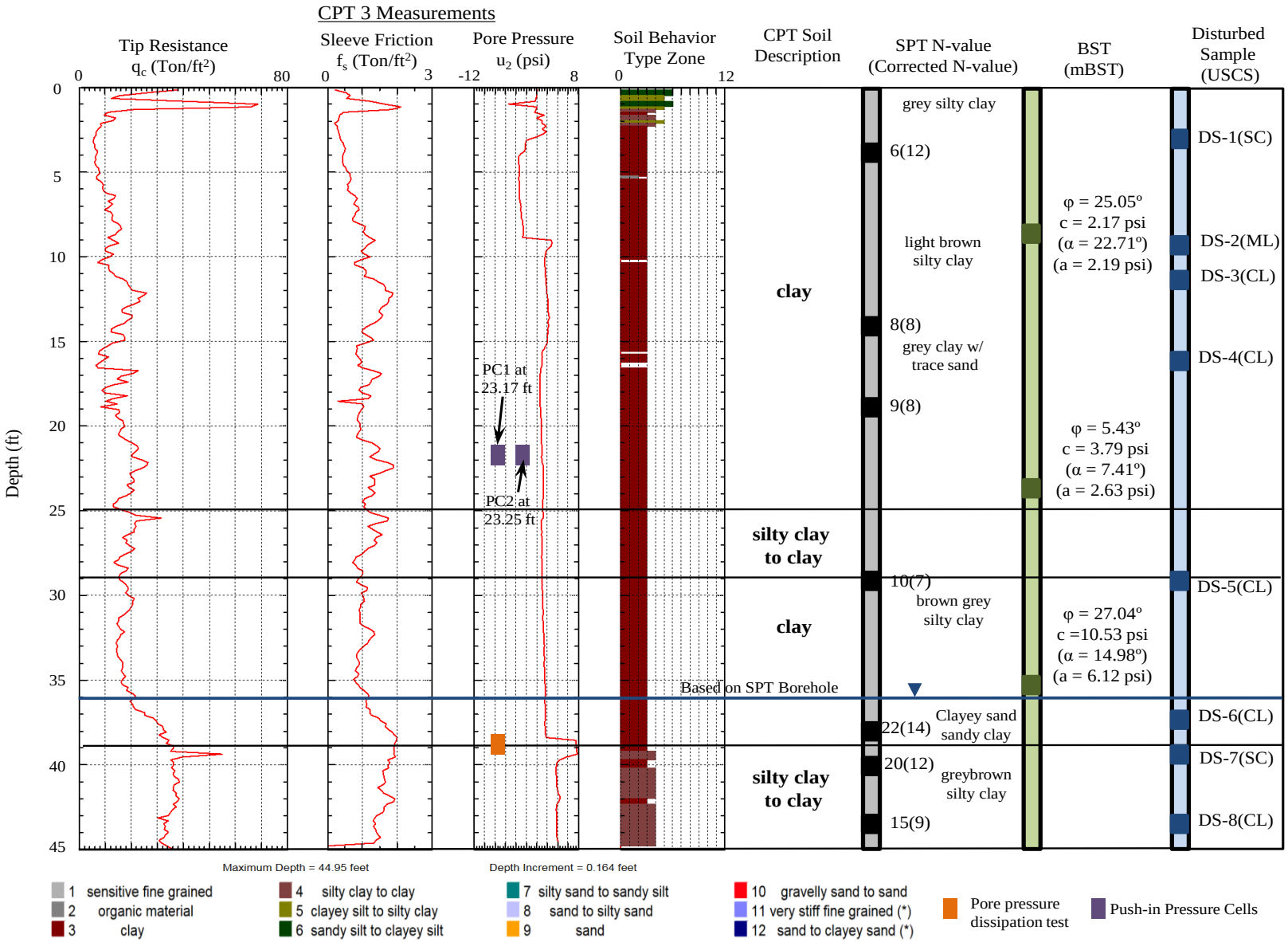

Figure 3.2. In-situ soil investigations and soil profile for ISU5 at Clarke County (CPT 3)

3.2. Cone Penetration Tests (CPT)

Cone Penetration Tests (CPT) were performed in accordance with ASTM Standard D5778. Geotechnical Services, Inc. (GSI) performed all CPT tests at locations shown in Appendix A. The CPT investigation utilized a 20-ton capacity, truck-mounted rig hydraulically advancing a Hogentogler Type 2, 10-ton subtraction cone, as shown in Figure 3.3. The electronic peizocone has a 60º tip angle, tip area of 1.55-in^2 (10-cm^2), a net area ratio of 0.8, and a friction sleeve area of 23.25-in^2 (150-cm^2). During the CPT, the cone was pushed into the ground at a controlled rate of around 1-in/s, while the uncorrected tip resistance (q_c), local sleeve friction (F_s) and pore pressure (u_2) measurements were collected at every 2-in. (50-mm) interval, as presented in Figure 3.2 for ISU5 and in Appendix B for all sites. Soil types, as shown in Figure 3.2, were identified using a simplified soil classification chart for a standard electric friction cone adapted from Robertson & Campanella (1983).

Figure 3.3. Typical Cone Penetration Test (CPT)

In addition, pore pressure dissipation tests were conducted at selected depths, as indicated in Figure 3.2 for ISU5 and in Appendix B for other sites. The results of these pore pressure dissipation tests were used to estimate the horizontal coefficient of consolidation (C_h) based on the strain path method reported by Houlsby and Teh (1988) and techniques suggested by Sully and Campanella (1994) for fine-grained soil. The pore pressure dissipation for ISU5 at 38.55-ft (11.75-m) depth, as shown in Figure 3.4, was conducted in a relatively hard and predominately fine-grained soil identified as silty clay to clay. Therefore, pore water pressure built up was measured, and due to dilation of soil, a long time was needed to re-saturate the cone tip before any pore pressure dissipation could be observed. The horizontal coefficient of consolidation (C_h) could not be estimated. Therefore, pore pressure dissipation for ISU2 at 35.4-ft (10.79-m) depth, as shown in Figure 3.5, is used to illustrate the calculation of C_h using Eq. 3-3 (Houlsby and Teh 1988). The rigidity index (I_R) is estimated using Eq. 3-4 and Eq. 3-5 (Mayne 2001).

Based on the normalized pore water pressure (B_q), the effective friction angle (ϕ') is calculated either by Eq. 3-6 for granular soil where $B_q < 0.1$ (Kulhawy and Mayne 1990) or by using Eq.3-7 for soils where $0.1 \leq B_q \leq 1.0$, as per an approach developed by the Norwegian University of Science and Technology (NTNU) and discussed by Mayne (2007). By normalizing the measured pore pressures with the maximum pore pressure of 64.18 psi and plotting this in a logarithmic scale, starting at the maximum pore pressure, against time, the time for reaching the 50% pore pressure dissipation (t_{50}) is estimated at 265 seconds (4.42 min) as shown in Figure 3.5. The effective friction angle (ϕ') of 27.63º is estimated using Eq. 3-7 and yields the constrained modulus parameter (M) of 1.10. Using the CPT measurements of q_c, u_2 and the net area ratio of 0.8, the corrected tip resistance (q_t) of 147.59 psi (1.02 MPa) and the rigidity index (I_R) of 17.47 are calculated. Finally the horizontal coefficient of consolidation (C_h) of 0.1152 in^2/min (74.32 mm^2/min) is calculated using Eq. 3-3. The summary of the related parameters and C_h is presented in Table 3.2.

$$C_h = \frac{T_{50} a_c^2 \sqrt{I_R}}{t_{50}} \tag{3-3}$$

$$I_R = \exp\left[\left(\frac{1.5}{M} + 2.925\right)\left(\frac{q_t - \sigma_{vo}}{q_t - u_2}\right) - 2.925\right] \tag{3-4}$$

$$M = \frac{6\sin\varphi'}{3 - \sin\varphi'} \tag{3-5}$$

$$\phi' = 17.6^o + 11^o \mathrm{Log}\left(\frac{q_t/\sigma_{atm}}{\sqrt{\sigma'_{vo}/\sigma_{atm}}}\right) \text{ for } B_q < 0.1 \tag{3-6}$$

$$\phi' = 29.5^o B_q^{0.121}\left(0.256 + 0.336 B_q + \mathrm{LogQ}\right) \text{ for } 0.1 \leq B_q \leq 1.0 \tag{3-7}$$

where

C_h = Horizontal coefficient of consolidation estimated using CPT results, in^2/min;
T_{50} = Modified time factor for Type 2 cone at 50% dissipation = 0.245;
a_c = Tip area of cone = 1.55-in^2, in^2;
I_R = Rigidity index evaluated directly from CPT data using Eq.3-4;
t_{50} = Measured time to reach 50% consolidation, sec;
q_t = Corrected tip resistance = q_c+u_2(1- net area ratio), psi;
q_c = Uncorrected measured tip resistance, psi;
σ_{vo} = Total vertical geostatic stress, psi;
u_2 = CPT measured pore pressure, psi;
ϕ' = Frictional angle, degree;
σ'_{vo} = Effective vertical geostatic stress, psi;
σ_{atm} = Atmospheric pressure = 1.47×10^{-5}, psi;
B_q = Normalized pore water pressure parameter = $(u_2-u_o)/(q_t-\sigma_{vo})$; and
Q = Normalized cone tip resistance = $(q_t-\sigma_{vo})/\sigma'_{vo}$.

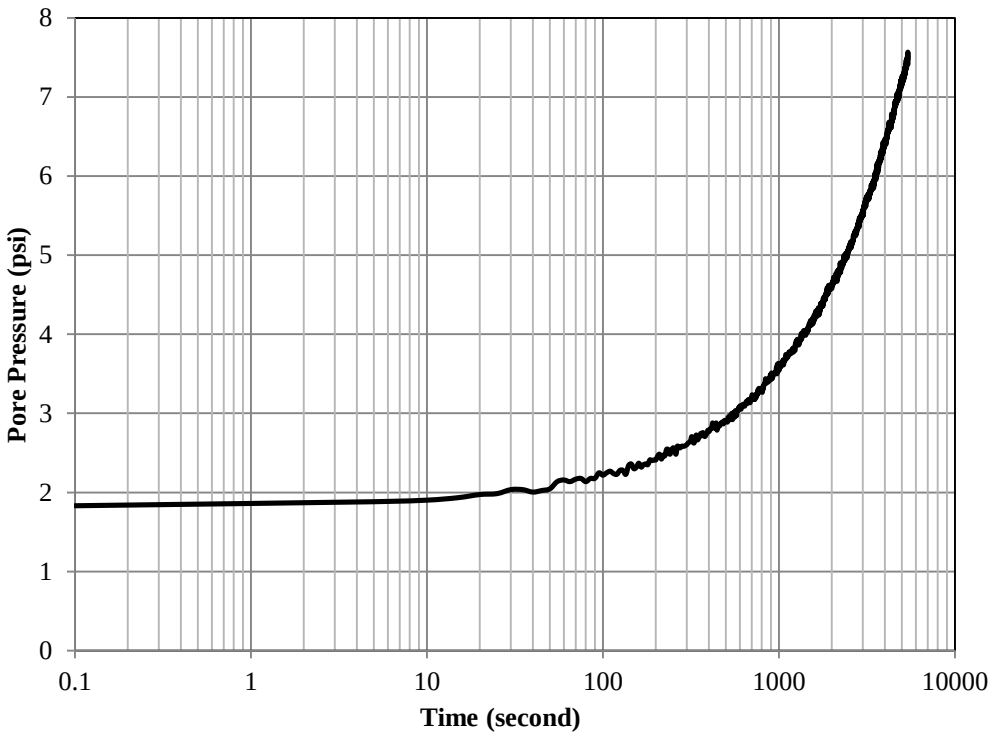

Figure 3.4. Increase in pore pressure for ISU5 at a depth of 38.55-ft

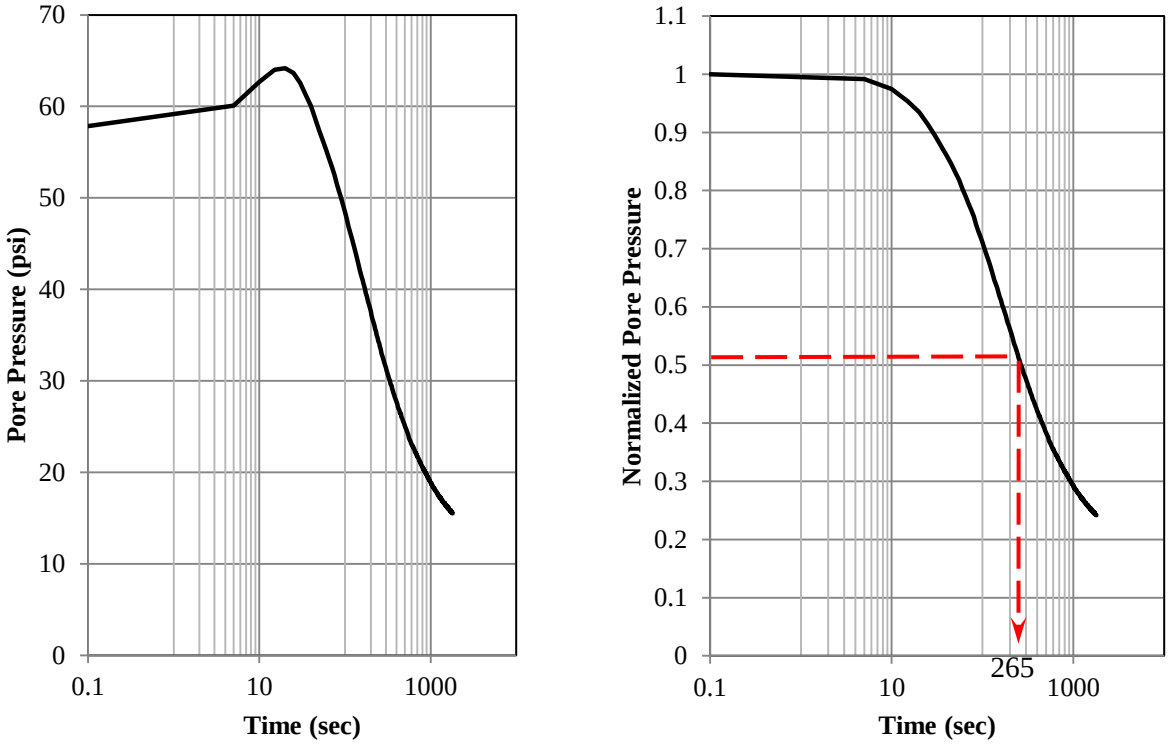

Figure 3.5. Pore pressure dissipation result for ISU2 at a depth of 35.4-ft

Table 3.2. Summary of soil parameters at depths of CPT dissipation tests

Project ID	Depth (ft)	t_{50} (min)	ϕ' (degree)	M	q_t (psi)	u_2 (psi)	σ_{vo} (psi)	I_R	C_h (in^2/min)
ISU2	35.40	4.42	27.72	1.10	147.59	57.40	18.24	25.13	0.1382
ISU3	22.15	31.27	11.94	0.44	228.47	38.20	17.31	58.37	0.0298
ISU4	19.50	43.42	24.66	0.97	239.71	4.13	12.54	4.01	0.0056
	21.00	64.78	38.71	1.58	1209.92	5.19	14.45	2.51	0.0030
	41.00	227.99	21.80	0.85	353.17	37.41	25.01	7.06	0.0014
	50.53	88.68	33.09	1.33	313.15	82.21	29.82	7.71	0.0038
ISU6	50.03	151.52	30.28	1.21	282.47	9.60	35.42	2.33	0.0012
ISU8	57.25	264.83	34.24	1.39	732.76	4.08	34.42	2.50	0.0007

The CPT soundings provide a nearly continuous subsurface soil profile and are used to estimate basic soil parameters such as effective friction angle (ϕ') as explained above, undrained shear strength (S_u), and over-consolidation ratio (OCR). The undrained shear strength (S_u) is estimated using a classical approach given by Eq. 3-8 (Mayne 2007). The over-consolidation ratio (OCR) for intact clays is estimated using Eq. 3-9 (Demers and Leroueil 2002). These estimated soil parameters are used in the static and dynamic pile analyses conducted later. The average soil parameters are summarized in Table 3.3 for ISU5 based on the CPT classified soil profiles, indicated in Figure 3.2, and are summarized in Appendix B for all sites.

$$S_u = \frac{q_t - \sigma_{vo}}{N_{kt}} \tag{3-8}$$

$$OCR = \frac{q_t - \sigma_{vo}}{\sigma'_{vo}} \tag{3-9}$$

where

N_{kt} = Bearing factor; 15 was assumed for representing the Iowa soil condition; and

Table 3.3. Summary of soil properties for ISU5 based on CPT

Soil Profiles	Depth (ft)	Soil Types	Average Effective Friction Angle, ϕ' (degree)	Average Undrained Shear Strength, S_u (psi)	Average Over-consolidation Ratio (OCR)
Layer 1	0 to 25	Clay	31.08	13.28	5.60
Layer 2	25 to 29	Silty Clay to Clay	29.94	15.71	3.11
Layer 3	29 to 39	Clay	29.72	16.46	2.63
Layer 4	39 to 45	Silty Clay to Clay	32.09	30.61	3.92

3.3. Borehole Shear Tests (BST)

Borehole shear tests (BST) were conducted at each test site, except ISU9 and ISU10, by the research team. BST equipment, as shown in Figure 3.6, was developed by Emeritus Professor Richard Handy of Iowa State University to rapidly and directly measure the in-situ effective shear strengths of soil in relation to applied normal pressure. A 3-in (75-mm) smooth hole was drilled to a desired depth. An expandable shear head with a pair of grooved shear plates was inserted into the hole and pushed against the sides of the hole with a predetermined normal pressure, starting from the top soil layer to minimize hole disturbance. After allowing time for soil consolidation, the shear head was slowly pulled upward to measure the shear stress (τ). Furthermore, the shear stress increments were continuously recorded at every 10 rotations of the crank, which was equivalent to 0.006-in. (0.152-mm) of the vertical shearing displacement. Repeating this process with increasing the normal stress (σ), a Mohr-Coulomb shear failure envelope, as shown in Figure 3.7 for ISU5 at 8.83-ft (2.69-m) depth, was generated based on the maximum shear stresses and the corresponding applied normal stresses, in order to determine the soil frictional angle (ϕ) and cohesion (c). The soil friction angle (ϕ) of 25.08º is the arctangent of the shear envelope slope of 0.47, and the soil cohesion is the vertical axis interception of 2.17 psi (14.96 KPa). The shear stress-displacement relationship at each applied normal stress is plotted in Figure 3.8. The results of BSTs for all sites are presented in Appendix B.

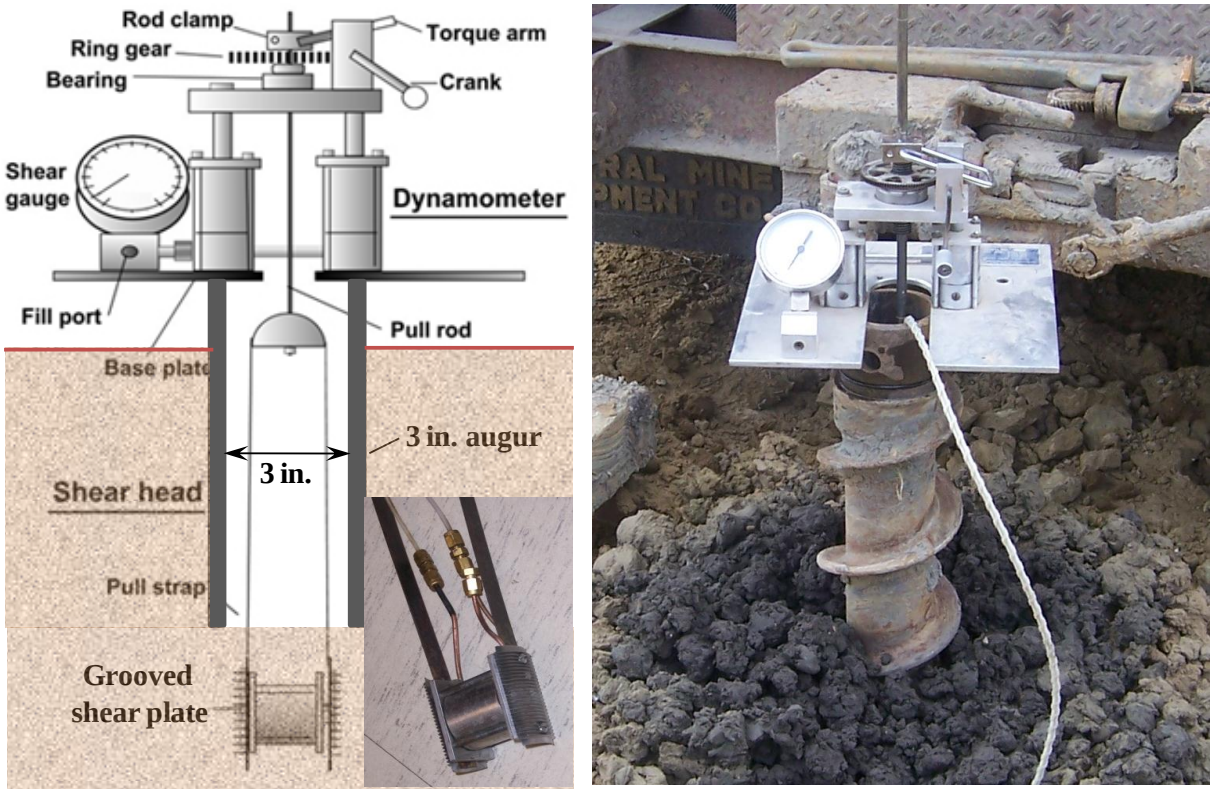

(a) Cross sectional view (b) Photo view

Figure 3.6. The conventional Borehole Shear Test (BST) equipment (adapted from Handy, 1986)

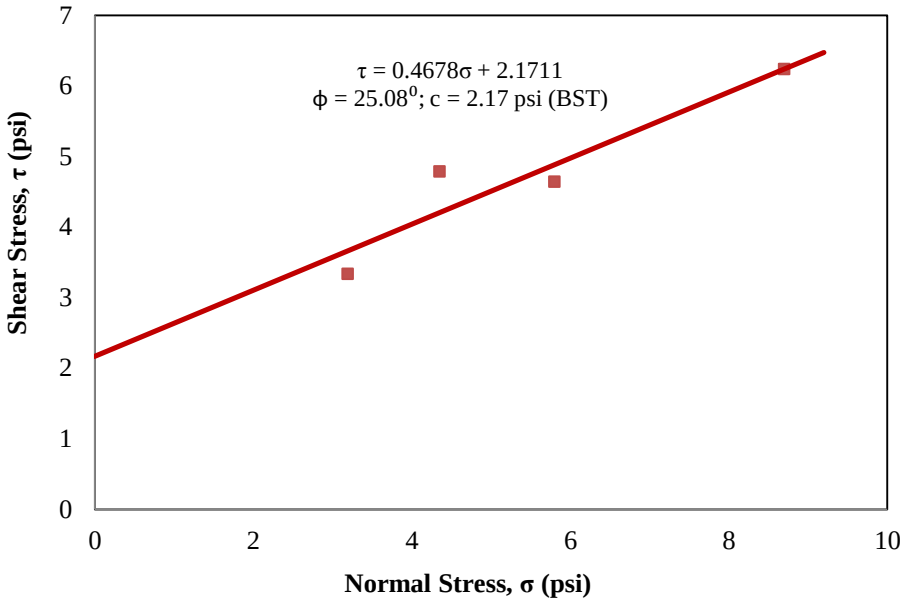

Figure 3.7. BST generated Mohr-Coulomb shear failure envelope for ISU5 at 8.83-ft depth

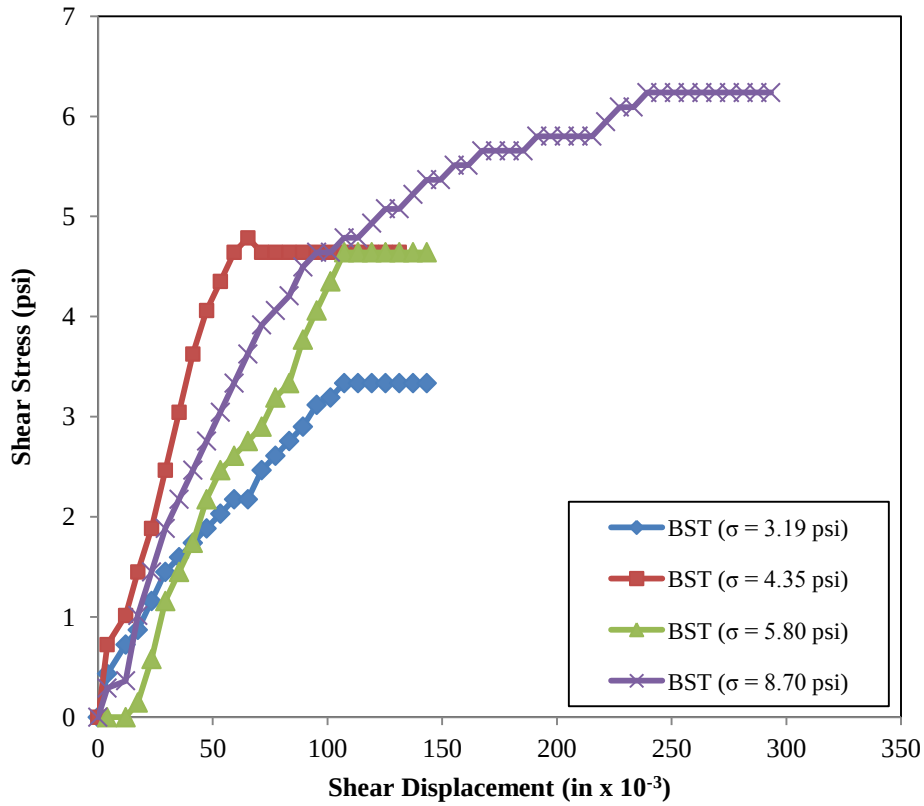

Figure 3.8. BST generated shear stress-displacement relationship at different applied normal stress for ISU5 at 8.83-ft depth

3.4. Modified Borehole Shear Tests (mBST)

Similar to conventional Borehole Shear Test (BST), the modified Borehole Shear Test (mBST) was performed using a pair of smoothed steel plates as shown in Figure 3.9 instead of using the BST's grooved steel plates. The modified Borehole Shear Test equipment was explicitly described by AbdelSalam et al. (2010). The mBST directly determines the frictional angle (α) and adhesion (a) between the smoothed steel plate and the contacted soil by measuring the shear displacement and the corresponding shear stresses (τ) at several applied normal stresses (σ). Figure 3.10 shows the relationships between the shear stresses and the shear displacements at four different applied normal stresses for ISU5 at 8.83-ft (2.69-m) depth. Taking the peak shear stress at each applied normal stress, the Mohr-Coulomb shear failure envelope was generated as shown in Figure 3.11. The interface frictional angle (α), between the steel plate and soil, of 20.75º is the arctangent of the envelope slope of 0.38, and the interface adhesion (a) is the vertical axis interception of 2.48 psi (17.10 KPa).

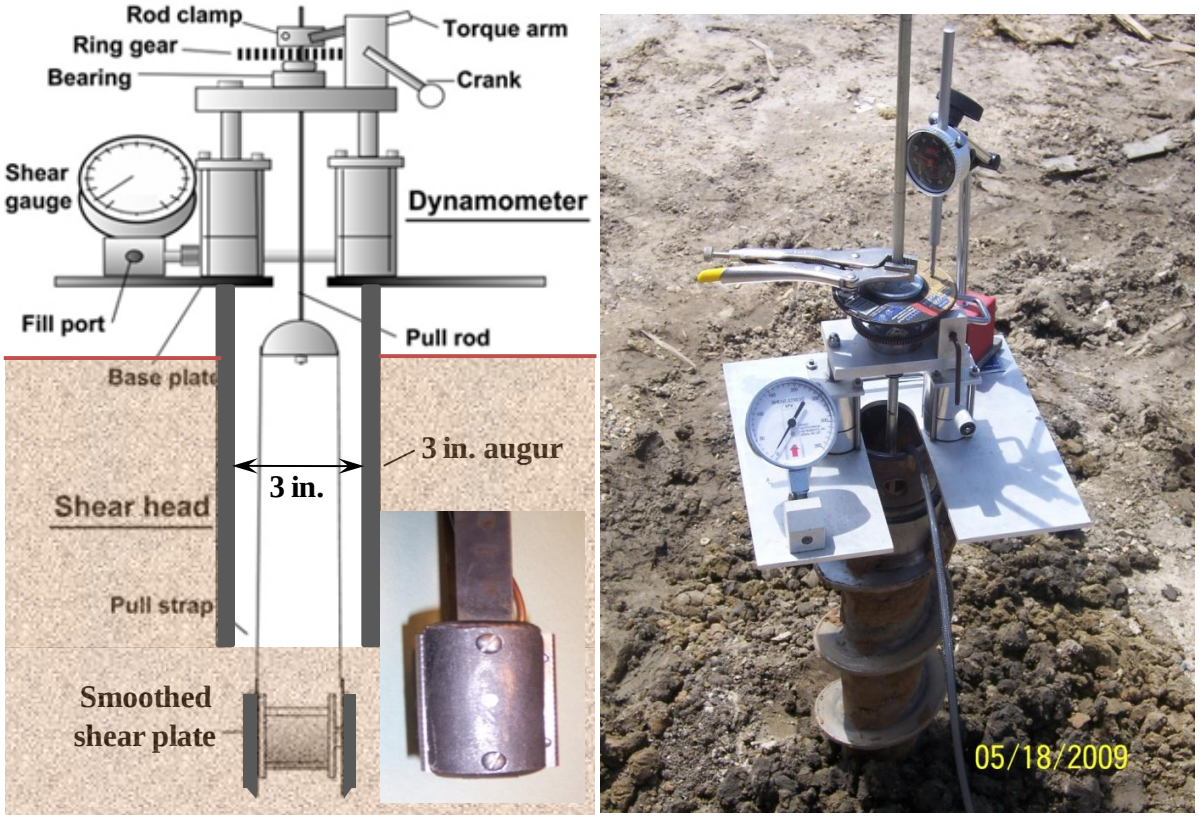

(a) Cross sectional view (b) Photo view

Figure 3.9. The modified Borehole Shear Test (mBST) equipment (adapted from Handy, 1986)

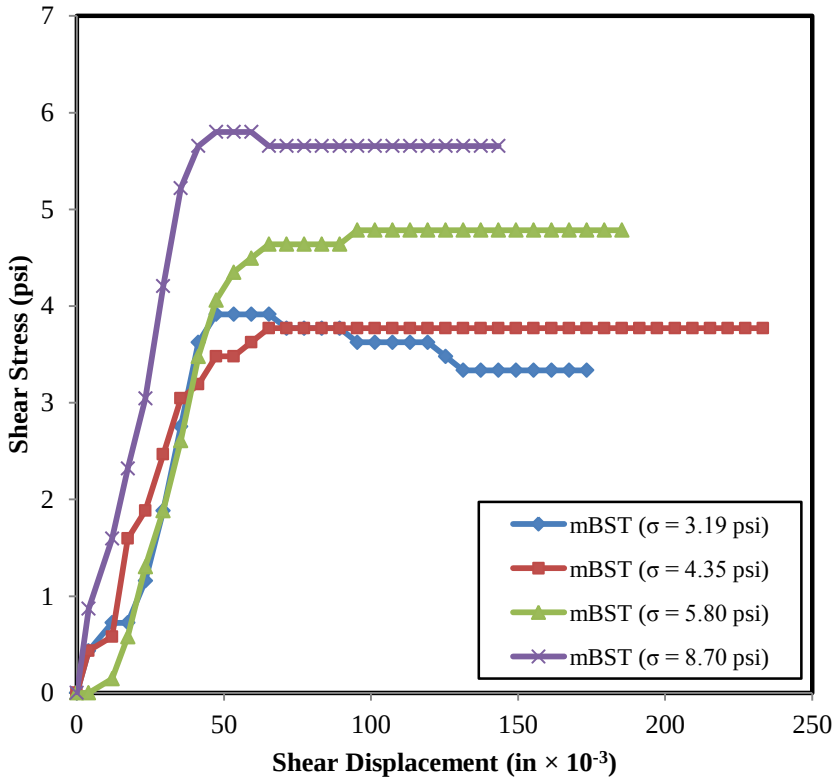

Figure 3.10. mBST generated shear stress-displacement relationship at different applied normal stress for ISU5 at 8.83-ft depth

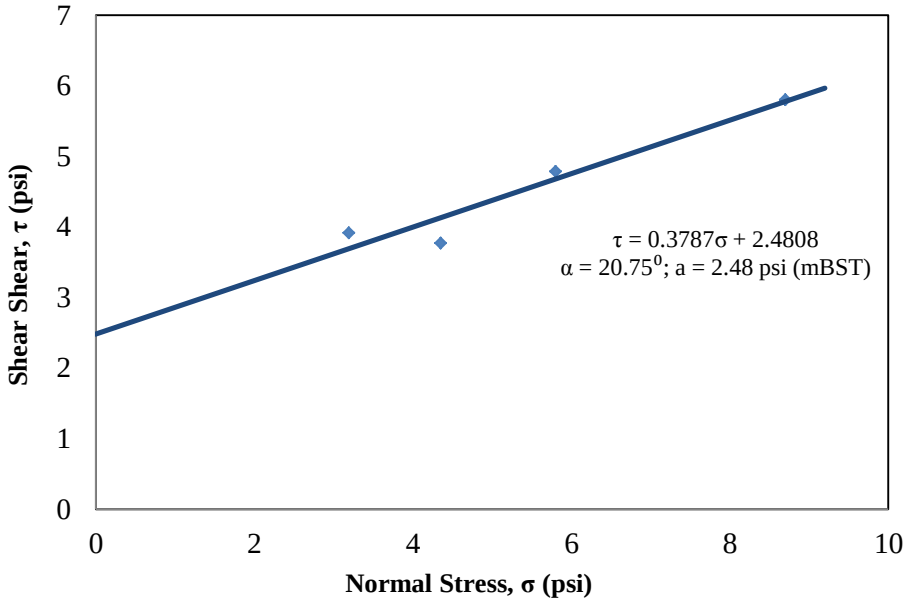

Figure 3.11. mBST generated Mohr-Coulomb interface shear failure envelop for ISU5 at 8.83 ft depth

3.5. Laboratory Soil Tests

3.5.1 Soil Grain Size Distribution

Disturbed samples collected from SPT boreholes at various depths were used in a soil gradation test in accordance with ASTM D6913 using sieve analysis, as shown in Figure 3.12 (a), for soil particle sizes greater than 0.0029-in (0.074-mm or No. 200 sieve). A hydrometer 151H that complied with ASTM E100, illustrated in Figure 3.12 (b), was used in accordance with ASTM D422 to determine the grain size distribution finer than 0.0029-in (0.074-mm). Combining the results obtained from the sieve analysis and the hydrometer test, a complete grain size distribution curve was generated, as shown in Figure 3.13, for the disturbed sample DS-1 collected at 3-ft (0.9-m) depth of ISU5. The particle sizes finer than 10%, 30% and 60%, denoted as D_{10}, D_{30}, and D_{60} respectively, for ISU5 were determined from the grain size distribution curve shown in Figure 3.13 and listed in Table 3.4.

(a) Sieve analysis (b) Hydrometer test (c) Atterberg's limit test

Figure 3.12. Laboratory soil tests

3.5.2. Atterberg Limits

In addition to performing the above soil gradation tests, Atterberg's limit tests were conducted in accordance with ASTM D4318, using equipment as shown in Figure 3.12 (c), to determine the plastic limit (PL) and liquid limit (LL). These Atterberg's limits are essential properties for classifying fine-grained soil. The plastic limit (PL) is the amount of moisture content in a soil when it starts to exhibit plastic behavior. It is determined when a thread of soil, rolled to a diameter of 0.12-in (3-mm), begins to crumble. The liquid limit (LL) is defined as the amount of moisture content in a soil when it changes from plastic to liquid behavior. The liquid limit is determined by placing the soil sample into the metal cup of the LL device, as shown in Figure 3.12 (c), and making a 0.5-in. (13-mm) groove down its center with a standardized tool. The number of blows required to close the groove is recorded and the moisture content at which it took 25 drops of the cup is defined as the liquid limit. The difference between the liquid limits and the plastic limits are defined as the plasticity indices (PI), which are listed in Table 3.4 for ISU5.

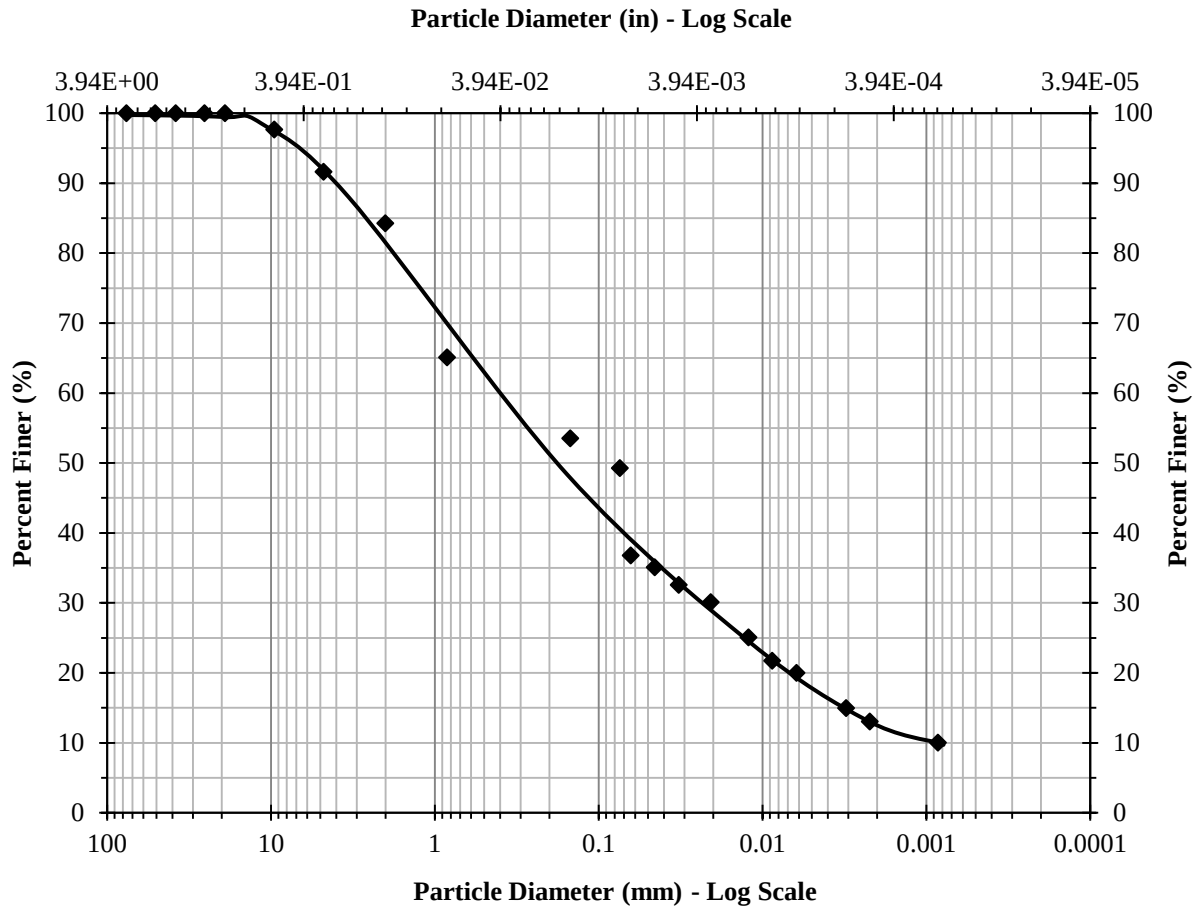

Figure 3.13. Grain size distribution curve for disturbed sample DS-1 at 3 ft depth of ISU5

3.5.3. Soil Classification

After performing the above soil gradation tests and Atterberg's limit tests and determining the essential soil properties, the soil was classified using the Unified Soil Classification System (USCS) in accordance with ASTM D2487. The results of the USCS soil classification are listed in Table 3.4 for ISU5 and are included in Appendix B for other sites. Estimated values for the natural moisture content (ω), void ratio (e), and saturated unit weight (γ_{sat}) properties of the soils tests are also included in Table 3.4 for ISU5 and in Appendix B. The natural moisture content (ω) is determined in accordance with ASTM D2216 and estimated using Eq. 3-10. The void ratio (e) is estimated using Eq. 3-11 by assuming 100% saturation (S) and a specific gravity (G) of 2.7. Using the estimated void ratio, the saturated unit weight (γ_{sat}) is estimated using Eq. 3-12.

$$\omega = \frac{W_w}{W_s} \tag{3-10}$$

$$e = \frac{\omega G}{S} \tag{3-11}$$

$$\gamma_{sat} = \frac{(G + e)\gamma_w}{1 + e} \quad (3\text{-}12)$$

where

ω = Moisture content, %;
W_w = Weight of moisture (water) in a soil sample, lb;
W_s = Weight of solid in a soil sample, lb;
e = Void ratio;
G = Specific gravity (assumed 2.7);
S = Degree of saturation (assumed 100%), %;
γ_w = Unit weight of water = 62.4 pcf; and
γ_{sat} = Saturated unit weight, pcf.

Table 3.4. Soil classification and properties for ISU5 obtained from gradation and Atterberg's limit tests

Disturbed Sample	Sample Depth (ft)	Soil Type (USCS)	D_{10} (in)	D_{30} (in)	D_{60} (in)	Liquid Limit, LL (%)	Plasticity Index, PI (%)	Moisture Content, ω (%)	Saturated Unit Weight, γ_{sat} (pcf)	Void Ratio, e
DS-1	3	SC	3.3E-5	8.1E-4	2.1E-2	26.31	11.27	20.39	130.82	0.55
DS-2	8 to 10	ML	9.0E-6	4.8E-4	2.7E-3	36.30	5.57	18.70	132.89	0.50
DS-3	10 to 12	CL	-	2.4E-4	2.6E-3	38.41	20.82	20.64	130.52	0.56
DS-4	16	CL	-	3.4E-4	2.7E-3	49.10	27.08	21.58	129.42	0.58
DS-5	28 to 30	CL	-	3.4E-4	2.8E-3	44.60	26.84	17.20	134.84	0.46
DS-6	37 to 38.5	CL	-	3.4E-4	2.7E-3	38.61	22.23	22.03	128.92	0.59
DS-7	38.5 to 40	SC	-	7.2E-4	6.4E-3	22.02	8.63	19.80	131.52	0.53
DS-8	43.5 to 45	CL	-	1.2E-4	2.6E-3	38.73	20.78	16.11	136.32	0.44
DS-9	48 to 50	CL	-	1E-4	2.4E-3	40.07	22.33	16.94	135.19	0.46

D_{10}, D_{20}, and D_{60} – particle sizes finer than 10%, 30% and 60%, respectively.

3.5.4. Laboratory Soil Consolidation Tests

The undisturbed samples collected in the 3-in. (75-mm) Shelby tubes from the SPT boreholes were extruded, trimmed and inserted into a consolidation ring for laboratory soil consolidation tests, performed in accordance with ASTM D2435. The consolidation ring, weighted at about 0.14 lb (65 g), has an inner diameter (D) around 2.51-in. (63.7-mm) and a height (H_o) of 0.79-in. (20.1-mm). The consolidation loading device and the consolidometer are shown in Figure 3.14.

(a) Consolidation loading equipment

(b) Consolidometer

Figure 3.14. Laboratory soil consolidation tests

Test method A (described in ASTM D2435) was performed with a constant load increment duration of at least 24 hrs. Soil specimen deformations at applied loading and unloading increments were measured at specified time intervals as indicated in the ASTM D2435. Double-sided drainage was allowed during all consolidation tests. The loading increments were 0.87 psi, 1.74 psi, 3.63 psi, 7.25 psi, 14.50 psi, 29.01 psi, 58.02 psi, 116.03 psi, and 232.06 psi. The unloading increments started from 232.06 psi to 116.03 psi, 29.01 psi, 7.25 psi, and 1.74 psi. The natural initial moisture contents (ω) of the soil samples were determined in accordance with ASTM D2216 and computed using Eq. 3-10. Assuming the specific gravity (G) of the soil to be 2.7 and having measured the dry soil mass in the consolidation ring (M_s), the initial height of the solid component of each soil specimen (H_s) is estimated using Eq. 3-13, where the water density (ρ_w) is taken as 0.036 pci (1 g/cm^3). Using the estimated initial solid height (H_s), the initial void ratio (e_o) of each soil specimen is calculated using Eq. 3-14. These initial soil properties are listed in Table 3.5.

$$H_s = \frac{M_s}{G\rho_w \pi \left(\frac{D}{2}\right)^2} \tag{3-13}$$

$$e_o = \frac{H_o - H_s}{H_s} \tag{3-14}$$

Based on the soil deformation measurement at each load increment, the void ratio (e) at each applied pressure (σ) is calculated using Eq. 3-15 and is plotted with the corresponding applied pressure in a logarithmic scale. Using the e-Log (σ) curve generated in Figure 3.15 for sample Clarke-25, the pre-consolidation stress (σ_c) is estimated using the Casagrande's Method as described in ASTM D2435. The over-consolidation ratio (OCR) is determined from the test using Eq. 3-16, which gives a ratio of the pre-consolidation stress (σ_c) and the total vertical effective stress (σ'_v). Besides calculating the over-consolidation ratio, the coefficient of consolidation (C_v) at each applied loading pressure is calculated using Eq. 3-17 based on Taylor's Square Root Time $(\sqrt{t})$ Method. The dimensionless time factor (T_{90}) for 90% consolidation was determined to be 0.848. The length of the drainage path for double-sided drainage (H_{dr}) was taken as half of the average specimen height at the applied loading increment. The time corresponding to the 90% consolidation (t_{90}) is estimated using the Taylor's Square Root Time $(\sqrt{t})$ Method. The results of the consolidation tests are summarized in Table 3.5.

$$e = \frac{H_o - \Delta H - H_s}{H_s} \tag{3-15}$$

$$OCR = \frac{\sigma_c}{\sigma'_v} \tag{3-16}$$

$$C_v = \frac{T_{90} H_{dr}^2}{t_{90}}; \text{where } H_{dr} = \frac{H_o + (H_o - \Delta H)}{4} \tag{3-17}$$

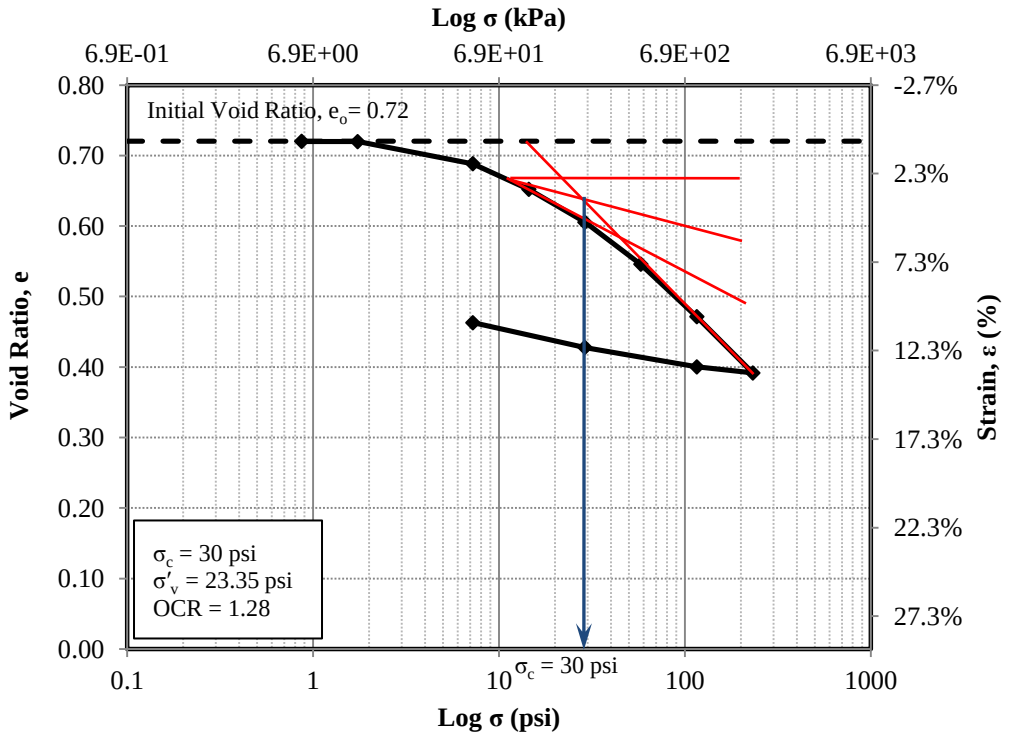

Figure 3.15. The e-log(σ) curve for evaluating pre-consolidation stress from Casagrande's Method for specimen Clarke-25

Table 3.5. Summary of the consolidation test results and analyses

Project ID	Sample - Depth in feet	Initial Moisture Content, ω (%)	Initial Solid Height, H_s (in)	Initial Void Ratio, e_o	Pre-consolidation Stress, σ_c (psi)	Effective Vertical Stress, σ'_v (psi)	Over Consolidation Ratio, OCR	Coefficient of Consolidation at σ'_v, C_v at (in^2/min)
ISU2	Mills-9	19.00	0.52	0.54	6.3	7.92	1.00[a]	0.023
	Mills-20	30.31	0.43	0.84	20	17.53	1.14	0.008
	Mills-30	25.69	0.43	0.86	30	28.56	1.05	0.020
	Mills-55	36.94	0.39	1.01	34	38.77	1.00[a]	0.018
ISU3	Polk-3	15.65	0.59	0.33	13	2.77	4.69	0.011
	Polk-27	27.18	0.49	0.62	28	18.37	1.52	0.012
	Polk-50	29.06	0.48	0.67	35	26.86	1.30	0.006
ISU4	Jas-15	13.10	0.59	0.33	26	10.5	2.48	0.019
	Jas-27	17.12	0.53	0.49	30	18.40	1.63	0.012
	Jas-45	15.09	0.57	0.40	23	27.07	1.00[a]	0.012
	Jas-60	15.41	0.56	0.42	36	34.95	1.03	0.007
ISU5	Clarke-8	21.82	0.48	0.64	33	7.42	4.45	0.017
	Clarke-25	25.91	0.46	0.72	30	23.35	1.28	0.014
	Clarke-35	15.13	0.56	0.40	17	31.29	1.00[a]	0.008
ISU6 and ISU7	Buc-12	32.26	0.42	0.86	16	13.31	1.20	0.005
	Buc-49	13.56	0.57	0.39	38	34.83	1.09	0.006
	Buc-59	15.07	0.56	0.40	34	37.06	1.00[a]	0.009
ISU8	Pow-3	23.19	0.49	0.62	10	2.26	4.43	0.020
	Pow-23	24.87	0.42	0.86	13.3	18.37	1.00[a]	0.030
	Pow-44	16.72	0.54	0.46	13	28.66	1.00[a]	0.011

[a] – round up to 1.00 for normally consolidated soils.

3.6. Pore Water and Lateral Earth Pressure Measurements

The in-situ pore water and total lateral earth pressures were measured using Geokon Model 4830 push-in pressure cells shown in Figure 3.16. As listed in Table 3.1, the push-in pressure cells were installed at ISU5, ISU6, ISU7, ISU8 and ISU10, and the locations are indicated with solid black crosses on the site layout plans in Appendix A. The push-in pressure cells were installed in a range of approximately 8-in. (200-mm) to 24-in. (600-mm) away from one of the flanges of a test pile. The elevations of the pressure cells are indicated on the soil profile as shown in Figure 3.2 for ISU5 and in Appendix B for ISU6, ISU7, ISU8, and ISU10. The pressure cell is fitted with an integral piezometer on one of the flat surfaces to measure pore water pressure. Before installing the pressure cell, the piezometer was saturated with water by drawing a vacuum on the circular porous sensor and allowing water to flow into the sensor when the vacuum was released, as shown in Figure 3.16. A thread is provided on the end of the cell to allow for installation using the SPT drill rods.

During the installation, the pressure cell was oriented, so that the circular porous sensor and the flat surface faced the proposed position of the flange of the test pile. The pressure cell was then slowly lowered into the ground through the SPT auger which had been drilled to the desired elevation. When the pressure cell reached the bottom of the drilled hole, it was pushed into the ground for about 14-in. (350-mm). The process of pushing the pressure cell created an increase in temperature, pore water and earth pressures surrounding the cell, therefore the cell was required to stabilize for at least 24 hours to reach both thermal and pressure equilibriums before taking any measurement as recommended by Suleiman et al. (2010) in Iowa soils. Readings were then taken at every 4 seconds during pile driving, re-strikes and static load test. However,

readings were taken only every 30 minutes between each re-strike event and between the last re-strike event and the static load test.

Temperature (T), pore water pressure and total lateral earth pressure are measured by the pressure cells. Initially, the pressure signals and temperature signal are transmitted from the pressure cell to a CR1000 data logger which stored data for the duration of testing, from the beginning of a pile driving to the end of a static load test. A data analysis program known as PC400 is used to collect the data from the data logger and to convert the data signals (R_i) into the actual pressures (P) using the polynomial pressure Eq. 3-18. Temperature (T) is part of the polynomial pressure equation for converting the pressure signals (R_i).

(a) Saturating pressure cells

(b) Installing pressure cells

(c) Stabilization and data acquisition system

(d) Measuring pore water pressure and lateral earth pressure

Figure 3.16. Measurement of pore water and lateral earth pressures using Geokon push-in pressure cells at the field

Each pressure cell is initially calibrated at Geokon's factory to determine the gage factors (A, B, and C), the thermal factor (κ) and the zero reading temperature (T_o). The calibrated factors and

T_o for each pressure cell used in the field are tabulated in Table 3.6. The pressure cells are differentiated and identified based on coil numbers, for example, cell No.1 consists of Coil 1 and Coil 1A, which are used to measure the total earth pressure signal and pore water pressure signal respectively.

$$P = AR_i^2 + BR_i + C + \kappa(T_i - T_o) \quad (3\text{-}18)$$

Table 3.6. Calibrated factors and zero reading temperature for each pressure cell

Pressure Cells ID	Test Piles	Linear Gage Factor, G (psi/digit)	Gage Factor, A	Gage Factor, B	Gage Factor, C	Thermal Factor, κ (psi/°C)	Zero Reading Temperature, T_o (°C)
Coil 1	ISU5, ISU7	0.00644	-2.70E-8	-6.01E-3	61.43	2.41E-4	24.7
Coil 1A	ISU5, ISU7	0.00662	-2.28E-8	-6.27E-3	62.08	9.63E-4	24.7
Coil 2	ISU5	0.00644	-3.05E-8	-6.17E-3	61.54	3.10E-3	24.5
Coil 2A	ISU5	0.00618	-2.45E-8	-5.99E-3	59.63	2.12E-4	24.5
Coil 3	ISU6	0.03833	-1.56E-7	-3.62E-2	329.65	1.39E-2	22
Coil 3A	ISU6	0.04152	-1.76E-7	-3.90E-2	357.88	2.38E-2	22
Coil 4	ISU6, ISU8	0.04081	-1.58E-7	-3.86E-2	353.75	6.46E-3	22
Coil 4A	ISU6, ISU8	0.04155	-1.99E-7	-3.88E-2	352.98	2.38E-2	22

After converting all signals, the actual in-situ total earth pressure and pore water pressure are plotted as a function of time, as shown in Figure 3.17 for pressure cell (PC) No.1 at approximately 23.17-ft (7.1-m) below ground with the groundwater table at 36-ft (11-m) and 8-in. (200-mm) away from the flange of the test pile ISU5. The time plotted is relative to the time at the end of driving. The events of pile driving, re-strikes and static load test are indicated on the plots to illustrate the effect of the events on the measured pressures. Although the PC1 was installed above the groundwater table, it was observed that the lateral earth pressure and the pore water pressure increased abruptly at the moment the driven pile toe reached the elevation of the PC1. The pore water pressure dissipated immediately when the pile toe was driven beyond the pressure cell. The pore pressure reached equilibrium and decreased gradually over time. In contrast, the lateral earth pressure increased gradually over time. The event of re-strikes increased the pore water pressure slightly which dissipated almost immediately and had no effect on the lateral earth pressure. The static load test had little or no effect on the measurements. Unlike PC1 at ISU5, the pore water pressures at ISU6 using PC3 and PC4 were recorded at 33-ft (10-m) below ground surface, with the groundwater table at 15-ft (4.6-m), as plotted in Figure 3.18 as function of time. Figure 3.18(a) shows the recorded data for the first 20-minute period. Accordingly, pore water pressure recorded using PC3 experienced a slight reduction in readings before the pile toe reached the depth of the device, but no significant change was recorded as the pile passed by the gauge location during driving. The recorded pore pressure progressively increased from 12 psi (84-kPa) to 14.6 psi (101-kPa) at PC3 and from 8 psi (55-kPa) to 9.3 psi (64-kPa) at PC4 between the time when the pile passed through the devices and BOR3. After BOR3, fluctuations in data during re-strike and static load test, as well as gradual dissipation of pressure with time, were generally seen (Figure 3.18(b)). For PC3, which was closer to the pile, the pore water pressure dissipation generally followed a logarithmic trend and reached a value of about 10 psi (68-kPa) within a day (i.e., around BOR5), almost returning to its hydrostatic state, which indicates complete dissipation in about seven days (i.e., around BOR7). Similarly, the

lateral earth pressure reduced over time. Overall, the restrikes and static load test had little effect on the measurements. The results of ISU7, ISU8, and ISU10 are included in Appendix B.

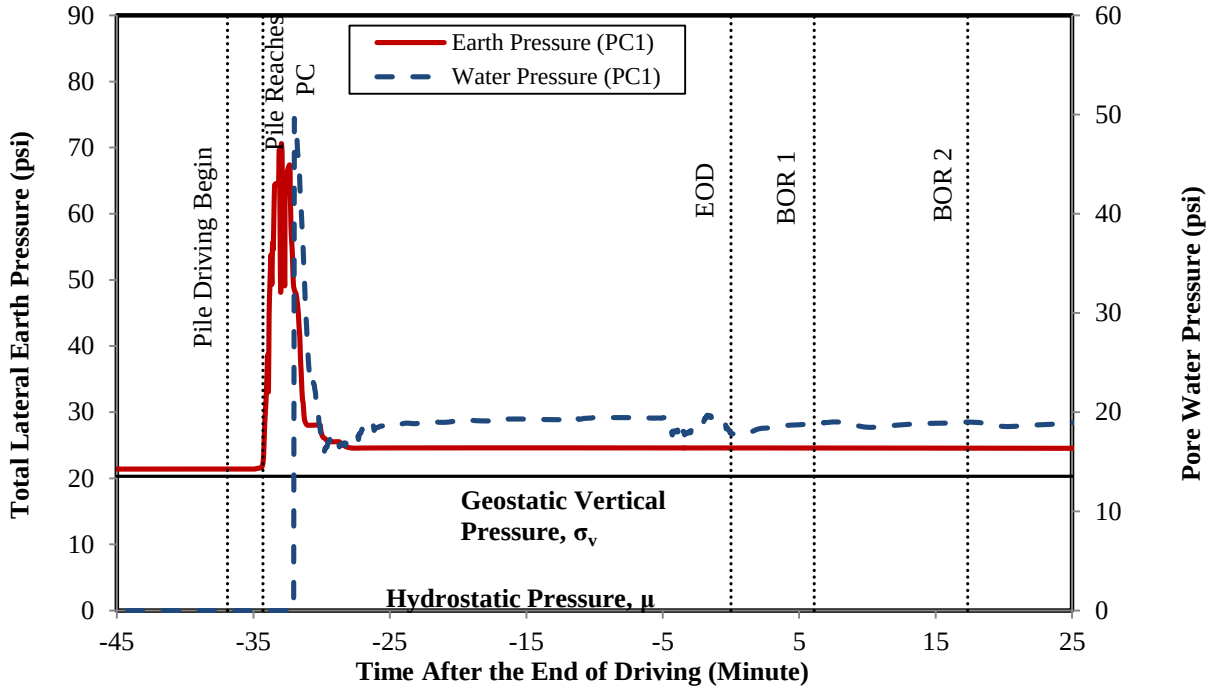

(a) Measured pressure versus time in minutes

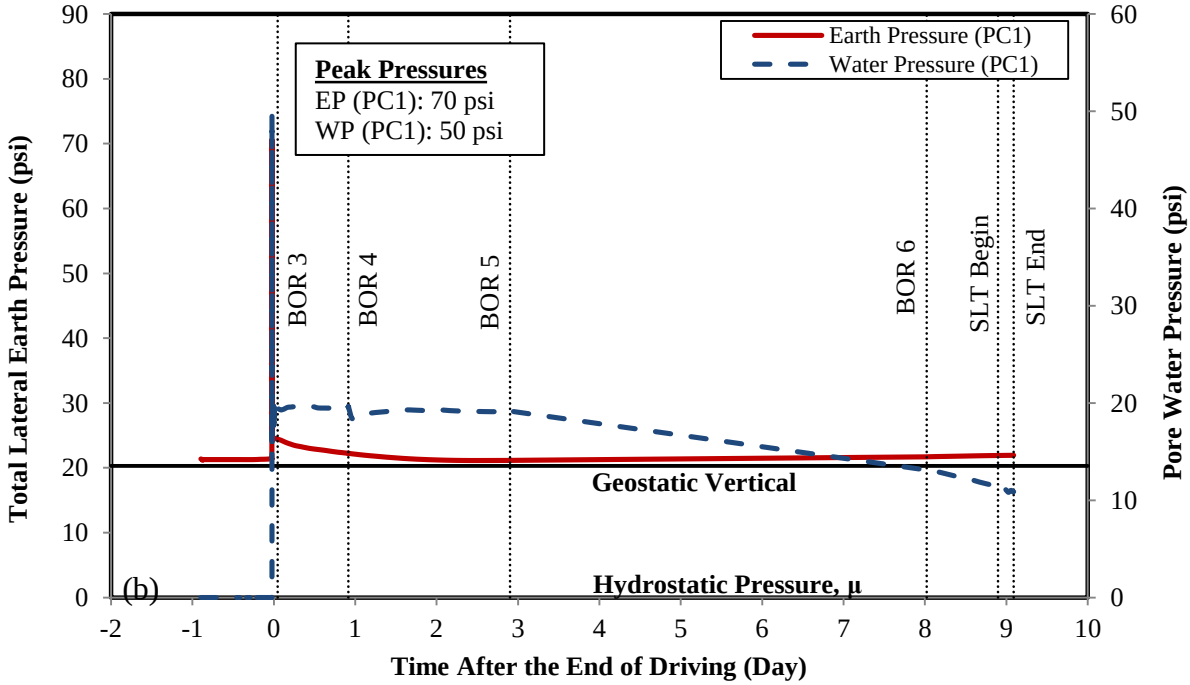

(b) Measured pressure versus time in days

Figure 3.17. Total lateral earth pressure and pore water pressure measurements from PC1 at test pile ISU5 with respect to the time

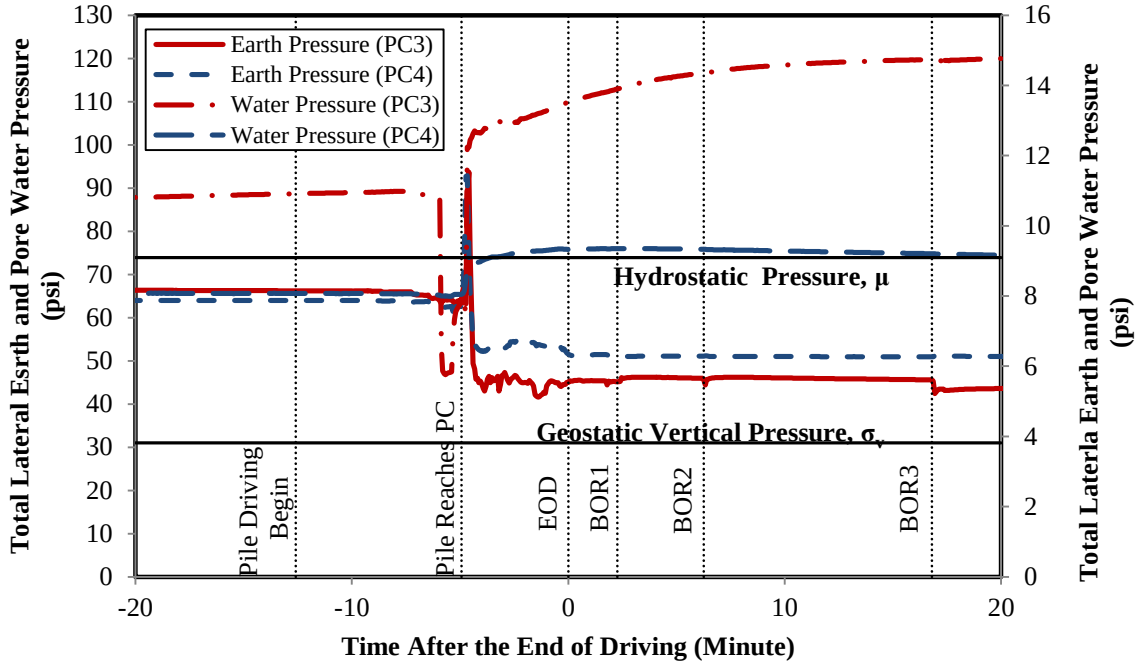

(a) Measured pressure versus time in minutes

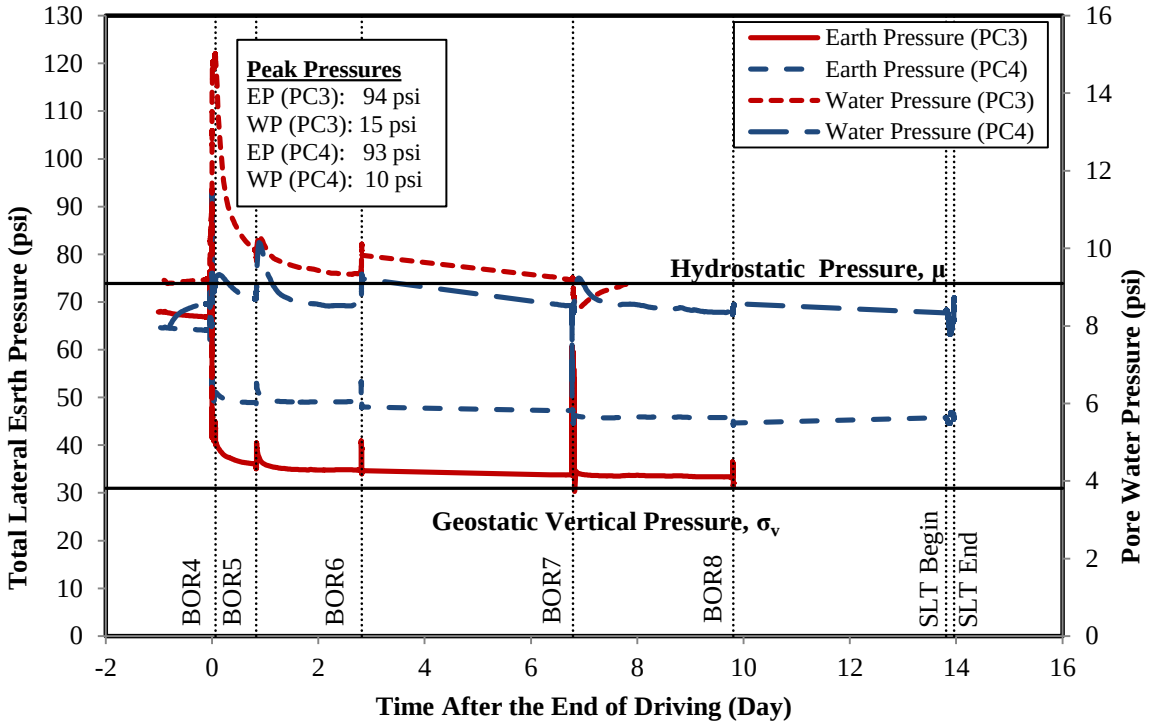

(b) Measured pressure versus time in days

Figure 3.18. Total lateral earth pressure and pore water pressure measurements from PC3 and PC4 at test pile ISU6 with respect to the time

CHAPTER 4: FULL-SCALE TESTS

4.1. Pile Type and Properties

A recent survey completed by AbdelSalam et al. (2008) indicates that the steel H-pile foundation is the most common bridge foundation used in the United States, especially in the Midwest. The Iowa Department of Transportation (Iowa DOT) conducted a total of 264 static pile load tests, between 1966 and 1989, to improve their pile foundation design practice. Of these tests, Roling et al. (2010) summarized that 164 (62 percent) of the tests were performed on steel H-piles, and 32 of these 164 contained sufficient pile, soil, hammer and driving information to be considered "usable data sets" for resistance factor calculations using the Wave Equation Analysis Program (WEAP) and dynamic formulas. Of the 32 usable steel H-piles, 29 were HP 10 x 42 steel piles (10-in. pile size and 42 lb/ft), 2 were HP 12 x 53 steel piles and one was HP 14 x 89 steel pile. Thus, HP 10 x 42 was used in the field tests except ISU1 at Mahaska County, where HP 10 x 57 steel pile was used. ASTM A572 Grade 50 steel with a yield strength (F_y) of 50 ksi (345 MPa) was selected and the relevant properties are listed in Table 4.1. The cross sectional view of the steel H-piles is shown in Figure 4.1. The pile impedance (Z) is determined using Eq. 4-1, where the elastic modulus (E) of 30,000 ksi (206,843 MPa) is used and the compressive wave speed (C) for steel piles is taken as 16,808 ft/s (5,123 m/s).

$$Z = \frac{EA}{C} \tag{4-1}$$

The American Association of State Highway and Transportation Officials (AASHTO) (2007) LRFD Bridge Design Specifications limit the pile stress to 0.6 F_y and 0.5 F_y under good driving and severe driving conditions respectively. Vande Voort (2008) noted that the stress limits reflect geotechnical concerns rather than structural limit states. In particular, the Iowa DOT LRFD Design Manual Section 6.2.6.1 specifies allowable pile stresses of 6 ksi (41 MPa), 9 ksi (62 MPa) and 12 ksi (83 MPa) for pile resistance levels 1, 2 and 3 respectively to limit and control pile settlement.

Table 4.1. A572 Grade 50 (F_y = 50 ksi) steel H-pile properties

Project ID	Pile Types	Cross Sectional Area, A (in^2)	Coating Area (ft^2/ft)	Depth, d (in)	Flange Width, b (in)	Flange Thicknes, t_f (in)	Web Thickness, t_w (in)	Pile Impedance, Z (kip-s/ft)
ISU1	HP 10 x 57	16.8	4.91	9.99	10.225	0.565	0.565	29.99
ISU2 to ISU10 and Iowa DOT Database	HP 10 x 42	12.4	4.83	9.70	10.075	0.420	0.415	22.13
Iowa DOT Database	HP 12 x 53	15.5	5.82	11.78	12.045	0.435	0.435	27.67
Iowa DOT Database	HP 14 x 89	26.1	7.02	13.83	14.695	0.615	0.615	46.59

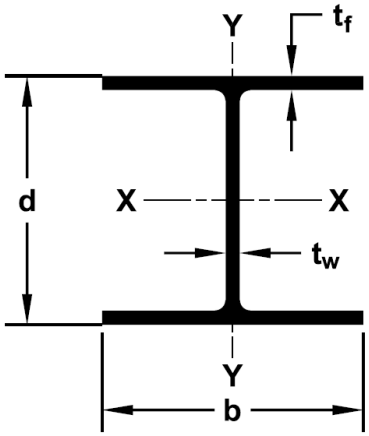

Figure 4.1. Cross sectional view of the steel H-piles

4.2. Hammer Types

Hammers are used for pile driving and re-strikes, with the hammer properties required for pile resistance estimations using dynamic analysis methods and dynamic formulas. Diesel hammers and external combustion hammers are the two main hammer types used in the State of Iowa. The hammer information of the Iowa DOT Pile Load Test Database (PILOT) was summarized by Roling et al. (2010). The hammer information of the field tests are summarized in Table 4.2. The hammers used in the field tests were Delmag manufactured open end diesel hammers, which operate on a two stroke engine cycle as shown in Figure 4.2. Delmag diesel hammers are single acting free fall hammers utilizing the principle of impact atomization (Delmag 2005). The driving mechanism of the hammers was described by Pile Dynamics, Inc. (2005). Some energy loss is incurred during the driving mechanism before the energy is transmitted to piles, thus an efficiency of 0.8 was determined by Pile Dynamics, Inc. (2005) for diesel hammers. Table 4.2 lists the weights of the hammer ram, cap and anvil, and the rated hammer energy, which were supplied by the piling contractors. The equivalent maximum hammer stroke is defined as the maximum height at which the hammer ram will rise or travel upwards resulting from the pile rebound and combustion pressure. The equivalent maximum hammer stroke is calculated by dividing the rated hammer energy with the ram weight.

Table 4.2. Summary of hammer information

Project ID	Hammer Types	Ram Weight (lb)	Cap Weight (lb)	Anvil Weight (lb)	Equivalent Max Hammer Stroke (ft)	Efficiency	Rated Hammer Energy (kip-ft)
ISU1	Delmag D19-42	4000	2000	753	10.81	0.8	43.24
ISU2	Delmag D19-42	4015	1920	753	10.77	0.8	43.23
ISU3	Delmag D19-32	4000	2000	753	10.61	0.8	42.44
ISU4	Delmag D19-42	4015	2000	750	10.81	0.8	43.24
ISU5	Delmag D16-32	3520	2050	810	11.42	0.8	40.20
ISU6 & ISU7	Delmag D19-42	4190	2000	750	10.21	0.8	42.80
ISU8	Delmag D19-42	4015	2000	750	10.81	0.8	43.24
ISU9	APE D19-42	4189	1345	749	11.25	0.8	47.34
ISU10	APE D19-42	4189	1345	749	11.25	0.8	47.34

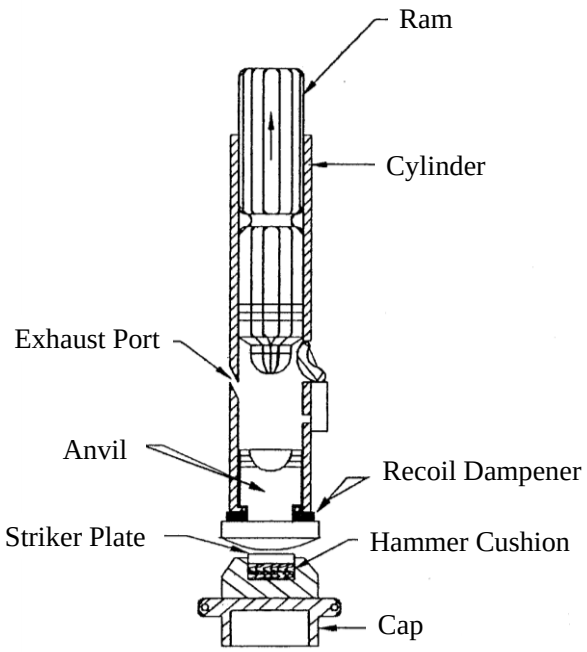

Figure 4.2. Single acting open end diesel hammer (adapted from Pile Dynamics, Inc., 2005)

4.3. Strain Gauge Instrumentation

Given the focus on vertical load testing, test piles were instrumented with strain gauges in pairs on each side of the webs at the neutral axis depth along the pile length as shown in Figure 4.3 and Figure 4.6. A combination of normal foil gauges and weldable gauges were used. The vertical distance between gauges varied along the pile length. The locations of the strain gauges were decided based on both the pile embedded length and the location of soil layer boundaries. Gauges were placed within 12-in (300-mm) above and below soil layer boundaries, and the distance between the pile toe and the nearest strain gauge was between 6-in (150-mm) to 12-in (300-mm).

The normal strain gauges were adhered onto the steel surfaces after being cleaned with acetone. M-coat was applied on the gauges for water resistance and flexible membranes were placed on top of the gauges for vibration protection. Subsequently, aluminum tapes were used to cover the gauges and the rubbers, and aluminum foil was wrapped around the cables, to prevent damage caused by welding sparks & heat. The strain gauges and cables were placed in a vertical line along the pile length, and the cables were tied to nuts welded to steel piles to prevent loosening during pile handling and driving. After completing the above steps, the gauges and cables were protected by 2-in x 2-in x 3/16 in thick (50-mm x 50-mm x 5-mm) angle bars welded on the steel pile webs (see Figure 4.3 and Figure 4.4) to prevent damage caused by welding sparks & heat, as well as direct soil contact during pile installation. The angle bars were welded with a continuous 6-in (150-mm) fillet weld at an interval of 24-in (600-mm). The angle bars at the pile toe were chamfered to form a pointed end as shown in Figure 4.5. Similar procedures were applied to the weldable gauges, except tack welding was used to adhere them to the steel piles. The strain gauge arrangements, along with soil profiles for other test piles, are included in Appendix C.

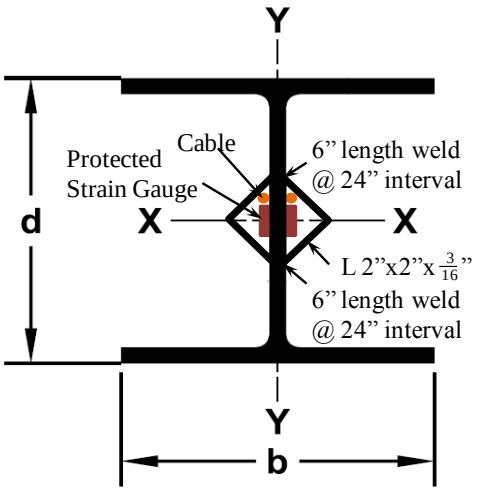

Figure 4.3. Strain gauges arrangement at a cross sectional view of a steel H-pile

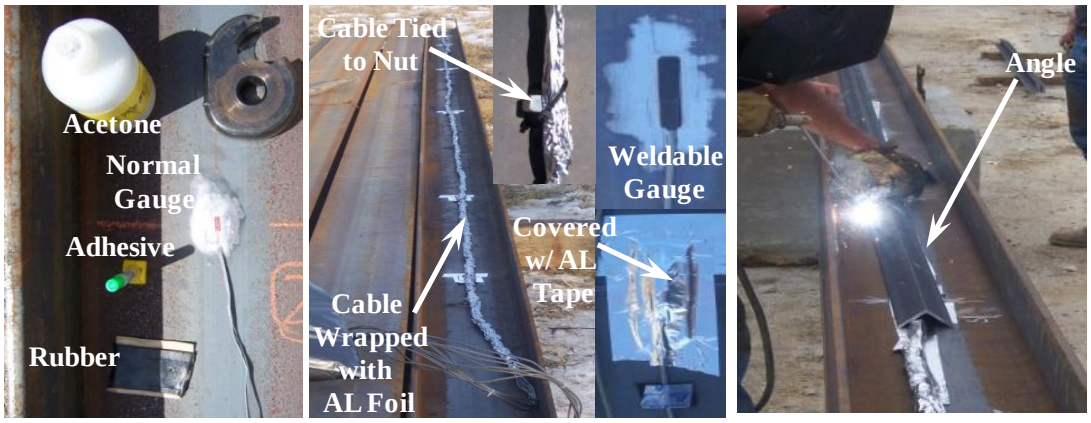

(a) Strain gauge installation (b) Strain gauge protection (c) Covered by angles

Figure 4.4. Strain gauges installation, protection, and covered by angles

Figure 4.5. Angle bars were chamfered to form a pointed end at pile toe

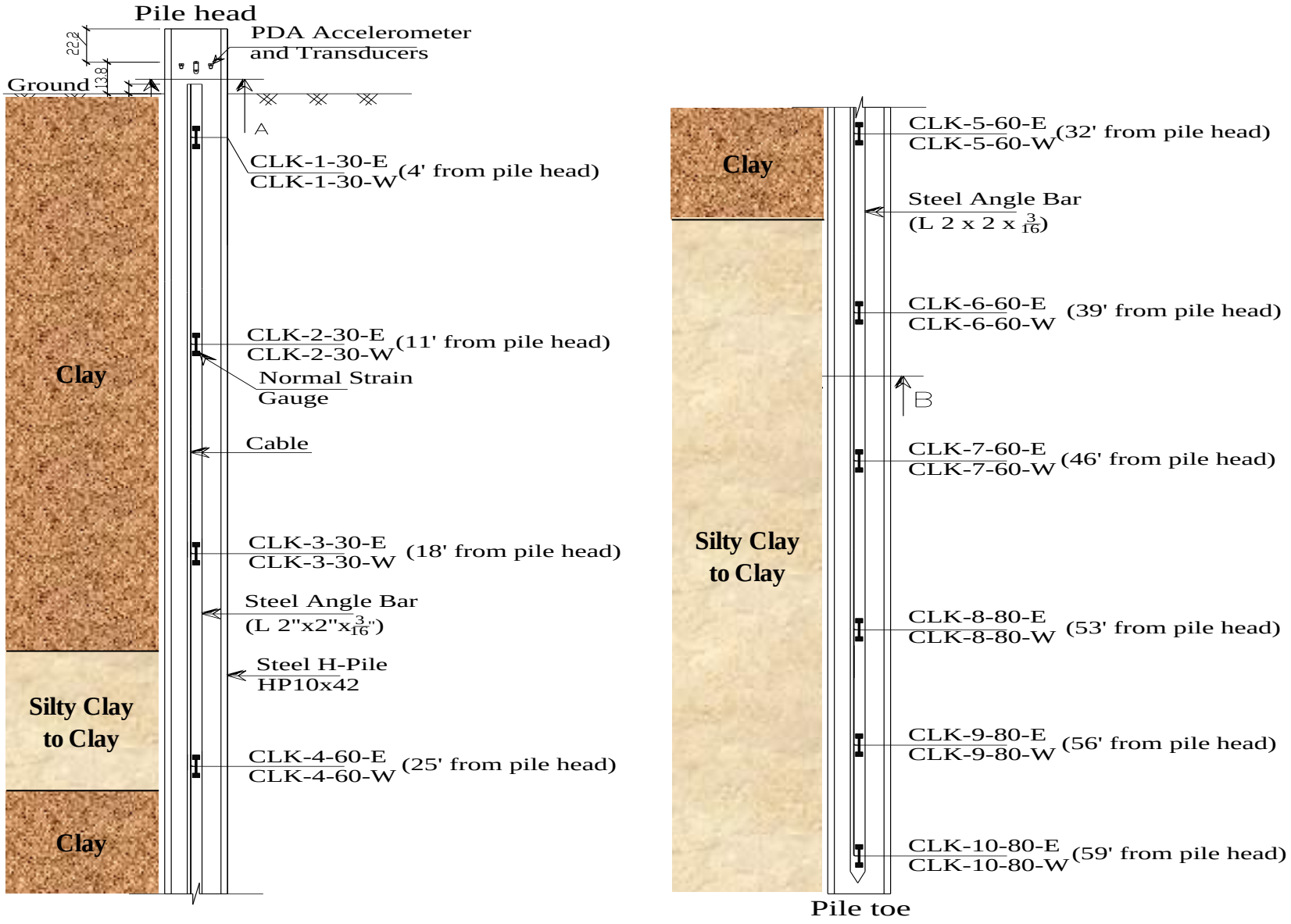

Figure 4.6. Location of strain gauges along the ISU5 test pile at Clarke County

4.4. Pile Driving Analyzer (PDA) Tests

Pile Driving Analyzer (PDA) tests were conducted in accordance with ASTM D4945 to investigate the development of soil resistances as a function of time, evaluate pile data quality, estimate pile resistance, assess soil resistance distribution, determine pile integrity, and evaluate driving system performance. Two strain transducers and two accelerometers were installed below the pile top at a distance of 3 times of the pile width, as shown in Figure 4.7. The strain transducers were bolted at the mid-depth of the web, and each of the accelerometers was bolted on the opposite side of the web at a distance of 3-in (75-mm) from the transducers. The PDA converts the strain and acceleration signals to force and velocity records as a function of time, as plotted in Figure 4.8 for ISU5. During pile driving, a record of force and velocity was continuously collected and displayed by the PDA at every hammer impact on the test pile until the end of driving (EOD). After the end of driving, all the test piles except ISU1 were re-struck or re-tapped using the same hammers (see Table 4.2) at a schedule listed in Table 4.3. During the re-strikes, the force and velocity records were collected using the PDA. The main purpose of performing the re-strikes is to investigate the change in pile resistance as a function of time. The gain in pile resistance over time is referred to as pile setup and it has been observed by many researchers, including Salgado (2008) who believed that the phenomenon is mostly due to the dissipation of pore pressure and the healing of remolded soil near the pile over time. The PDA records during the entire re-strikes for ISU5 are shown in Figure 4.9, and the PDA records for other test piles are included in Appendix C.

Table 4.3. Schedule of re-strikes and PDA tests

Project ID	Number of Days after EOD							
	1st Re-strike	2nd Re-strike	3rd Re-strike	4th Re-strike	5th Re-strike	6th Re-strike	7th Re-strike	8th Re-strike
ISU2	0.17	0.92	2.97	-	-	-	-	-
ISU3	0.0028	0.0073	0.017	1.11	1.95	-	-	-
ISU4	0.0041	0.016	0.04097	0.74	1.74	4.75	-	-
ISU5	5.38E-3	0.013	0.048	0.92	2.90	7.92	-	-
ISU6	1.60E-3	0.0044	0.012	0.07	0.83	2.82	6.79	9.81
ISU7	1.86E-3	0.006	0.015	0.80	2.77	6.76	9.76	-
ISU8	7.07E-3	0.011	0.039	0.97	3.97	4.95	-	-
ISU9	3.87E-3	0.011	0.038	0.69	2.87	9.77	-	-
ISU10	3.78E-3	0.011	0.039	0.64	4.64	-	-	-

The PDA uses the Case Method, developed by Professor Goble and his students at Case Western Reserve University, which is based on the principle of wave mechanics to determine the static pile resistance. Using the force and velocity records, the PDA estimates the total soil resistance (RTL) using Eq. 4-2. Goble et al. (1975) assumed that the total soil resistance was a combination of static and dynamic resistances, where the dynamic soil resistance was a linear function of a viscous damping coefficient and the pile toe velocity. Goble et al. (1975) defined the viscous damping coefficient as a product of a Case damping factor (J_c) and a pile impedance (Z). The recommended J_c values, specified by Hannigan et al. (1998), are shown in Table 4.4. The original J_c values were determined by Goble et al. (1975), with the updated J_c values determined by Dynamic, Inc. (1996) using an additional database. The single best J_c value was selected from the correlation study for each soil type and tabulated under the "Best Correlation Value" in Table 4.4.

Subtracting the dynamic soil resistance from the total soil resistance, the static soil resistance (RSP) can be derived from Eq. 4-3. After calculating all RSP values for the data set, where a different RSP is found at each given time relative to the force and velocity values for that time, the maximum calculated RSP value is then assigned as the maximum static resistance (RMX) for the tested soil. For example the force (F1) and velocity (V1) at time of initial impact for ISU5 at the EOD are 396 kips (1,762 kN) and 14.5 ft/s (4.42 m/s) respectively, and the F2 and V2 are 108 kips (480 kN) and 0 ft/s respectively. For the HP 10 x 42 steel pile (where E=30,000 ksi (206,843 MPa), A=12.4 in^2 (80 cm^2) and C=16,808 ft/s (5,123 m/s)), the RTL is computed at 413 kips (1,837 kN). Knowing the RTL and assuming J_c of 0.70 for silty clay soil at the pile toe, the RSP is computed at 200 kips (890 kN). After searching for the maximum RSP for the entire record, the RMX is found to be 200 kips (890 kN). The pile static resistance is assumed equal to the estimated RMX value.

$$\mathrm{RTL} = \frac{1}{2}[\mathrm{F1} + \mathrm{F2}] + \frac{1}{2}[\mathrm{V1} - \mathrm{V2}]\frac{\mathrm{EA}}{\mathrm{C}} \tag{4-2}$$

$$\mathrm{RSP} = \mathrm{RTL} - \mathrm{J_c}\left[\frac{\mathrm{EA}}{\mathrm{C}}\mathrm{V1} + \mathrm{F1} - \mathrm{RTL}\right] \tag{4-3}$$

where

RTL = Total soil resistance at time t_1 of initial hammer impact, kip;
RSP = Static soil resistance at time t_1 of initial hammer impact, kip;
F1 = Force measured at transducer location at time t_1, kip;
F2 = Force measured at transducer location at time $t_2 = t_1 + 2L/C$, kip;
V1 = Velocity measured at accelerometer location at time t_1, ft/s;
V2 = Velocity measured at accelerometer location at time $t_2 = t_1 + 2L/C$, ft/s;
E = Modulus of elasticity of the steel H-piles, ksi;
A = Cross sectional area of the steel H-piles, in^2;
C = Compressive wave speed of the steel H-piles, ft/s;
L = The pile length below the transducers or LE used in the PDA, ft; and
J_c = Dimensionless Case damping factor.

Table 4.4. Summary of Case damping factors

Soil Type at Pile Toe	Original Case Damping Factor	Best Correlation Value	Updated Case Damping Factor
Clean Sand	0.05 to 0.20	0.05	0.10 to 0.15
Silty Sand, Sandy Silt	0.15 to 0.30	0.15	0.15 to 0.25
Silt	0.20 to 0.45	0.3	0.25 to 0.40
Silty Clay, Clayey Silt	0.40 to 0.70	0.55	0.40 to 0.70
Clay	0.60 to 1.10	1.10	0.70 or higher

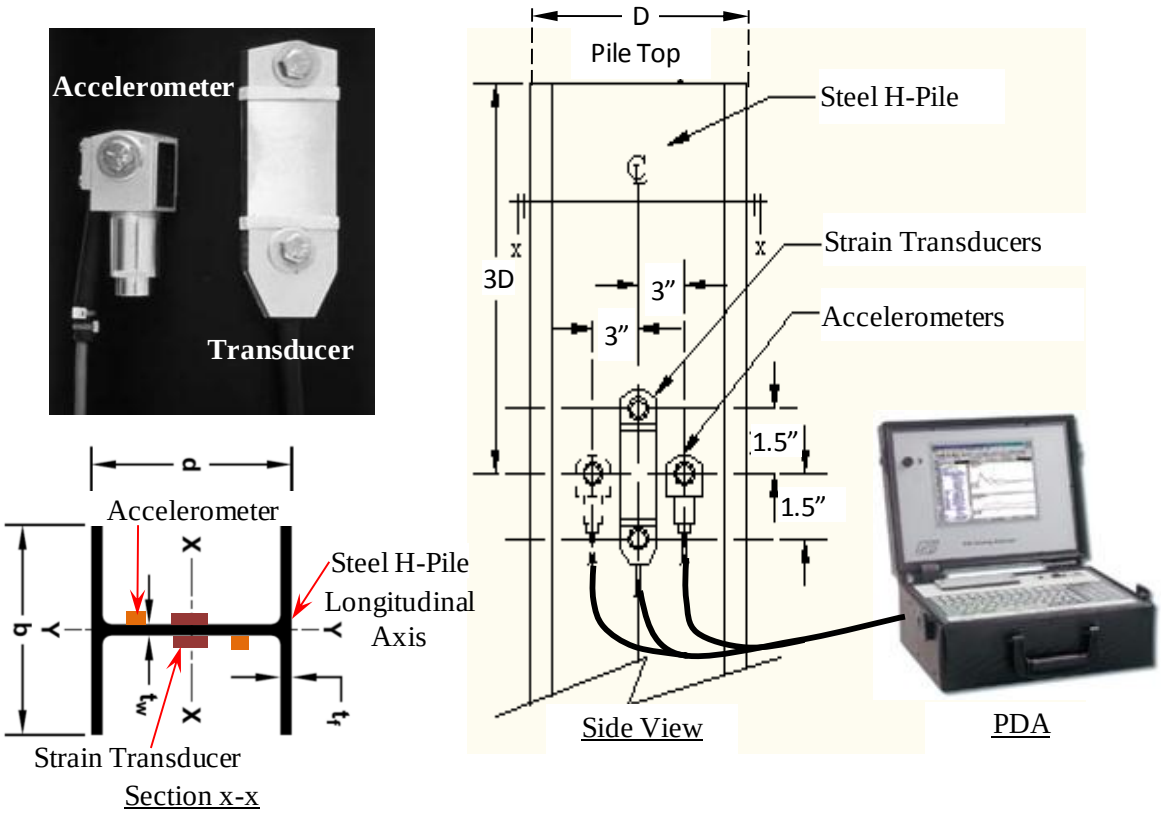

Figure 4.7. Typical Pile Driving Analyzer (PDA) set up (from Pile Dynamics, Inc., 1996)

Furthermore, the PDA was also used to assess soil resistance distribution along an embedded pile length. The PDA estimates the shaft resistance (SFR) using Eq. 4-4, and the end bearing is determined by subtracting the SFR from the estimated pile static resistance (assumed as RMX). Using the velocity record and the computed wave-up (W_u) of the test pile, as illustrated by ISU5 at EOD as shown in Figure 4.10, the total shaft resistance (SFT) is estimated by extrapolating the wave-up curve (solid line) and intersecting with the vertical line at the point where the measured velocity (dash line) reaches zero (Case Western Reserve University et al. 2008), and the SFT is determined at 375 kips (1,668 kN). Wave-up is defined as the upward moving wave force as given by Eq. 4-5. The RMX at J_c of 0.7 was determined early at 200 kips (890 kN), and similarly, the RX0 which is equal to RMX at J_c of zero is estimated at 413 kips (1,837 kN). Thus, the shaft resistance is computed at 182 kips (810 kN) using Eq. 4-4, which is 91% of the pile resistance. As such, only 18 kips (80 kN), or 9%, is contributed from the end bearing. Table 4.5 summarizes the Case damping factor (J_c) used, PDA estimated pile static resistance (RMX) and shaft resistances (SFR) at both EOD and re-strikes.

$$SFR = SFT\left(\frac{RMX}{RX0}\right) \tag{4-4}$$

$$W_u = \frac{1}{2}\left(F - \frac{EA}{C}V\right) \tag{4-5}$$

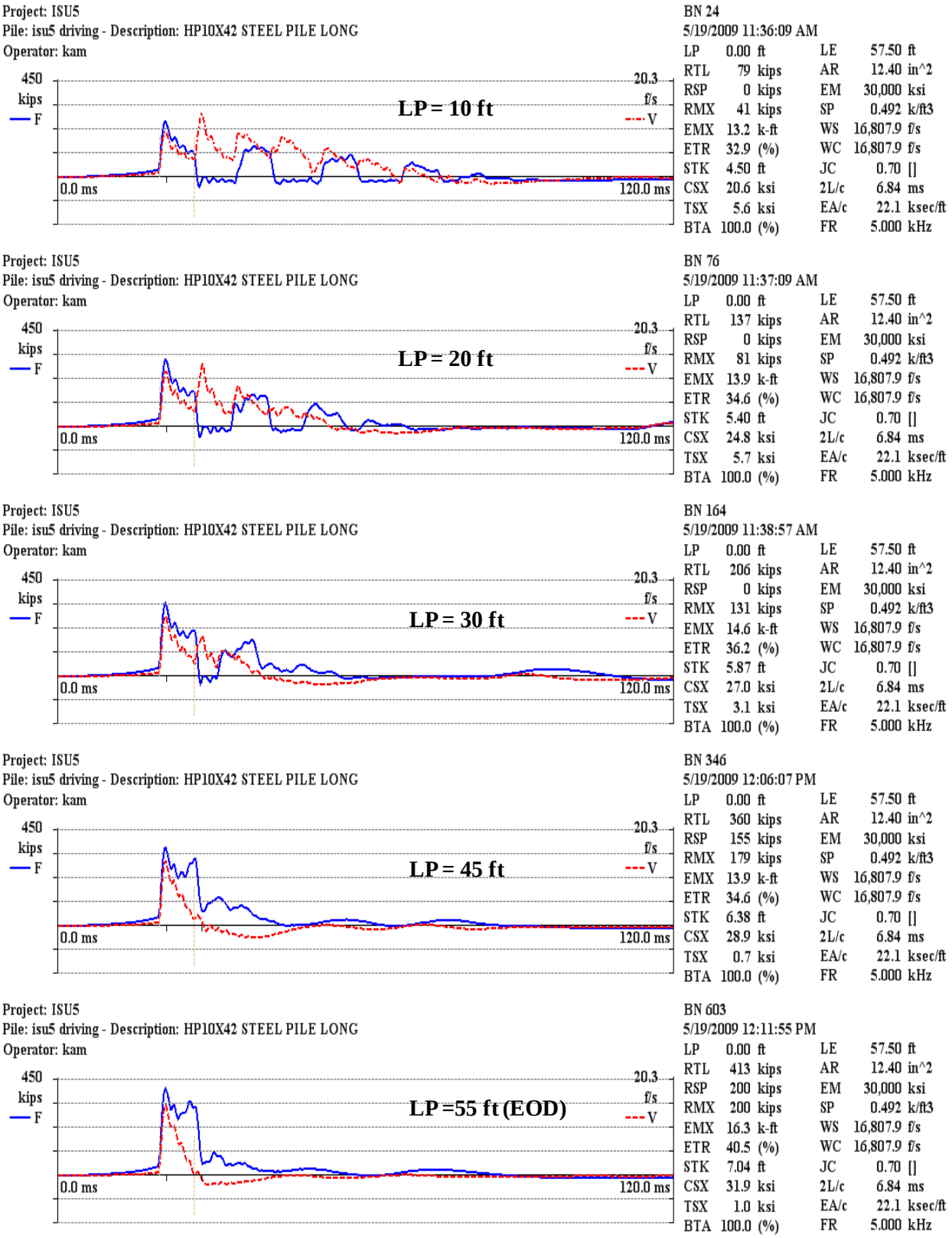

Figure 4.8. PDA force and velocity records during driving and at EOD for ISU5

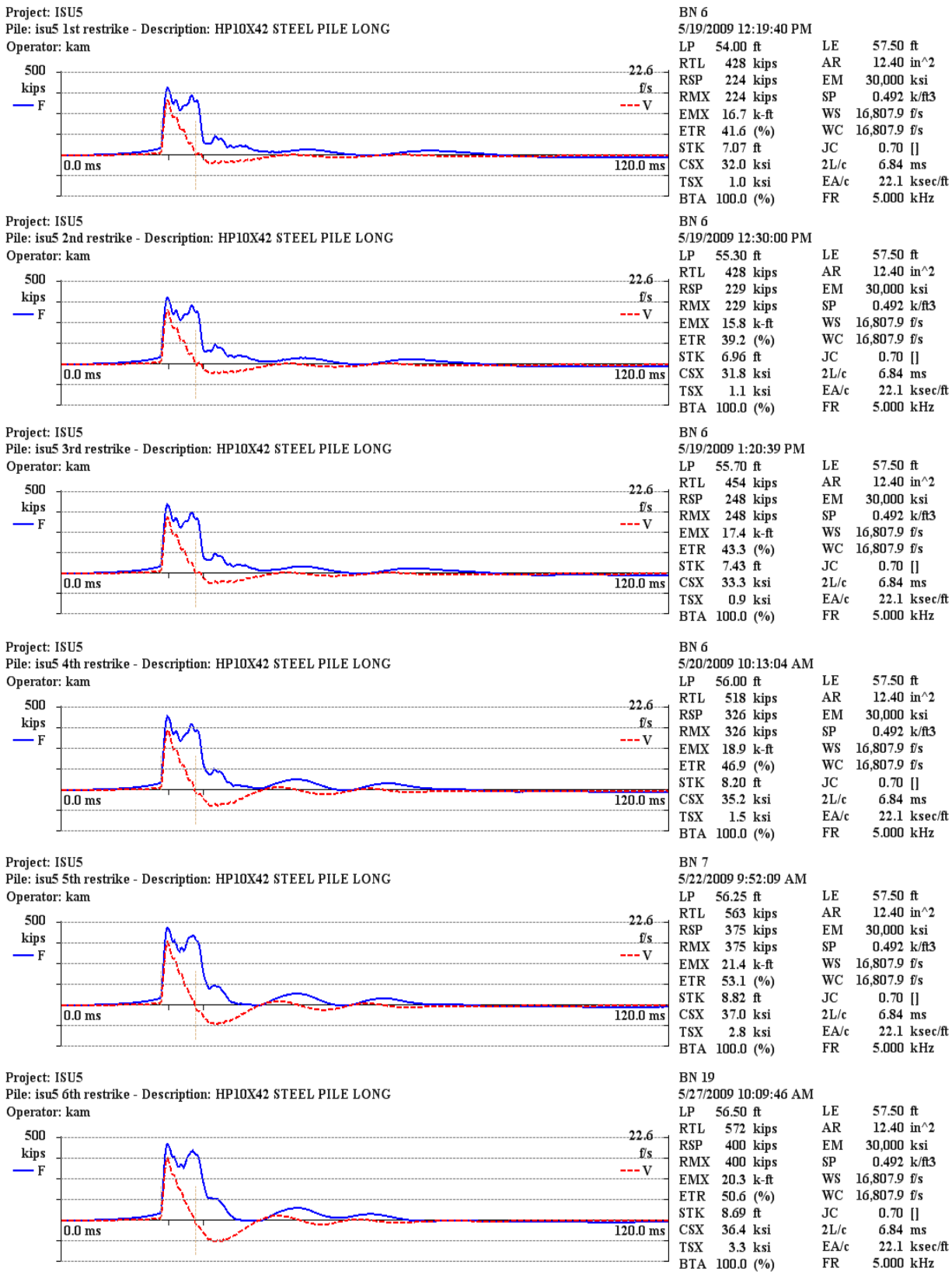

Figure 4.9. PDA force and velocity records during re-strikes for ISU5

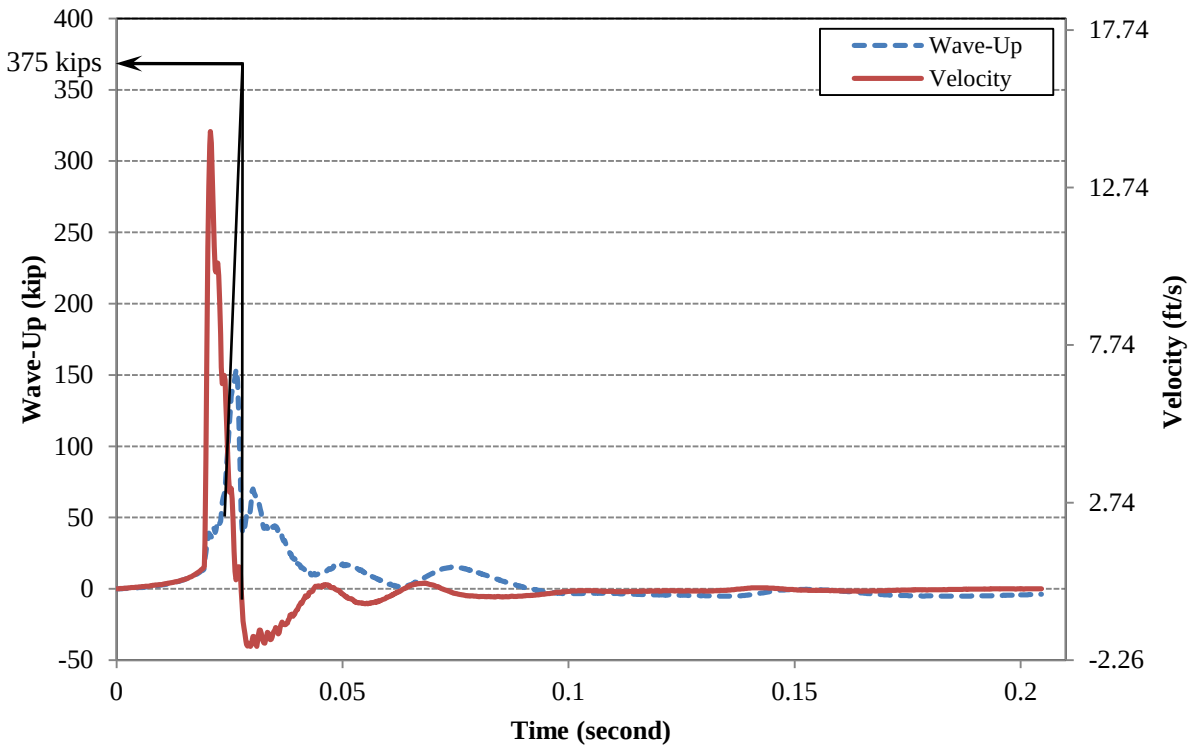

Figure 4.10. Wave-up and velocity measurement for ISU5 at EOD used to determine shaft resistance

Table 4.5. Summary of J_c, PDA estimated pile static (RMX) and shaft resistances (SFR)

Project ID	J_c	Pile Static Resistance (Pile Shaft Resistance), kips								
		EOD	1st Re-strike	2nd Re-strike	3rd Re-strike	4th Re-strike	5th Re-strike	6th Re-strike	7th Re-strike	8th Re-strike
ISU1	0.7	141 (118)	-	-	-	-	-	-	-	-
ISU2	0.7	107 (87)	148 (132)	162 (145)	146 (137)	-	-	-	-	-
ISU3	1.1	120 (119)	117 (117)	123 (122)	128 (128)	157 (144)	163 (150)	-	-	-
ISU4	0.7	143 (107)	144 (110)	143 (109)	154 (142)	161 (152)	162 (148)	223 (185)	-	-
ISU5	0.7	200 (182)	224 (200)	229 (203)	248 (217)	326 (279)	375 (329)	400 (350)	-	-
ISU6	0.7	146 (144)	151 (149)	149 (149)	145 (142)	167 (159)	195 (181)	231 (211)	266 (255)	310 (261)
ISU7	1.1	0	0	11(3)	0	31(19)	66(48)	95(76)	93(73)	-
ISU8	0.7	164 (142)	161 (148)	169 (156)	161 (148)	180 (170)	177 (177)	208 (200)	-	-
ISU9	0.2	226 (226)	217 (216)	215 (199)	220 (186)	227 (198)	229 (189)	233 (189)	-	-
ISU10	0.2	158 (117)	160 (124)	163 (134)	166 (138)	170 (143)	175 (123)	-	-	-

The PDA can also be used to evaluate driving system performance. The maximum energy (EMX) transferred from a hammer to a steel H-pile is calculated using Eq. 4-6, based on the force and velocity records. The performance of the hammers, as indicated in Table 4.2, is evaluated in terms of the energy transferred ratio (ETR) given by Eq. 4-7, which is defined as the ratio of maximum energy (EMX) and the manufacturer's rated hammer energy. For example the EMX for ISU5 at EOD is determined at 16.3 k-ft (22 kN-m). When dividing the EMX by the manufacturer's rated hammer energy of 40.20 k-ft (55 kN-m) as given in Table 4.2 for ISU5, the ETR of 40.5% is determined. Hannigan et al. (1998) suggests the hammer performance is considered satisfactory when the estimated ETR is higher than the mean value of 34.3% for a diesel hammer on steel. Likins et al. (2004) estimated the hammer stroke (STK) of an open end diesel hammer by using an equivalent hammer blow rate (BPM), as given by Eq. 4-8. The hammer stroke for ISU5 at EOD with the PDA measured BPM of 44.4 is estimated to be 7.04-ft (2.15-m).

$$\mathrm{EMX} = \mathrm{Max}\left[\sum \mathrm{F(t)\,V(t)\Delta t}\right] \tag{4-6}$$

$$\mathrm{ETR} = \frac{\mathrm{EMX}}{\mathrm{Rated\ Energy}} \tag{4-7}$$

$$\mathrm{STK} = 4.02\left(\frac{60}{\mathrm{BPM}}\right)^2 - 0.3 \tag{4-8}$$

To monitor the pile integrity during driving, the PDA calculates the maximum compressive (CSX) and tensile (TSX) stresses for each hammer impact and compares this with the allowable stresses specified by the PDA users. The AASHTO (2007) LRFD Bridge Design Specifications have limited the allowable stress of a steel H-pile to $0.9F_y$ for both compression and tension. For example, the allowable stress for a Grade 50 HP 10 x 42 steel pile with a cross sectional area (A) of 12.4-in^2 (80-cm^2) is 45 ksi (310 MPa). The maximum measured compressive force (positive) for ISU5 at EOD is 396 kips (1,762 kN), and the maximum compressive stress (CSX) is calculated at 31.9 ksi (220 MPa). Similarly, the maximum measured tensile force (negative) is 12 ksi (83 MPa), which yields the maximum tensile stress (TSX) of 1 ksi (7 MPa). Since neither of the measured stresses exceeds the AASHTO allowable stress limit, the pile integrity during driving is ensured.

However, pile quality cannot be evaluated solely based on measured pile stresses. Pile can be damaged even if the measured stresses do not exceed the allowable stress limit. Rausche and Goble (1979) derived the integrity factor (BTA) in order to describe the degree of convergence between the force and velocity records within a period 2L/C, where L is the pile length and C is the wave speed, which give an indication of a reduction in the pile impedance (Z). The BTA value is determined using Eq. 4-9, and the severity of pile damage is decided using the classification defined by Rausche and Goble (1979), given in Table 4.6, under the presumption that BTA indicates how much the pile cross section integrity is retained. For an undamaged pile, such as ISU5 at EOD, no convergence (i.e., crossing between force and velocity records) occurs before 2L/C, therefore the α term is zero and BTM equal to 1 (or 100%).

$$BTA = \frac{1-\alpha}{1+\alpha};\ \alpha = \frac{ZV_d - F_d}{2\left(F1 - (F^* - ZV^*)\right)} \quad (4\text{-}9)$$

where

BTA = Degree of convergence between force and velocity records before 2L/C;
α = Defining term, dimensionless;
Z = Pile impedance (see Eq. 4-1), k-s/ft;
V_d = Velocity at location of pile damage after convergence occurred, ft/s;
F_d = Force at location of pile damage after convergence occurred, kip;
F1 = Force at initial hammer impact, kip;
F^* = Force at the time before the increase in the velocity become noticeable and before convergence, kip; and
V^* = Velocity at the time when it started to increase toward convergence, ft/s.

Table 4.6. Pile damage classification

BTA (Percentage)	Severity of Damage
1.0 (100%)	Undamaged
0.8 – 1.0 (80% - 100%)	Slight damage
0.6 – 0.8 (60% - 80%)	Damage
Below 0.6 (below 60%)	Broken

The PDA force and velocity signals are used as an input for the CAse Pile Wave Analysis Program (CAPWAP) to improve the estimations of static shaft resistance, end bearing, the load settlement curve, and to determine the dynamic soil parameters (i.e., quakes and damping factors). For additional detailed descriptions of the PDA, refer to Ng (2011).

4.5. CAse Pile Wave Analysis Program (CAPWAP)

CAse Pile Wave Analysis Program (CAPWAP) method was developed by Professor Goble and his students in the 1970s. It is a computer program which uses the PDA records as input data for a more accurate analysis and estimation of the pile resistance, soil resistance distribution and dynamic soil properties. CAPWAP is used to refine the PDA results at the end of driving and at re-strikes by performing a signal matching process with the combination of several analytical techniques, as described by Pile Dynamics, Inc. (2000). CAPWAP adopts the soil-pile model developed by Smith (1962) and uses the wave equation algorithm in the analysis. Figure 4.11 shows the CAPWAP model for the 60-ft (18.3-m) long HP 10 x 42 steel pile for ISU5 at Clarke County. CAPWAP considers the pile length below the location of the PDA transducers and accelerometers, which is 57.5-ft (17.5-m) for the ISU5 example mentioned. The pile model is divided into user specified segments of pile masses (m) with approximately equal length, and each pile mass is connected with a series of elastic springs and linear viscous dampers. The ISU5 example comprised 22 pile segments of around 2.6-ft (0.8-m) in length. The CAPWAP soil model at an alternate pile segment is represented by an elastic-plastic spring and a linear damper, as shown in Figure 4.11. The elastic-plastic spring is characterized by two parameters, static soil resistance at the soil segment (R_s) and soil quake (q), and the linear damper is characterized by

the damping coefficient (C_s). CAPWAP approximately relates the damping coefficient to the Smith damping factor (J_s) and the Case damping factor (J_c), using Eqs. 4-10 and 4-11 respectively. It is important to note that any variation in static soil resistance (R_s) will affect the J_s value, but not the J_c value. For a detailed description of CAPWAP, refer to Pile Dynamics, Inc. (2000).

$$J_s \cong \frac{C_s}{R_s} \tag{4-10}$$

$$J_c \cong \frac{\sum C_s}{Z} \tag{4-11}$$

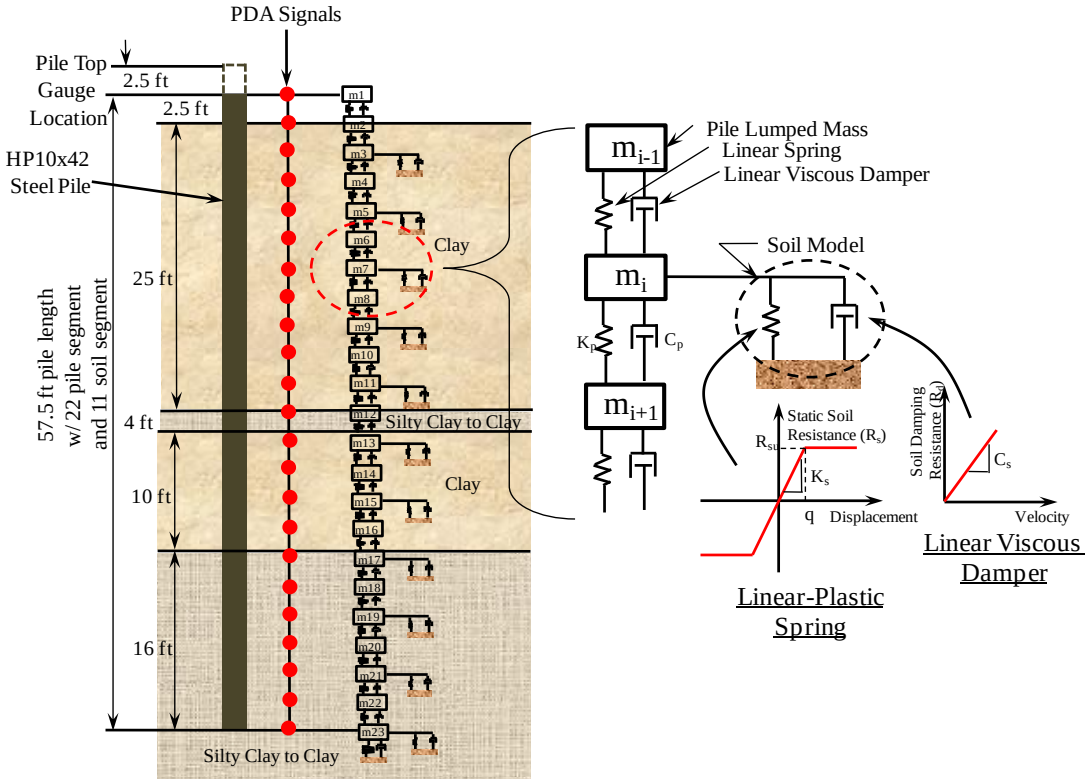

Figure 4.11. Typical CAPWAP model for ISU5 at EOD

The soil resistance at each soil segment, soil quake and either the Smith's damping factor or the Case damping factor are adjusted until the best signal matching is achieved, as shown in Figure 4.12 for ISU5 at EOD. The summation of all adjusted soil resistances along the pile shaft gives the soil shaft resistance, and total pile resistance is determined by adding the shaft resistance with the soil resistance at the pile toe. Table 4.7 summarizes the CAPWAP estimated pile capacities and shaft resistances at EOD and re-strikes for all test piles. A constant soil quake is used for all soil segments along the shaft and a different quake value is used for the soil model at the pile toe. The adjusted soil quake values for shaft and toe at EOD and re-strikes for all test sites are summarized in Table 4.8, and Smith's damping factors are summarized in Table 4.9.

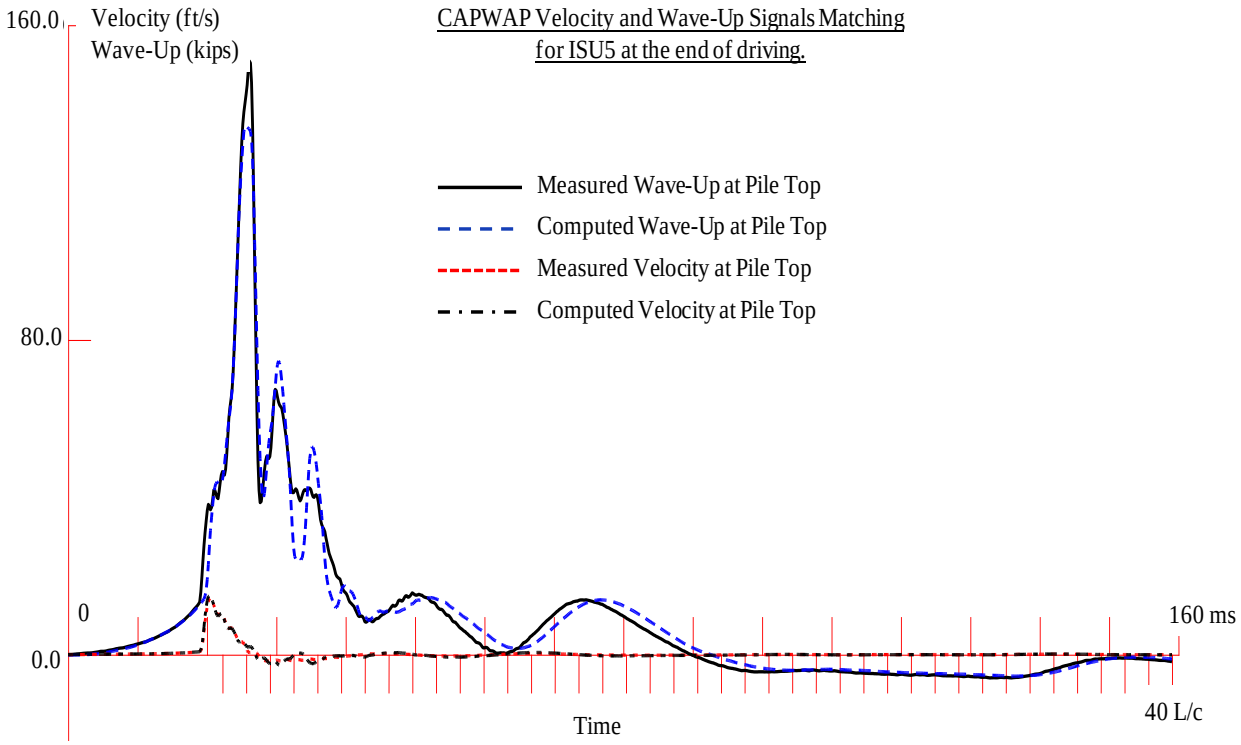

Figure 4.12. Results of CAPWAP signals matching for ISU5 at EOD

Table 4.7. Summary of CAPWAP estimated total pile resistances and shaft resistances

Project ID	Total Pile Resistance (Shaft Resistance), kips								
	EOD	1st Re-strike	2nd Re-strike	3rd Re-strike	4th Re-strike	5th Re-strike	6th Re-strike	7th Re-strike	8th Re-strike
ISU1	142 (96)	-	-	-	-	-	-	-	-
ISU2	81 (67)	116 (101)	130 (114)	130 (114)	-	-	-	-	-
ISU3	99 (85)	103 (88)	105 (89)	130 (113)	143 (127)	148 (130)	-	-	-
ISU4	102 (88)	105 (90)	109 (93)	121 (107)	135 (117)	144 (127)	154 (138)	-	-
ISU5	178 (124)	189 (135)	215 (160)	220 (165)	233 (175)	235 (177)	245 (186)	-	-
ISU6	145 (123)	140 (117)	149 (125)	148 (124)	177 (161)	187 (162)	197 (171)	211 (185)	211 (186)
ISU7	12(0)	13(1)	19(10)	32(18)	43(27)	67(47)	69(60)	75(67)	-
ISU8	140 (123)	143 (134)	146 (137)	153 (139)	155 (135)	159 (120)	160 (117)	-	-
ISU9	169 (138)	168 (127)	166 (139)	161 (131)	159 (127)	157 (124)	155 (115)	-	-
ISU10	121 (103)	105 (86)	106 (89)	114 (96)	121 (103)	118 (100)	-	-	-

Table 4.8. Summary of CAPWAP estimated soil quake values

Project ID	Shaft Quake (Toe Quake), in								
	EOD	1st Re-strike	2nd Re-strike	3rd Re-strike	4th Re-strike	5th Re-strike	6th Re-strike	7th Re-strike	8th Re-strike
ISU1	0.07 (0.93)	-	-	-	-	-	-	-	-
ISU2	0.05 (0.45)	0.11 (0.28)	0.11 (0.49)	0.25 (0.41)	-	-	-	-	-
ISU3	0.24 (0.04)	0.25 (0.04)	0.20 (0.04)	0.06 (0.18)	0.12 (0.29)	0.14 (0.20)	-	-	-
ISU4	0.07 (0.16)	0.10 (0.36)	0.08 (0.25)	0.07 (0.23)	0.07 (0.40)	0.12 (0.39)	0.04 (0.50)	-	-
ISU5	0.07 (0.38)	0.05 (0.09)	0.06 (0.10)	0.05 (0.10)	0.07 (0.16)	0.04 (0.16)	0.05 (0.08)	-	-
ISU6	0.10 (0.31)	0.09 (0.24)	0.10 (0.41)	0.08 (0.22)	0.05 (0.10)	0.28 (0.15)	0.22 (0.22)	0.31 (0.30)	0.26 (0.25)
ISU7	0.37 (0.28)	0.15 (0.17)	0.15 (0.16)	0.14 (0.04)	0.05 (0.06)	0.04 (0.28)	0.09 (0.16)	0.06 (0.10)	-
ISU8	0.11 (0.25)	0.10 (0.27)	0.10 (0.26)	0.15 (0.35)	0.14 (0.28)	0.13 (0.51)	0.12 (0.24)	-	-
ISU9	0.05 (1.00)	0.05 (0.84)	0.06 (0.86)	0.09 (0.76)	0.07 (0.92)	0.14 (0.82)	0.05 (0.89)	-	-
ISU10	0.10 (0.99)	0.11 (0.91)	0.11 (0.88)	0.12 (0.15)	0.10 (0.98)	0.11 (0.33)	-	-	-

Table 4.9. Summary of CAPWAP estimated soil Smith's damping factors

Project ID	Shaft Damping Factor (Toe Damping Factor), s/ft								
	EOD	1st Re-strike	2nd Re-strike	3rd Re-strike	4th Re-strike	5th Re-strike	6th Re-strike	7th Re-strike	8th Re-strike
ISU1	0.082 (0.063)	-	-	-	-	-	-	-	-
ISU2	0.130 (0.160)	0.124 (0.140)	0.148 (0.250)	0.169 (0.348)	-	-	-	-	-
ISU3	0.095 (0.159)	0.118 (0.127)	0.120 (0.099)	0.064 (0.107)	0.105 (0.070)	0.128 (0.118)	-	-	-
ISU4	0.122 (0.05)	0.132 (0.086)	0.112 (0.181)	0.102 (0.123)	0.153 (0.221)	0.164 (0.448)	0.227 (0.315)	-	-
ISU5	0.241 (0.038)	0.203 (0.066)	0.140 (0.067)	0.164 (0.027)	0.215 (0.110)	0.262 (0.028)	0.203 (0.386)	-	-
ISU6	0.062 (0.086)	0.064 (0.080)	0.075 (0.115)	0.074 (0.158)	0.089 (0.092)	0.151 (0.200)	0.139 (0.384)	0.166 (0.345)	0.189 (0.290)
ISU7	0.398 (0.074)	0.230 (0.209)	0.083 (0.126)	0.099 (0.136)	0.094 (0.104)	0.107 (0.027)	0.110 (0.078)	0.097 (0.182)	-
ISU8	0.092 (0.134)	0.109 (0.167)	0.128 (0.156)	0.134 (0.193)	0.146 (0.398)	0.178 (0.366)	0.147 (0.191)	-	-
ISU9	0.053 (0.189)	0.088 (0.077)	0.082 (0.135)	0.108 (0.217)	0.092 (0.202)	0.117 (0.222)	0.153 (0.140)	-	-
ISU10	0.084 (0.074)	0.088 (0.186)	0.098 (0.134)	0.095 (0.060)	0.084 (0.124)	0.061 (0.051)	-	-	-

4.6. Wave Equation Analysis Program (WEAP)

Wave equation analysis method was first introduced by Smith (1962) and was adopted and upgraded by Goble and Rausche (1976) into a commercial program known as WEAP program. WEAP is a one-dimensional wave equation analysis software program that simulates the motion and force on a pile when driven by an impact or vibratory hammer. It is used to assess the behavior of a pile with different hammers, prior to the pile actually being driven. WEAP requires input describing the modeling of a hammer driving system, a pile and the surrounding soil properties and from this computes the blow count, axial driven stress, hammer performance, and pile bearing resistance. Similar to the CAPWAP model, WEAP models the pile and surrounding soil in a series of masses, springs and viscous dampers, as shown in Figure 4.13. Unlike CAPWAP, which uses PDA records to replace the hammer driving system, WEAP completely models different hammer driving systems, with different combinations of masses, springs and/or dampers, and the latest commercial Windows^{TM} operated WEAP program (GRLWEAP) even includes a database of various hammer types. Modifications of hammer efficiency, pressure and stroke values, which represent the actual hammer used, are also allowed.

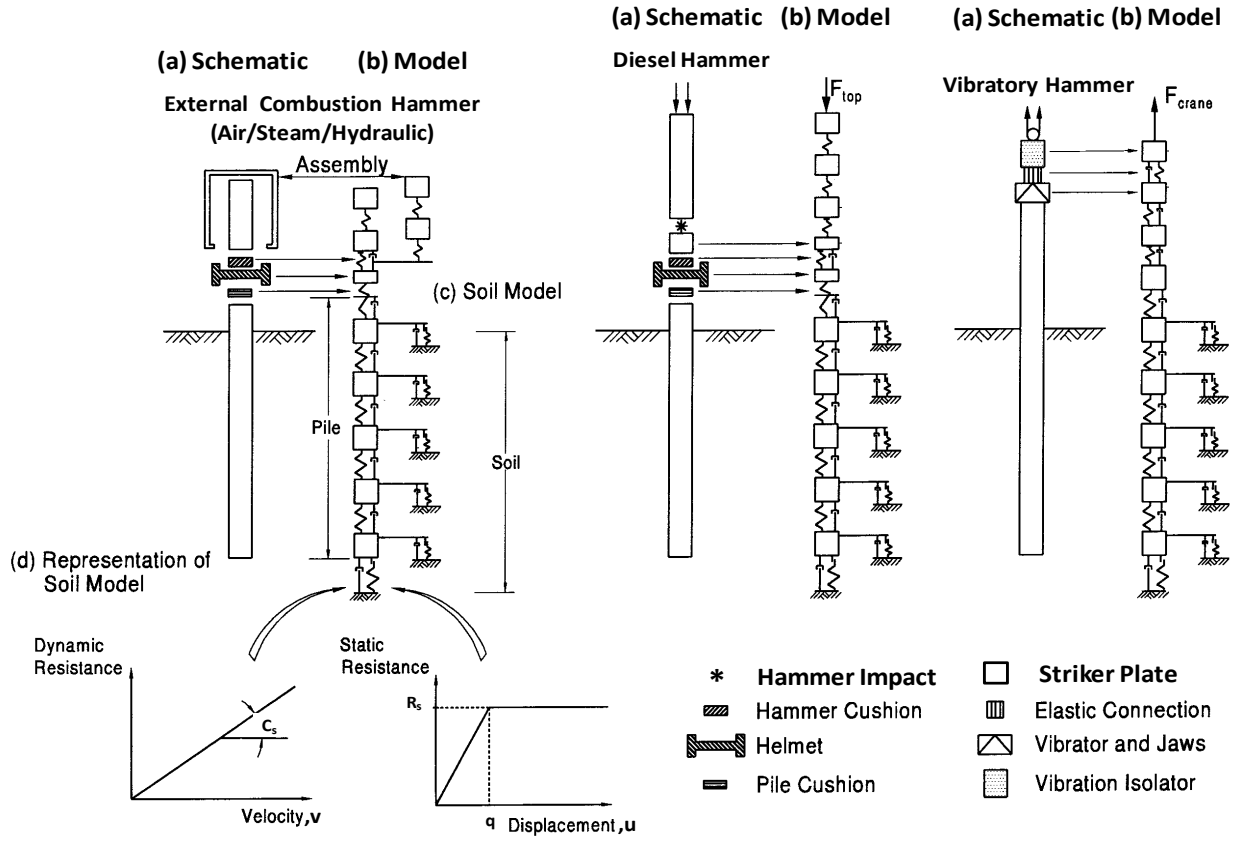

Figure 4.13. Wave equation models for different hammers (adapted from Hannigan et al. 1998)

Knowing the pile properties, as listed in Table 4.1, and the hammer types, as listed in Table 4.2, used in the field tests, WEAP analyses were performed at EOD and re-strikes. Five different procedures of inputting soil profile data into WEAP were carried out, including: 1) GRLWEAP soil type based method (ST); 2) GRLWEAP SPT N-value based method (SA); 3) the Federal

Highway Administration (FHWA) DRIVEN program; 4) Iowa Blue Book (Iowa DOT steel pile Design Chart); and 5) Iowa DOT current approach. The static analysis methods used in the static soil resistance estimation for each procedure are summarized in Table 4.10. The methodology used in each procedure is briefly described in the following subsections; for a detailed description, refer to Ng (2011).

4.6.1 GRLWEAP soil type based method (ST)

The GRLWEAP soil type based method (ST) provides the easiest procedure of inputting the soil information. It requires only the identification of soil types, which aids the input process and simplifies the soil resistance calculation for both bearing graph and driveability analyses. The corresponding soil parameters stored in the GRLWEAP are based on the Bowles (1996) and Fellenius (1996) recommendations, given in Table 4.11 for cohesionless soils and Table 4.12 for cohesive soils. ST method uses the β-method and the modified α-method to estimate the unit shaft (q_s) and unit toe (q_t) resistances for non-cohesive soils and cohesive soils respectively.

4.6.2 GRLWEAP SPT N-value based method (SA)

The GRLWEAP SPT N-value based method (SA) requires the input of soil types, unit weights and uncorrected SPT N-values. These soil parameters can be obtained from the in-situ SPT tests and laboratory soil tests, or they can be estimated using Bowles (1996) recommendations, given in Table 4.13 for cohesionless soils and Table 4.14 for cohesive soils, in the absence of soil test results. The unit shaft and toe resistances are calculated based on the static analysis methods listed in Table 4.10.

4.6.3 FHWA's DRIVEN Program

DRIVEN program generates the entire soil profile of a full pile depth and creates an input file for WEAP analysis. It requires the soil unit weight for all soil types, which are obtained either from laboratory soil tests, or from Table 4.13 for cohesionless soils and Table 4.14 for cohesive soils. SPT N-value is used to define cohesionless soil characteristic and undrained shear strength (S_u) is required to define the cohesive soil strength. The undrained shear strength (S_u) is estimated either from the CPT, described in Section 3.2, or by taking half of the unconfined compressive strength (q_u) given in Table 4.14. Next, the unit shaft and toe resistances are calculated based on static analysis methods, as listed in Table 4.10. For a detailed description of the DRIVEN program, refer to FHWA DRIVEN User's Manual (Mathias and Cribbs 1998).

4.6.4 Iowa Blue Book Method

WEAP analysis based on the Iowa Blue Book method uses the Iowa DOT pile design charts, as shown in Table 4.15 and Table 4.16, for determining the unit shaft (q_s) and unit toe (q_t) resistances. The friction value (in kips/ft) is chosen from the design chart with reference to the width of the steel H-pile, the soil description and the SPT N-value, then this is divided by the perimeter of the boxed section of a steel H-pile to determine the unit shaft resistance. For example, the unit shaft for ISU5 (HP 10 x 42 steel H-pile) at about 19-ft (5.8-m) depth with a clay soil and a SPT N-value of 9 (see Figure 3.2) is calculated at 0.601 ksf (29 kPa), found by dividing the friction value of 2.0 kip/ft with the square perimeter of 3.33-ft (1-m). However, a surface perimeter for the H section was assumed for calculating the unit shaft for sand or

cohesionless soil. The toe resistance (in kips) is determined by multiplying the unit end bearing value (in ksi) with the cross sectional area of the H-pile for any soil conditions, assuming soil plug does not occur in cohesive or clay soil. The calculated unit shaft resistance and the toe resistances, as tabulated in Table 4.17 and Table 4.18 respectively, shall be inserted directly into the WEAP's variable resistance distribution table for driveability and bearing graph analyses.

4.6.5 Iowa DOT Method

The Iowa DOT method uses the SPT N-values as the only soil parameter, which is input into the WEAP's variable resistance distribution table, with respect to the depth where the SPT N-values are taken. Static geotechnical analysis and driveability analysis are not able to be performed since the SPT N-values only serve to define the relative and approximate stiffness of the soil profile. However, a bearing graph analysis can be performed to estimate pile resistance.

Despite the various procedures of inputting the soil profiles, the following assumptions are made and applied to all procedures during the WEAP analysis.

1) Water table remains constant at EOD and at re-strikes
2) The percentage of shaft resistance used in the bearing graph analysis is determined and assumed from the static geotechnical analysis
3) No residual stress analysis is considered
4) The soil geostatic stress within the pre-drilling depth is treated as an overburden pressure, and the pile embedded length does not include the pre-drilling depth
5) Bearing graph analysis based on an equal distribution of total pile capacity on shaft and toe components are selected.

Soil quake (q) and damping coefficient (C_s) are the dynamic soil parameters that describe the soil model. The WEAP recommended soil quake values for shaft and toe soil segments are given in Table 4.19, and are used in the five procedures of defining the soil profile. Five approaches are available in WEAP to define the damping coefficient; however the Smith damping (Eq. 4-10) is the most commonly used in practice. For a detailed description of the five damping options, refer to Pile Dynamics, Inc (2005). The relationship between the damping coefficient (C_s) and the Smith's damping factor (J_s) is given by Eq. 4-10. The WEAP recommended Smith's damping factors for shaft and toe soil segments, as outlined in Table 4.20 are used in the WEAP analyses for all procedures except the Iowa DOT method. The damping factors used in the Iowa DOT method are given in Table 4.21 based on different soil types. Furthermore, the Smith's damping factors are applied consistently to all soil segments, whereas in the Iowa DOT method various damping factors are chosen, from Table 4.21, based on different soil layers along a pile.

Table 4.10. Summary of static analysis methods used in the five soil profile input procedures

Input Procedure	Soil Types							
	Sand (Non-cohesive, drained)		Silt (Non-cohesive, drained)		Silt (Cohesive, undrained)		Clay (Cohesive, undrained)	
	Unit Shaft	Unit Toe	Unit Shaft	Unit Toe	Unit Shaft	Unit Toe	Unit Shaft	Unit Toe
ST (Soil Type Based Method: PDI, 2005)	β-method (Esrig and Kirby 1979)		β-method (Esrig and Kirby 1979)		Modified α-method based on unconfined compressive strength		Modified α-method based on unconfined compressive strength	
SA (SPT N-Value Based Method: PDI, 2005)	$k_o \tan\varphi' \sigma'_v \leq 5$ ksf	4.18 N ≤ 250 ksf	Bjerrum-Borland β-method (based on Fellenius 1996 linear interpolation of β)	$N_t \sigma'_v \leq 125$ ksf (N_t from Fellenius 1996)	Bjerrum-Borland β-method (based on Fellenius 1996 linear interpolation of β)	$N_t \sigma'_v \leq 125$ ksf (N_t from Fellenius 1996)	$k_o \tan\varphi' \sigma'_v \leq 1.6$ ksf	1.127 N ≤ 68 ksf
DRIVEN (FHWA, Mathias and Cribbs, 1998)	Nordlund (1963,1979) Thurman (1964)	Nordlund/ Thurman limited by Meyerhoff (1976)	Nordlund (1963,1979) Thurman (1964)	Nordlund/ Thurman limited by Meyerhoff (1976)	α-method (Tomlinson 1971)	$9S_u$ (Tomlinson 1971)	α-method (Tomlinson 1971)	$9S_u$ (Tomlinson 1971)
Blue Book (Iowa DOT Design Chart, Dirks and Kam, 1994)	Meyerhoff's semi-empirical method	Wave Equation concept using SPT N-values	Meyerhoff's semi-empirical method	Wave Equation concept using SPT N-values	α-method (Tomlinson 1971)	Wave Equation concept using SPT N-values	α-method (Tomlinson 1971)	Wave Equation concept using SPT N-values
Iowa DOT current practice	Used SPT N-values and variable pile profile option in the WEAP							

Table 4.11. Soil Parameters for cohesionless soils

Soil Type	SPT N-Value	Friction Angle (Degree)	Unit Weight (lb/ft^3)	β Value	Toe Bearing Capacity Coefficient (N_t)	Maximum Unit Shaft Resistance, q_s (ksf)	Maximum Unit Toe Resistance, q_t (ksf)
Very Loose	2	25 - 30	85.9	0.203	12.1	0.5	50
Loose	7	27 - 32	101.8	0.242	18.1	1.0	100
Medium	20	30 - 35	117.8	0.313	33.2	1.5	150
Dense	40	35 - 40	124.1	0.483	86.0	2.0	200
Very Dense	50+	38 - 43	140.0	0.627	147.0	4.0	400

Table 4.12. Soil Parameters for cohesive soils

Soil Type	SPT N-Value	Unconfined Compressive Strength, q_u (ksf)	Unit Weight (lb/ft^3)	Maximum Unit Shaft Resistance, q_s (ksf)	Maximum Unit Toe Resistance, q_t (ksf)
Very Soft	1	0.25	111.4	0.07	1.13
Soft	3	0.75	111.4	0.22	3.38
Medium	6	1.50	117.8	0.40	6.77
Stiff	12	3.00	130.5	0.80	13.53
Very Stiff	24	6.00	130.5	1.33	27.07
Hard	32+	8.00	120.9 – 140.0	1.61	36.10

Table 4.13. Empirical values for ø, D_r, and γ of cohesionless soils based on Bowles (1996)

Description	Very Loose	Loose	Medium	Dense	Very Dense
Relative Density, Dr	0 - 0.15	0.15 - 0.35	0.35 - 0.65	0.65 - 0.85	0.85 - 1.00
Corrected N-values	0 - 4	4 - 10	10 - 30	30 - 50	50+
Approximate frictional angle, ø	25 - 30˚	27 - 32˚	30 - 35˚	35 - 40˚	38 - 43˚
Approximate moist unit weight, γ (lb/ft^3)	70.0 - 99.9	89.8 - 115.2	110.1 - 129.9	110.1 - 140.0	129.9 - 150.2

Table 4.14. Empirical values for q_u and γ of cohesive soils based on Bowles (1996)

Description	Very Soft	Soft	Medium	Stiff	Very Stiff	Hard
Unconfined compressive strength, q_u (ksf)	0 - 0.5	0.5 - 1.0	1.0 - 2.0	2.0 - 4.0	4.0 - 8.0	8.0+
Uncorrected N-values	0 - 2	2 - 4	4 - 8	8 - 16	16 - 32	32+
Saturated unit weight, γ (lb/ft^3)	100.6 - 119.7	100.6 - 119.7	110.1 - 129.9	119.7 - 140.0	119.7 - 140.0	119.7 - 140.0

Table 4.15. Iowa pile design chart for friction bearing Grade 50 steel H-piles

SOIL DESCRIPTION	LRFD DRIVEN PILE FOUNDATION GEOTECHNICAL RESISTANCE CHART, ENGLISH UNITS				
	SPT N-VALUE		ESTIMATED NOMINAL RESISTANCE VALUES FOR FRICTION PILE IN KIPS/FT		
Alluvium or Loess	**MEAN**	**RANGE**	**HP 10**	**HP 12**	**HP 14**
Very soft silty clay	1	0 - 1	0.4	0.8	0.8
Soft silty clay	3	2 - 4	0.8	1.2	1.2
Stiff silty clay	6	4 - 8	1.2	1.6	2.0
Firm silty clay	11	7 - 15	2.0	2.4	2.8
Stiff silt	6	3 - 7	1.2	1.6	1.6
Stiff sandy silt	6	4 - 8	1.2	1.6	1.6
Stiff sandy clay	6	4 - 8	1.2	1.6	2.0
Silty sand	8	3 - 13	1.2	1.2	1.6
Clayey sand	13	6 - 20	1.6	2.0	2.8
Fine sand	15	8 - 22	2.0	2.4	2.8
Coarse sand	20	12 - 28	2.8	3.2	3.6
Gravely sand	21	11 - 31	2.8	3.2	3.6
Granular material	> 40	-	4.0	4.8	5.6
Glacial Clay	**MEAN**	**RANGE**	**HP 10**	**HP 12**	**HP 14**
Firm silty glacial clay	11	7 - 15	2.4	2.8	3.2
Firm clay (gumbotil)	12	9 - 15	2.4	2.8	3.2
Firm glacial clay[(1)]	11	7 - 15	2.8 [3.2]	3.2 [4.0]	3.6 [4.4]
Firm sandy glacial clay[(1)]	13	9 - 15	2.8 [3.2]	3.2 [4.0]	3.6 [4.4]
Firm-very firm glacial clay[(1)]	14	11 - 17	2.8 [4.0]	3.2 [4.8]	3.6 [5.6]
Very firm glacial clay[(1)]	24	17 - 30	2.8 [4.0]	3.2 [4.8]	3.6 [5.6]
Very firm sandy glacial clay[(1)]	25	15 - 30	2.8 [4.0]	3.2 [4.8]	3.6 [5.6]
Cohesive or glacial material[(1)]	> 35	-	2.8 [4.0]	3.2 [4.8]	3.6 [5.6]

[(1)] - For double entries the upper value is for an embedded pile within 30 feet of the natural ground elevation, and the lower value [ ] is for pile depths more than 30 feet below the natural ground elevation.

Table 4.16. Iowa pile design chart for end bearing Grade 50 steel H-piles

SOIL DESCRIPTION	LRFD DRIVEN PILE FOUNDATION GEOTECHNICAL RESISTANCE CHART, ENGLISH UNITS				
	SPT N-VALUE		ESTIMATED NOMINAL RESISTANCE VALUES FOR END BEARING PILE IN KSI		
	MEAN	RANGE	HP 10	HP 12	HP 14
Granular material	< 15	-	Do not consider end bearing		
Fine or medium sand	15	-			
Coarse sand	20	-			
Gravely sand	21	-			
Granular material	25	-			
	-	25 - 50	2-4	2-4	2-4
	-	50 - 100	4-8	4-8	4-8
	-	100 - 300	8-16	8-16	8-18
	-	> 300	18	18	18
Bedrock	-	100 - 200	12	12	12
	-	> 200	18	18	18
Cohesive material	12	10 - 50	Do not consider end bearing		
	20	-	1	1	1
	25	-	2	2	2
	50	-	4	4	4
	100	-	7	7	7

Table 4.17. Revised Iowa pile design chart used in WEAP for friction bearing Grade 50 steel H-piles

SOIL DESCRIPTION	LRFD DRIVEN PILE FOUNDATION GEOTECHNICAL RESISTANCE CHART, ENGLISH UNITS				
	SPT N-VALUE		ESTIMATED NOMINAL RESISTANCE VALUES FOR FRICTION PILE IN KIPS PER SQUARE FOOT (KSF)		
Alluvium or Loess	**MEAN**	**RANGE**	**HP 10**	**HP 12**	**HP 14**
Very soft silty clay	1	0 - 1	0.12	0.20	0.17
Soft silty clay	3	2 - 4	0.24	0.30	0.26
Stiff silty clay	6	4 - 8	0.36	0.40	0.43
Firm silty clay	11	7 - 15	0.60	0.60	0.60
Stiff silt	6	3 - 7	0.36	0.40	0.34
Stiff sandy silt	6	4 - 8	0.36	0.40	0.34
Stiff sandy clay	6	4 - 8	0.36	0.40	0.43
Silty sand	8	3 - 13	0.25	0.21	0.23
Clayey sand	13	6 - 20	0.33	0.34	0.40
Fine sand	15	8 - 22	0.41	0.41	0.40
Coarse sand	20	12 - 28	0.58	0.55	0.52
Gravely sand	21	11 - 31	0.58	0.55	0.52
Granular material	> 40	-	0.83	0.82	0.80
Glacial Clay	**MEAN**	**RANGE**	**HP 10**	**HP 12**	**HP 14**
Firm silty glacial clay	11	7 - 15	0.72	0.70	0.69
Firm clay (gumbotil)	12	9 - 15	0.72	0.70	0.69
Firm glacial clay[(1)]	11	7 - 15	0.84 [0.96]	0.80 [1.00]	0.77 [0.94]
Firm sandy glacial clay[(1)]	13	9 - 15	0.84 [0.96]	0.80 [1.00]	0.77 [0.94]
Firm-very firm glacial clay[(1)]	14	11 - 17	0.84 [1.20]	0.80 [1.20]	0.77 [1.20]
Very firm glacial clay[(1)]	24	17 - 30	0.84 [1.20]	0.80 [1.20]	0.77 [1.20]
Very firm sandy glacial clay[(1)]	25	15 - 30	0.84 [1.20]	0.80 [1.20]	0.77 [1.20]
Cohesive or glacial material[(1)]	> 35	-	0.84 [1.20]	0.80 [1.20]	0.77 [1.20]

[(1)] - For double entries the upper value is for an embedded pile within 30 feet of the natural ground elevation, and the lower value [ ] is for pile depths more than 30 feet below the natural ground elevation.

Table 4.18. Revised Iowa pile design chart used in WEAP for end bearing Grade 50 steel H-piles

SOIL DESCRIPTION	LRFD DRIVEN PILE FOUNDATION GEOTECHNICAL RESISTANCE CHART, ENGLISH UNITS				
	SPT N-VALUE		ESTIMATED NOMINAL RESISTANCE VALUES FOR END BEARING PILE IN KIPS		
	MEAN	RANGE	HP 10	HP 12	HP 14
Granular material	< 15	-	Do not consider end bearing		
Fine or medium sand	15	-			
Coarse sand	20	-			
Gravely sand	21	-			
Granular material	25	-			
	-	25 - 50	24.8-49.6	31-62	42.8-85.6
	-	50 - 100	49.6-99.2	62-124	85.6-171.2
	-	100 - 300	99.2-198.4	124-248	171.2-385.2
	-	> 300	223.2	279	385.2
Bedrock	-	100 - 200	148.8	186	256.8
	-	> 200	223.2	279	385.2
Cohesive material	12	10 - 50	Do not consider end bearing		
	20	-	12.4	15.5	21.4
	25	-	24.8	31	42.8
	50	-	49.6	62	85.6
	100	-	86.8	108.5	149.8

Table 4.19. WEAP recommended soil quake values (Pile Dynamics, Inc., 2005)

Soil Type (Pile Type)	Shaft Quake (in)	Toe Quake (in)
All soil types, soft rock (Non-displacement piles)	0.10	0.10
Very dense or hard soils (Displacement piles of diameter or width D)	0.10	D/120
Loose or soft soils (Displacement piles of diameter or width D)	0.10	D/60
Hard rock (All pile types)	0.10	0.04

Table 4.20. WEAP recommended Smith's damping factors used in ST, SA, Driven and Iowa Blue Book (Pile Dynamics, Inc., 2005)

Soil Types	Smith's Shaft Damping Factor (s/ft)	Smith's Toe Damping Factor (s/ft)
Non-cohesive soils	0.05	0.15
Cohesive soils	0.20	0.15

Table 4.21. Damping factors used in the Iowa DOT method

Soil Types	Shaft Damping Factor (s/ft)	Toe Damping Factor (s/ft)
Rock	0.05	0.05
Boulder & Gravel or Gravel Sand	0.10	0.05
Medium Sand or Fine Sand	0.10	0.10
Packed Sand	0.10	0.05
Silt	0.15	0.12
Silty Clay, Silty Clay, Sandy Clay or Firm Sandy Glacial Clay	0.12	0.12
Firm Clay	0.15	0.12
Firm Glacial Clay or Firm Silty Glacial Clay	0.15	0.15

Pile capacities at EOD and re-strikes are estimated using the measured hammer blow count, as listed in Table 4.22. The hammer blow count is defined as the amount of hammer blows required to cause one foot (1-ft) pile penetration into the ground. Using the measured hammer blow count, the corresponding pile resistance at each loading stage is determined from the WEAP generated bearing graph. For example, the pile resistance of 166 kips (738 kN) is determined from the bearing graph, as shown in Figure 4.14 for ISU5 at EOD using the Iowa DOT method with respect to the measured blow count of 26. Table 4.23 presents the estimated pile capacities for all events (EOD and re-strikes) using the five soil profile input procedures. Furthermore, given the hammer information, WEAP estimates the hammer stroke as a function of hammer blow count, as seen in Figure 4.14 for ISU5 at EOD. The bearing graph analysis also generates relationships between pile compressive/tensile stresses and hammer blow count, as illustrated in Figure 4.15 for ISU5 at EOD. In this example, both the compressive (38.25 ksi or 264 MPa) and tensile (6.7 ksi or 46 MPa) stresses at the hammer blow count of 26 are less than the allowable driving stress of 45 ksi (310 MPa) for a Grade 50 steel H-pile. The WEAP analysis shows that the pile is not overstressed at EOD. In general, WEAP is used to evaluate hammer performance, ensure pile integrity, and estimate pile resistance, however the estimated

hammer strokes and pile stresses are not tabulated here because the main purpose of performing the WEAP analysis on this occasion is to estimate pile capacities.

Table 4.22. Measured hammer blow count at EOD and re-strikes

Project ID	Measured Hammer Blow Count (blow/ft)								
	EOD	1st Re-strike	2nd Re-strike	3rd Re-strike	4th Re-strike	5th Re-strike	6th Re-strike	7th Re-strike	8th Re-strike
ISU1	13	-	-	-	-	-	-	-	-
ISU2	10	14	18	22	-	-	-	-	-
ISU3	10	16	16	16	18	20	-	-	-
ISU4	13	15	18	16	21	24	26	-	-
ISU5	26	36	37	38	44	54	72	-	-
ISU6	21	20	22	25	29	38	44	53	60
ISU7	1	3	3	3	7	7	8	8	-
ISU8	19	20	21	21	28	30	31	-	-
ISU9	17	15	16	15	17	14	15	-	-
ISU10	15	10	10	12	14	12	-	-	-

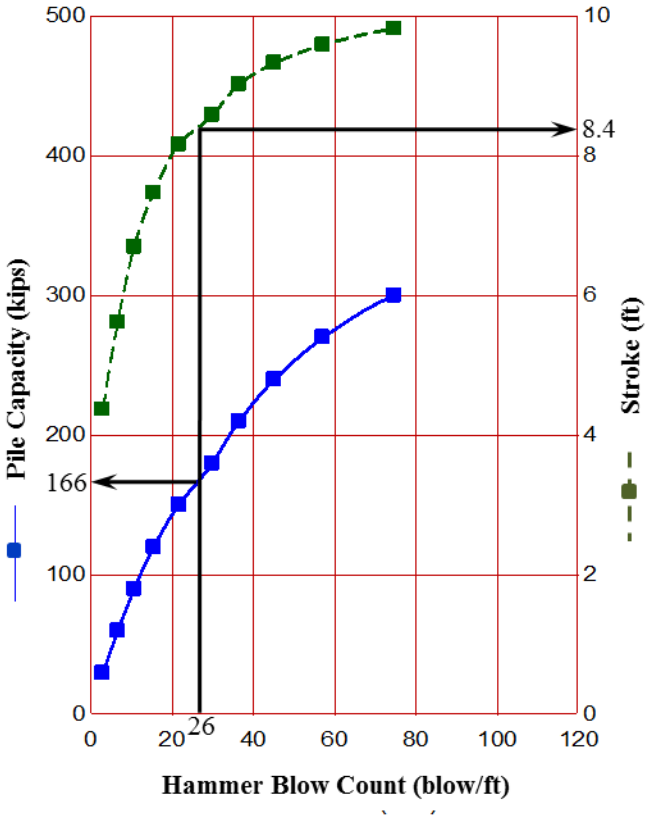

Figure 4.14. WEAP generated bearing graph for ISU5 at EOD using the Iowa DOT method

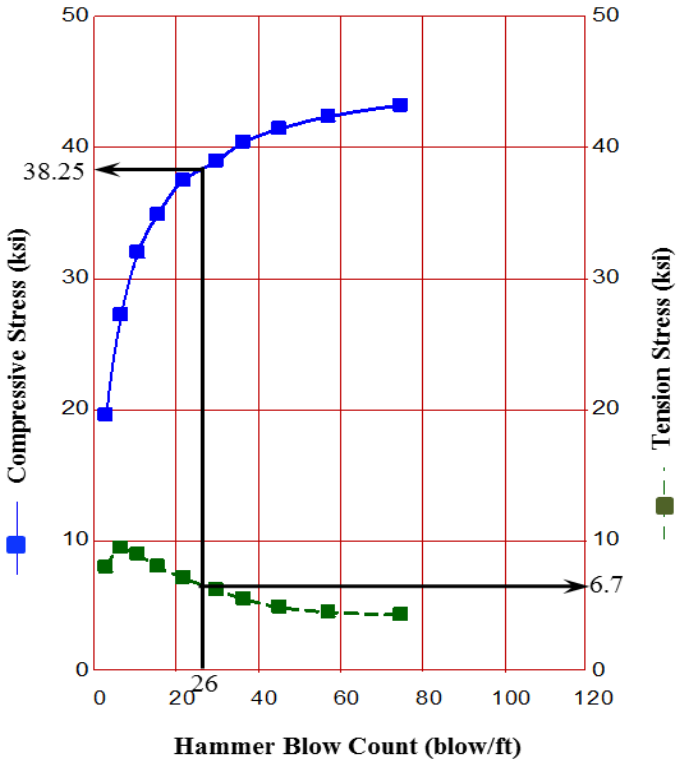

Figure 4.15. WEAP estimated pile stresses for ISU5 at EOD using the Iowa DOT method

Table 4.23. Summary of WEAP estimated pile capacities for all loading stages and all test piles using different soil input options

Project ID	WEAP Estimated Pile Resistance using ST Method (kip)								
	EOD	1st Re-strike	2nd Re-strike	3rd Re-strike	4th Re-strike	5th Re-strike	6th Re-strike	7th Re-strike	8th Re-strike
ISU1	107	-	-	-	-	-	-	-	-
ISU2	77	101	123	138	-	-	-	-	-
ISU3	82	110	110	110	121	161	-	-	-
ISU4	98	110	127	116	139	152	160	-	-
ISU5	144	180	184	187	206	232	261	-	-
ISU6	135	129	138	149	162	191	211	231	245
ISU7	8	24	30	31	62	65	68	70	-
ISU8	137	143	145	148	173	179	183	-	-
ISU9	178	162	171	163	177	159	161	-	-
ISU10	154	114	114	131	147	135	-	-	-
Project ID	**WEAP Estimated Pile Resistance using SA Method (kip)**								
	EOD	**1st Re-strike**	**2nd Re-strike**	**3rd Re-strike**	**4th Re-strike**	**5th Re-strike**	**6th Re-strike**	**7th Re-strike**	**8th Re-strike**
ISU1	102	-	-	-	-	-	-	-	-
ISU2	77	101	123	139	-	-	-	-	-
ISU3	82	111	111	111	121	132	-	-	-
ISU4	95	106	122	112	133	147	154	-	-
ISU5	143	178	182	185	203	228	256	-	-
ISU6	138	133	142	153	166	198	217	239	252
ISU7	9	23	28	29	58	61	64	65	-
ISU8	138	145	146	149	177	179	183	-	-
ISU9	160	149	155	149	160	144	146	-	-
ISU10	159	117	117	135	151	138	-	-	-

Project ID	WEAP Estimated Pile Resistance using DRIVEN Method (kip)								
	EOD	1st Re-strike	2nd Re-strike	3rd Re-strike	4th Re-strike	5th Re-strike	6th Re-strike	7th Re-strike	8th Re-strike
ISU1	131	-	-	-	-	-	-	-	-
ISU2	78	102	124	139	-	-	-	-	-
ISU3	82	111	111	111	122	132	-	-	-
ISU4	95	106	122	112	133	147	155	-	-
ISU5	142	177	181	184	201	224	252	-	-
ISU6	135	130	139	149	163	193	213	234	247
ISU7	13	23	28	29	58	61	64	66	-
ISU8	125	131	133	136	160	166	170	-	-
ISU9	185	169	177	169	183	164	166	-	-
ISU10	162	119	119	138	154	141	-	-	-
Project ID	**WEAP Estimated Pile Resistance using Blue Book Method (kip)**								
	EOD	**1st Re-strike**	**2nd Re-strike**	**3rd Re-strike**	**4th Re-strike**	**5th Re-strike**	**6th Re-strike**	**7th Re-strike**	**8th Re-strike**
ISU1	106	-	-	-	-	-	-	-	-
ISU2	77	100	123	138	-	-	-	-	-
ISU3	82	111	111	111	121	131	-	-	-
ISU4	95	106	122	112	133	147	155	-	-
ISU5	143	178	182	185	203	227	256	-	-
ISU6	140	133	143	153	167	198	217	240	252
ISU7	9	24	27	29	58	61	64	66	-
ISU8	136	143	144	147	172	179	182	-	-
ISU9	166	152	159	152	164	148	150	-	-
ISU10	154	112	113	130	145	133	-	-	-
Project ID	**WEAP Estimated Pile Resistance using Iowa DOT Method (kip)**								
	EOD	**1st Re-strike**	**2nd Re-strike**	**3rd Re-strike**	**4th Re-strike**	**5th Re-strike**	**6th Re-strike**	**7th Re-strike**	**8th Re-strike**
ISU1	117	-	-	-	-	-	-	-	-
ISU2	95	123	150	169	-	-	-	-	-
ISU3	92	133	133	133	146	160	-	-	-
ISU4	115	127	146	134	159	174	183	-	-
ISU5	166	208	212	216	236	263	295	-	-
ISU6	164	158	168	179	195	230	252	276	291
ISU7	10	25	30	32	65	68	71	73	-
ISU8	152	160	161	164	190	198	202	-	-
ISU9	155	142	148	141	154	138	139	-	-
ISU10	143	107	107	121	135	123	-	-	-

4.7. Vertical Static Load Tests

After completing all the re-strikes, vertical static load tests were performed on the test piles in accordance with ASTM D1143 Procedure A: Quick test method. AASHTO (2007) LRFD bridge specifications require that the static load test shall be performed a minimum of five (5) days after the pile is installed and the quick load test method shall be used to measure the pile resistance. The schematic diagram of the static axial load test for ISU5 at Clarke County, using a hydraulic jack acting against a frame utilizing two anchored reaction piles, is shown in Figure 4.17. After installing the test pile, two HP 10 x 42 anchor piles were installed with 72-in. (1.8-m) exposed lengths, in line with the test pile and with a minimum clear distance of five (5) times the diameter of the largest pile (total clearance of 50-in or 1.3-m), as shown in Figure 4.18. This is in accordance with AASHTO (2007) specifications, which require a minimum distance of 30-in (760-mm) or 2.5 diameters in order to avoid any influence of the anchor piles on the test pile.

Note that the test pile and the anchored piles were oriented with all the flanges parallel to each other for the ease of setting up the static load test frame.

Some of the test piles experienced minimal local bucking on the flanges near the pile head due to hard driving, as illustrated in Figure 4.16. The buckled section, usually of about 6-in. (150-mm) to 12-in. (300-mm), was cut off to provide a level and even surface before the loading jack and steel plates were placed on the test pile. After the anchored piles had been driven, four (4) 40-in. (1-m) pile segments were prepared and continuously welded onto the flanges of the anchored piles, as shown in Figure 4.19. The main reaction beam was lifted and placed on top of the anchored piles, with the clamping beams and height adjusters then placed atop the reaction beam. The 3-in. (75-mm) diameter steel rods were then lowered through holes in the height adjusters and clamping beams and through the spaces between the flanges of the 40-in. (1-m) pile segments. Sleeved rod nuts were tightened against the bottom plate directly underneath the 40-in. (1-m) pile segment. The completed static load test frame is shown in Figure 4.19. Next, steel plates were placed on top of the test pile and followed by a 200 ton (1,779 kN) hydraulic jack, cylindrical steel tube and load cell. The remaining gap between the load cell and the bottom of the main reaction beam was filled with layers of shim plates. The hydraulic jack was connected to an electrical pump which extended and retrieved the jack during the loading and unloading stages respectively.

The amount of force applied vertically on the test pile was measured and recorded by the load cell, which was connected to a data acquisition system. When a vertical load was applied on the test pile, an equal and opposite vertical load was exerted upward on the main reaction beam, which was resisted by the clamping beams and height adjusters at both ends. The resisting force on the clamping beams and height adjusters was transferred to the 3-in. (75-mm) diameter steel rods which reacted against the steel plates on the bottom of the 40-in (1-m) pile segments, welded onto the anchored piles. The vertical load was eventually transferred to the anchored piles, which were supported by the shaft soil resistance along their embedded length of 54-ft (16.5-m). Since the test pile had a similar embedded length and was mainly a frictional pile, the static load test frame system provided a safety factor of about 2.0, due to the friction resistance of the anchor piles.

Figure 4.16. Minimal buckling on flanges at pile head

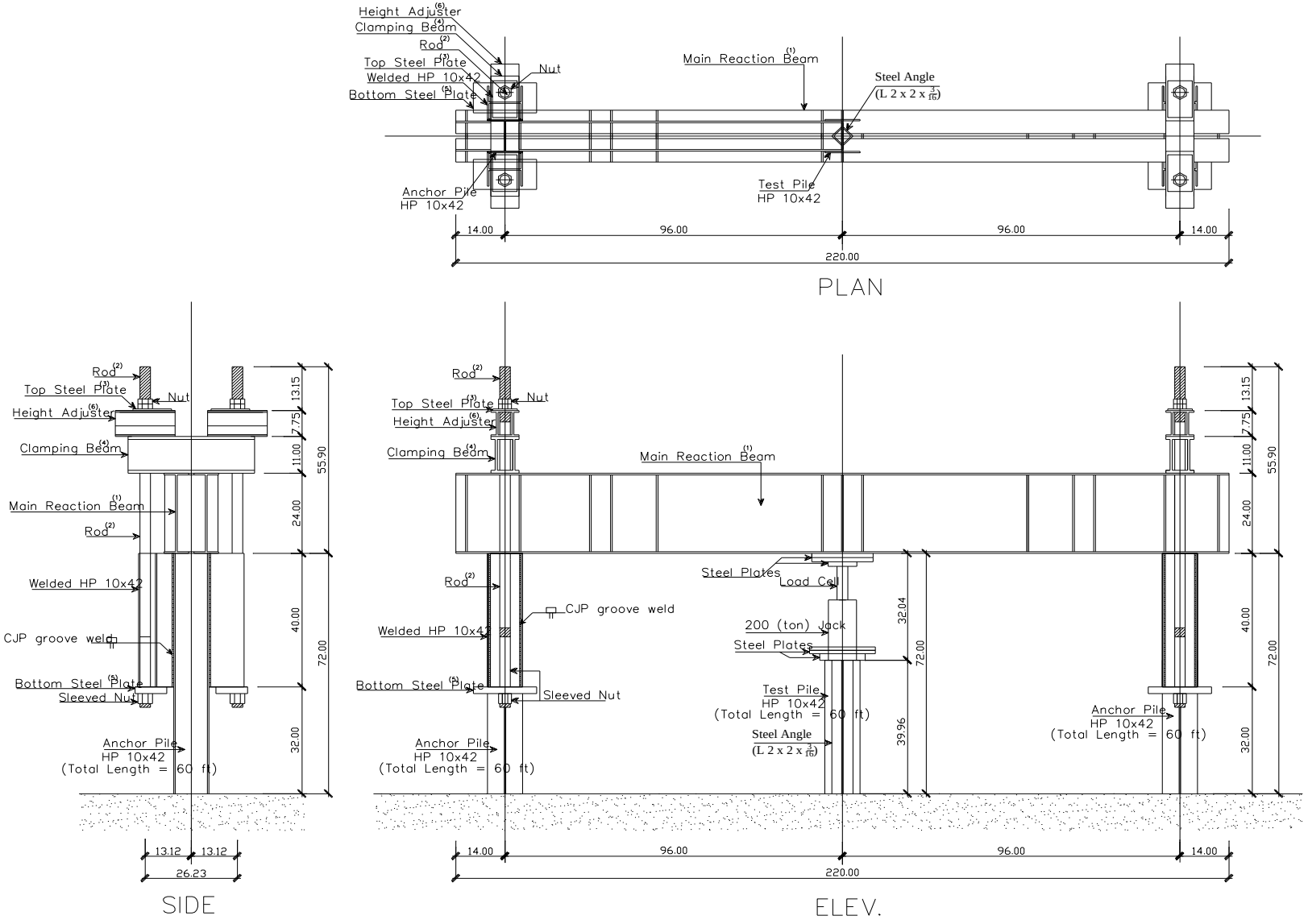

Figure 4.17. Schematic drawing of vertical static load test for ISU5 at Clarke County

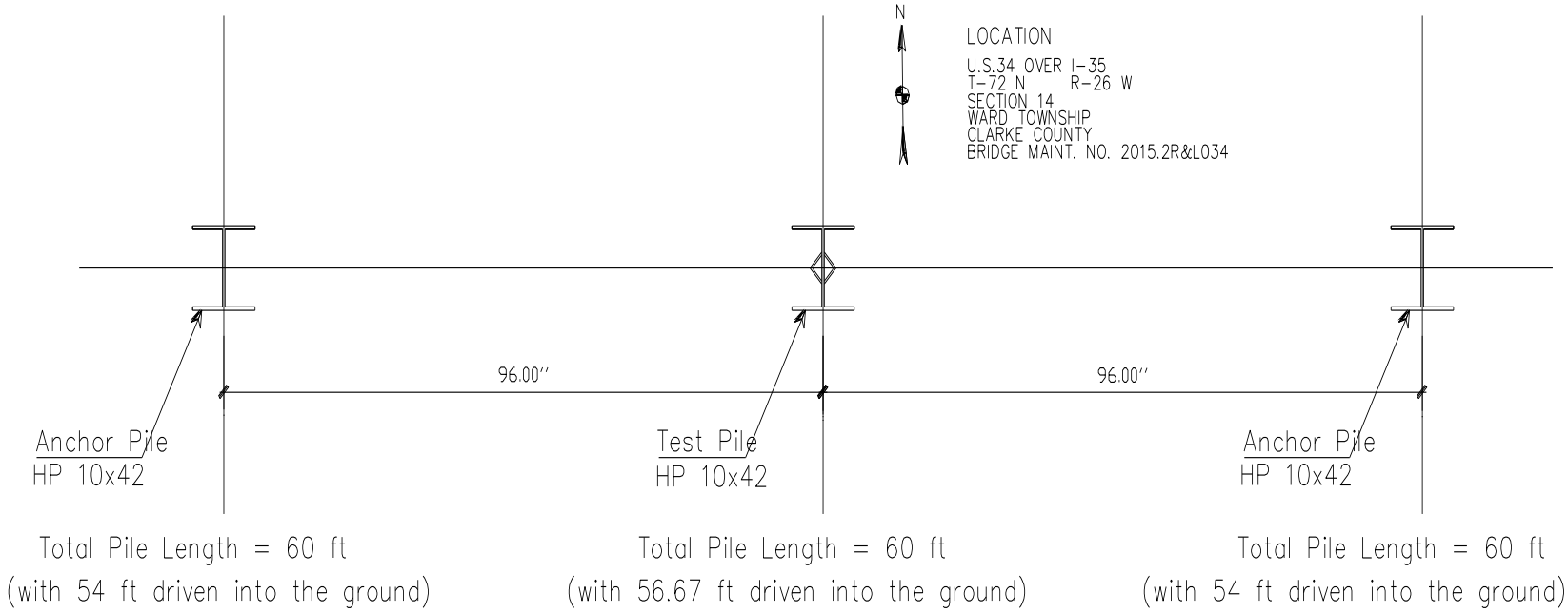

Figure 4.18. Configuration of two anchor piles and a test pile for ISU5 at Clarke County

(a) Welded 40 in. short segment onto flanges

(b) A test pile between two anchored piles

(c) Assembled a main reaction beam, clamping beams and height adjusters; Fastened with steel rods

(d) Placed load cell and jack between test pile and beam

(e) Set up data acquisition system

(f) Completed static load test frame

Figure 4.19. Setting up of the static load test

During testing readings from strain gauges installed along the pile and displacement gauges were recorded at load increments of 5% of the anticipated failure load. During each load interval, the load was kept constant for a time interval of not less than four (4) minutes and not more than fifteen (15) minutes. During the unloading testing stage, a similar procedure was applied at 10% load decrement. The strain gauge instrumentation is described in detail in Section 4-3 and the displacement transducers instrumentation is shown in Figure 4.20. Four (4) 10-in. (250-mm) stroke displacement transducers were utilized, with each pair located close to both sides of the test pile flanges. The displacement gauges were bolted on 2×4-in. (40×90-mm) wooden reference beams, which were supported by wooden ladders approximately 3-ft (900-mm) away from the test pile on either side, as shown in Figure 4.19 and Figure 4.20. This setting allowed the measurement of vertical pile movement independent of any movement of the loading frame. The extendable strings of the displacement transducers were connected to eye hooks mounted on wooden blocks adhered to the flanges of the test pile, as illustrated in Figure 4.20.

Vertical pile displacement was recorded during each static load test and a load displacement curve was plotted for each test pile to determine the pile resistance, using the Davisson's criteria, as shown in Figure 4.21 for ISU5. The procedure of determining the pile resistance is given by: (1) drawing the pile elastic stiffness line (dashed-orange line), calculated using Eq. 4-12; (2) offsetting the line by an additional displacement (δΔ), given by Eq. 4-13, to form the Davisson's line (red line); (3) identifying the intersection point (in green circle) between the Davisson's line and the load-displacement curve (blue line); and (4) determining the applied load (Q) corresponding to the intersection point. Due to the contribution of soil stiffness surrounding ISU5, Figure 4.21 shows that the load displacement curve was plotted above the pile elastic stiffness line. The measured pile capacities from static load tests based on the Davisson's criteria are summarized in Table 4.24 and the load-displacement curves are included in Appendix C for all test piles. The distribution of the measured pile capacities along the embedded pile length is described in Section 5.

$$\Delta_e = \frac{QL}{AE} \tag{4-12}$$

$$\delta\Delta = 0.15 + \frac{D}{120} \tag{4-13}$$

where

Δ_e = Pile structural elastic displacement, in;
Q = Applied static load on top of the test pile, kip;
L = Total pile length, in;
A = Cross-sectional area of the test pile, in^2;
E = Modulus of elasticity of the test pile, ksi;
$\delta\Delta$ = Additional displacement for offsetting the pile elastic line, in; and
D = Pile width or diameter, in.

Figure 4.20. Pile top vertical displacement transducers instrumentation

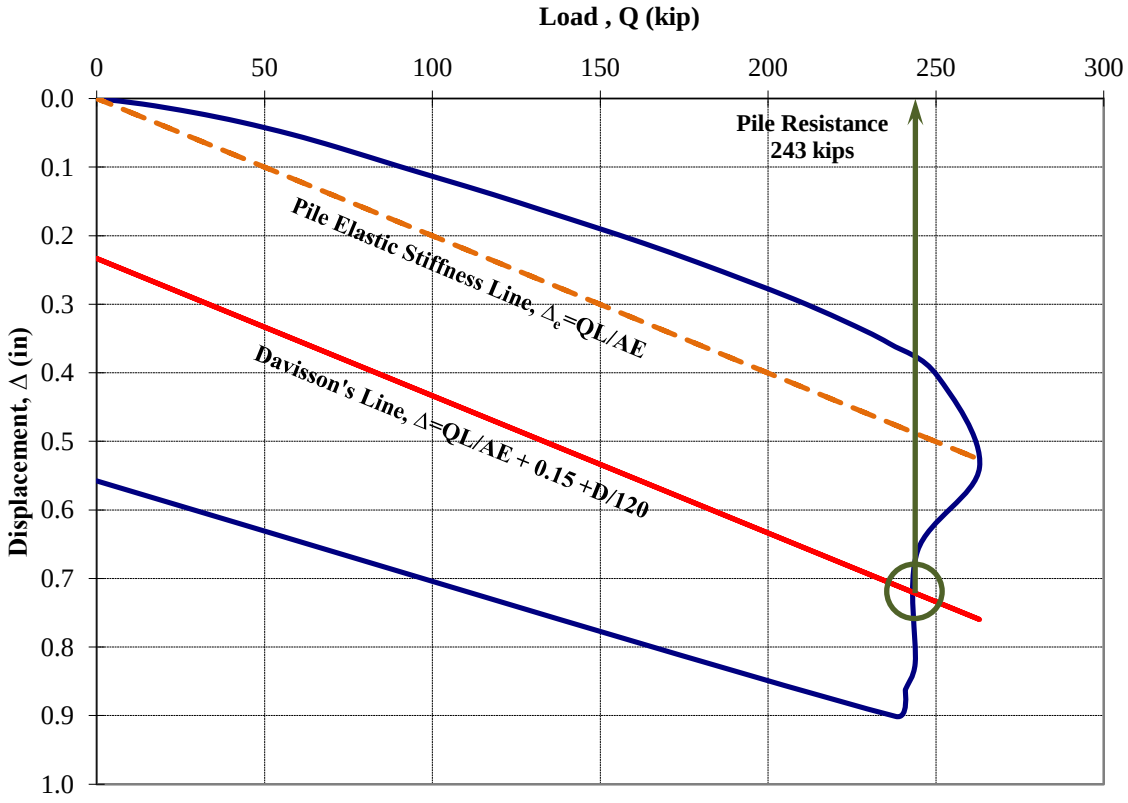

Figure 4.21. A load-displacement curve and Davisson's criteria for ISU5 at Clarke County

Table 4.24. Summary of static load test results

Project ID	Number of Days after EOD	Embedded Pile Length before Static Load Test (ft)	Measured Pile Resistance (kip)
ISU1	100	32.50	212
ISU2	9	55.83	125
ISU3	36	51.00	150
ISU4	16	56.78	154
ISU5	9	56.67	243
ISU6	14	57.2	213
ISU7	13	26.9	53
ISU8	15	57.21	162
ISU9	25	49.5	158
ISU10	6	49.17	127

CHAPTER 5: INTERPRETATION AND ANALYSIS OF FIELD DATA

5.1. Introduction

The aforementioned experimental research studies generate important data for concurrent analytical and computational investigations. In pursuing the objectives of this research for pile resistance quantifications and LRFD resistance factor calibrations, the soil properties measured, using both in-situ and laboratory tests, and pile responses measured, during re-strikes and from static load tests (SLTs), were interpreted and analyzed. The strain measurements collected from SLTs were employed to evaluate the pile load distribution along the embedded pile length and to determine the shaft resistance and end bearing. Particularly, using the static load test results and soil properties measured using mBST, load transfer analyses were performed by AbdelSalam (2010) using TZPILE software to simulate the pile load-displacement relationship. In addition, the measured soil properties were correlated with the increase in pile resistances as a function of time (i.e., pile setup), determined using dynamic analysis methods during re-strikes and measured using SLTs. Due to the economic benefits of incorporating pile setup during pile designs in cohesive soil, pile setup analytical quantification methods were developed in terms of measured soil properties. The proposed setup methods were validated using PILOT database. To expand the application of the proposed pile setup methods, LRFD resistance factors for pile setup were calibrated by Ng (2011), from which the recommendations were documented in the LRFD Report Volume III by AbdelSalam et al. (2011). Additional detailed data interpretation and analyses have also been performed on static analysis methods by AbdelSalam (2010), dynamic analysis methods by Ng (2011) and dynamic formulae by Roling (2010).

5.2. Pile Resistance Distribution

The measured strains (ε) along an embedded test pile length during the static load test were converted to pile forces (F) using Eq. (5-1) at each load increment (Q) based on pile elastic modulus (E) and pile cross-sectional area (A). The distribution of pile forces for test pile ISU5 is drawn in Figure 5.1, and similar force distributions for other test piles are included in the Appendix D.1.

$$F = \varepsilon E A \tag{5-1}$$

The force distribution for ISU5 corresponding to the nominal measured pile resistance (Q_m) of 243 kips (1081 kN) based on the Davisson's criteria (indicated by the solid line without markers shown in Figure 5.1) was established by interpolation of the force distribution curves relating to 236.2 kips (1050 kN) and 250.4 kips (1114 kN). By extending the slope of the pile force curve along the pile length over the bottom two pairs of strain data, the end bearing contribution was estimated at the toe of each pile. In this case, the end bearing component at the embedded pile length of 56.67-ft (17.28-m) was 55.5 kips (247 kN) or 23% of the total pile resistance of 243 kips (1081 kN). Subtracting the end bearing resistance from the total nominal pile resistance, the shaft resistance for ISU5 was determined to be 187.5 kips (834 kN). Table 5.1 lists the shaft resistance and end bearing for all test piles except ISU1, which had no strain instrumentation, and ISU6, ISU7 and ISU10, for which a large number of strain gauges failed during the test and thus this information could not be extracted with sufficient accuracy. For comparison with the

measurements obtained from SLTs, the shaft resistance and end bearing values estimated at the last re-strike using CAPWAP are reported in Table 5.1. It is important to note from both results that the total pile resistance is comprised predominately of the shaft resistance, while the end bearing contribution ranges only between 2% to 28% of the total pile resistance.

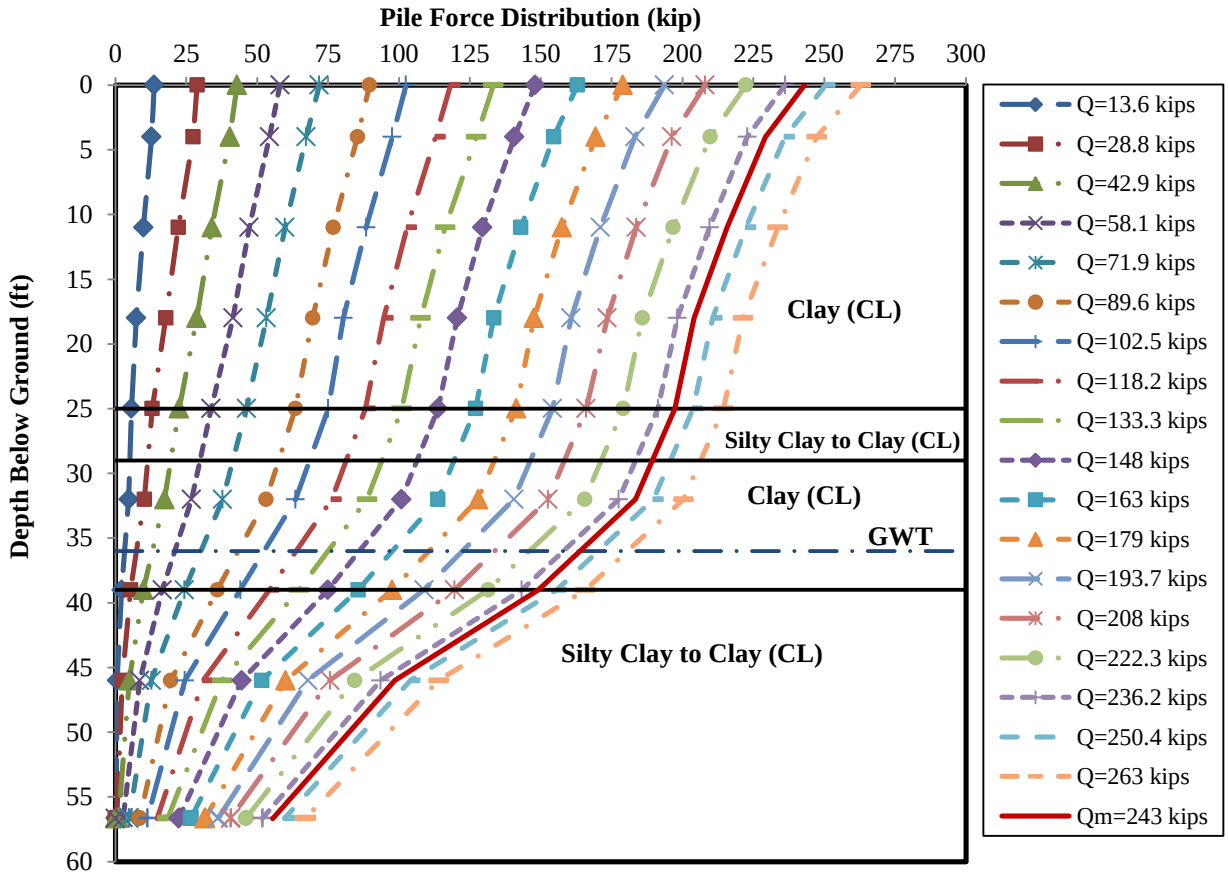

Figure 5.1. Pile force distribution along the embedded pile length of test pile ISU5

Following this, the SLT shaft resistance distribution is systematically determined from the pile force distribution curve at the nominal pile resistance (Q_m) by calculating the difference in forces of two consecutive gauges and plotting these differences with respect to their median locations, as shown in Figure 5.2 for ISU5 and represented by a smoothed line without markers. For a comparative purpose, similar shaft resistance distributions estimated using CAPWAP during the beginning of re-strikes (BOR) are plotted in Figure 5.2. It was observed that the shaft resistance was higher at the stiffer soil layer between 30-ft and 50-ft (9-m and 15-m), characterized with relatively large uncorrected SPT N-values of 20 and 22. The estimated distributions generally follow the trend of the measured distribution, where the differences between estimated and measured resistances reduce from EOD to BOR6. Similar observations are noticed on other test piles as presented in Appendix D.2.

Table 5.1. Summary of shaft resistance and end bearing from static load test results and last re-strike using CAPWAP

Project ID	Soil Type	Static Load Test Results		Last Re-strike Using CAPWAP	
		Shaft Resistance, kip (Percent Total)	End Bearing, kip (Percent Total)	Shaft Resistance, kip (Percent Total)	End Bearing, kip (Percent Total)
ISU1	Mixed	–	–	96 (68%)[a]	46 (32%)[a]
ISU2	Clay	111 (89%)	14 (11%)	114 (88%)	16 (12%)
ISU3	Clay	136 (91%)	14 (9%)	130 (88%)	18 (12%)
ISU4	Clay	151 (98%)	3 (2%)	138 (90%)	16 (10%)
ISU5	Clay	187.5 (77%)	55.5 (23%)	186 (76%)	59 (24%)
ISU6	Clay	–	–	186 (88%)	25 (12%)
ISU7	Mixed	–	–	67 (89%)	8 (11%)
ISU8	Mixed	136 (84%)	26 (16%)	117(73%)	43 (27%)
ISU9	Sand	114 (72%)	44 (28%)	115 (74%)	40 (26%)
ISU10	Sand	–	–	100 (85%)	18 (15%)

[a] – based on end of driving condition.

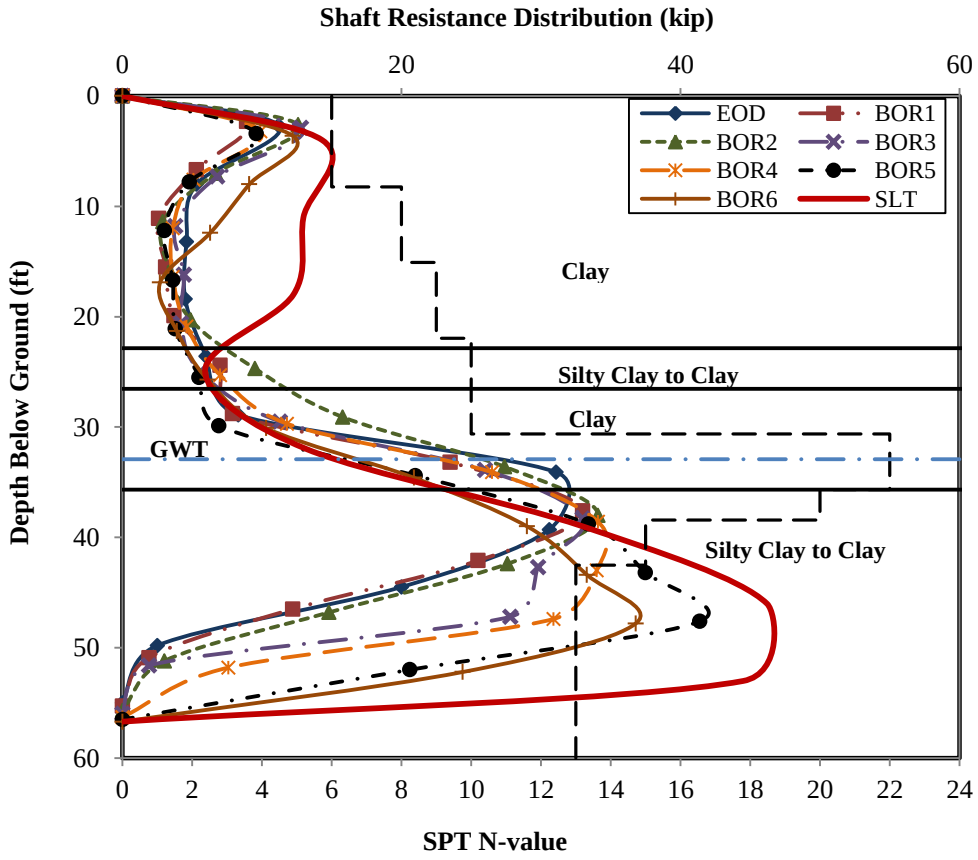

Figure 5.2. SLT measured and CAPWAP estimated pile shaft resistance distributions for test pile ISU5

5.3. Load Transfer Analysis Using mBST and TZPILE Program

The modified Borehole Shear Test (mBST) was used to improve the prediction of the load-displacement relationship and the load distribution for axially loaded friction piles in cohesive soils using a load-transfer analysis (t-z method). Previously, empirical formulas with soil laboratory or in-situ tests, such as the Cone Penetration Test (CPT), have been used for deriving the t-z curves required for this analysis, but the mBST enables direct field measurement of these curves along the soil-pile interface. Three full-scale, instrumented, static vertical load tests conducted on steel H-piles (ISU4, ISU5 and ISU8) were used in this study. The t-z analysis was used to model these three piles utilizing the TZPILE software. Different t-z curves were used in the models, based on: (1) empirical correlations with CPT; and (2) direct measurements from the mBST. When compared to the measured responses from the static vertical load tests, the mBST-based models showed a significant improvement in the prediction accuracy compared to the CPT-based models. The findings in this report may help to incorporate serviceability limits into the design of deep foundations. The major findings from this study are summarized as follows:

- The pile load-displacement relationship predicted using t-z curves based on empirical correlations with CPT data (TZ-CPT) significantly overestimated the soil-pile interface properties, the first portion of the load-displacement response, and the pile capacity by as much as 50%
- The pile load-displacement response calculated using t-z curves obtained from mBST data (TZ-mBST) provided a close match of the slope of the first portion of the measured load-displacement responses (i.e., the load-displacement curve before the start of plunging) and an acceptable estimate of the pile capacity (with differences ranging from 17% to 25% for the three test sites)
- Ignoring the end-bearing component (q-w curve) in the t-z analysis did not significantly affect the results in the case of friction steel H-piles
- Based on overall response predictions for the three (3) test sites, the TZ-mBST model has proven to provide a better match of the measured SLT results when compared with the TZ-CPT model.

Finally, the mBST is a simple and a cost effective in-situ test that captures the soil-pile interface and can be directly used in the load-transfer analysis to simulate the load-displacement behavior at the pile head and the load distribution along the pile length. For a more detailed description of this study, refer to AbdelSalam (2010).

5.4. Interpretation of Push-In Pressure Cell Measurements

Lateral earth and pore water pressures, in cohesive soil layers near test piles ISU5, ISU6, ISU7 and ISU8, as well as in a cohesionless soil layer near test pile ISU10, were measured using push-in pressure cells (PCs). Two cases with respect to the ground water elevation and PCs in cohesive soil layers were explicitly described. The first case, referring to PC1 at ISU5, was installed approximately 23-ft (7-m) below the ground surface and above the water table, which is at 36-ft (11-m) below ground level at this location, whilst for the second case, referring to PC3 and PC4 at ISU6, the PCs were installed approximately 33-ft (10-m) below the ground surface and also below the water table, which lies at 15-ft (4.6-m) below ground level. The measurements for ISU5 and ISU6 are plotted in Figure 3.17 and in Appendix B.6 respectively.

Similar observations were briefly described for PC1 at ISU7 (below water table) and PC4 at ISU8 (above water table) with their measurements presented in Appendix B.6.

The initial pore water pressure recorded by PC1 at ISU5 began with a zero value. Due to the process of PC installation that created a passive stress concentration around the PC, the initial lateral earth pressure (σ_h) was slightly higher than the estimated geostatic vertical pressure (σ_v). The initial pile driving had no effect on either the total lateral earth or pore water pressures. However, when the pile toe reached the PC1 elevation, at about 23.2-ft (7-m), the lateral earth pressure and pore water pressure increased almost instantaneously, to about 70 psi (486 kPa) and 50 psi (345 kPa) respectively. Next, the lateral earth pressure and pore water pressure reduced immediately to about 25 psi (169 kPa) and 19 psi (130 kPa) respectively. It is important to note that this phenomenon occurred before EOD. The pore water pressure then continued to decrease with time even when the SLT was performed at 9 days after EOD. As expected from the dissipation of pore water pressure, the lateral earth pressure increased slowly with time. Figure 3.17 shows that the re-strike and SLT events had insignificant effects on both pressures.

Similar observations were noticed from PC4 at ISU8, at which the lateral earth and pore water pressures instantaneously increased, to about 45 psi (310 kPa) and 3 psi (21 kPa) respectively, when the pile toe reached the PC4 elevation. The lateral earth pressure reduced immediately to its initial value, while the pore water pressure reduced slightly and gradually with time.

For the second case, the PC measurements at ISU6, plotted in Appendix B.6, show both σ_h values increased, to about 94 psi (640 kPa), when the pile toe reached the PC elevations. Before the EOD, the effect of remolding from the continuous pile driving process reduced the σ_h value at PC3 to a relative lower value, of 45 psi (310 kPa), than that at PC4, of 52 psi (360 kPa), which was placed 15-in. (380-mm) further away than PC3 at a distance of 24-in. (610-mm) from ISU6. On the other hand, the water pressure at PC3 increased to a relative higher magnitude of 15 psi (101 kPa) when compared to 9 psi (64 kPa) at PC4. These PC measurements showed that the PC3 water pressure did not reduce immediately; instead, it increased from the moment when the pile toe reached the PC3 sensor to BOR3. This phenomenon can be explained by the denser surrounding cohesive soil, indicated with a relatively high SPT N-value of 16, coupled with its smaller measured vertical coefficient of consolidation of about 0.006 in^2/min (0.039 cm^2/min). Beginning approximately 1.6 hours after EOD (i.e., at BOR4), the PC3 water pressure logarithmically dissipated about 4 psi (30 kPa) over the period of one day and had almost completely dissipated to its hydrostatic state in seven days, whereas the PC4 water pressure logarithmically reduced with a smaller value of 1 psi (7 kPa).

Since PC1 at ISU7 was installed at a location about 5-ft (1.5-m) away from ISU6 (see Appendix A) and at an elevation 6-ft (1.8-m) above PC3 and PC4 at ISU6 (see Appendix B.1), the measurements obtained from PC1 shared similar observations. Both lateral earth and pore water pressures increased, to about 48 psi (331 kPa) and 5.6 psi (39 kPa) respectively, when the pile toe reached the PC1 elevation. The pore water pressure did not reduce immediately after driving and its dissipation only began after BOR1. Unlike ISU5 and ISU8, the re-strikes and SLT events slightly influenced the PC measurements at ISU6 and ISU7, however, the overall logarithmic trends were not affected by these events.

Dissipation of pore water pressure began when the maximum pressure induced by pile driving was developed. At least 50% of the excess pore water pressure dissipated within 10 minutes at ISU5 and 4.8 hours at ISU6. Relating the different rate in pore water pressure dissipation, pile resistance at ISU5 increased rapidly, to 21% within 20 minutes (BOR1), while ISU6 required a longer time delay, of about 1.6 hours (BOR4), to reach the same percentage increase in the pile resistance (refer to Table 4.3 and Table 4.7). The continuous logarithmic dissipation of pore water pressure with time explains the similar pile setup trend, which is further described in Section 5.5. Due to the presence of moisture content in cohesive soils, dissipation of pore water pressure occurred regardless of the ground water elevation. This observation concludes that pile setup occurs along the embedded pile length which is surrounded with cohesive soils. However, the rate of pore water dissipation in a cohesive soil layer is dependent on its respective ground water elevation. The results showed that a higher rate of pore water pressure dissipation was experienced at soil layers above the water table, which led to a higher pile setup rate. In other words, a pile embedded in a cohesive soil profile with a relatively high ground water elevation requires a longer time to achieve the desired pile setup.

Alternatively, measurements obtained from PC4 at ISU10, installed in the cohesionless soil layer (sand) at 10-ft (3-m) below ground, revealed that both lateral earth and pore water pressures dissipated immediately, from the maximum values of 39.5 psi (272 kPa) and 4.5 psi (31 kPa) to their respective initial values before EOD (see Appendix B.6). The water pressure returned to the estimated hydrostatic pressure of 3.5 psi (24 kPa) and the lateral earth pressure remained constantly larger than the estimated geostatic vertical pressure of 9.7 psi (67 kPa). This observation was consistent with the minimal variation in pile resistance over time predicted using CAPWAP during the re-strike events, as reported in Table 4.7 and re-plotted in Figure 5.6. As such, it is concluded that pile setup does not occur in this cohesionless layer, due to the rapid and complete dissipation of the excess pore water pressure before the EOD.

5.5. Pile Responses over Time

5.5.1 Pile Driving Resistance

Pile responses in terms of pile driving resistances at three different pile-embedded soil profiles, clay, mixed soil and sand, were evaluated as a function of embedded pile length and time. The pile driving resistances were referenced to the hammer blow counts, which were video-recorded during driving, at EOD and during re-strikes, as reported in Table 4.22. Pile driving resistances for test piles ISU5, ISU8 and ISU9, as plotted in Figure 5.3, were selected to represent the clay, mixed soil and sand profiles respectively. Figure 5.3 shows that pile driving resistance increased as embedded pile length accumulated during pile installation. However, due to the effect of pile setup, with its trivial embedded pile length increment during re-strikes, the hammer blow count of ISU5 significantly increased from 30 at EOD condition to 72 at BOR6 after 7.92 days of pile installation (see Figure 5.3(a)). Similar phenomenon was observed at ISU8 for the mixed soil profile in Figure 5.3(b). In contrast, ISU9, which was embedded in the sand profile, did not experience the similar continuous increase in pile driving resistance after EOD as observed at ISU5 and ISU8. Confirmed by similar observations from the remaining test piles, included in Appendix D.1, it is concluded that pile setup occurs in the clay and mixed soil profiles but not in the sand profile.

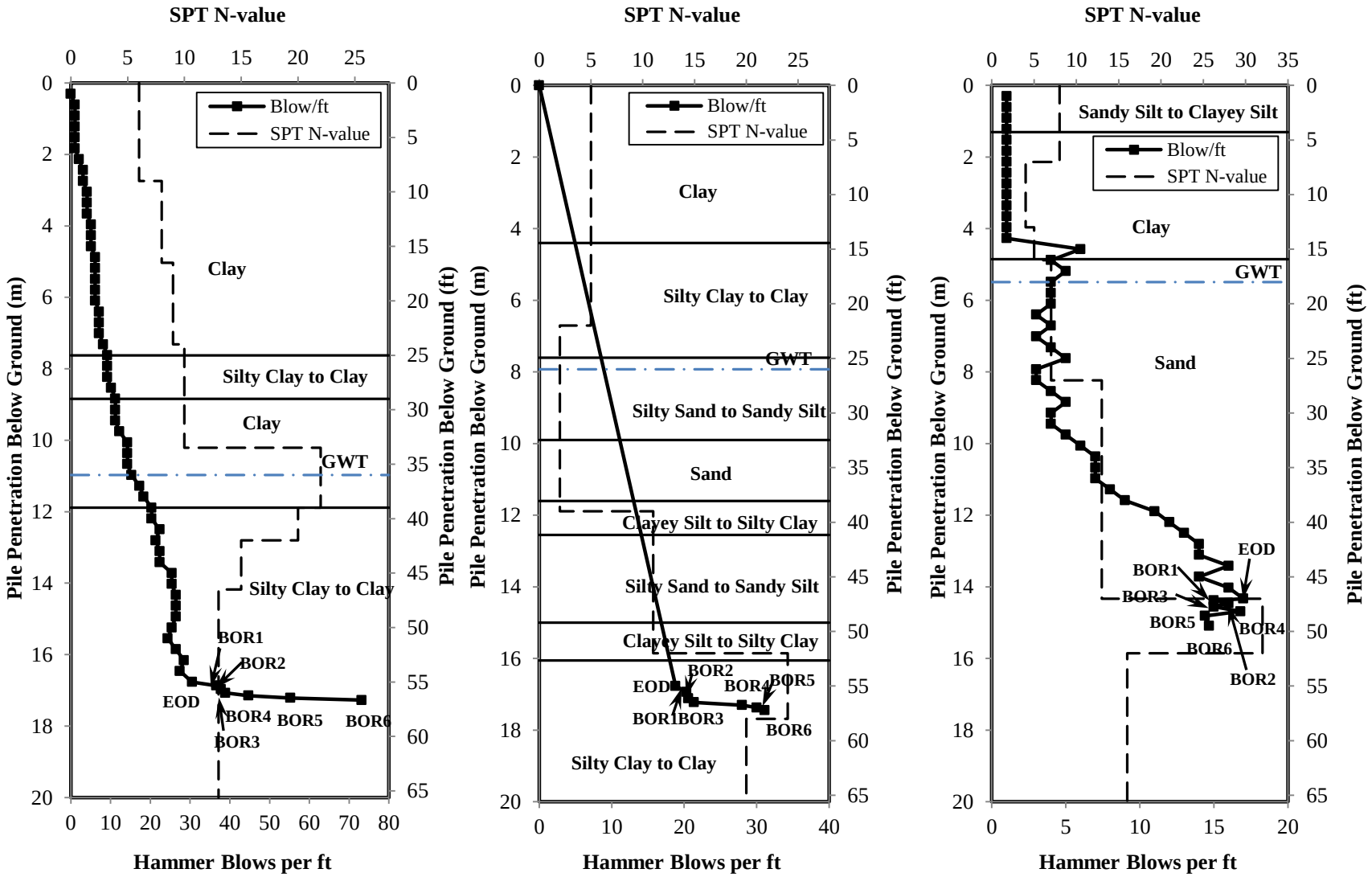

(a) ISU5 for clay profile (b) ISU8 for mixed profile (c) ISU9 for sand profile

Figure 5.3. Pile driving resistance in terms of hammer blow count

5.5.2 Relationship Between Pile Resistance and Time

Total pile resistances (R_t) estimated using WEAP and CAPWAP, summarized in Table 4.23 and Table 4.7 respectively, were plotted against the time (t) at when the re-strikes were performed (see Table 4.3). Among the five soil profile input procedures used in WEAP, only the results estimated using the Iowa Blue Book method (refer to Section 4.6.4 for detailed description) were presented for a comparative purpose. In addition, pile resistances measured using the static load tests, given in Table 4.24, were included to verify the relationship between pile resistance and time. Figure 5.4 and Figure 5.5 show that the increase in total pile resistance has a logarithmic relationship with time for both clay and mixed soil profiles, respectively. Not only do the resistances estimated during re-strikes, using both WEAP and CAPWAP, follow the logarithmic trend, but also the resistances measured at SLT agree with the trend. Alternatively, Figure 5.6 shows that the total resistance of test pile ISU10, embedded in sand profile, did not increase as much as observed in the clay and mixed soil profiles, while the resistance of ISU9 decreased with time. These results agreed with the observations described in Section 5.4 based on the contrasting pore water pressure measurements between cohesive and cohesionless soils and agreed with the conclusion made in Section 5.5.1.

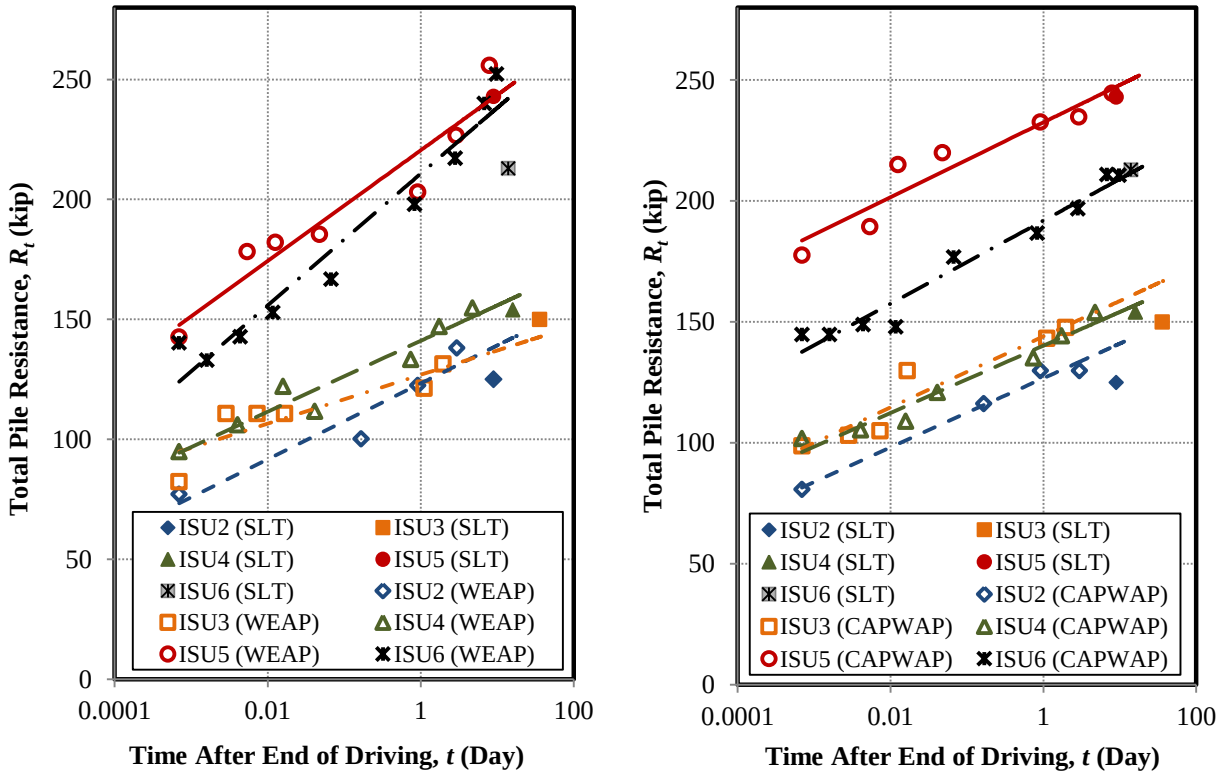

(a) WEAP-Iowa Blue Book Procedure (b) CAPWAP

Figure 5.4. Relationship between total pile resistance and time for clay profile

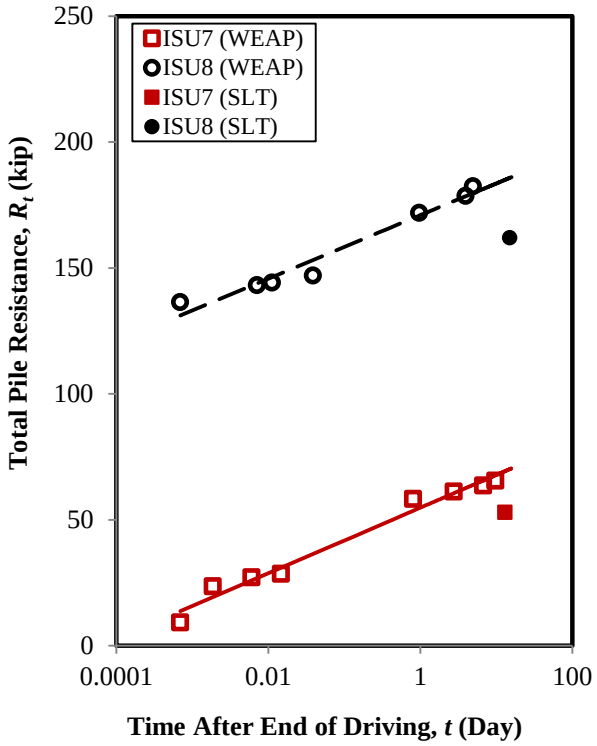

(a) WEAP-Iowa Blue Book Procedure

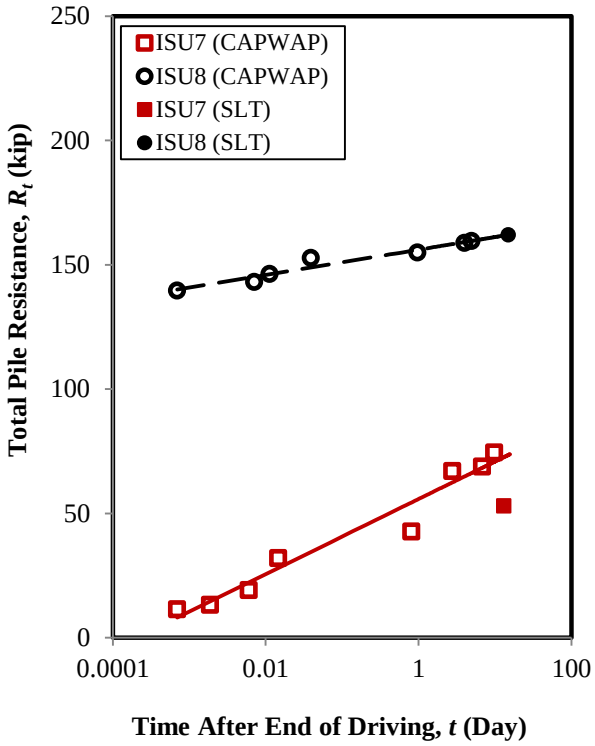

(b) CAPWAP

Figure 5.5. Relationship between total pile resistance and time for mixed soil profile

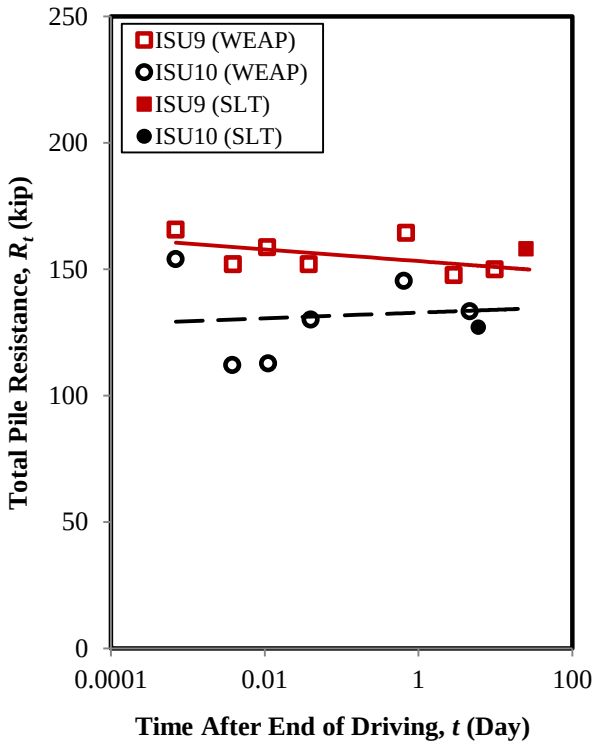

(a) WEAP-Iowa Blue Book Procedure

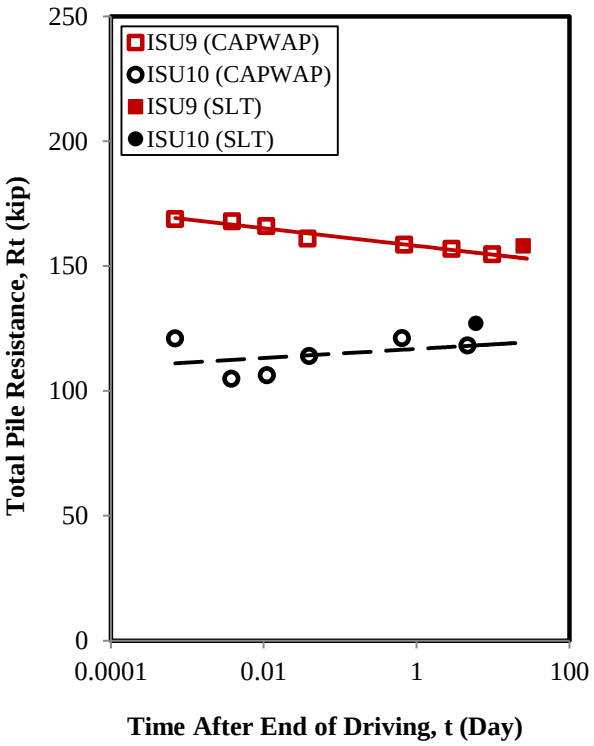

(b) CAPWAP

Figure 5.6. Relationship between total pile resistance and time for sand profile

Table 5.2 summarizes the percent increase in each pile resistance component (ΔR) with reference to its corresponding WEAP or CAPWAP estimated initial pile resistance component at EOD (R_{EOD}) in the clay soil profile. The increases in total pile resistance, shaft resistance and end bearing resistance are listed separately to illustrate the different effects on setup. Both shaft resistance and end bearing increased with time after EOD. Referring to the last re-strikes of all test piles, the increase in CAPWAP calculated shaft resistance ranged from 51% to 71% while the end bearing resistance increased by 8% to 21%. Since the end bearing component on average was about 16% of the total resistance, the impact of setup estimated for this component is not significant. Furthermore, the CAPWAP pile setup estimate on shaft resistance correlated well with the corresponding SLT measurements, in Table 5.2, that indicates 52% to 66% increase in shaft resistance due to setup. This observation concludes that the setup largely affects the shaft resistance of steel H-piles. Among the five test piles, ISU2 had the greatest gain in total pile capacity and shaft resistance and ISU3 had the greatest gain in end bearing. The correlations between pile setup and soil properties were discussed in Section 5.6. Furthermore, referring to ISU5 as an example, the total pile resistance increased by 31% within a day after pile installation (i.e., at BOR4) while the total increase at 7.9 days was only 38% using CAPWAP and 37% using SLT. This observation indicated that pile resistance increased immediately and significantly after pile installation which agreed with the rapid pore water dissipation recorded using the PC described in Section 5.4.

Table 5.2. Percent increase in pile resistance based on CAPWAP and SLT measurements

Test Site	Type of event	Time after EOD, t (day)	WEAP, $\Delta R_t/R_{EOD}$ (%)	CAPWAP, $\Delta R/R_{EOD}$ (%)			SLT			
				Total	Shaft	End Bearing	$\Delta R_t/R_{EOD\text{-}WEAP}$ (%)	$\Delta R_t/R_{EOD\text{-}CAPWAP}$ (%)		
							Total	Total	Shaft	End Bearing
ISU2	BOR1	0.17	31 %	44 %	52 %	6 %	62 %	55 %	66 %	3 %
	BOR2	0.92	59 %	61 %	71 %	12 %				
	BOR3	2.97	80 %	61 %	71 %	13 %				
ISU3	BOR1	2.85E-3	36 %	4 %	4 %	10 %	84 %	52 %	60 %	3 %
	BOR2	7.30E-3	36 %	6 %	5 %	16 %				
	BOR3	1.66E-2	36 %	31 %	33 %	22 %				
	BOR4	1.11	49 %	45 %	49 %	21 %				
	BOR5	1.96	61 %	49 %	54 %	21 %				
ISU4	BOR1	4.05E-3	12 %	4 %	1 %	17 %	62 %	51 %	n/a	n/a
	BOR2	1.58E-2	29 %	7 %	5 %	17 %				
	BOR3	0.04	18 %	19 %	19 %	15 %				
	BOR4	0.74	40 %	33 %	36 %	14 %				
	BOR5	1.74	55 %	42 %	46 %	13 %				
	BOR6	4.75	63 %	51 %	57 %	14 %				
ISU5	BOR1	5.38E-3	24 %	7 %	9 %	1 %	70 %	37 %	52 %	3 %
	BOR2	1.26E-2	27 %	21 %	30 %	2 %				
	BOR3	4.78E-2	30 %	24 %	33 %	3 %				
	BOR4	0.92	42 %	31 %	41 %	7 %				
	BOR5	2.90	59 %	32 %	43 %	7 %				
	BOR6	7.92	79 %	38 %	51 %	8 %				
ISU6	BOR1	1.60E-3	-4 %	0 %	0 %	0 %	54%	47 %	n/a	n/a
	BOR2	4.36E-3	3 %	3 %	2 %	6 %				
	BOR3	1.17E-2	10 %	2 %	1 %	7 %				
	BOR4	6.71E-2	20 %	22 %	24 %	11 %				
	BOR5	0.83	43 %	29 %	32 %	12 %				
	BOR6	2.82	57 %	36 %	40 %	15 %				
	BOR7	6.79	73 %	46 %	51 %	17 %				
	BOR8	9.81	82 %	46 %	51 %	16 %				

To investigate the contribution of shaft resistance and end bearing components to pile setup in clay profile, the shaft resistance and end bearing components estimated using CAPWAP are plotted against time (t), as shown in Figure 5.7. The reasonably good fit of trend lines reveals that both shaft resistance and end bearing components increase logarithmically with time. However, the increase in shaft resistance is larger than that in the end bearing at a given time, indicated by the steeper slope of the shaft resistance component. Hence, it is acknowledged that pile setup in clay profile results predominantly from the shaft resistance with minimal input from the end bearing, as similarly described in the previous paragraph. For the mixed soil profile, Figure 5.8 similarly shows that the shaft resistance generally follows the logarithmic trend while the end bearing randomly deviates somewhat along the logarithmic trend line. Unlike the clay profile shown in Figure 5.7, the decrease in shaft resistance and the increase in end bearing with time at ISU8 indicate that pile setup is contributed mostly from the end bearing. Compared with the clay profile, this different observation might have been complicated by the presence of cohesionless soil layers (layers 2, 4, and 6 as shown in Appendix B.1) along about 40% of the 57.21-ft (17.44-m) embedded pile length, while the pile toe was fully embedded in a cohesive soil layer (classified as CL in accordance with the USCS). The inconsistent observations between ISU7 and ISU8 and the limited field tests available in the mixed soil profile pose challenges in establishing a general conclusion for pile setup in this profile.

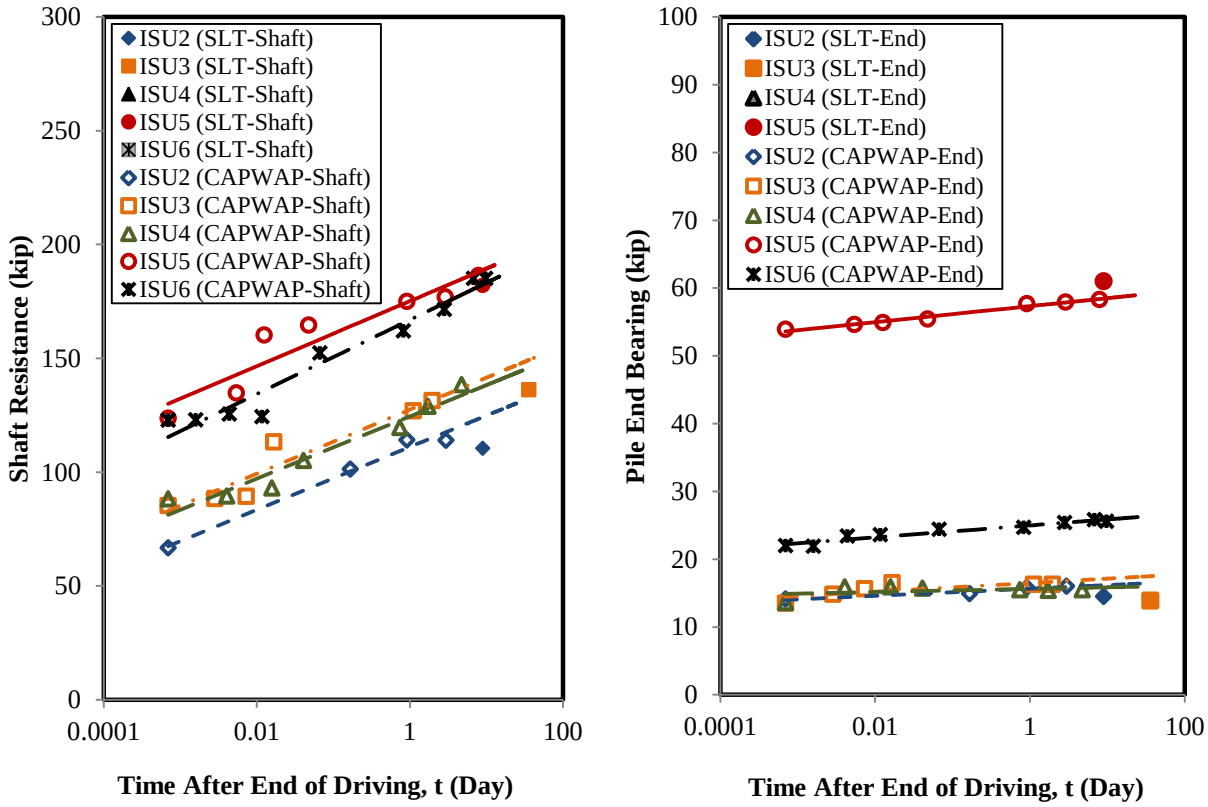

(a) Shaft Resistance vs Time (b) End Bearing vs Time

Figure 5.7. Relationship between resistance components and time for clay profile

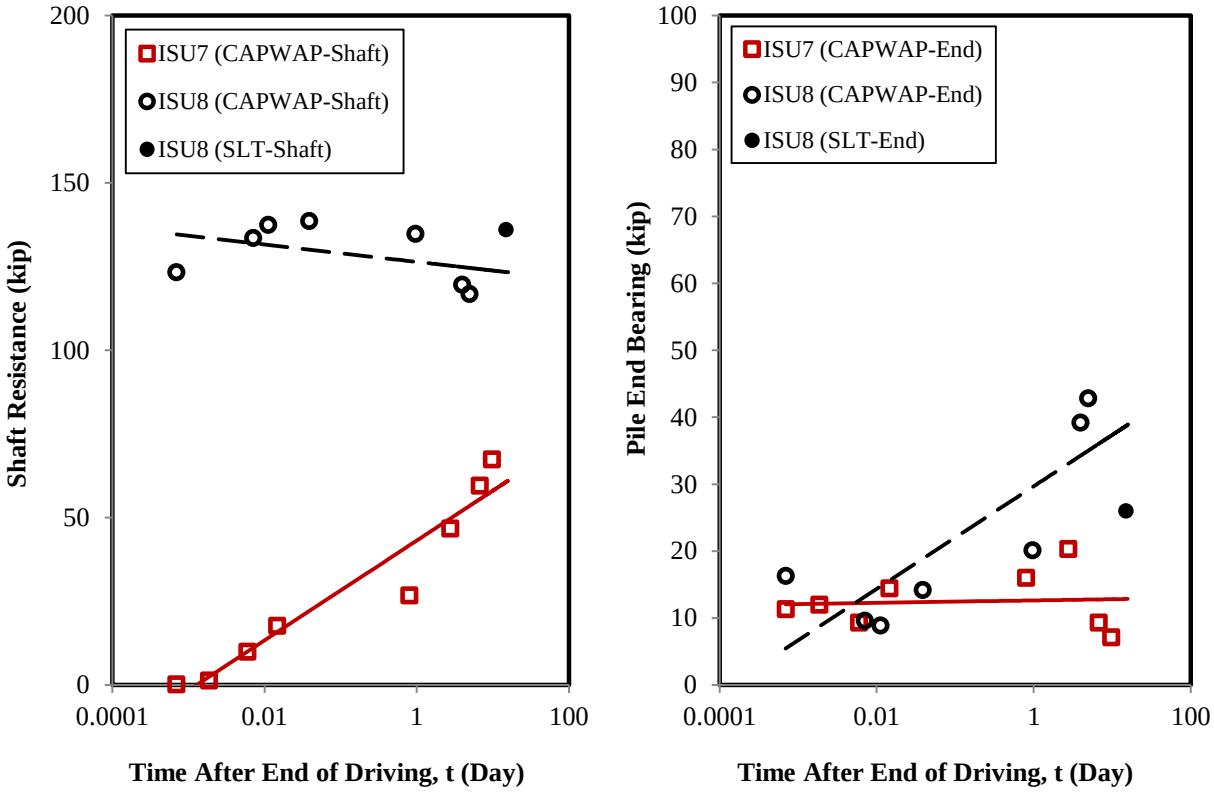

(a) Shaft Resistance vs Time (b) End Bearing vs Time

Figure 5.8. Relationship between resistance components and time for mixed soil profile

5.6. Pile Setup in Clay Profile

The aforementioned observations confirmed the logarithmic relationship between pile setup and time in the clay profile. When accounted for accurately, integration of pile setup will lead to more cost-effective design as it will reduce the number of piles and/or pile length in the clay profile. However, there are several limitations associated with the existing pile setup knowledge, and there are currently no methods available to confidently account for the effects of pile setup in foundation designs. These limitations arise from the lack of: a) sufficient and detailed dynamic and static field test data as a function of time for accurate pile setup evaluation; b) detailed subsurface investigations and monitoring of soil stresses to quantify pile setup (Komurka et al. 2003); and c) a systematic reliability-based method to account for pile setup in the LRFD approach. The extensive field tests carried out herein involved detailed pile setup measurements, using WEAP and CAPWAP, as well as soil investigations. These tests provide the opportunity to: 1) assess the influence of various soil properties on pile setup, as discussed in Section 5.6.1; and 2) develop two pile setup quantification methods in terms of commonly measured SPT N-value and/or CPT determined coefficient of consolidation, as discussed in Section 5.6.2. Along with the five field test results, twelve data points from the PILOT database were selected to validate the proposed pile setup quantification methods established for WEAP, discussed in Section 5.6.3. Since the PILOT database does not contain any PDA records for CAPWAP analyses, only the five field tests were used in validating the pile setup methods established for CAPWAP. To incorporate pile setup into LRFD, a new calibration procedure using the reliability theory was established in Section 5.6.4.

5.6.1 Influence of Various Soil Properties on Pile Setup

Since the pile setup largely increases the shaft resistance, a detailed correlation study between soil properties and percent increase in shaft resistance ($\Delta R/R_{EOD}$) was performed. For illustrative purposes, the correlation study of ISU5 has been explicitly described, whilst studies for the remaining four test piles are included in Appendix D.4. The percent increase in shaft resistance calculated for ISU5 using CAPWAP, between EOD and the last re-strike, was plotted along the embedded pile length, in Figure 5.9, together with the measured vertical coefficient of consolidation (C_v), SPT N-value, over consolidation ratio (OCR), soil compressibility index (C_c), and plasticity index (PI). Since the horizontal coefficient of consolidation (C_h) was not successfully measured at ISU5 due to the time required to achieve 50% pore water pressure dissipation, it can be related to the SPT N-values as shown in Figure 5.10. A similar shaft gain distribution of $\Delta R/R_{EOD}$ for the SLT, the percent difference between the measured shaft resistance from SLT at 9 days after EOD and the CAPWAP calculated shaft resistance at EOD, is also included in Figure 5.9 for comparative purposes. It is interesting to note that the distributions of percent increase in shaft resistance ($\Delta R/R_{EOD}$) for both CAPWAP and SLT have a similar trend, although the magnitudes are sometimes significantly different, which can be attributed to the standard CAPWAP signal matching procedure that uses constant damping and quake values to achieve a best match.

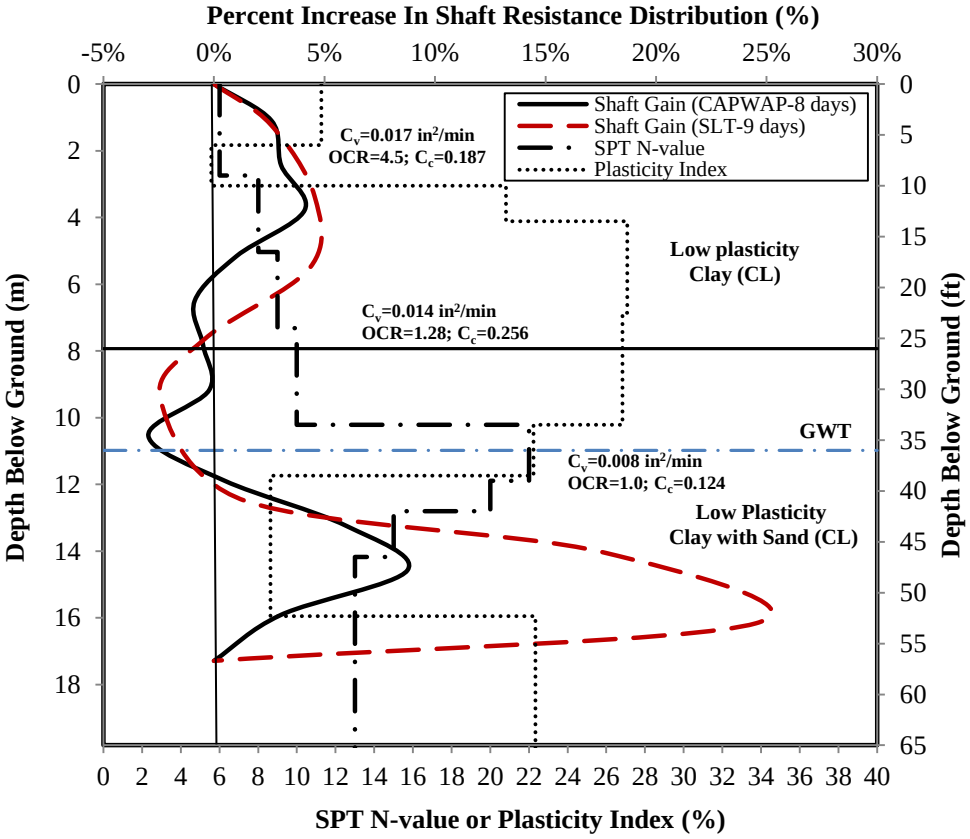

Figure 5.9. Relationship between soil properties and increase in shaft resistance for ISU5

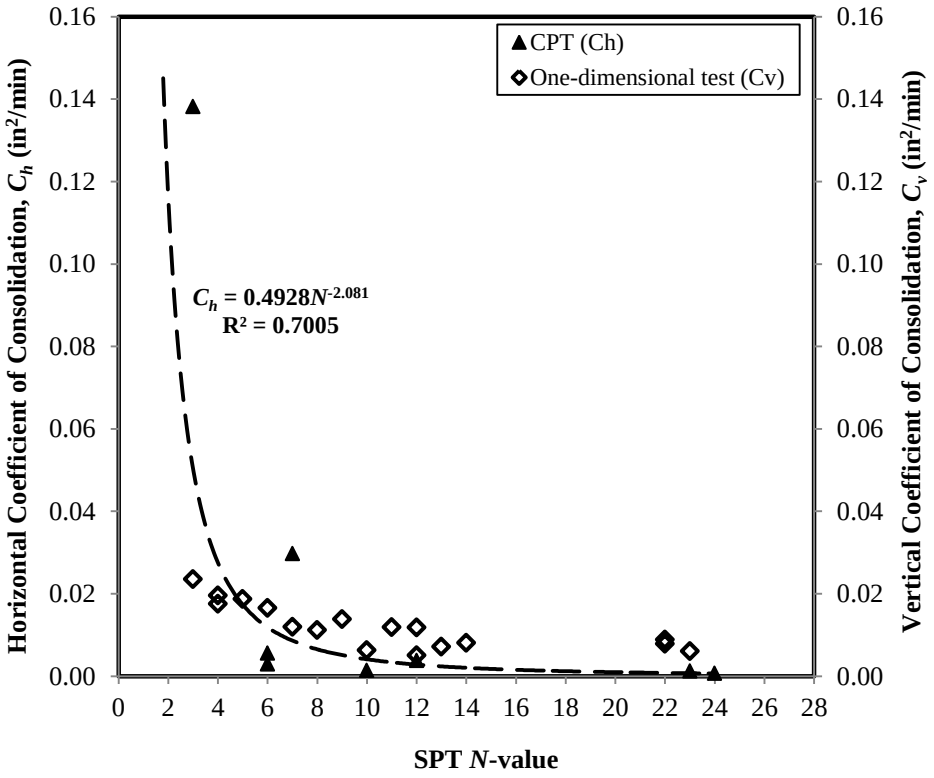

Figure 5.10. Correlations of both vertical and horizontal coefficients of consolidation with SPT N-values

The SLT-based shaft gain distribution, shown in Figure 5.9, illustrates that the $\Delta R/R_{EOD}$ increased by about 5% in the 16-ft (5-m) thick top soil layer, which was characterized with relatively large C_v values, ranging between 0.014 in^2/min (0.089 cm^2/min) and 0.017 in^2/min (0.107 cm^2/min), and small SPT N-values, ranging between 6 and 9. This $\Delta R/R_{EOD}$ continued to reduce to a depth of around 36-ft (11-m) from ground surface, where the surrounding cohesive soil layer has the smallest C_v of 0.008 in^2/min (0.051 cm^2/min) and the highest SPT N-value of 22. With the combined effects of the overburden pressure and the reduction in SPT N-value, from 22 to 13, below the 36-ft (11-m) depth, the $\Delta R/R_{EOD}$ indicated a peak increase of about 25%. This observation suggests a direct relationship between pile setup along the shaft and the coefficient of consolidation, plus an inverse relationship between pile setup and SPT N-value (or a direct correlation with the horizontal coefficient of consolidation, as indicated by Figure 5.10).

Besides comparing with SPT N-value and coefficient of consolidation, pile setup was also compared with other soil properties, including over consolidation ratio (OCR), compressibility index (C_c) and plastic index (PI). Figure 5.9 reveals an inverse relationship between the measured PI and the $\Delta R/R_{EOD}$. For instance, within the cohesive soil layers with low PI values, of 5.6% and 8.6% at 10-ft (3-m) and 47-ft (14-m) respectively, the shaft resistances increased. Hence, a pile embedded in a cohesive soil with low PI will experience a large $\Delta R/R_{EOD}$ at any given time. Furthermore, Zheng et al. (2010) concluded that a low compressive cohesive soil with a small C_c value dissipated the excess pore water pressure faster. Relating this conclusion to pile setup, this means C_c value should have an inverse relationship with $\Delta R/R_{EOD}$, however,

Figure 5.9 reveals no such relationship, especially at the 11-m (36-ft) depth where $\Delta R/R_{EOD}$ reduced despite having the lowest C_c of 0.124.

To further expand upon the observations presented above using data from ISU5, the percent increase in total pile resistance, shaft resistance and end bearing estimated for all five test piles using CAPWAP were compared with weighted average C_h, C_v, PI and SPT N-values, allowing variation of soil thicknesses along the embedded pile length to be included. For soil layers where the CPT dissipation test was not conducted or the 50% consolidation was not achieved, the horizontal coefficient of consolidation (C_h) was estimated using the SPT N-value, based on the correlation developed from field test results presented in Figure 5.10. Table 5.3 summarizes the findings together with the weighted average soil properties along the pile shaft and near the pile toe for each test site, whilst Figure 5.11 gives a graphical representation of the same data for each of the soil variables affecting pile setup, at approximately 1 day after EOD for all sites.

Table 5.3. Average soil properties along pile shaft and near pile toe

Test Site	SPT N-value		C_h (in^2/min)		C_v (in^2/min)		PI (%)	
	Shaft	Toe	Shaft	Toe	Shaft	Toe	Shaft	Toe
ISU2	5	4	0.0322	0.0276	0.0195	0.0175	14.86	28.40
ISU3	8	10	0.0070	0.0040	0.0158	0.0150	9.95	8.15
ISU4	10	13	0.0087	0.0023	0.0146	0.0155	15.44	13.06
ISU5	12	13	0.0043	0.0023	0.0140	0.0132	18.17	22.33
ISU6	14	22	0.0034	0.0008	0.0132	0.0143	9.22	7.43

At 1 day after EOD, Figure 5.11(a) shows that the increase in total pile resistance and shaft resistance is inversely proportional to SPT N-value for all five piles. Similarly, Figure 5.11(b) and (c) show that total pile resistance and shaft resistance of a pile increase linearly with the C_h and C_v values, respectively. However, Figure 5.11(d) shows that total pile resistance and shaft resistance increase with PI between 8% and 12%, which mainly represent the sandy low plasticity clay soils surrounding test piles ISU3 and ISU6 (see Appendix B). However, the continuous increase in PI above 12%, which represents the mostly low plasticity clay soils, with a higher affinity for water, at the test sites of ISU2, ISU4 and ISU5, results in a reduction of both total pile resistance and shaft resistance. Although the end bearing components were included in these figures, no clear correlations between the soil properties and the end bearing component are evident, as expected. This is largely due to relatively large deviations in the data resulting from: a) smaller contributions of the end bearing to total pile resistance; and b) small errors in the estimation of shaft resistance causing larger error to the end bearing components. The insignificance of the impact of the end bearing has also been confirmed by the comparable trends observed for both the shaft resistance and total pile resistance.

Most importantly, Figure 5.11 strongly supports the prospect of using routine in-situ (i.e., SPTs and/or CPTs with pore water pressure dissipation tests) and/or laboratory soil testing procedures (i.e., one-dimensional consolidation tests) to quantitatively estimate pile setup for use in the LRFD approach. Detailed laboratory soil classifications, PI estimations and soil layer identifications are also an essential part of our recommended systematic approach for routine and accurate pile setup estimations within the LRFD framework.

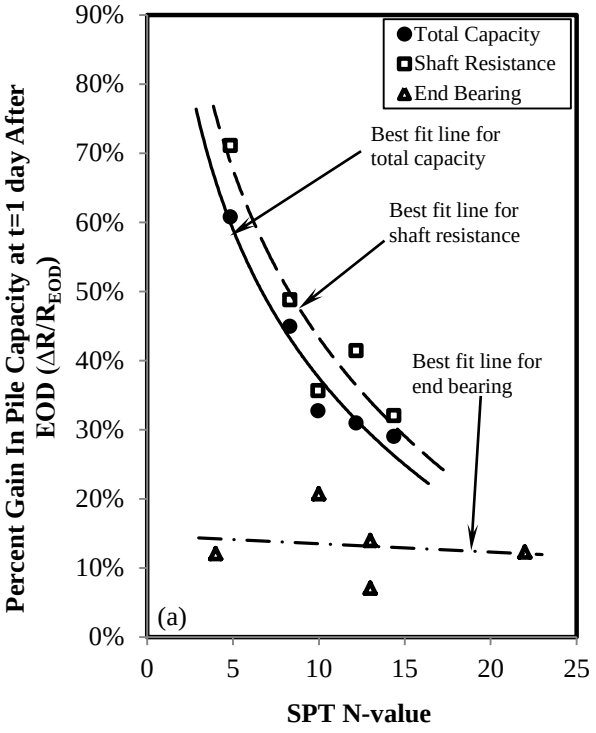

(a) Relation with SPT *N*-value

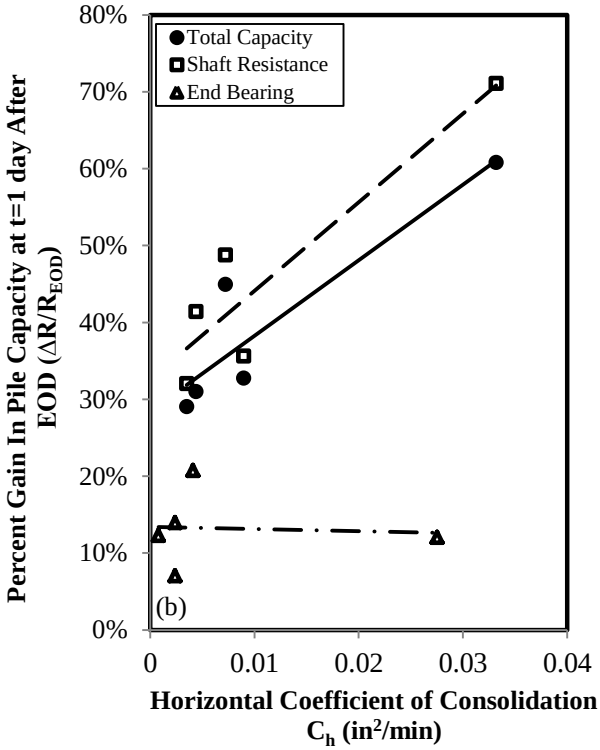

(b) Relation with C_h

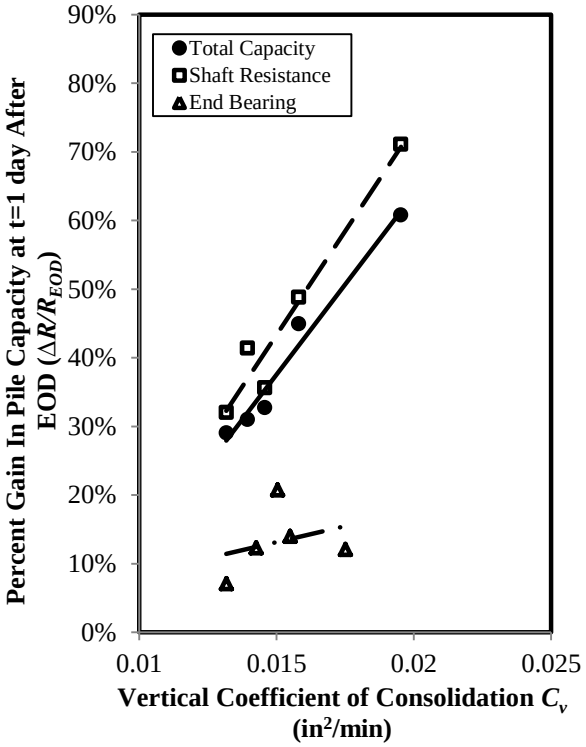

(c) Relation with C_v

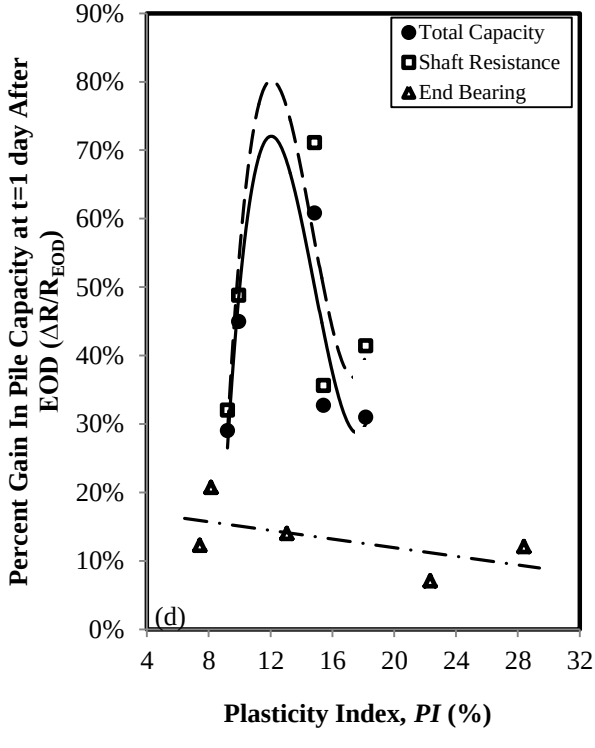

(d) Relation with *PI*

Figure 5.11. Relationships between percent gain in pile capacity and (a) SPT N-value, (b) C_h, (c) C_v, and (d) PI, estimated at a time of 1 day after EOD for all sites

5.6.2 Development of Pile Setup Analytical Quantification Methods

Using the field test results of steel H-piles driven in the clay soil profile, two analytical methods were established to quantify pile setup. Although existing methods found in literature, such as Skov and Denver (1988), have been utilized for decades, they require inconvenient re-strikes during construction and rarely correlate with any soil properties, even though these properties significantly influence the pile setup. To account for these limitations, the proposed methods were developed in terms of soil properties that can be measured using in-situ soil investigations, such as SPT and CPT. For convenient practical applications, the methods utilize the initial pile resistance estimated at the EOD condition (R_{EOD}) using either WEAP or CAPWAP. The first method described (CPT & SPT based setup method) incorporates the average SPT N-value (N_a) and horizontal coefficient of consolidation (C_h) determined from CPT to represent the surrounding soils, and employs an equivalent pile radius to represent the pile geometry. The average SPT N-value is calculated by weighting the measured N-value (N_i) at each cohesive soil layer, i, along the pile shaft by its thickness (ℓ_i) for the total number, n, of cohesive layers situated along the embedded pile length, simply expressed as:

$$N_a = \frac{\sum_{i=1}^{n} N_i \ell_i}{\sum_{i=1}^{n} \ell_i} \tag{5-2}$$

To further simplify the pile setup estimation for routine practical applications, the second method described (SPT based setup method) considers only the commonly used average SPT N-value.

When total pile resistance (R_t) and time (t), as shown in Figure 5.4, are normalized by initial pile resistance (R_{EOD}) and initial time (t_{EOD}) at EOD condition respectively, a linear relationship between normalized pile capacity (R_t/R_{EOD}) and logarithmic normalized time ($Log_{10}(t/t_{EOD})$) for each test pile is observed (see Figure 5.12 (a) and (b)), based on CAPWAP and WEAP analyses. To correct pile resistance gain resulting from additional pile penetrations during re-strikes, normalized pile resistance was multiplied with normalized pile embedded pile length (L_{EOD}/L_t). In order to satisfy the logarithmic relationship and to consider the immediate gain in pile resistance measured after EOD, the time at EOD (t_{EOD}) was assumed to be 1 minute (0.000693 day).

Each linear best fit line was generated using a linear regression analysis based on re-strike results, as indicated by open markers. Most linear lines fit reasonably well with the results, indicated with good coefficients of determination (R^2). For a comparative purpose, static load test results, indicated by filled markers, were also included. The slope (C) of each linear best fit line describes the rate of pile resistance gain, i.e., a linear line with a larger slope indicates a higher percentage of pile resistance gain or provides a larger normalized pile resistance (R_t/R_{EOD}) at a given time. It is important to recognize that the magnitude of the slope (C) is not a unique constant for all piles but its variation is dependent on the surrounding cohesive soil properties. The equation for the linear best fit lines can be expressed as:

$$\frac{R_t}{R_{EOD}} = \left[C\log_{10}\left(\frac{t}{t_{EOD}}\right) + 1\right]\left(\frac{L_t}{L_{EOD}}\right) \tag{5-3}$$

5.6.2.1 CPT & SPT based setup method

It is evident from the field test results (see Figure 5.7) that pile setup mostly occurs along a pile shaft, hence, only the cohesive soil layers along the pile shaft are considered. Ng (2011) derived that the pile setup rate (C) can be expressed as:

$$C = f_c\left(\frac{C_h}{N_a r_p^2}\right) + f_r \qquad (5\text{-}4)$$

where

f_c = consolidation factor (see Table 5.4), min.$^{-1}$;
f_r = remolding recovery factor (see Table 5.4);
C_h = horizontal coefficient of consolidation as described in Section 5.2, in^2/min.;
N_a = average SPT N-value given by Eq. (5-2); and
r_p = equivalent pile radius, in.

Using the pile setup rate (C) determined from Figure 5.12, the relationships between the pile setup rate and measured soil parameters (SPT N-value and C_h), summarized in Table 5.3, were plotted (see Figure 5.13) to evaluate the f_c and f_r factors for CAPWAP and WEAP (using Iowa Blue Book as soil profile input method for illustrative purposes). The f_c and f_r factors are tabulated in Table 5.4 together with the coefficients of determination (R^2), which indicate the accuracy of future pile setup rate predictions using Eq. (5-4). This clearly demonstrates that pile setup rates estimated using CAPWAP will provide a better accuracy than WEAP estimates.

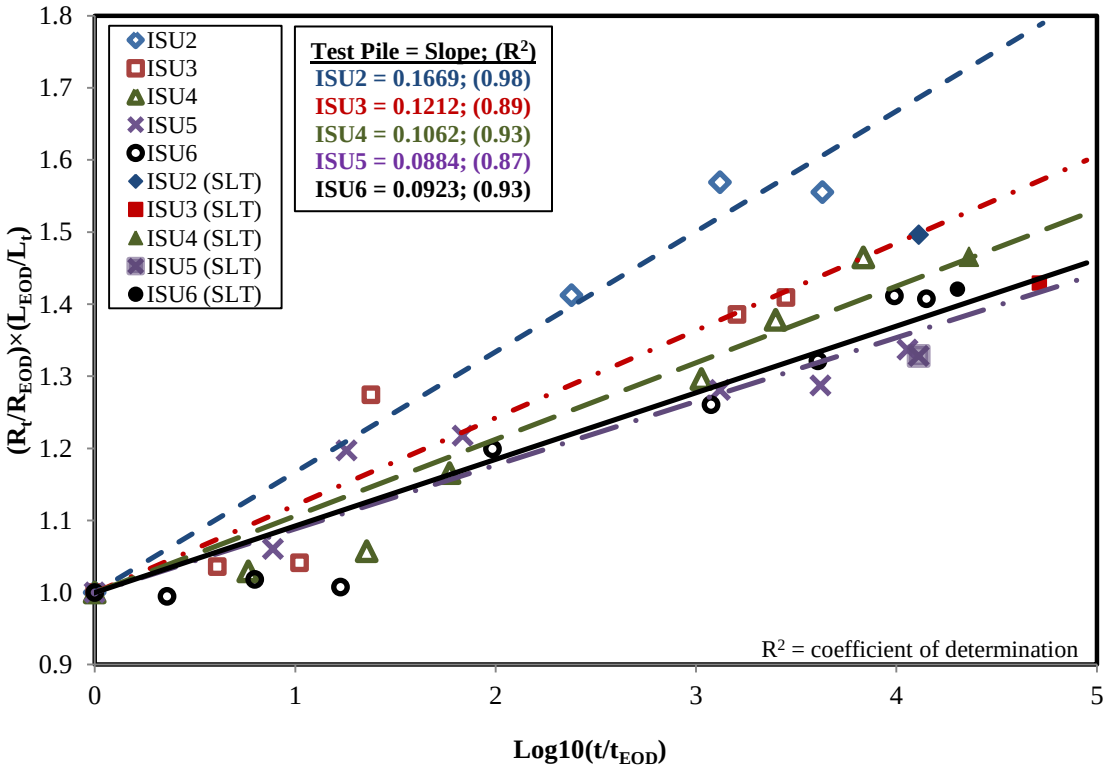

(a) Based on CAPWAP analysis

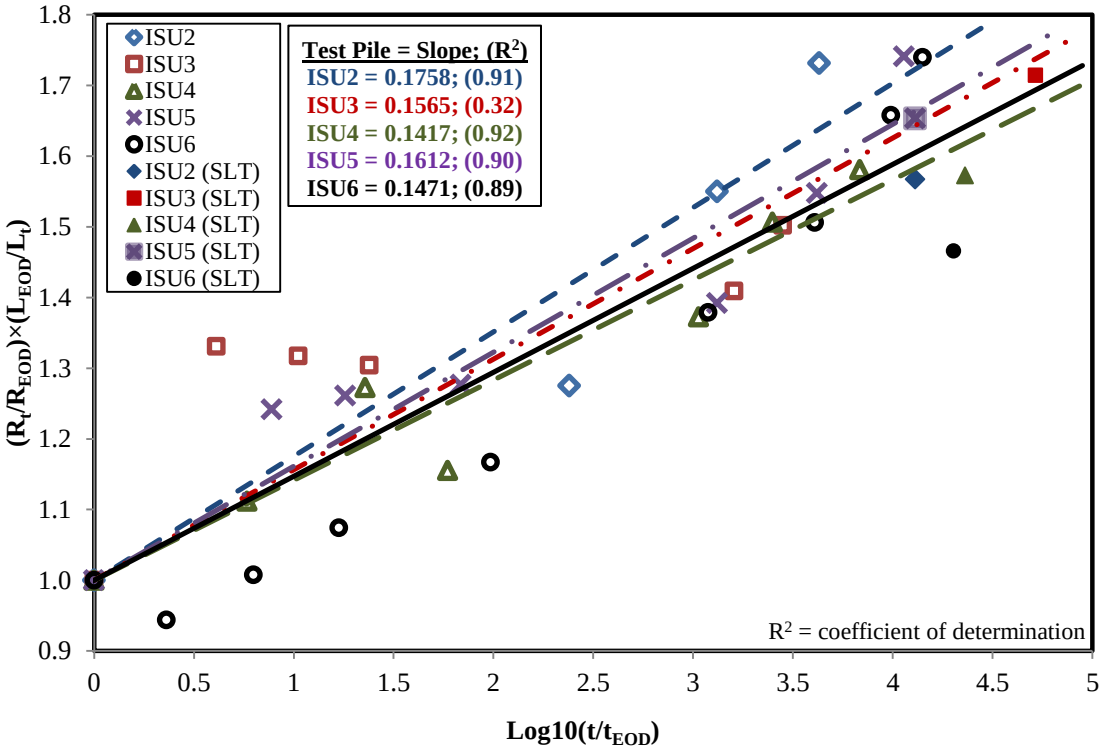

(b) Based on WEAP analysis using Iowa Blue Book as soil profile input method

Figure 5.12. Linear best fit lines of normalized pile resistance and logarithmic normalized time

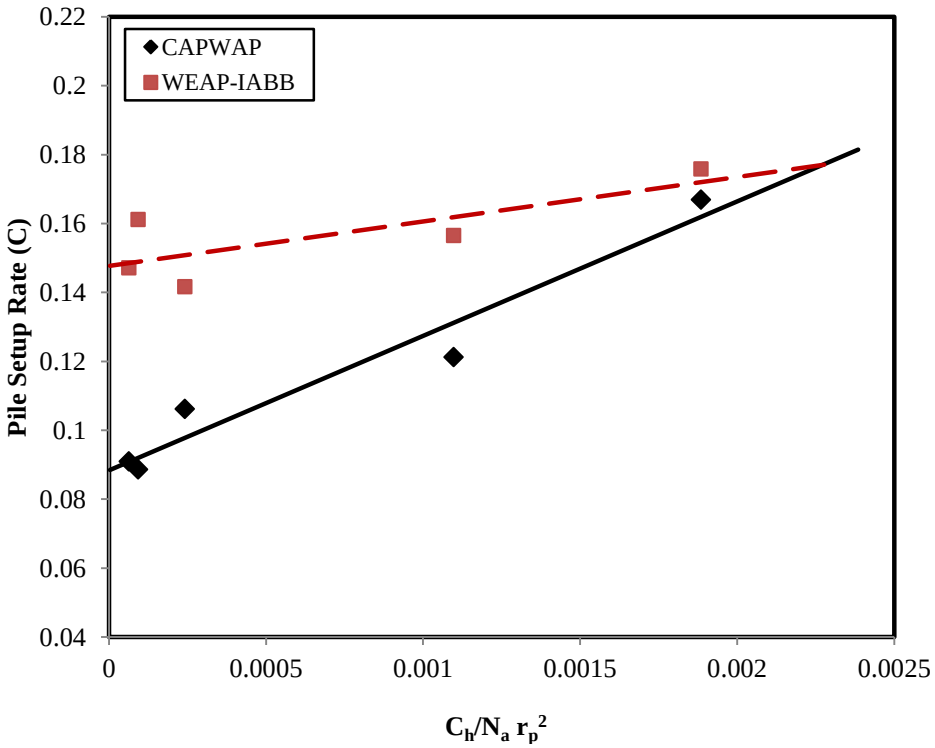

Figure 5.13. Correlation between pile setup rate (C) and soil parameters with pile radius

Table 5.4. The consolidation (f_c) and remolding recovery (f_r) factors

Method	Consolidation Factor, f_c ($min.^{-1}$)	Remolding Recovery Factor, f_r	Coefficient of Determination, R^2
CAPWAP	39.048	0.088	0.95
WEAP-ST	19.565	0.155	0.39
WEAP-SA	13.780	0.150	0.65
WEAP-DRIVEN	13.590	0.149	0.70
WEAP-Iowa Blue Book	12.889	0.148	0.60
WEAP-Iowa DOT	15.497	0.147	0.60

5.6.2.2 SPT based setup method

In order to simplify the pile setup estimation during designs based on the commonly used SPT, the pile setup rates determined, from Figure 5.12, are directly compared with the corresponding average SPT N-values, given in Table 5.3. Figure 5.14 shows best fitted power-function relationships between pile setup rates and SPT N-values. More generally, these relationships can be expressed as:

$$C = \frac{a}{N_a^b} \tag{5-5}$$

where

a = method dependent scale factor (see Table 5.5);
b = method dependent concave factor (see Table 5.5); and
N_a = average SPT N-value given by Eq. (5-2).

The a and b factors are tabulated in Table 5.5 together with the coefficients of determination (R^2), which indicate the accuracy of future pile setup rate predictions using Eq. (5-5). Figure 5.14 shows that the increase in pile resistance is inversely proportional to SPT N-values. Hence, a pile embedded in a denser clayey soil represented with a higher average SPT N-value experiences a smaller gain in resistance. It is clearly shown that pile setup rate will be best estimated using CAPWAP. Among the five different soil profile input procedures used in WEAP, Iowa Blue Book procedure, which resulted in the highest R^2 of 0.52, is recommended for the total pile resistance (R_t) estimation using Eq. (5-6), which was derived by substituting Eq. (5-5) into Eq. (5-3). It is important to recognize in the case for WEAP that the CPT&SPT based method gives a better pile setup prediction than the SPT based method.

$$\frac{R_t}{R_{EOD}} = \left[\frac{a\ \log_{10}\left(\frac{t}{t_{EOD}}\right)}{(N_a)^b} + 1\right]\left(\frac{L}{L_{EOD}}\right) \tag{5-6}$$

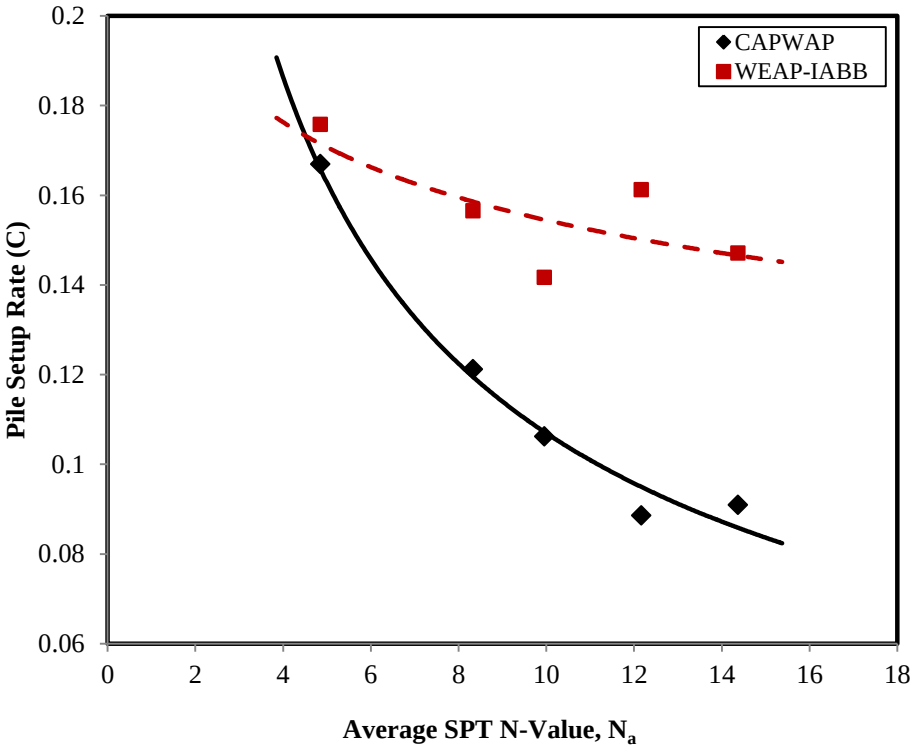

Figure 5.14. Correlation between pile setup rate (C) and average SPT N-value

Table 5.5. Scale (a) and concave (b) factors

Method	a	b	Coefficient of Determination, R^2
CAPWAP	0.432	0.606	0.97
WEAP-ST	0.243	0.168	0.24
WEAP-SA	0.217	0.141	0.47
WEAP-DRIVEN	0.214	0.136	0.48
WEAP-Iowa Blue Book	0.215	0.144	0.52
WEAP-Iowa DOT	0.246	0.192	0.26

To provide pile designers a quick and convenient approach to estimate total pile resistance including setup resistance using either WEAP (Iowa Blue Book procedure) or CAPWAP, Eq. (5-6) was transformed into pile setup design charts in terms of corrected normalized pile resistance $((R_t/R_{EOD})\times(L_{EOD}/L))$ based on a range of average SPT N-value (N_a), between 1 and 50, and a time lapsed (t), at days 1, 3, 5, 7, 14, 21 and 30 after EOD, as plotted in Figure 5.15.

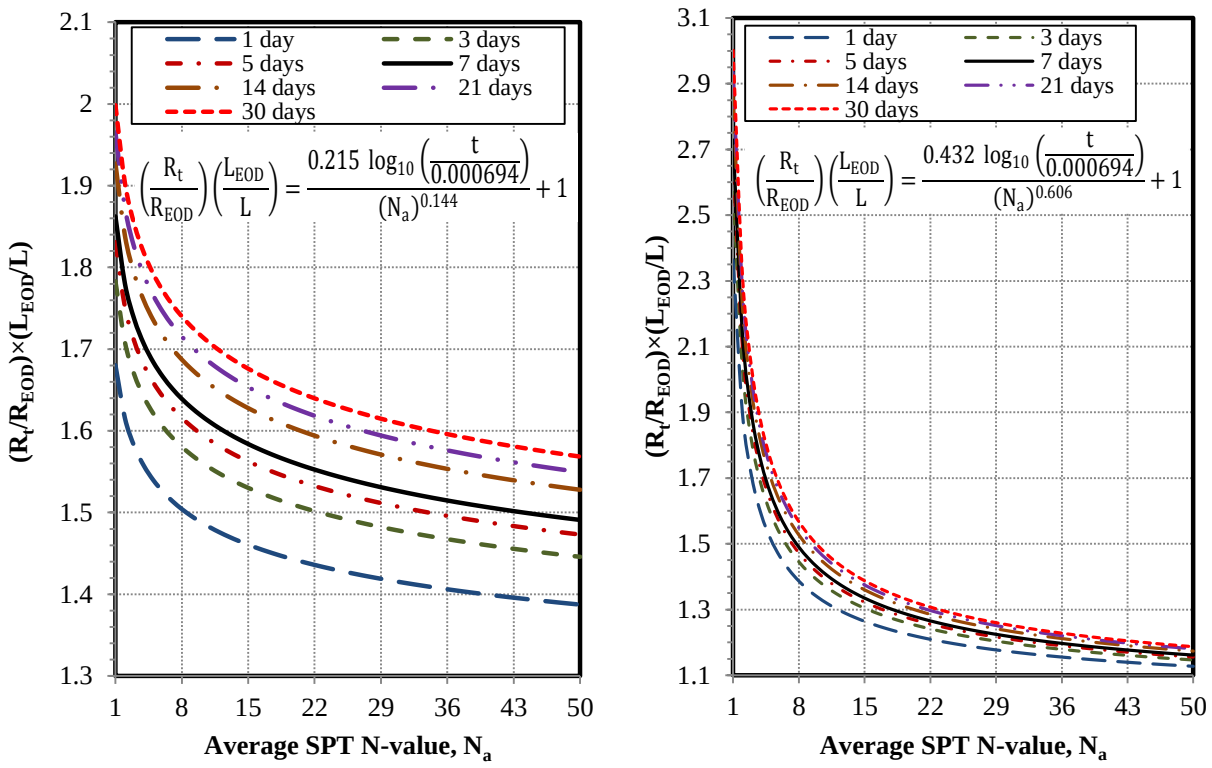

(a) WEAP (Iowa Blue Book) (b) CAPWAP

Figure 5.15. Pile setup design charts for WEAP and CAPWAP

Although pile setup is estimated at a specified time, for example 7 days, after EOD during design, the estimated pile setup can be optionally verified during construction before the specified time. Verification of expected pile setup at 7 days is performed by comparing the pile resistance estimated using either WEAP or CAPWAP during re-strikes with the pile setup site verification charts given in Figure 5.16. Because pile re-strike is considered as an inconvenient construction practice, which is generally performed within a short time after pile installation, pile setup site verification charts are a more convenient means to confirm the pile setup estimated during design. For instance, referring to Figure 5.16(a), the pile resistance ratio of 1.55 measured using WEAP from a re-strike at 2 days after EOD (represented by Line A) coincides with a dashed line that corresponds to an average SPT N-value of 8. Following along the same dashed line, the pile resistance ratio of 1.65 (or 65% increase in pile resistance) is determined from the chart as occurring at 7 days after EOD (represented by Line B). Finally, the determined 65% increase in pile resistance can be verified against the initially estimated setup resistance, so the amount of expected setup is ensured early before the design setup time of 7 days.

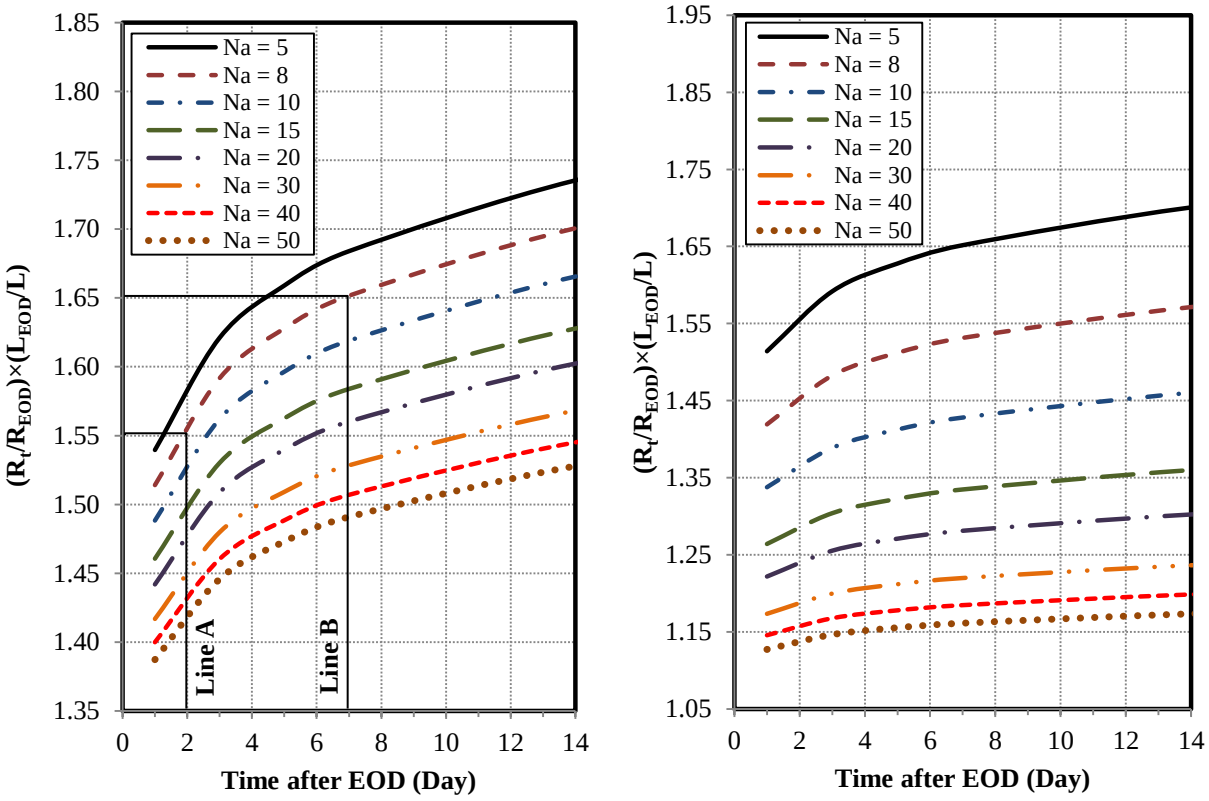

(a) WEAP (Iowa Blue Book) (b) CAPWAP

Figure 5.16. Pile setup site verification charts for WEAP and CAPWAP

5.6.3 Pile Setup Validation

To validate the proposed pile setup quantification methods based on WEAP, twelve data points with piles embedded in the clay profile were selected from PILOT, as listed in Table 5.6, along with the recently completed five field tests. Since PILOT contains no PDA record, only the field tests were used in the validation of the pile setup methods based on CAPWAP. Based on the calculated average soil parameters (N_a and/or C_h) the total pile resistance (R_t), including pile setup resistance, was computed using the CPT&SPT based setup method (Eq. (5-3) and Eq. (5-4)) and SPT based setup method (Eq. (5-6)) for both CAPWAP and WEAP, as listed in Table 5.7. To illustrate the effect of pile setup, pile resistances estimated at EOD condition (i.e., without considering pile setup) and pile resistances estimated at the time of load tests were compared with the measured pile resistances using static load tests, as shown in Figure 5.17. When considering pile setup effect using the two proposed methods for CAPWAP, Figure 5.17(a) illustrates that the mean values (μ) shift towards unity, from 1.483 to 0.978 and 0.995, and the standard deviations (StDev or δ) reduce from 0.069 to 0.052 and 0.058 for CPT&SPT based setup method and SPT based setup method, respectively. Similar results are observed for setup methods using WEAP, as illustrated from Figure 5.17(b). This clearly shows that the proposed pile setup methods have adequately and consistently predicted the increase in pile resistances at the given time when the corresponding measured values were taken. This statistical assessment validates the proposed pile setup methods. Additional validations were documented in Ng (2011).

Table 5.6. Summary of the twelve data records from PILOT

Project ID	County in Iowa	Pile Type	Pile Penetration (ft)	Hammer Type	Soil Profile Description	Average SPT N-value, N_a	Average C_h (in^2/min)	Time After EOD, t (day)	SLT Measured Pile Resistance at Time t (kip)	WEAP-IABB Estimated Pile Resistance at EOD (kip)
6	Decatur	HP 10 × 42	53	Gravity #732	Glacial clay	14.47	0.00631	3	118	71
12	Linn	HP 10 × 42	23.78	Kobe K-13	Glacial clay	29.90	0.00045	5	204	155
42	Linn	HP 10 × 42	23.5	Kobe K-13	Glacial clay	22.20	0.00147	5	82	85
44	Linn	HP 10 × 42	36.5	Delmag D-22	Sandy silty clay	22.34	0.00083	5	136	94
51	Johnson	HP 10 × 42	29.5	Kobe K-13	Silt/glacial clay	40.00	0.00022	3	190	128
57	Hamilton	HP 10 × 42	57	Gravity #2107	Glacial clay	9.77	0.00469	4	168	94
62	Kossuth	HP 10 × 42	45	MKT DE-30B	Glacial clay	36.05	0.00279	5	100	76
63	Jasper	HP 10 × 42	63	Gravity	Silt on glacial clay	8.32	0.00665	2	66	59
64	Jasper	HP 10 × 42	71	Gravity	Silt on glacial clay	10.52	0.00479	1	122	71
67	Audubon	HP 10 × 42	32	Delmag D-12	Glacial clay	20.00	0.00094	4	140	121
102	Poweshiek	HP 10 × 42	43	Gravity #203	Silt/glacial clay	16.45	0.00620	8	130	84
109	Poweshiek	HP 12 × 53	51	Delmag D-12	Glacial clay	17.36	0.00204	3	176	147

Table 5.7. Summary of the estimated pile resistance including setup

Project ID	Pile Resistance Based on SPT & CPT (Eq. 5-3 & Eq. 5-4) (kip)		Pile Resistance Based On SPT (Eq. 5-6) (kip)	
	CAPWAP	WEAP-Iowa Blue Book	CAPWAP	WEAP-Iowa Blue Book
6	Not Available	109	Not Available	108
12		243		234
42		133		130
44		134		144
51		197		187
57		146		148
62		119		113
63		90		91
64		104		105
67		188		184
102		135		134
109		226		223
ISU2	139	136	136	132
ISU3	153	150	154	144
ISU4	150	162	149	159
ISU5	252	237	247	231
ISU6	208	238	198	229

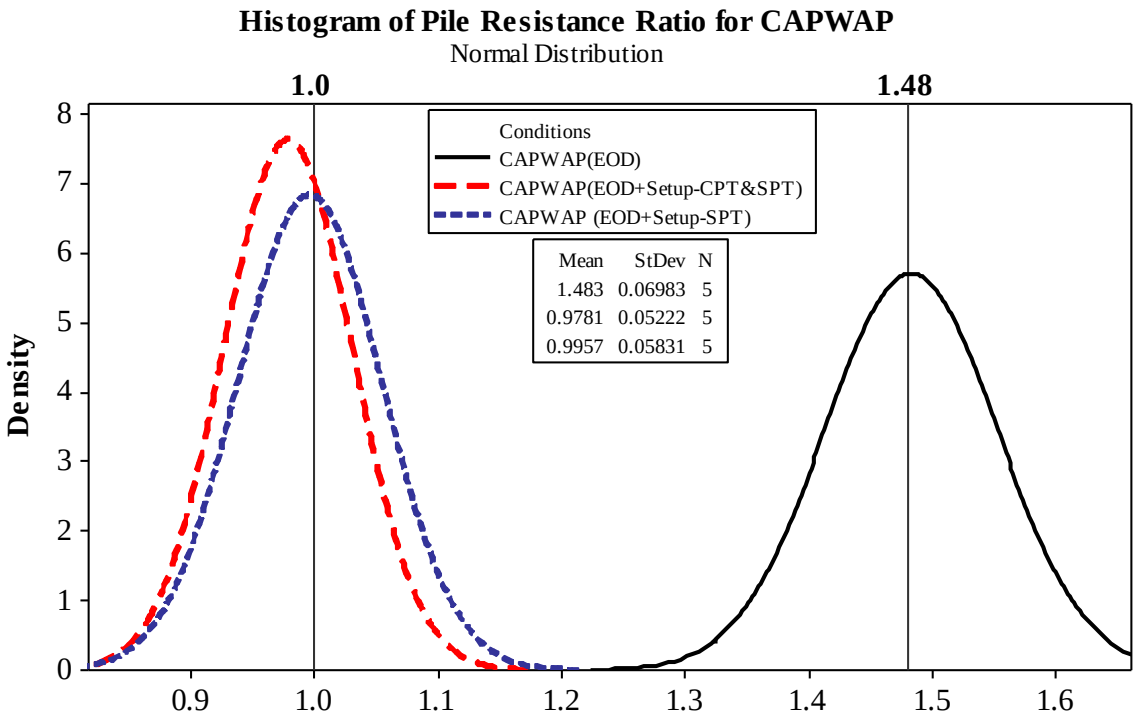

(a) CAPWAP

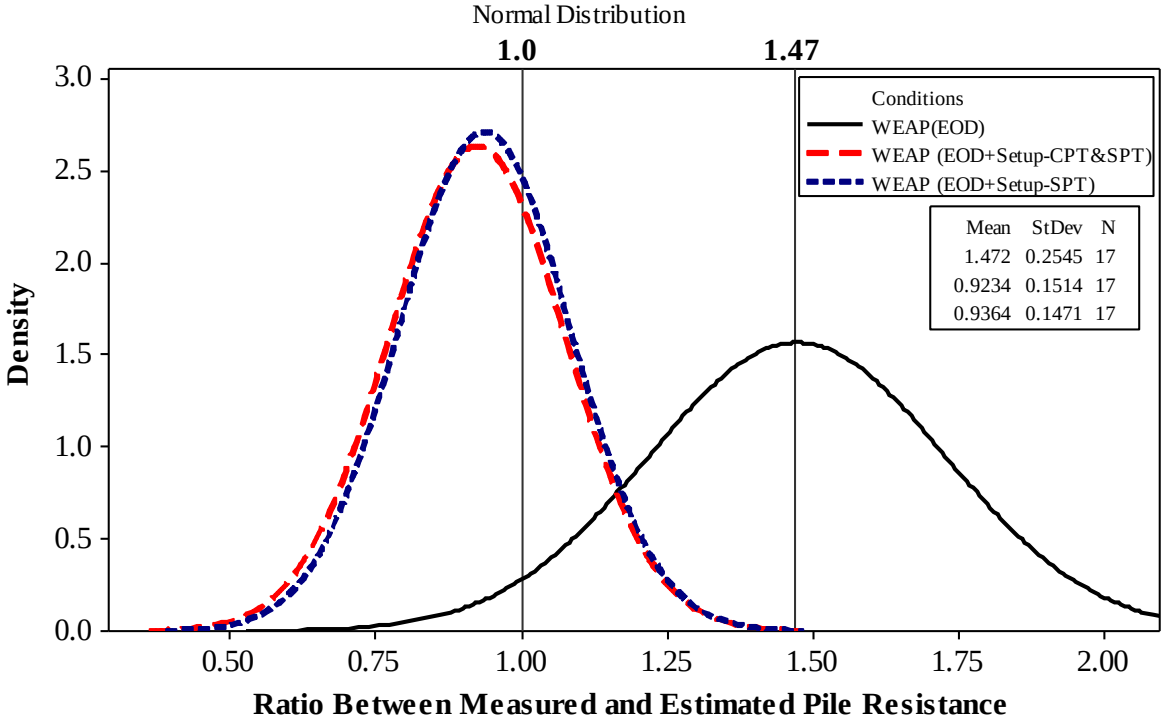

(b) WEAP based on Iowa Blue Book soil input procedure

Figure 5.17. Pile setup comparison and validation

Following the validation of the proposed pile setup methods, the confidence of the methods in terms of the pile resistance ratio (R_m/R_t) at different confidence intervals can be expressed as:

$$\left(\frac{R_m}{R_t}\right)_{\substack{\text{upper}\\\text{bound}}} = \mu + z \times \frac{\delta}{\sqrt{n}}$$
$$\left(\frac{R_m}{R_t}\right)_{\substack{\text{lower}\\\text{bound}}} = \mu - z \times \frac{\delta}{\sqrt{n}} \quad (5\text{-}7)$$

where

μ = mean value of the pile resistance ratio;
z = standard normal parameter based on a chosen percent of confidence interval (CI);
δ = standard of deviation of the pile resistance ratio; and
n = sample size.

Using the statistical parameters (μ, δ and n) calculated in Figure 5.17, the upper and lower limits of the population mean values of the pile resistance ratios for 80%, 85%, 90%, 95%, and 98% confidence intervals (CIs) are calculated, using Eq. (5-7), and plotted in Figure 5.18 (a) and (b) for the CPT & SPT based and SPT based pile setup methods respectively. Figure 5.18 shows that the upper limits increase and the lower limits decrease with increasing CIs from 80% to 98%. In an attempt to determine the amount of pile setup that can be confidently applied directly to production piles in the State of North Carolina, Kim and Kreider (2007) suggested the use of 98% and 90% CIs for individual piles and pile groups with redundancy, respectively, which were assumed based on their field observations. Applying this similar recommendation in the case of an individual pile by considering a 98% CI, the pile resistance ratio for WEAP ranges between 0.85 and 1.02 (refer to Figure 5.18 (b) for an illustrative purpose). In other words, there is 98% confidence that the SPT based pile setup method when used in conjunction with WEAP will predict the R_t with an error falling between -17.2% and 1.9%. Similarly, in the case of a pile group foundation considering a 90% CI, the proposed SPT based pile setup when used in conjunction with WEAP, the error will fall between -13.9% and -0.5%. The anticipated errors of the pile setup methods at various confidence levels are summarized in Table 5.8. It is generally observed that the range of errors is smaller for pile setup methods used in conjunction with CAPWAP than those with WEAP.

Table 5.8. Anticipated errors of the pile setup methods at various confidence levels

Confidence Level	Anticipated Errors (%)			
	SPT & CPT Based Setup Method		SPT Based Setup Method	
	CAPWAP	WEAP-Iowa Blue Book	CAPWAP	WEAP-Iowa Blue Book
80	-5.5% to 0.8%	-14.2% to -3.1%	-4% to 2.8%	-12.2% to -1.8%
90	-6.4% to 1.7%	-15.9% to -1.6%	-4.9% to 3.8%	-13.9% to -0.5%
98	-8.2% to 3.1%	-19.3% to 0.9%	-7% to 5.3%	-17.2% to 1.9%

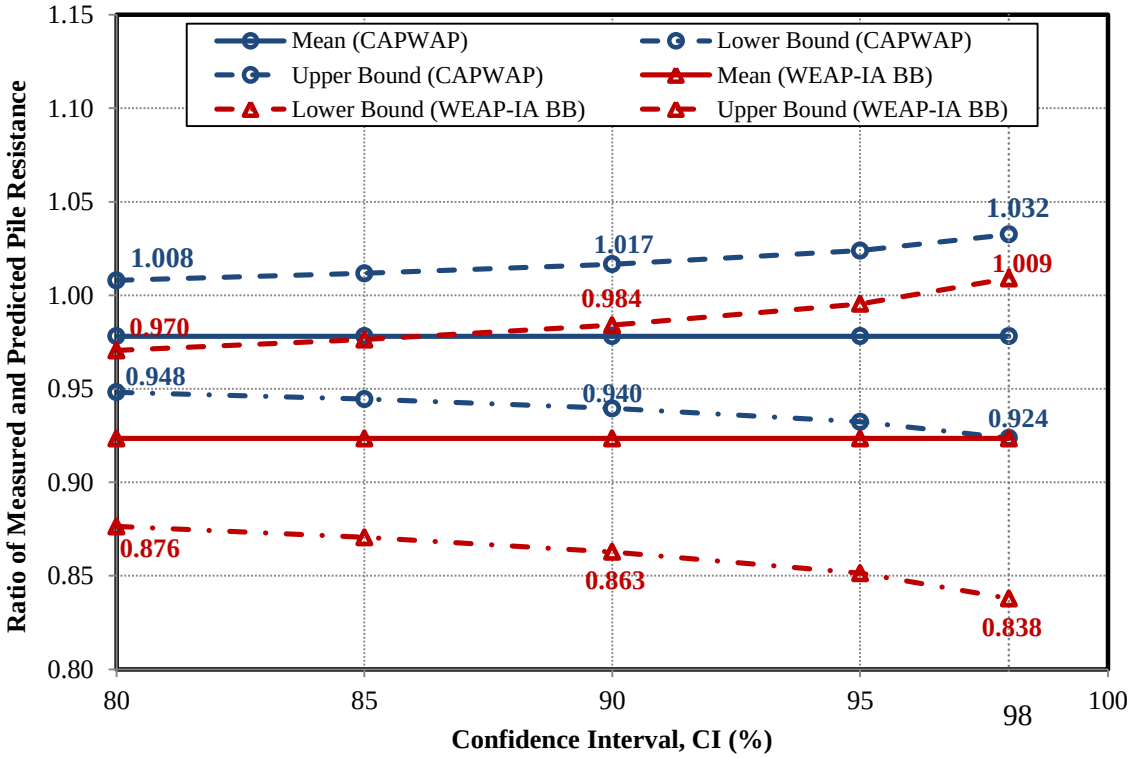

(a) CPT & SPT based pile setup method

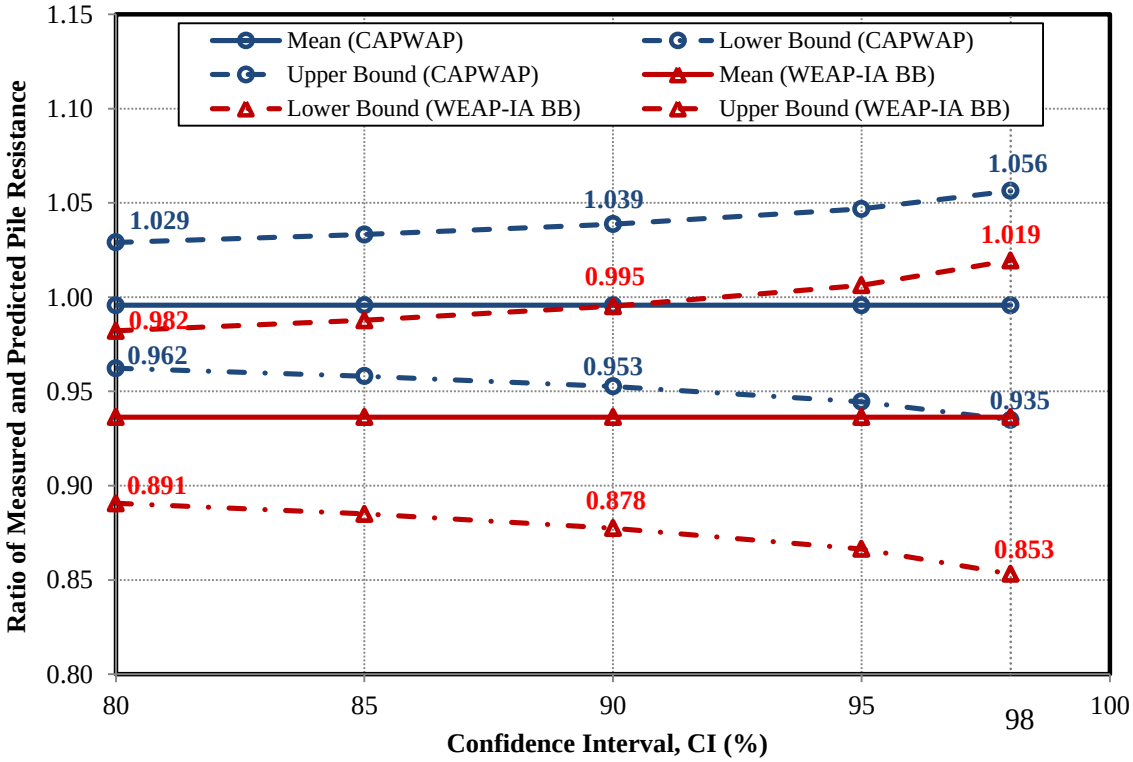

(b) SPT based pile setup method

Figure 5.18. Pile setup confidence levels

5.6.4 LRFD Calibration for Pile Setup

Although pile setup has been systematically quantified using the aforementioned proposed methods, the setup quantification has its own uncertainties resulting from in-situ measurements of soil properties and the semi-empirical approach adapted for the effects of setup. To incorporate such a pile setup estimate in LRFD satisfactorily, it should be realized that the impact of the uncertainties associated with the initial pile resistance at EOD (R_{EOD}), estimated using the dynamic analysis methods, and the pile setup resistance (R_{setup}), estimated using the proposed methods, are different and they should be accounted for simultaneously to reach the same target reliability index. While ensuring that the reliability theory based LRFD framework is adequately followed in this process, it also enables incorporation of two resistance factors: one for the initial pile resistance and other for the pile setup resistance. In order to provide a general and closed-form solution, the derivation of the resistance factors for pile setup follows the First Order Second Moment (FOSM) method. To illustrate this, the following evaluation is based on the proposed SPT based pile setup method using Eq. (5-6) for WEAP based on the Iowa Blue Book soil input procedure.

In order to evaluate the uncertainties associated with initial pile resistance at EOD and setup, twelve data records from PILOT, as listed in Table 5.6, along with the five field tests were used. To compare the various sources of uncertainties in terms of coefficient of correlation (COV_R), two different resistance ratio estimators (RRE) for EOD condition ($R_{m\text{-}EOD}/R_{e\text{-}EOD}$) and for setup ($R_{m\text{-}setup}/R_{e\text{-}setup}$), based on the measured (R_m) and estimated (R_e) pile resistances, were calculated, as listed in Table 5.9. Since pile resistances were measured using SLT at time (t) after EOD, the measured pile resistances at EOD ($R_{m\text{-}EOD}$) for the data points from PILOT were adjusted using the SPT based pile setup Eq. (5-6) while the CAPWAP estimates at EOD were used for the data points from field tests. The measured pile setup resistance ($R_{m\text{-}setup}$) was determined to be the difference between the SLT measured pile resistance at any time ($R_{m\text{-}t}$) and the initial pile resistance at EOD ($R_{m\text{-}EOD}$). Figure 5.19 shows the different theoretical normal distribution curves, representing different COV values of 0.181 and 0.330 for EOD and setup respectively, and highlights the different uncertainties associated with initial pile resistance at EOD and setup resistance. The large difference in COV values confirms the disparity in the associated uncertainties and promotes the development of resistance factors separately for EOD condition and effects of setup.

Considering the AASHTO (2007) strength I load combination for axially loaded piles, the equation of the resistance factor for pile setup (φ_{setup}) was derived as:

$$\varphi_{setup} = \frac{\lambda_{setup}\left[\dfrac{\gamma_D\left(\frac{Q_D}{Q_L}\right)+\gamma_L}{1+\left(\frac{Q_D}{Q_L}\right)} - \varphi_{EOD}\alpha\right]}{\left(\dfrac{\lambda_D\left(\frac{Q_D}{Q_L}\right)+\lambda_L}{1+\left(\frac{Q_D}{Q_L}\right)}\right)e^{\beta_T\sqrt{\ln\left[\left(1+COV_{R_{EOD}}^2+COV_{R_{setup}}^2\right)\left(1+COV_{Q_D}^2+COV_{Q_L}^2\right)\right]}}\sqrt{\dfrac{\left(1+COV_{Q_D}^2+COV_{Q_L}^2\right)}{\left(1+COV_{R_{EOD}}^2+COV_{R_{setup}}^2\right)}} - \lambda_{EOD}\alpha} \quad (5\text{-}8)$$

where

λ_{EOD} = the resistance bias factor of the resistance ratio estimator for EOD;
λ_{setup} = the resistance bias factor of the resistance ratio estimator for setup;
COV_{REOD} = the coefficient of variation of the resistance ratio estimator for EOD;
COV_{Rsetup} = the coefficient of variation of the resistance ratio estimator for setup;
φ_{EOD} = resistance factor for initial pile resistance at EOD;
α = ratio between initial pile resistance and total serviced dead and live loads, $(R_{EOD}/(Q_D+Q_L))$;
β_T = target reliability index;
γ_D, γ_L = the dead load factor (1.25) and live load factor (1.75);
λ_D, λ_L = the dead load bias (1.05) and live load bias (1.15);
COV_D, COV_L = the coefficients of variation of dead load (0.1) and live load (0.2); and
Q_D/Q_L = dead to live load ratio.

Table 5.9. Summary of resistance ratio estimators for EOD and setup

Project ID	Measured Pile Resistance at EOD, $R_{m\text{-}EOD}$ (kip)	Measured Pile Setup Resistance, $R_{m\text{-}setup}$ (kip)	Estimated Pile Resistance at EOD, $R_{e\text{-}EOD}$ (kip)	Estimated Pile Setup Resistance, $R_{e\text{-}setup}$ (kip)	RRE for EOD ($R_{m\text{-}EOD}/R_{e\text{-}EOD}$)	RRE for Setup ($R_{m\text{-}setup}/R_{e\text{-}setup}$)
6	77[a]	47[c]	71	38	1.09	1.26
12	135[a]	49[c]	155	79	0.87	0.62
42	54[a]	28[c]	85	45	0.63	0.63
44	89[a]	42[c]	94	50	0.95	0.84
51	130[a]	62[c]	128	59	1.02	1.05
57	106[a]	75[c]	94	55	1.14	1.37
62	67[a]	24[c]	76	37	0.88	0.65
63	43[a]	23[c]	59	32	0.72	0.72
64	82[a]	51[c]	71	34	1.16	1.49
67	92[a]	48[c]	121	63	0.76	0.76
102	82[a]	46[c]	84	49	0.97	0.92
109	116[a]	29[c]	147	76	0.79	0.38
ISU2	81[b]	44[d]	77	54	1.05	0.81
ISU3	99[b]	51[d]	82	62	1.20	0.83
ISU4	102[b]	52[d]	95	64	1.07	0.82
ISU5	178[b]	65[d]	143	88	1.24	0.74
ISU6	145[b]	68[d]	140	89	1.03	0.77

[a] – adjusted from SPT based pile setup equation;
[b] – CAPWAP estimates at EOD;
[c] – difference between SLT measured pile resistance at time (t) and initial pile resistance at EOD using WEAP; and
[d] – difference between SLT measured pile resistance at time (t) and initial pile resistance at EOD using CAPWAP.

The detailed derivation of Eq. (5-8), based on the original FOSM and its assumptions of lognormal distribution and a mutually independent relationship between load and resistance, were explicitly described by Ng (2011). Eq. (5-8) reveals that the φ_{setup} value is dependent on various parameters. The probabilistic characteristics (γ, λ and COV) of the random variables Q_D and Q_L are defined in Eq. (5-8) with the recommended values recapitulated in parentheses (Nowak 1999). The probabilistic characteristics (λ and COV) of the random variables R_{EOD} and R_{setup} were determined in Figure 5.19. The target reliability indices (β_T) of 2.33 (corresponding to 1% probability of failure) and 3.00 (corresponding to 0.1% probability of failure), as recommended, for representing redundant and non-redundant pile groups respectively (Paikowsky et al. 2004), were selected for the calculations. Neglecting the effect of pile setup and assuming the Q_D/Q_L ratio of 2.0, the φ_{EOD} values were determined to be 0.66 and 0.55 for the

β_T values of 2.33 and 3.00, respectively, using the original FOSM. Therefore, the φ_{setup} value can be determined depending on the α value, the only remaining unknown, as plotted in Figure 5.20. This figure illustrates that with an increase in α values from 0.2 to 1.73 the φ_{setup} values reduce by a factor of 2.2 and 1.7 for β_T values of 2.33 and 3.00, respectively. It also shows that the φ_{setup} values for β_T value of 2.33 are greater than those for β_T value of 3.00, except when α values become greater than 1.73 where the opposite is seen. The continuous increase in α values correlates with φ_{setup} values that reduce towards zero. This means that pile setup effect could be ignored in pile design at an extremely high R_{EOD} value with respect to total load. Similar observations are observed for the efficiency factors (φ/λ). It is reasonable for Eq. (5-8) to yield a smaller φ_{setup} value when the estimated R_{EOD} is much higher than the loads, so the computed total factored pile resistances are not significantly larger than the factored loads, resulting in an over conservative design. Therefore, an efficient driven pile system shall consider the optimum contribution from pile setup resistance by having a smaller α value, which may be accomplished by having a smaller pile group with a shorter individual pile length.

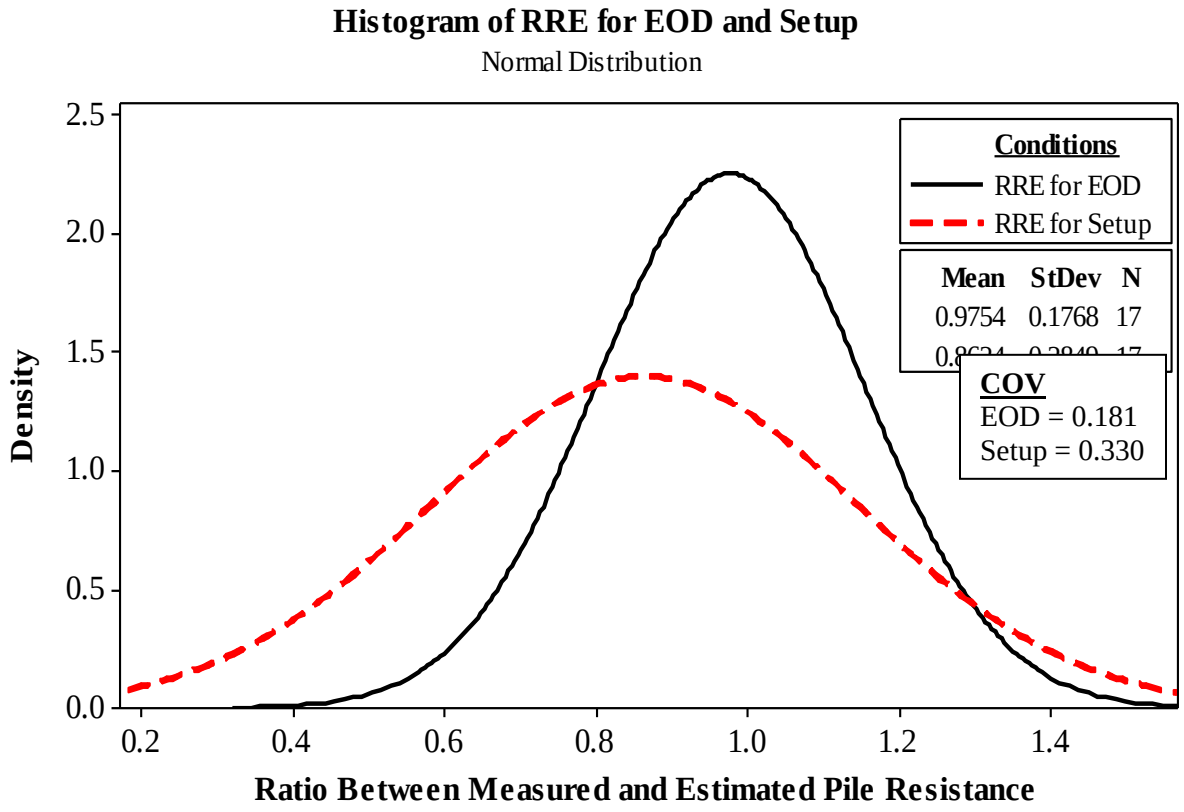

Figure 5.19. Different uncertainties involved between EOD and setup

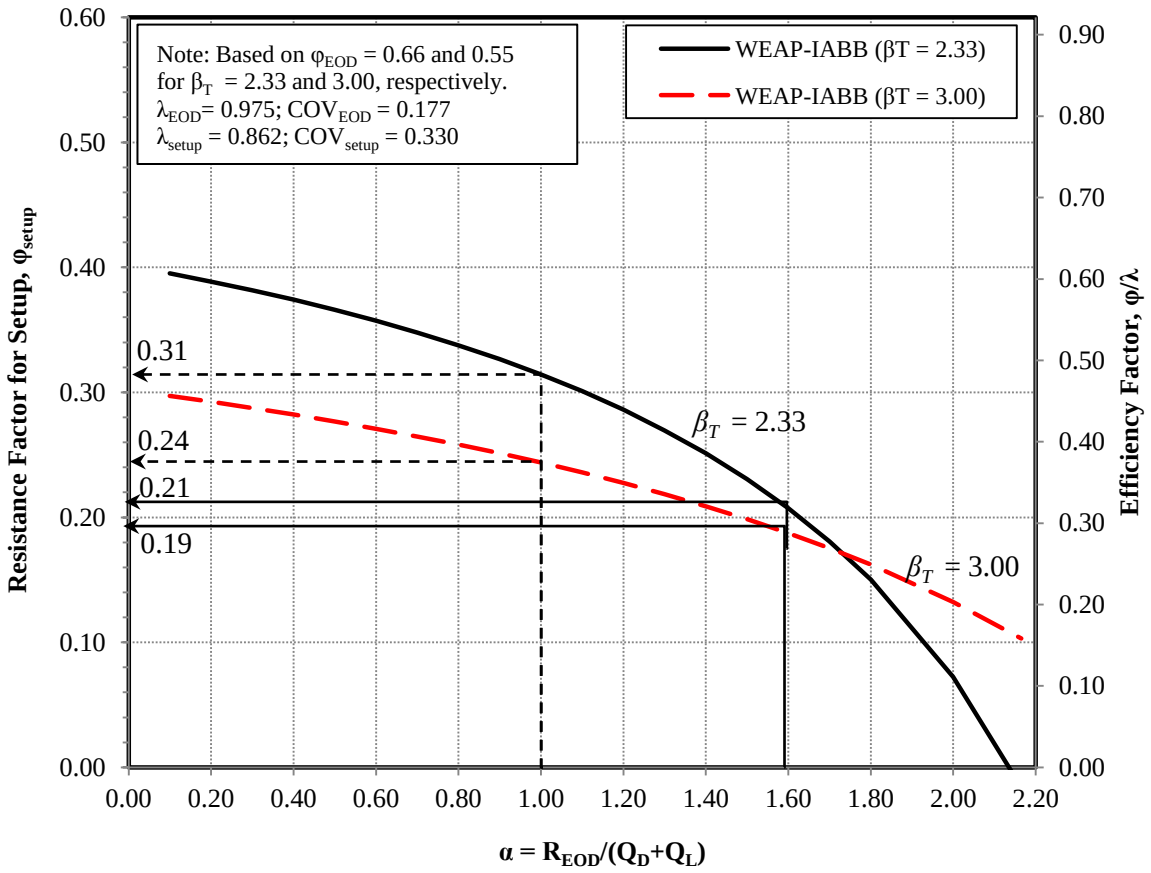

Figure 5.20. Resistance factor for pile setup resistance

To reflect the Iowa DOT's current practice, α values were computed based on design and driving information of production piles installed at six ISU's field test sites as summarized in Table 5.10. The location of abutments, production pile sizes, soil profiles classified in accordance to the procedure described in Section 2.1.2, and actual driven pile lengths are summarized. Given the total serviced load (Q_D+Q_L) exerting on each production pile and the measured driving resistance determined at EOD (R_{EOD}) using WEAP, α value (i.e., $\frac{R_{EOD}}{Q_D+Q_L}$) is calculated for each location except for those with either no driving information or situated in a mixed soil profile. Figure 5.21 shows the histogram and theoretical normal distribution of the computed α values given in Table 5.10. Among the five calculated α values, three values fall between 2.0 and 3.0 while the other two are greater than 3.0. Based on the theoretical normal distribution, the mean and standard deviation were determined to be 2.74 and 0.41, respectively. If this average α value of 2.74 would have been used to determine φ_{setup} from Figure 5.20, the contribution of pile setup will be neglected in the proposed LRFD framework (i.e., φ_{setup} is less than zero) . Before making any recommendations, α values were re-evaluated based on additional and independent data sets given by Iowa DOT on completed production steel H-piles as summarized in Table 5.11. These additional data were taken from 17 project sites at 10 different counties in Iowa. The location of the production piles, pile sizes, description of embedded soils, and plan pile lengths are tabulated accordingly. A total of 604 piles was selected for a similar analysis, and the histogram and theoretical normal distribution of α values are shown in Figure 5.22. The normal distribution shows that the mean and standard deviation are 2.78 and 0.95, respectively. This mean value of

2.78 is comparable to the mean value of 2.74 determined in Figure 5.21, in which the effect of pile setup would be neglected. Furthermore, most of the α values shown in both Figure 5.21 and Figure 5.22 are higher than the target value of 2.0, which is determined based on current Iowa LRFD design practice as illustrated

$$\alpha = \frac{R}{Q_T} = \frac{\gamma}{\varphi} = \frac{1.45}{0.725} = 2.0 \quad (5\text{-}9)$$

where

R = the nominal pile resistance estimated using Iowa Blue Book;
Q_T = total service load or dead plus live loads;
φ = resistance factor of 0.725 currently used in a pile design using Iowa Blue Book method; and
γ = equivalent load factor of 1.45 adopted by Iowa DOT.

Table 5.10. Summary of information on production piles at ISU test sites

Production Piles at Location of ISU's Test Pile	Abutment	Production Pile Size	Classified Soil Profile	Actual Driven Length (ft)	Serviced Load Per Pile, Q_D+Q_L (kip)	Measured Nominal Driving Resistance at EOD, R_{EOD} (kip)	Calculated α Value
ISU1	South	HP 10 × 57	Clay	48.6	86.1	269.6	3.13
	North	HP 10 × 57	Clay	58.3	86.1	260.8	3.03
ISU2	South	HP 10 × 42	Mixed	No driving information			
	North	HP 10 × 42	Mixed				
ISU3	South	HP 10 × 57	Clay	78.8	92	268	2.91
	North	HP 10 × 57	Clay	79.3	92	232	2.52
ISU4	West	HP 10 × 57	Clay	No driving information			
	East	HP 10 × 57	Clay	72.4	94	200	2.13
ISU5	West	HP 10 × 57	Clay	No driving information			
	East	HP 10 × 57	Clay				
ISU6	South	HP 10 × 42	Mixed	49.1	62.3	176	-
	North	HP 10 × 42	Mixed	46.9	62.3	116	-

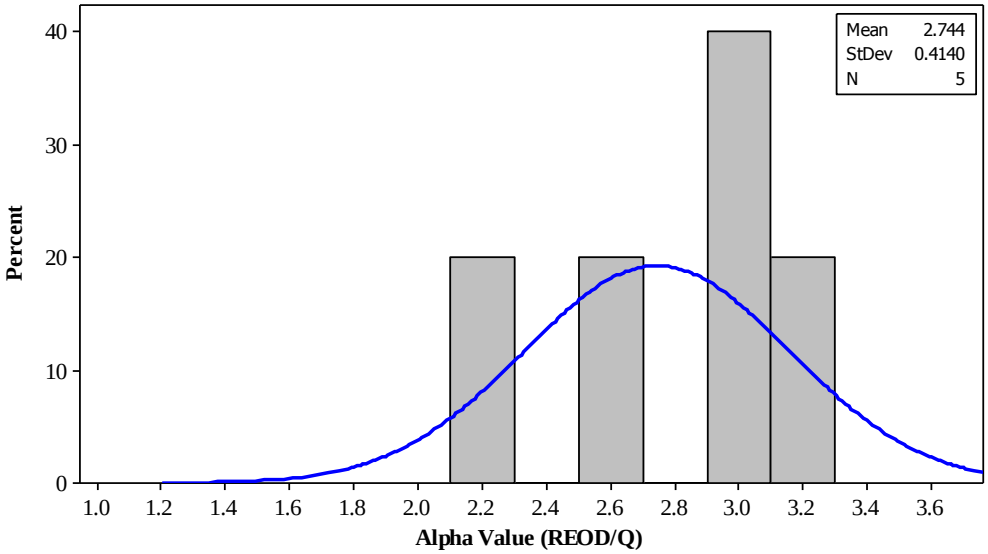

Figure 5.21. Histogram and theoretical normal distribution of α values based on information of production piles at ISU field test sites

Table 5.11. Summary of additional data on production piles in Iowa

Iowa County-ID Number	Pier/Abutment	Production Pile Size	Soil Description	Total Number of Piles	Plan Pile Length (ft)
Lee-135	Pier 2	HP 10 × 57	Sandy Glacial Clay	29	45
	North Abutment	HP 10 × 57		12	60
Buena Vista-53	West Abutment	HP 10 × 42	Firm Sandy Glacial Clay over Very Firm Glacial Clay	7	60
	East Abutment	HP 10 × 42		7	60
	Pier 1 West	HP 12 × 53		13	60
	Pier 2 East	HP 12 × 53		13	60
Jasper-44	West Abutment	HP 10 × 57	Silty Clay	7	70 & 80
	Pier 2	HP 12 × 53	Stiff Silty Clay to Very Firm Glacial Clay	14	70
	East Abutment	HP 10 × 57		7	75 & 80
Dickinson-35	East Abutment	HP 10 × 57	Sandy Lean Clay	6	60
	West Abutment	HP 10 × 57	Firm Sandy Lean Clay	6	60
	East Pier	HP 12 × 53	Very Firm Glacial Clay	8	60
Plymouth-40	West Abutment	HP 10 × 57	Silty Clay - Glacial Clay	6	80
	East Pier	HP 10 × 57	Very Firm Glacial Clay	12	70
Wright-63	East Abutment	HP 10 × 42	Glacial Clay	5	45
	West Abutment	HP 10 × 42		5	45
Carroll-122	South Abutment	HP 10 × 42	Silty Clay to Firm Glacial Clay	7	55
	North Abutment	HP 10 × 42		7	55
Cedar-82	South Abutment	HP 10 × 57	Silty Clay to Firm Glacial Clay	5	80
	North Abutment	HP 10 × 57		5	80
	Pier 1	HP 10 × 57		22	55
	Pier 3	HP 10 × 57		22	55
	Pier 2	HP 10 × 57		22	60
Tama-114	Pier	HP 10 × 57	Silty Clay to Firm Glacial Clay	27	44.28
	North Abutment	HP 10 × 57		12	63.96
	South Abutment	HP 10 × 57		13	70
Tama-119	Pier	HP 10 × 57	Very Firm Glacial Clay	27	45
	North Abutment	HP 10 × 57	Silty Clay to Very Firm Glacial Clay	14	60
	South Abutment	HP 10 × 57		13	60
Lee-130	Pier	HP 10 × 57	Firm Sandy Glacial Clay	36	50
Lee-147	SBL S. Abutment	HP 10 × 57	Stiff Silty Clay to Very Firm Glacial Clay	8	80
	NBL N. Abutment	HP 10 × 57		8	80
	SBL Pier 1	HP 10 × 57	Firm Glacial Clay	24	55
	NBL S. Abutment	HP 10 × 57	Stiff Silty Clay	8	75
	NBL Pier 1	HP 10 × 57	Firm Glacial Clay	24	55
Lee-148	South Abutment	HP 10 × 57	Silty Clay	12	60
	Pier	HP 10 × 57	Very Firm Glacial Clay	26	40
Lee-157	East Abutment	HP 10 × 57	Stiff Silty Clay to Firm Glacial Clay	11	70
	West Abutment	HP 10 × 57		11	70
Lee-138	West Abutment	HP 10 × 57	Silty Clay to Glacial Clay	7	70
	East Abutment	HP 10 × 57		7	70
	Pier 1	HP 12 × 53		27	45
Buena Vista-57	West Pier	HP 10 × 57	Glacial Clay to Gravelly Sand	12	65
	West Abutment	HP 10 × 57	Soft Silty Clay to Very Firm Glacial Clay	6	70
Johnson-285	Pier 1	HP 10 × 57	Sandy Lean Clay	24	55

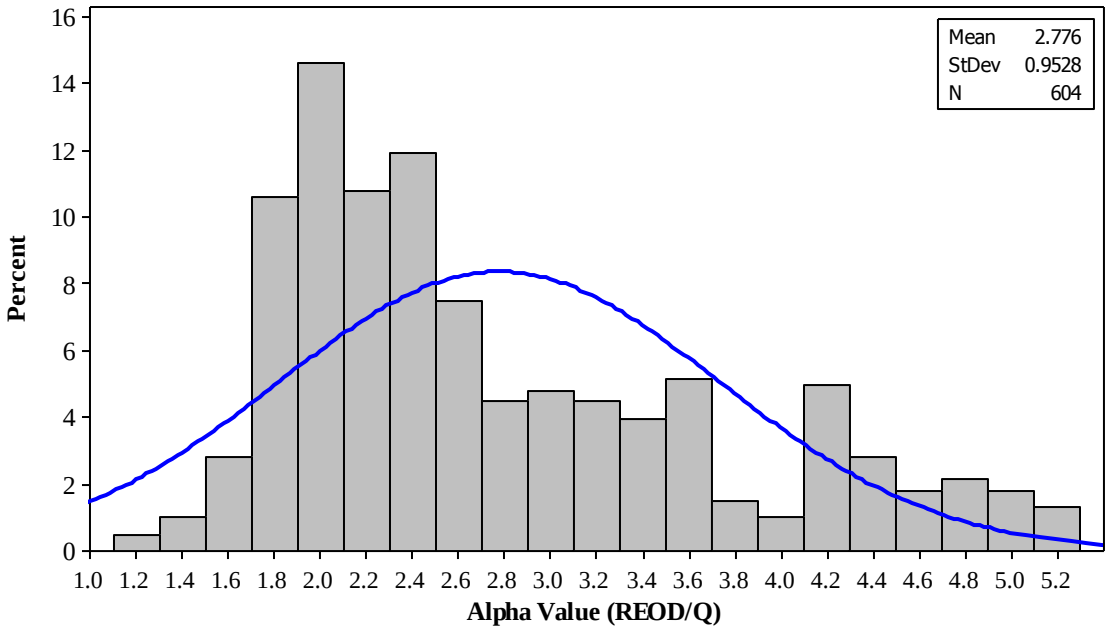

Figure 5.22. Histogram and theoretical normal distribution of α values based on additional data of production piles in Iowa

This comparison shows that most of the production piles were installed with higher capacities than that required using Eq. (5-9). In other words, the production piles were conservatively installed. In contrast, to eliminate an additional safety margin incurred to R_{EOD}, which has been accounted for using φ_{EOD} in Eq. (5-8), a lowest α value of 1.0 can be assumed. Referring to Figure 5.20 based on α value of 1.0, φ_{setup} values of 0.31 and 0.24 can be determined for the β_T values of 2.33 and 3.00, respectively. However, these φ_{setup} values could be high based upon the actual results revealed in Figure 5.21 and Figure 5.22 with an average α value of about 2.7 as well as the target α value of 2.0. To compromise between the conservatism observed in the actual production pile constructions and the idealistic condition that eliminates the additional safety margin to the R_{EOD}, α value of 1.8 can be selected between the lowest value of 1.0 and the average value of 2.7. Alternatively, α value of 1.5 can be selected between the lowest value of 1.0 and the target value of 2.0. If α value of 1.6 is chosen between 1.5 and 1.8 for pile designs in Iowa, φ_{setup} values of 0.21 and 0.19 can be reasonably recommended for the β_T values of 2.33 and 3.00, respectively. In this recommendation, only about 20% of the pile setup resistance estimated using the proposed methods described in Section 5.6.2 will be considered in the LRFD of steel H-pile foundations.

CHAPTER 6: SUMMARY

Because of the mandate imposed by the Federal Highway Administration (FHWA) on the implementation of Load Resistance Factor Design (LRFD) in all new bridge projects initiated after October 1, 2007, the Iowa Highway Research Board (IHRB) sponsored the research project TR-573 to develop the LRFD commendations for the State of Iowa based on the Pile Load Test (PILOT) database. PILOT contains pile information about past projects completed by the Iowa Department of Transportation (Iowa DOT) from 1966 until the late 1980s. To populate PILOT, especially for dynamic analysis, two add-on research projects (TR-583 and TR-584) were included to conduct ten (10) full-scale field tests in Iowa to increase the data points for LRFD resistance factors calculation, develop LRFD recommendations for dynamic methods, and validate the results of LRFD calibration.

The most common steel H-piles were used in the ten field sites which were selected from Iowa DOT bridge projects. Chapter 2 describes the six criteria established for selecting the ten field testing locations. Appendix A shows the layout of the test pile locations. When the test sites were selected, detailed soil in-situ investigations and laboratory tests were performed to characterize the soils surrounding the test piles. Standard Penetration Tests (SPT), Cone Penetration Tests (CPT), Borehole Shear Tests (BST), and modified Borehole Shear Tests (mBST) were the four selected in-situ soil investigations. In addition, push-in pressure cells (PCs) were installed near test piles ISU5, ISU6, ISU7, ISU8, and ISU10 to measure total lateral earth pressure and pore water pressure during driving, re-strikes, and static load tests. Soil samples collected from SPT boreholes were used for laboratory testing which consisted of basic soil characterization (i.e., gradation, Atterberg's limits and moisture content) and consolidation tests. The detailed descriptions of both in-situ and laboratory soil tests are presented in Chapter 3 and the results of the soil tests are included in the Appendix B.

Besides characterizing the surrounding soils, the properties of the ASTM A572 Grade 50 steel H-piles and the hammer driving systems are described and presented in Chapter 4. The test piles were instrumented with strain gauges along their embedded lengths before being driven into the ground. The details of the strain gauge instrumentations are described in Chapter 4 and their arrangements are included in Appendix C. The test piles were also instrumented with a pair of transducers and accelerometers near the pile head for Pile Driving Analyzer (PDA) tests.

The PDA tests were conducted during pile driving, at the end of driving (EOD), and at several re-strikes. The test piles were re-struck at several durations after EOD and before static load tests. The PDA force and velocity records at each event (given in Appendix C) were used in the CAse Pile Wave Analysis Program (CAPWAP) method for a more accurate pile resistance estimation, which was achieved by performing signal matching.

Hammer blow counts were recorded at EOD and re-strikes and were used in the Wave Equation Analysis Program (WEAP) bearing graph analysis to determine the pile resistance. Five soil profile input procedures were used in WEAP analysis: 1) GRLWEAP soil type based method (ST); 2) GRLWEAP SPT N-value based method (SA); 3) the Federal Highway Administration (FHWA) DRIVEN program; 4) Iowa Blue Book (Iowa DOT steel pile Design Chart); and 5) Iowa DOT current approach. The estimated pile capacities and their respective dynamic soil properties for PDA, CAPWAP, and WEAP are tabulated in Chapter 4.

After completing all re-strikes, vertical static load tests were performed on the test piles in according with ASTM D1143 Procedure A: Quick test method. The pile resistance was determined from the load-displacement graph based on the Davisson's criteria. Also, force distributions were calculated from the strain measurements at each load increment. The procedure of performing the static load tests is described in Chapter 4 and the results are given in Appendix C.

CHAPTER 7: CONCLUSIONS

The extensive experimental research studies generated important data for concurrent analytical and computational investigations. Results from re-strikes and static load tests were compared. The SLT measured load-displacements were compared with the simulated results obtained using TZ-mBST model. The relationship between PC measurements and estimated pile responses was assessed. The variation in pile responses was evaluated with respect to the time elapsed after pile installation and was correlated with the surrounding soil properties. Two analytical pile setup quantification methods were developed and validated. A new calibration procedure was developed to incorporate pile setup into LRFD. The results of this research project led to the following conclusions:

1. Total pile resistance is contributed predominantly from shaft resistance while end bearing ranges between 2% to 28% of the total resistance.

2. Shaft resistance is higher at a stiffer soil layer, represented with a relatively large uncorrected SPT N-value.

3. The TZ-mBST model has proven to provide a better match of the measured SLT load-displacement relationship when compared with TZ-CPT model.

4. The continuous logarithmic dissipation of pore water pressure with time explains the observed pile setup trend. Alternatively for the cohesionless soil layer, the immediate and complete pore water dissipation before EOD explains the minimal variation in pile resistance over time.

5. Comparison of the measured pile driving resistances concludes that pile setup occurs in piles embedded in clay and mixed soil profiles but not in sand profile. The re-strike and load test measurements show that the increase in total pile resistance has a general logarithmic trend with respect to time for clay and mixed soil profiles. Furthermore, the field test results indicate that pile resistance increases immediately and significantly after pile installation, and thus, the performance of re-strikes within a day after EOD is reasonably recommended. The CAPWAP results in clay profile reveal that both shaft resistance and end bearing increase logarithmically with time, and pile setup is contributed predominantly from the shaft resistance and minimally from the end bearing. Unlike the clay profile, test pile ISU8 in the mixed soil profile experienced a contrasting observation.

6. The experimental results confirmed that the amount of increase in shaft resistance at a given time was dependent on the combined effects of the: (1) soil permeability, which was measured directly using the coefficient of consolidation or indirectly using the SPT N-values; (2) soil compressibility, which was measured using the plasticity index (PI) values; and (3) corresponding thicknesses of all the cohesive layers along the embedded pile length. The quantitative correlation studies specifically revealed that the increases in total pile capacity and shaft resistance of a pile embedded in a cohesive clay soil were directly proportional to C_v or C_h and were inversely proportional to SPT N-values and PI values larger than 12%. However, they were directly proportional to PI values smaller

than 12% for a pile embedded in a sandy cohesive soil. Alternatively, the increase in the end bearing component showed no significant correlations to either SPT N-values or C_h values, but was directly proportional to the C_v and inversely proportional to the PI values.

7. Based on the field test results and the successful correlation studies, two analytical quantification methods were established to estimate the pile setup rate (C) in a clay profile using the influential soil properties measured from the commonly used SPT & CPT and using the dynamic analysis methods (WEAP and CAPWAP). The first method, given by Eq. (5-4), involves both SPT and CPT while the second method, given by Eq. (5-5), involves only SPT. The quantification of pile setup rate in terms of soil properties avoids the inconvenient re-strikes and allows the estimation of pile resistance at any time (t) using Eq. (5-3).

8. Using twelve data records from PILOT along with the five field tests, the confidence of the proposed pile setup methods were validated, as illustrated in Figure 5.17 and summarized in Table 5.8, at various confidence levels. The maximum error falls between -17.2% and 1.9%, based on the SPT based setup method when used in conjunction with WEAP at the 98% confidence interval. Generally, the range of the errors is smaller for pile setup methods when used in conjunction with CAPWAP than those with WEAP.

9. Recognizing the difference in uncertainties associated with the estimations of initial pile resistance at EOD and pile setup resistance, representing different COV values of 0.181 and 0.330 for WEAP, separate resistance factors are calculated for both initial pile resistance and setup resistance to ensure the reliability theory based LRFD framework is adequately followed. Considering the AASHTO (2007) strength I load combination for axially loaded piles, the resistance factor for pile setup (φ_{setup}) is calculated using Eq. (5-8), derived based on FOSM and explicitly described by Ng (2011). For a typical α value of 1.6, Q_D/Q_L ratio of 2.0, and φ_{EOD} of 0.66 for the β_T=2.33, the φ_{setup} value of 0.21 can be conservatively recommended.

REFERENCES

AbdelSalam, S. S. (2010). Behavior Characterization & Development of LRFD Resistance Factors for Axially Loaded Steel H-Piles of Bridge Foundations, Ph D Dissertation. Ames, IA: Iowa State University.

AbdelSalam, S., Sritharan, S., Suleiman, M. T., Ng, K. W., & Roling, M. J. (2011). Development of LRFD Procedures for Bridge Pile Foundations In Iowa - Volume III: Recommended Resistance Factors with Consideration to Construction Control and Setup. Ames, IA: Iowa State University - Institute for Transportation.

AbdulSalam, S., Sritharan, S., & Suleiman, M. (2008). Current Design and Construction Practices of Bridge Pile Foundations. Proceeding of the International Foundations Congress and Equipment Expo. Orlando, Florida: ASCE.

American Association of State Highway and Transportation Officials (AASHTO). (2007). AASHTO LRFD Bridge Design Specifications, Customary U.S. Units, Forth Ed. Washington, D.C.: AASHTO.

Bowles, J. (1996). Foundation Analysis and Design. Fifth Edition. The Mcgraw-Hill Companies, Inc.

Case Western Reserve Univeristy, GRL Engineers, I., & Pile Dynamics, I. (2008, October 20-22). GRL Case Dynamic Foundation Testing Seminar and Workshops. Cleveland, OH.

Das, B. M. (1990). Principles of Foundation Engineering (2nd ed.). Boston: PWS-KENT Publishing Company.

Delmag. (2005, February). Delmag. Retrieved from Delmag Diesel Pile Hammer: http://www.delmag.com/diesel-pile-hammer.html

Demers, D., & Leroueil, S. (2002). Evaluation of Preconsolidation Pressure and the Overconsolidation Ratio from Piezocone Tests of Clay Deposits in Quebac. Canadian Geotechnical Journal, 39(1), 174-192.

Dirks, K. L., & Kam, P. (1989; revised 1994). Foundation Soils Information Chart: Pile Foundation. Ames: Iowa Department of Transportation: Highway Division: Soils Survey Section.

Esrig, M., & Kirby, R. (1979). Soil Capacity for Supporting Deep Foundation Members in Clay. ASTM STP No. 670, 27-63.

Fellenius, B. (1996). Basic of Foundation Design. Richmond, Columbia: BiTech Publishers.

Goble, G., Likins, G., & Rausche, F. (1975). Bearing Capacity of Piles from Dynamic Measurements. Final Report. Cleveland, Ohio: Department of Civil Engineering, Case Western Reserve University.

Handy, R. L. (1986). Borehole Shear Test and Slope Stability. Proceedings of the ASCE Specialty Conference on In Situ Tests: Use of In Situ Tests in Geotechnical Engineering Blacksburg, Virginia: ASCE, pp. 161-175.

Hannigan, P., Goble, G., Thendean, G., Likins, G., & Rausche, F. (1998). Design and Construction of Driven Pile Foundations - Vol. II, FHWA-HI-97-013. Washington, D.C.: National Highway Institute, Federal Highway Administration, U.S. Department of Transportation.

Houlsby, G., & Teh, C. (1988). Analysis of the Peizocone in Clay. Penetration Testing 1988, 2, 777-783.

Kim, K. J., & Kreider, C. A. (2004). Measured Soil Setup of Steel HP Piles from Windsor Bypass Project in North Caralina. Transportation Research Record: Journal of the Transportation Research Board, 3-11.

Komurka, V. E., Wagner, A. B., & Edil, T. B. (2003). Estimating Soil/Pile Set-Up, Final Report. Wisconsin: Wagner Komurka Geotechnical Group, Inc. and University of Wisconsin-Madison.

Kulhawy, F. H., & Mayne, P. (1990). Manual on Estimating Soil Properties for Foundation Design. Palo Alto, California: Electric Power Research Institute.

Liao, S. S., & Whitman, R. V. (1986). Overburden Correction Factors for SPT in Sand. Journal of Geotechnical Engineering, 112(3), 373-377.

Likins, G., Piscsalko, G., Rausche, F., & Hussein, M. (2004). Real Time Monitoring Solutions for Deep Foundation Testing. 83rd Annual Transportation Research Board Meeting (pp. 1-18). Washington, D.C.: Transportation Research Board.

Mathias, D., & Cribbs, M. (1998). Driven 1.0:A Microsoft Window TM Based Program for Determining Ultimate Vertical Static Pile Capacity. Publication No. FHWA-Sa-98-074. Washington, D.C.: National Highway Institute, Federal Highway Administration, U.S. Department of Transportation.

Mayne, P. W. (2001). Stress-Strain-Strength-Flow Parameters from Enhanced In-Situ Tests. Proceedings, International Conference on In-Situ Measurement of Soil Properties and Case Histories, (pp. 27-48). Bali, Indonesia.

Mayne, P. W. (2006). In-Situ Test Calibrations for Evaluating Soil Parameters. Characterization and Engineering Properties of Natural Soils II (Proceedings Singapore Workshop). Taylor & Francis Group, London, United Kingdom.

Mayne, P. W. (2007). Cone Penetration Test: A Synthesis of Highway Practice. Washington, D. C.: Transportation Research Board.

Meyerhof, G. (1976). Bearing Capacity and Settlement of Pile Foundations. Journal of Geotechnical Engineering Division, ASCE, Vol. 102, No. GT3, Proc. Paper 11962, 195-228.

Ng, K. W. (2011). Pile Setup, Dynamic Construction Control, and Load and Resistance Factor Design of Vertically-Loaded Steel H-Piles. Ph.D. Thesis. Iowa State University, Ames, IA.

Nordlund, R. (1963). Bearing Capacity of Piles in Cohesionless Soils. Journal of Soil Mechanics and Foundation, ASCE, SM-3.

Nordlund, R. (1979). Point Bearing and Shaft Friction of Piles in Sand. 5th Annual Fundamentals of Deep Foundation Design. Rolla, Missouri: University of Missouri-Rolla.

Nowak, A. (1999). Calibration of LRFD Bridge Design Code. NCHRP Report 368. Washington, D. C.: Transportation Research Board.

Pile Dynamics, Inc. (1996). Pile Driving Analyzer Manual: Model PAK. Cleveland, Ohio: Pile Dynamics, Inc.

Pile Dynamics, Inc. (2000). CAPWAP for Windows Manual. Cleveland, Ohio: Pile Dynamics, Inc.

Pile Dynamics, Inc. (2005). GRLWEAP Wave Equation Analysis of Pile Driving: Procedures and Models Version 2005. Cleveland, Ohio: Pile Dynamics, Inc.

Rausche, F., & Goble, G. (1979). Determination of Pile Damage by Top Measurements. Philadelphia, PA: American Society for Testing and Materials.

Robertson, P., & Campanella, R. (1983). Interpretation of Cone Penetration Tests, Part I (Sand) and Part II (Clay). University of California at Berkeley, Civil Engineering Department. Berkeley: Soil Mechanics Series No. 60.

Roling, J. M. (2010). Establishment of a Suitable Dynamic Formula for the Construction control of Driven Piles and its Calibration for Load and Resistance Factor Design, MS Thesis. Ames, IA: Iowa State University.

Roling, M., Sritharan, S., Suleiman, M., Ng, K. W., & AbdelSalam, S. (2010). Development of LRFD Design Procedures for Bridge Piles in Iowa-Electronic Database. Final Report Vol. I. IHRB Project No. TR-573. Ames, Iowa: Institute for Transportation, Iowa State University.

Salgado, R. (2008). The Engineering of Foundations. New York: McGraw-Hill.

Skov, R., & Denver, H. (1988). Time-Dependence of Bearing Capacity of Piles. Proceeding of 3rd international Conference on application of Stress-Waves Theory to Piles, (pp. 879-888). Ottawa, Ontario, Canada.

Smith, E. (1962). Pile-Driving Analysis by the Wave Equation. Journal of the Soil Mechanics and Foundation Division, ASCE, paper No. 3306, Vol. 127, Part 1, 1145-1193.

Suleiman, M. T., Stevens, L., Jahren, C. T., Ceylan, H., and Conway, W. M. (2010). Identification of Practices, Design, Construction, and Repair Using Trenchless Technology. Final Research Report. Iowa Department of Transportation Project Number IHRB-06-09, Ames, Iowa: Institute for Transportation, Iowa State University.

Sully, J., & Campanella, R. (1994). Evaluation of Field CPTU Dissipation Data in Overconsolidated Fine-Grained Soils. XIII ICSMFE (p. 4). New Delhi, India: XIII CIMSTF.

Thurman, A. (1964). Computed Load Capacity and Movement of Friction and End-Bearing Piles Embedded in Uniform and Stratified Soil. Ph.D. Thesis. Carnegie Institute of Technology.

Tomlinson, M. (1971). Some Effects of Pile Driving on Skin Friction. Proceedings Conference on Behavior of Piles (pp. 107-114). London: ICE.

Vande Voort, T., Suleiman, M., & Sritharan, S. (2008). Design and Performance Verification of UHPC Piles for Deep Foundations (Final Report). IHRB Project No. TR-558. Ames Iowa: Institute for Transportation, Iowa State University.

Wroth, C., & Wood, D. W. (1978). The Correlation of Index Properties with Some Basic Engineering Properties of Soils. Canadian Geotechnical Journal, 15(2), 137-145.

Zheng, J. J., Lu, Y. E., Yin, J. H., & Guo, J. (2010). Radial Consolidation with Variable Compressibility and Permeability Following Pile Installation. Computers and Geotechnics, 37(3), 408-412.

APPENDIX A: LOCATIONS OF TEST PILES AND IN SITU SOIL TESTS

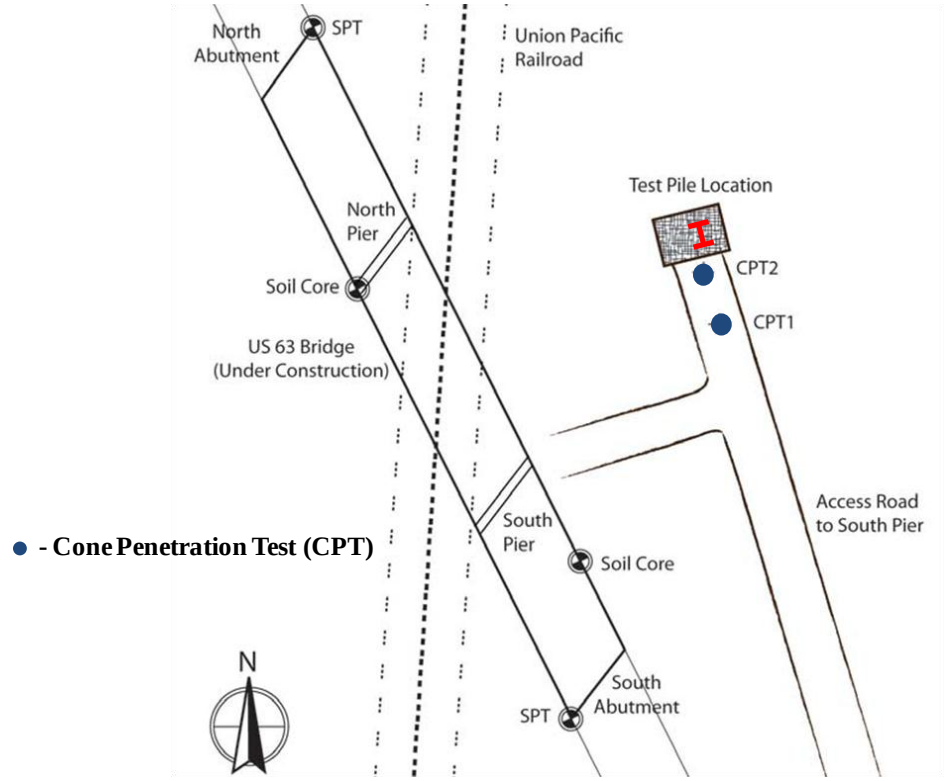

Figure A.1. Test Pile ISU1 at Mahaska County

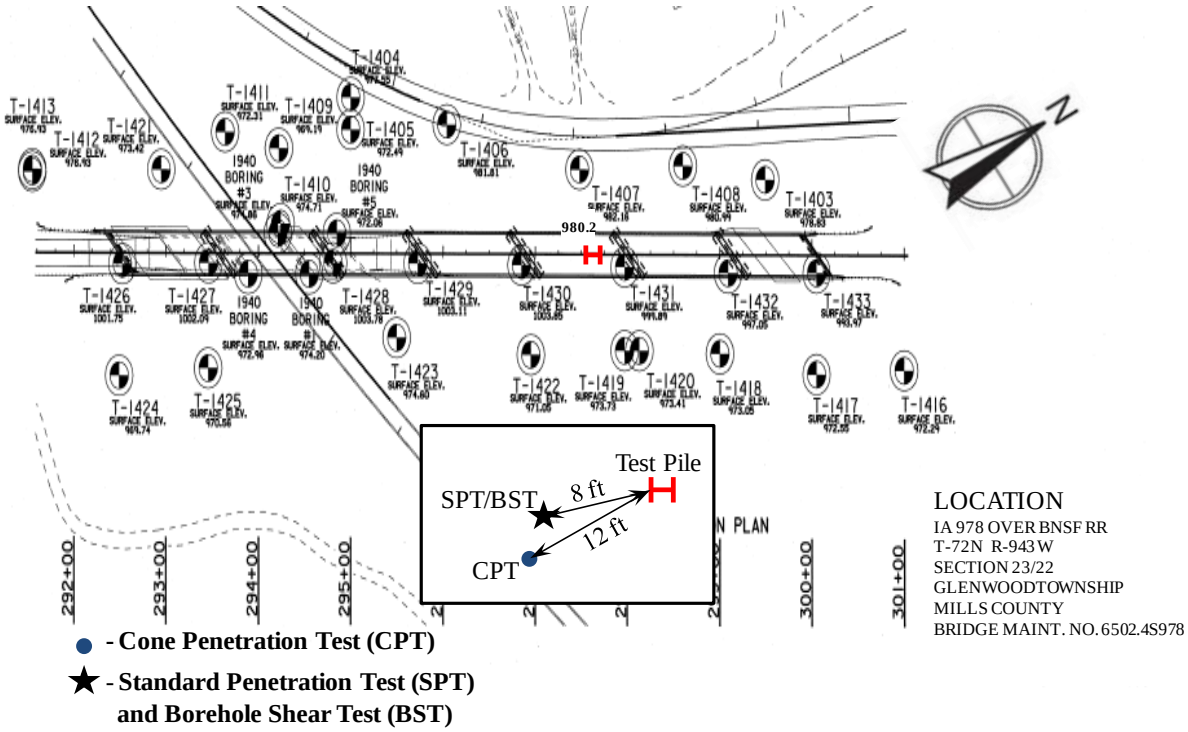

Figure A.2. Test Pile ISU2 at Mills County

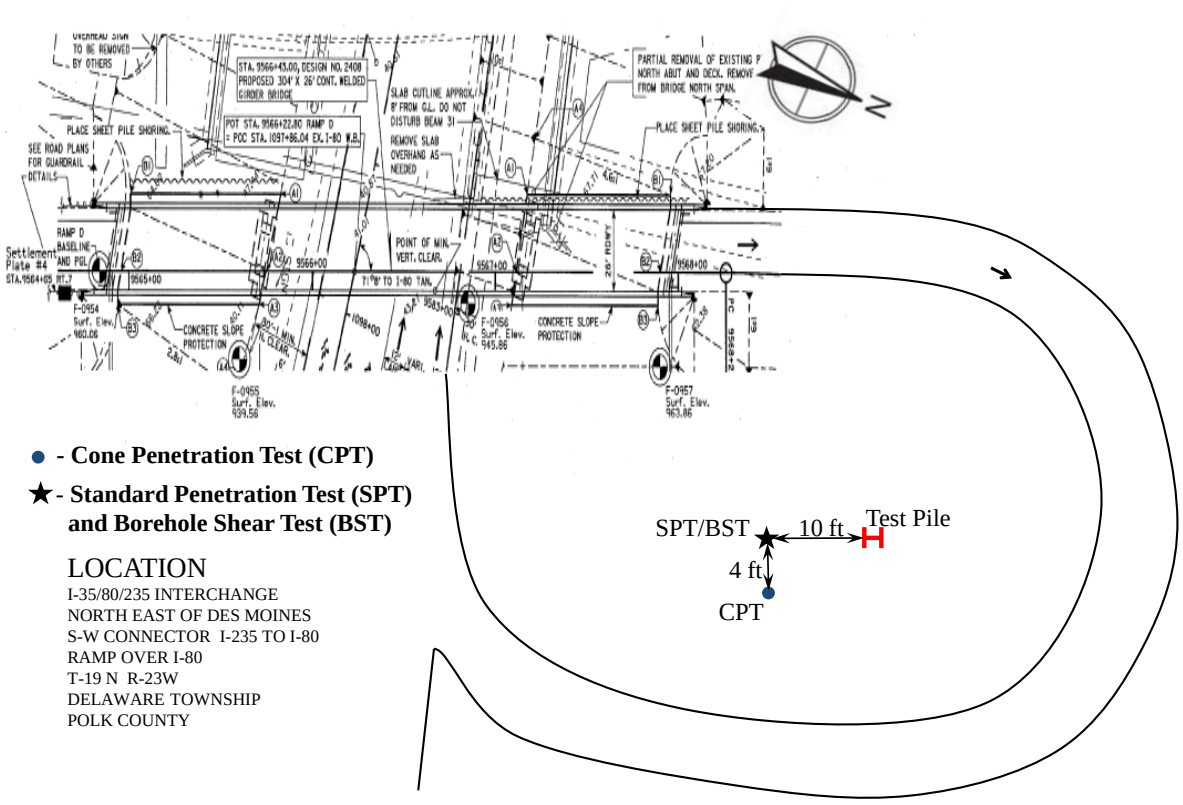

Figure A.3. Test Pile ISU3 at Polk County

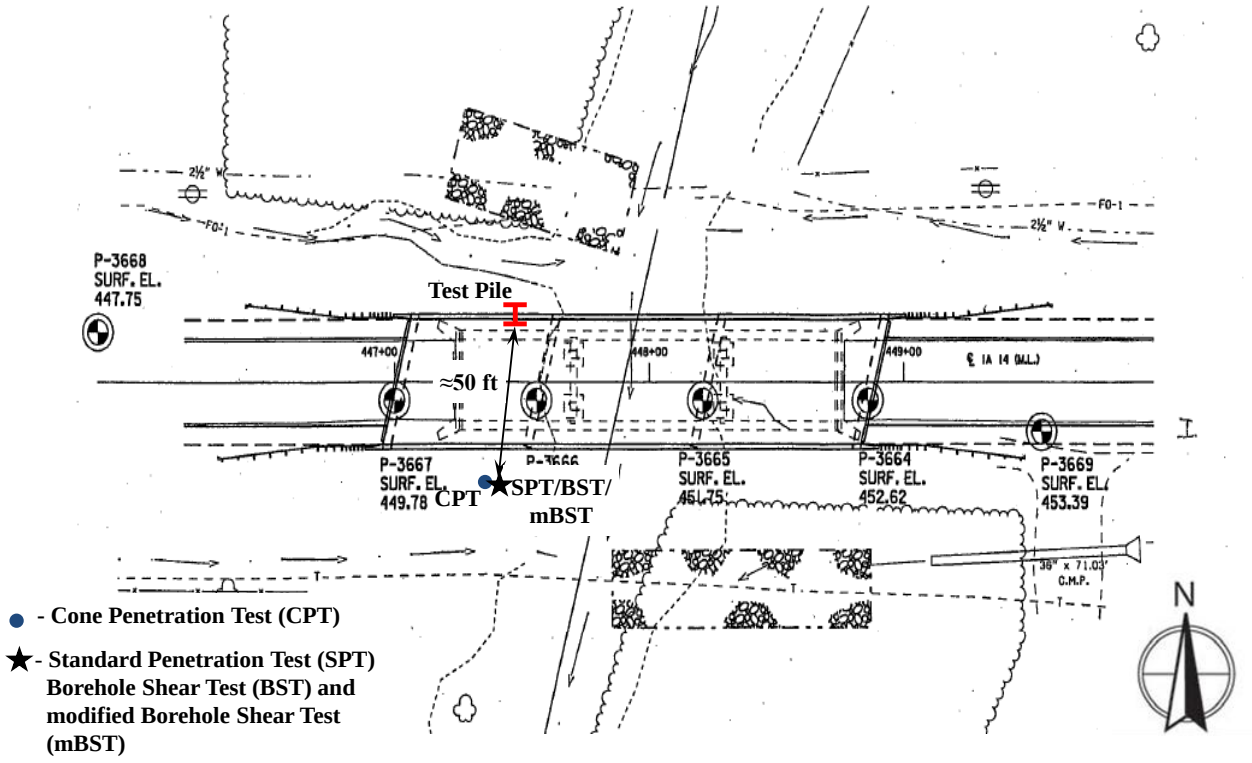

Figure A.4. Test Pile ISU4 at Jasper County

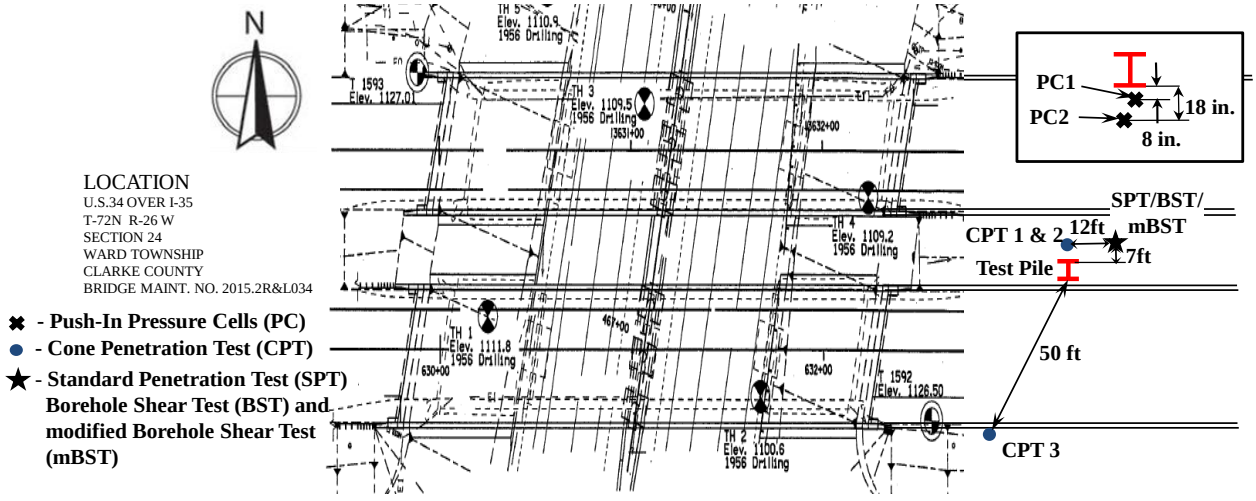

Figure A.5. Test Pile ISU5 at Clark County

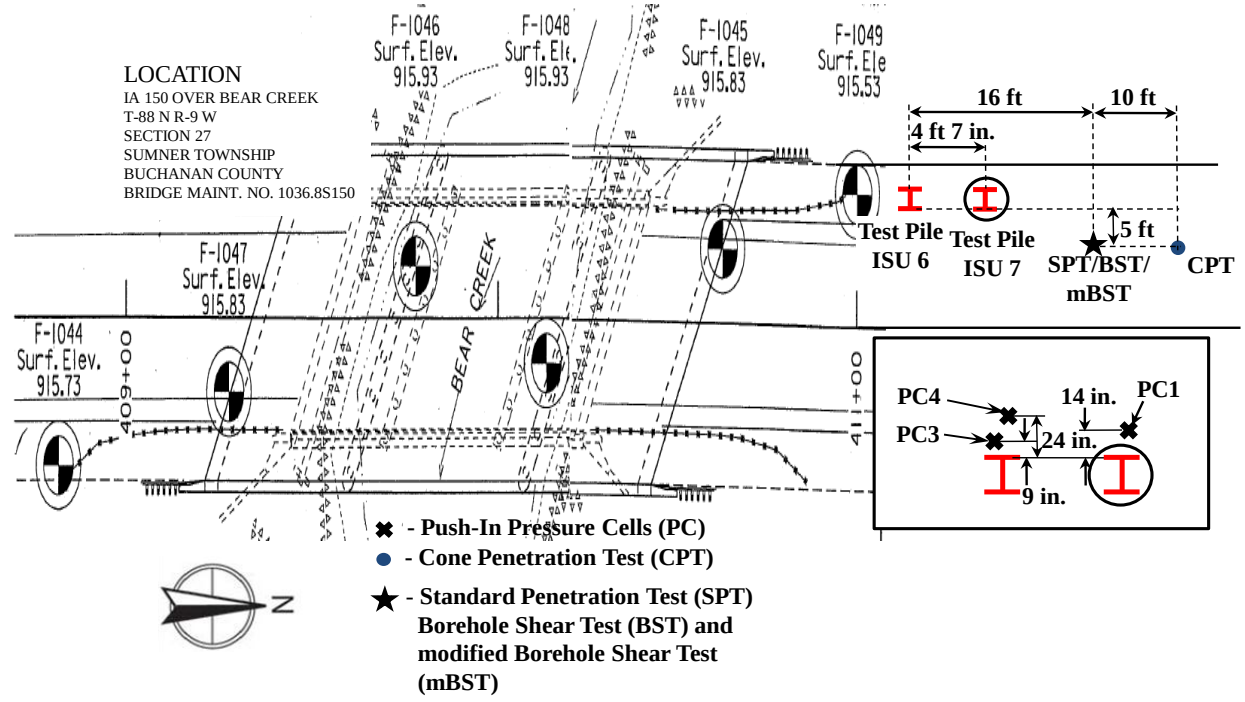

Figure A.6. Test Piles ISU6 and ISU7 at Buchanan County

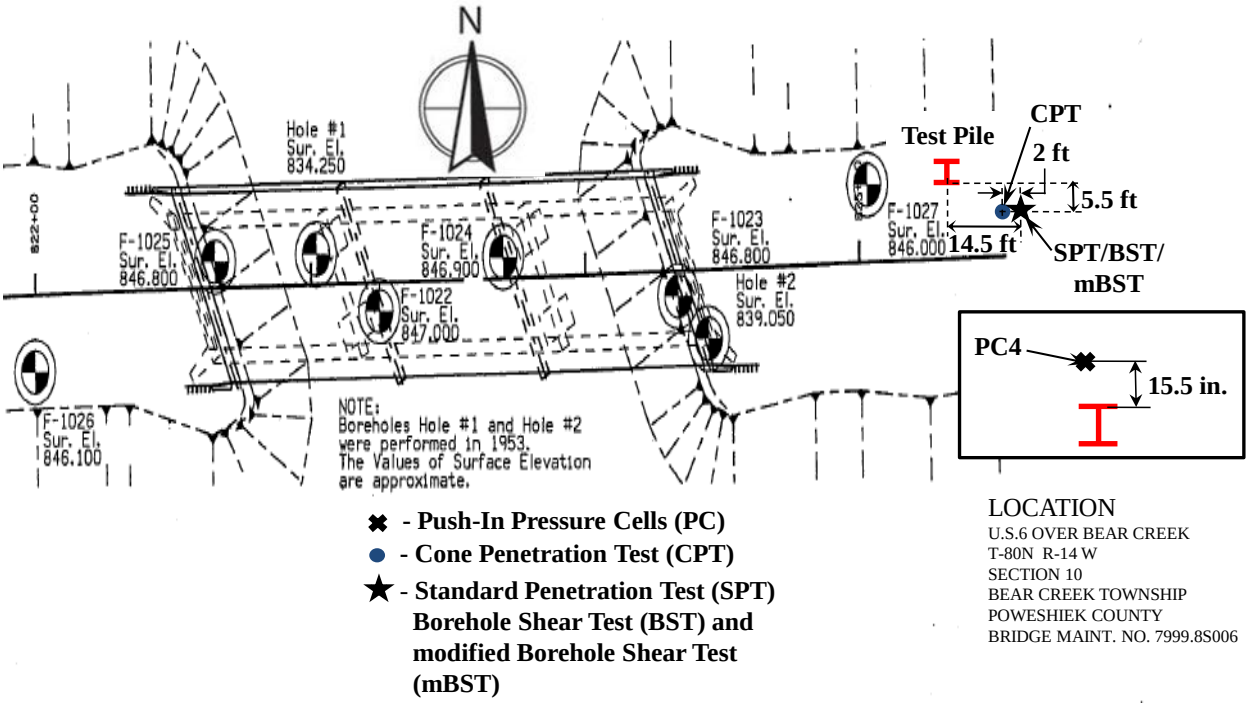

Figure A.7. Test Pile ISU8 at Poweshiek County

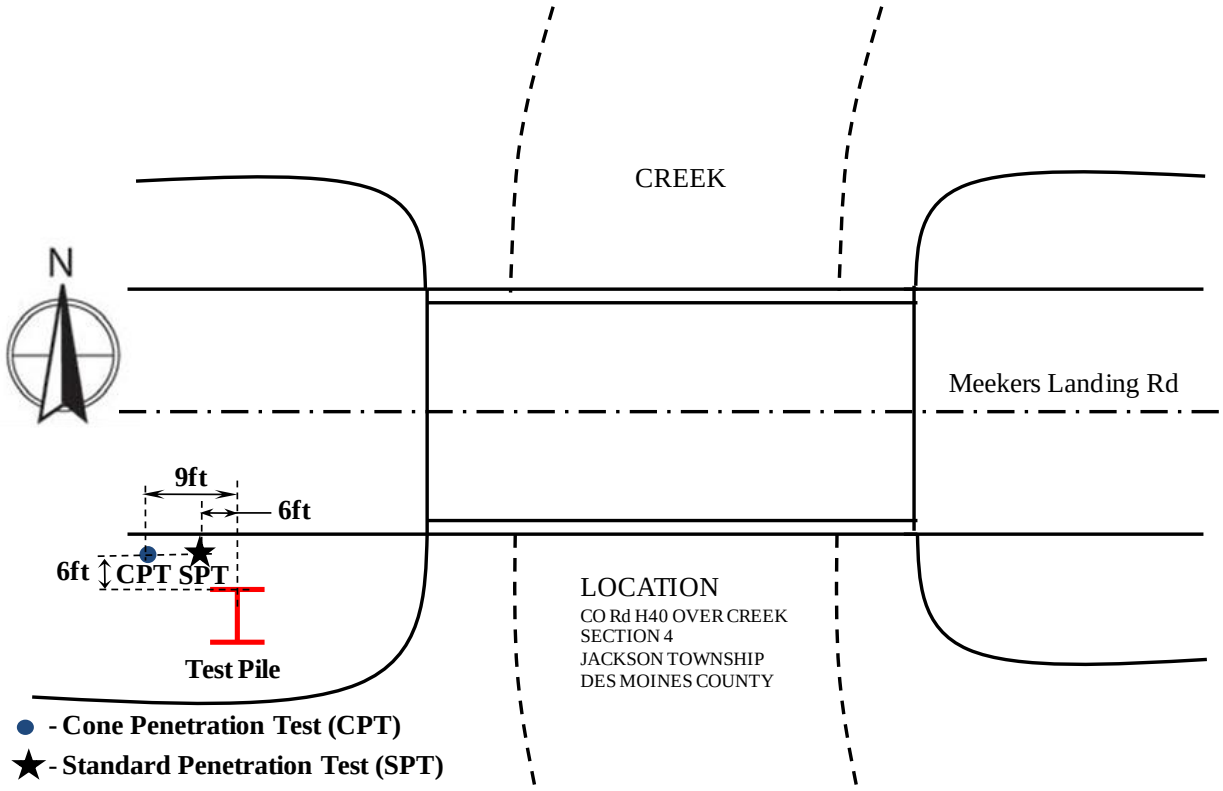

Figure A.8. Test Pile ISU9 at Des Moines County

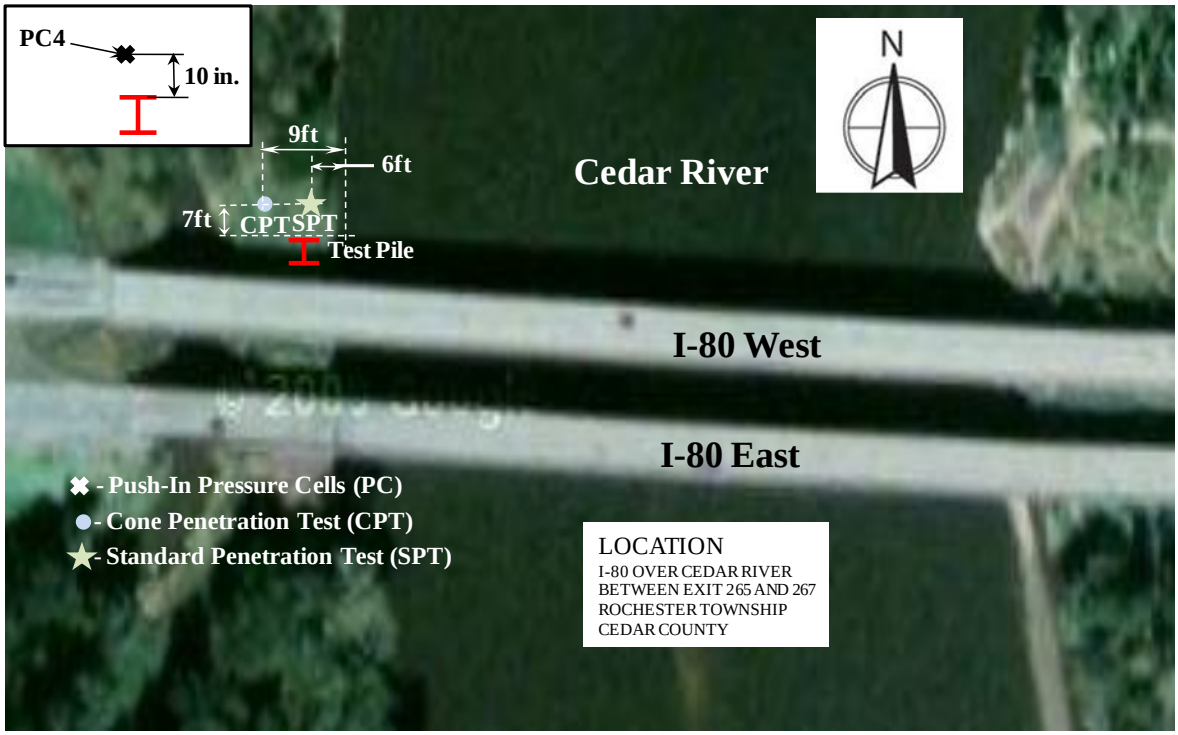

Figure A.9. Test Pile ISU10 at Cedar County

APPENDIX B: RESULTS OF IN SITU SOIL INVESTIGATIONS AND SOIL PROFILES

B.1. Diagrammatic soil profile

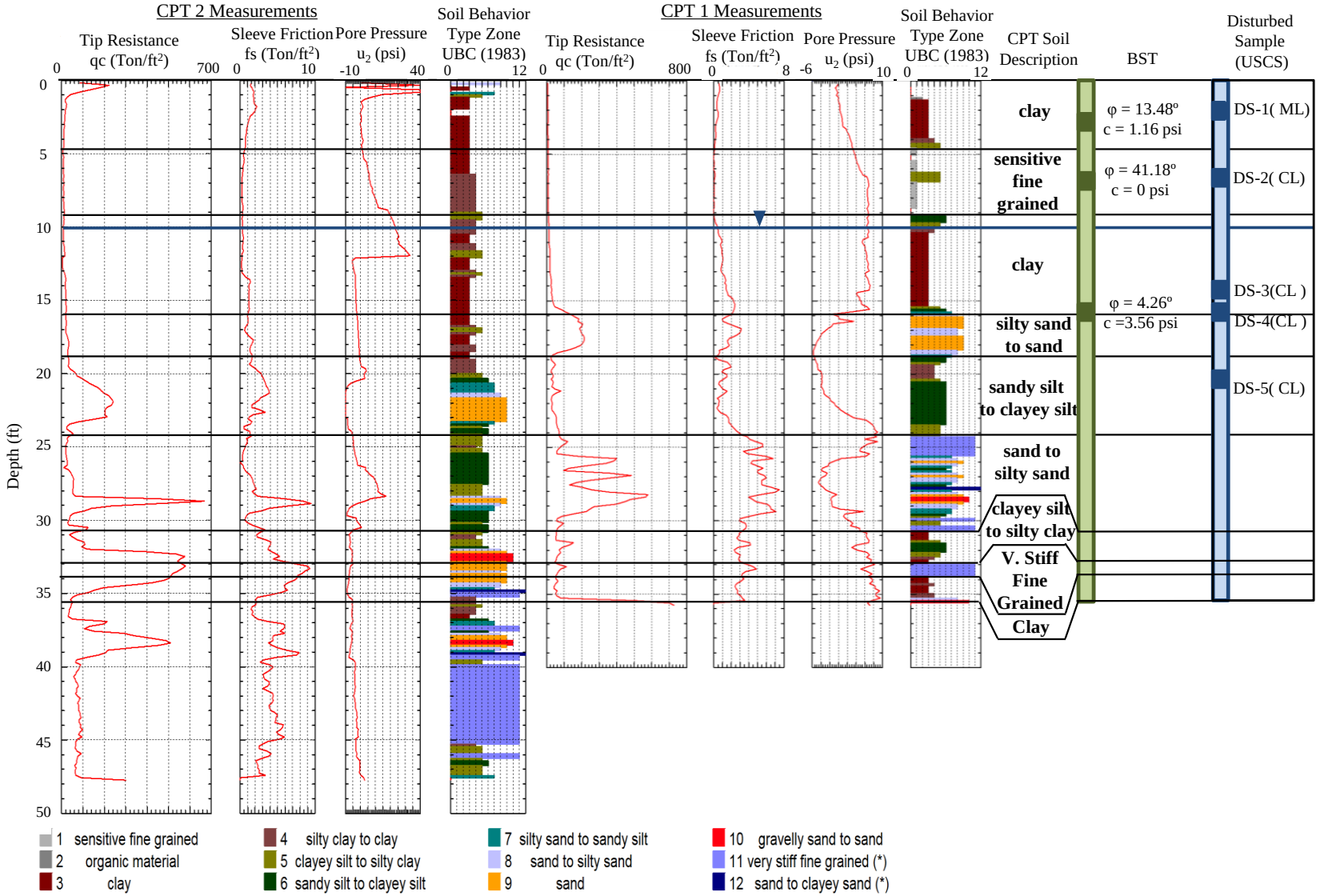

Figure B.1.1. In-situ soil investigations and soil profile for ISU1 at Mahaska County

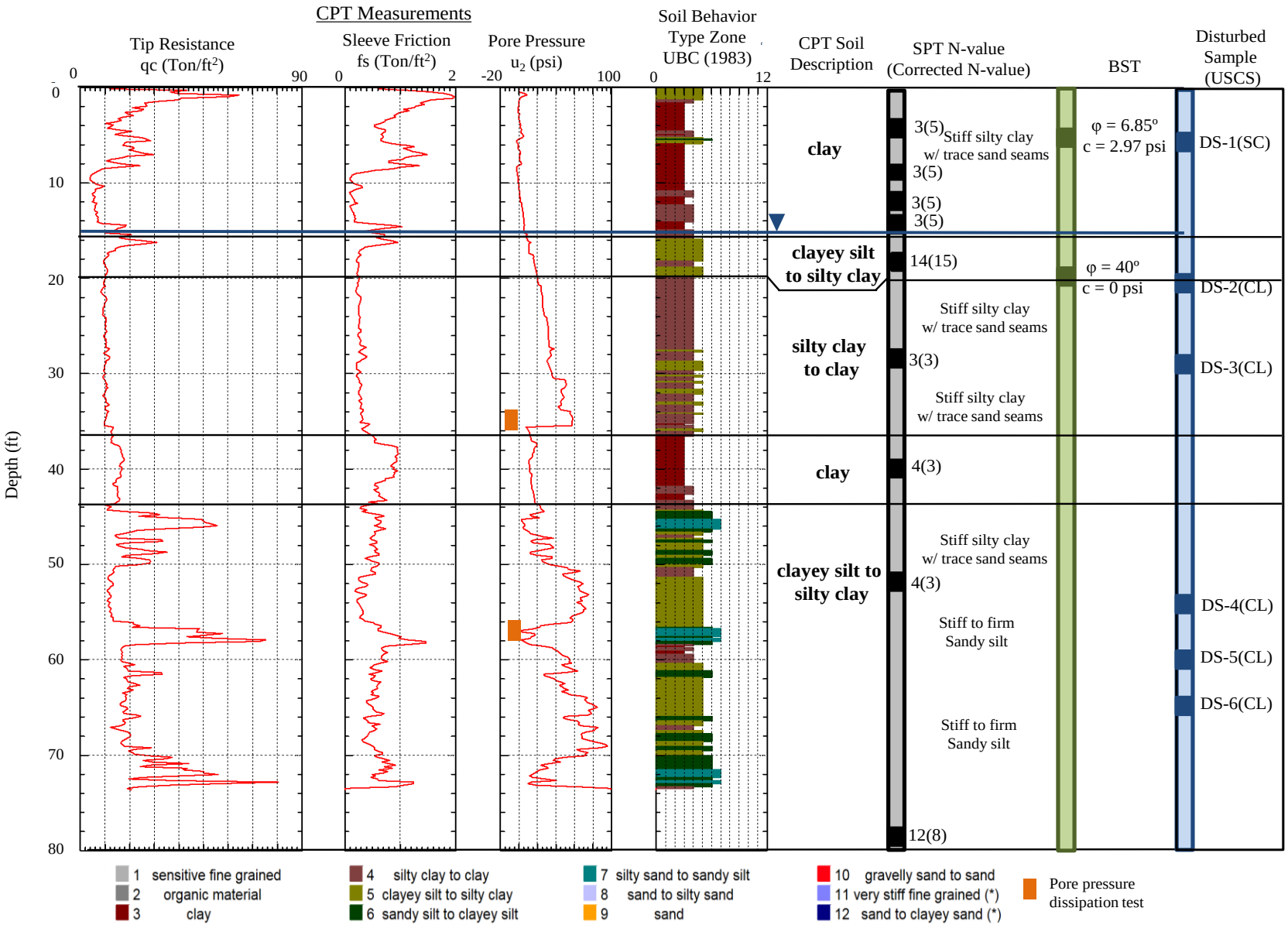

Figure B.1.2. In-situ soil investigations and soil profile for ISU2 at Mills County

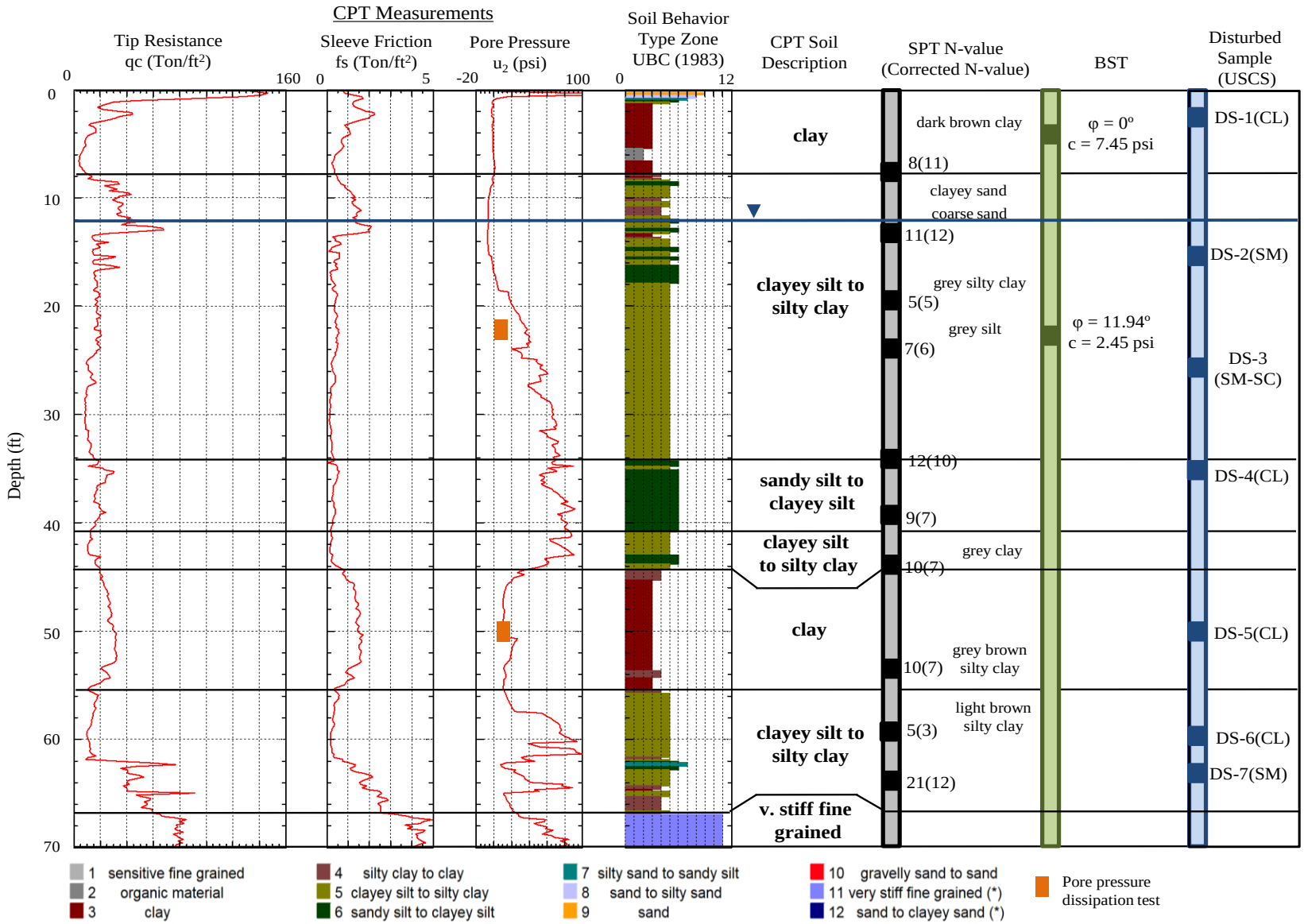

Figure B.1.3. In-situ soil investigations and soil profile for ISU3 at Polk County

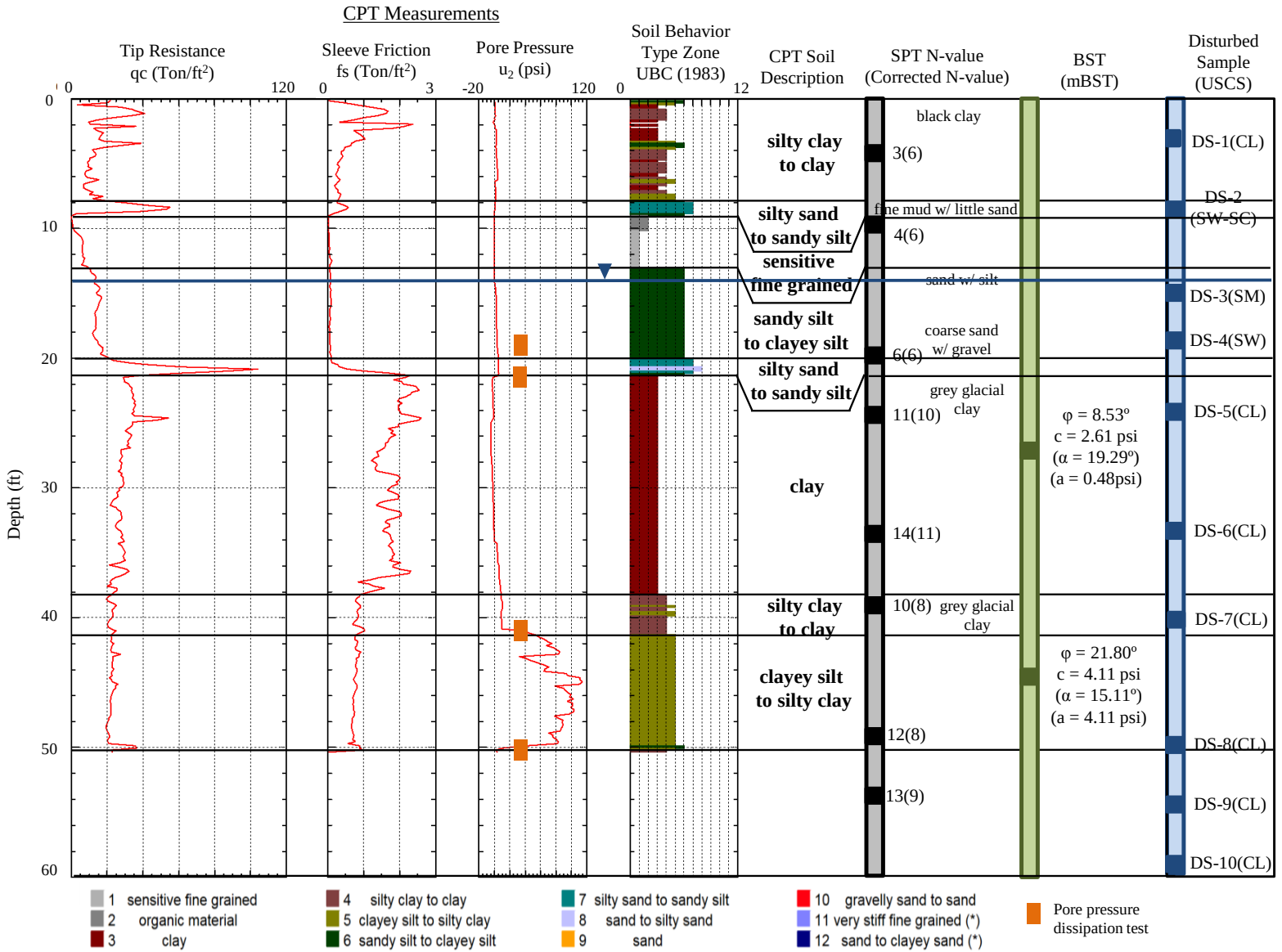

Figure B.1.4. In-situ soil investigations and soil profile for ISU4 at Jasper County

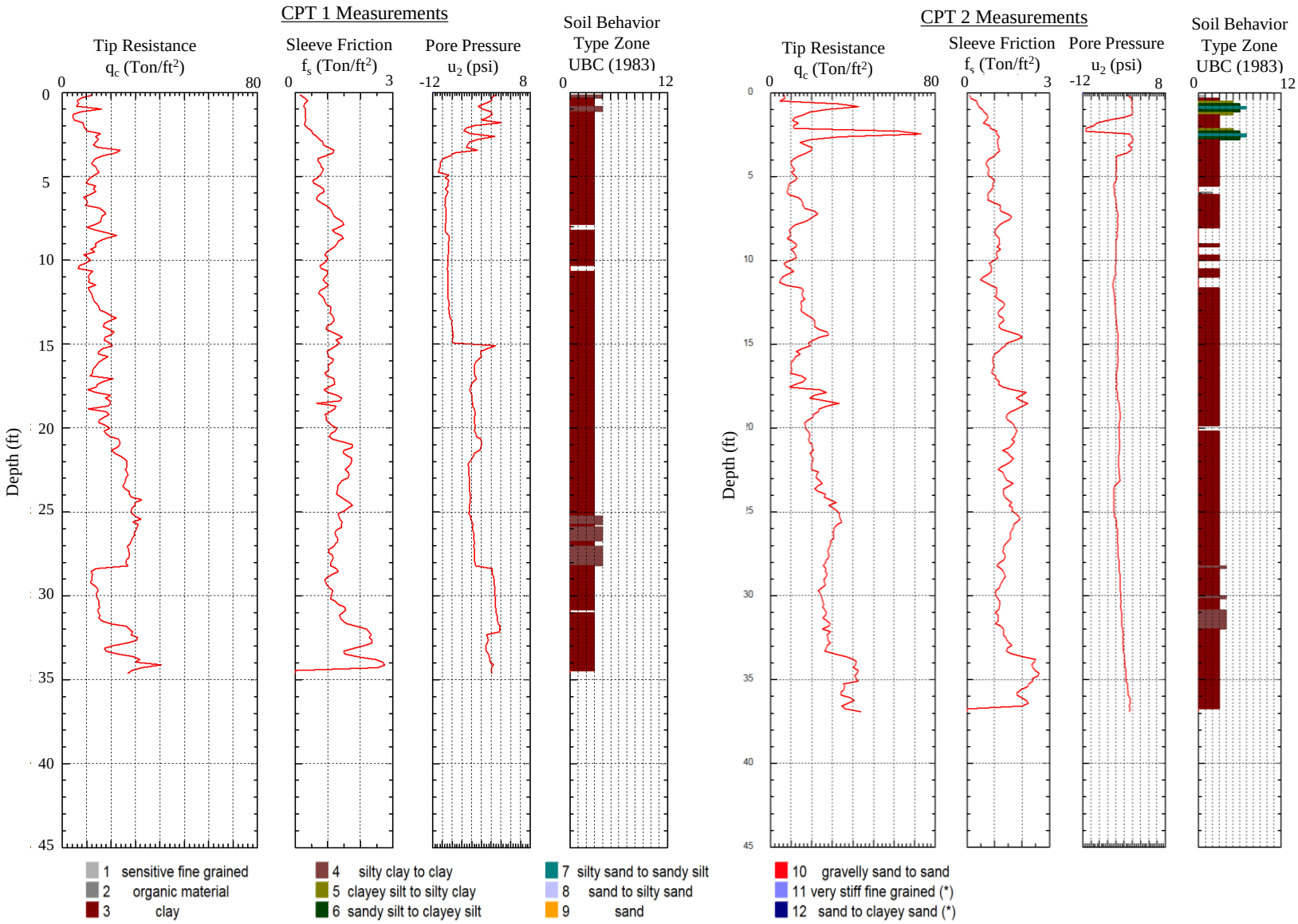

Figure B.1.5. Cone Penetration Tests and soil profile for ISU5 at Clarke County

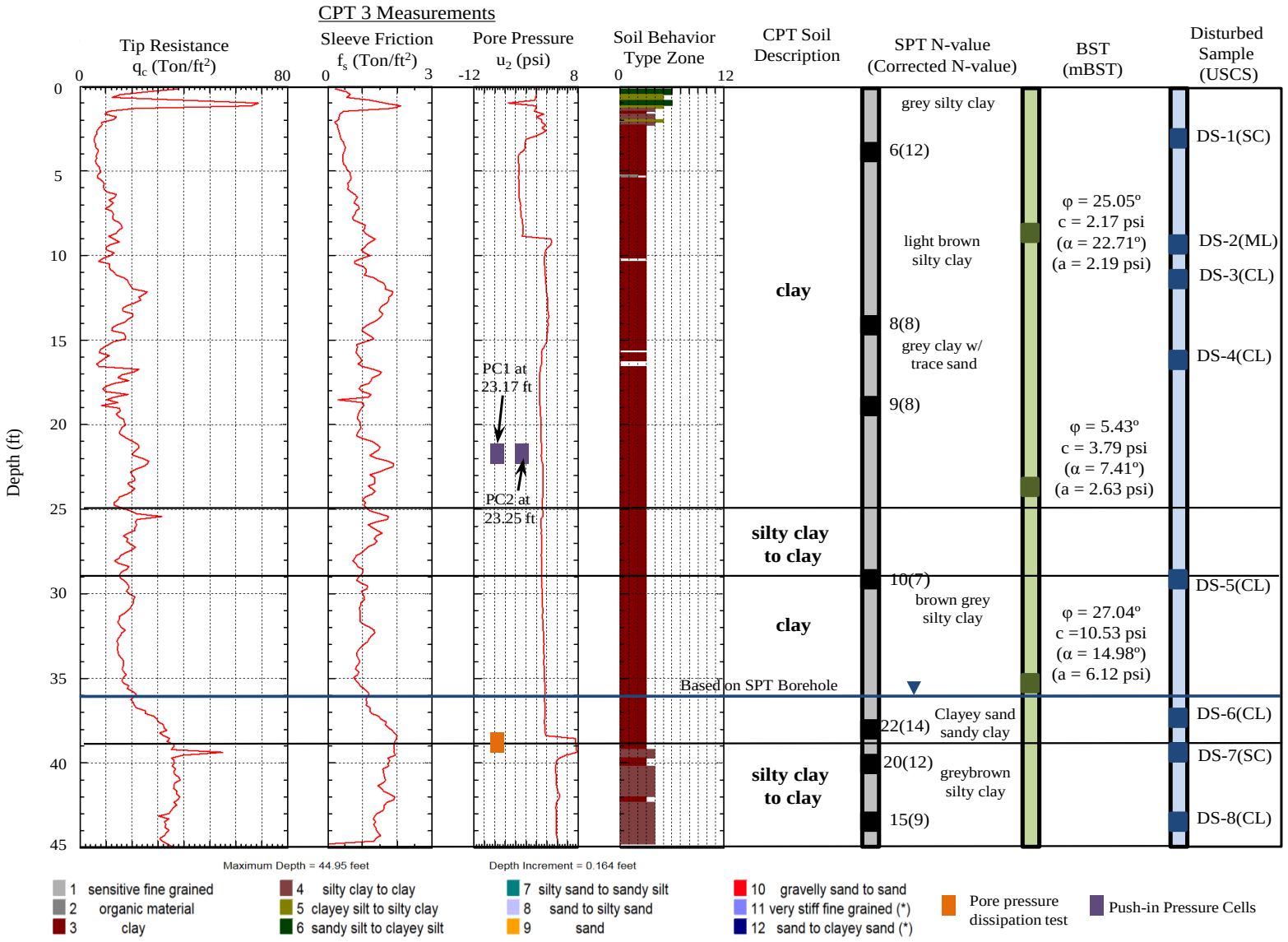

Figure B.1.6. In-situ soil investigations and soil profile for ISU5 at Clarke County

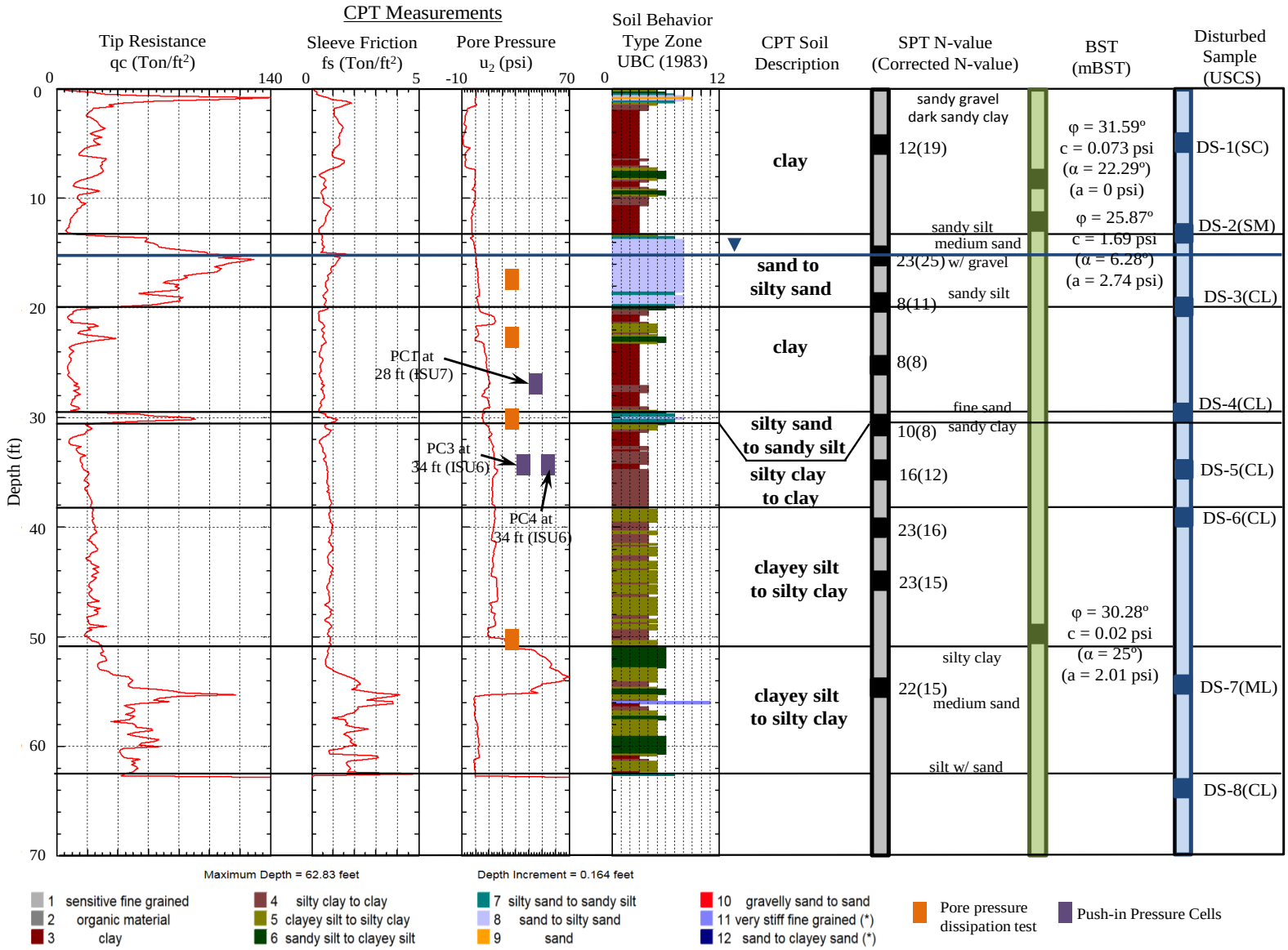

Figure B.1.7. In-situ soil investigations and soil profile for ISU6 and ISU7 at Buchanan County

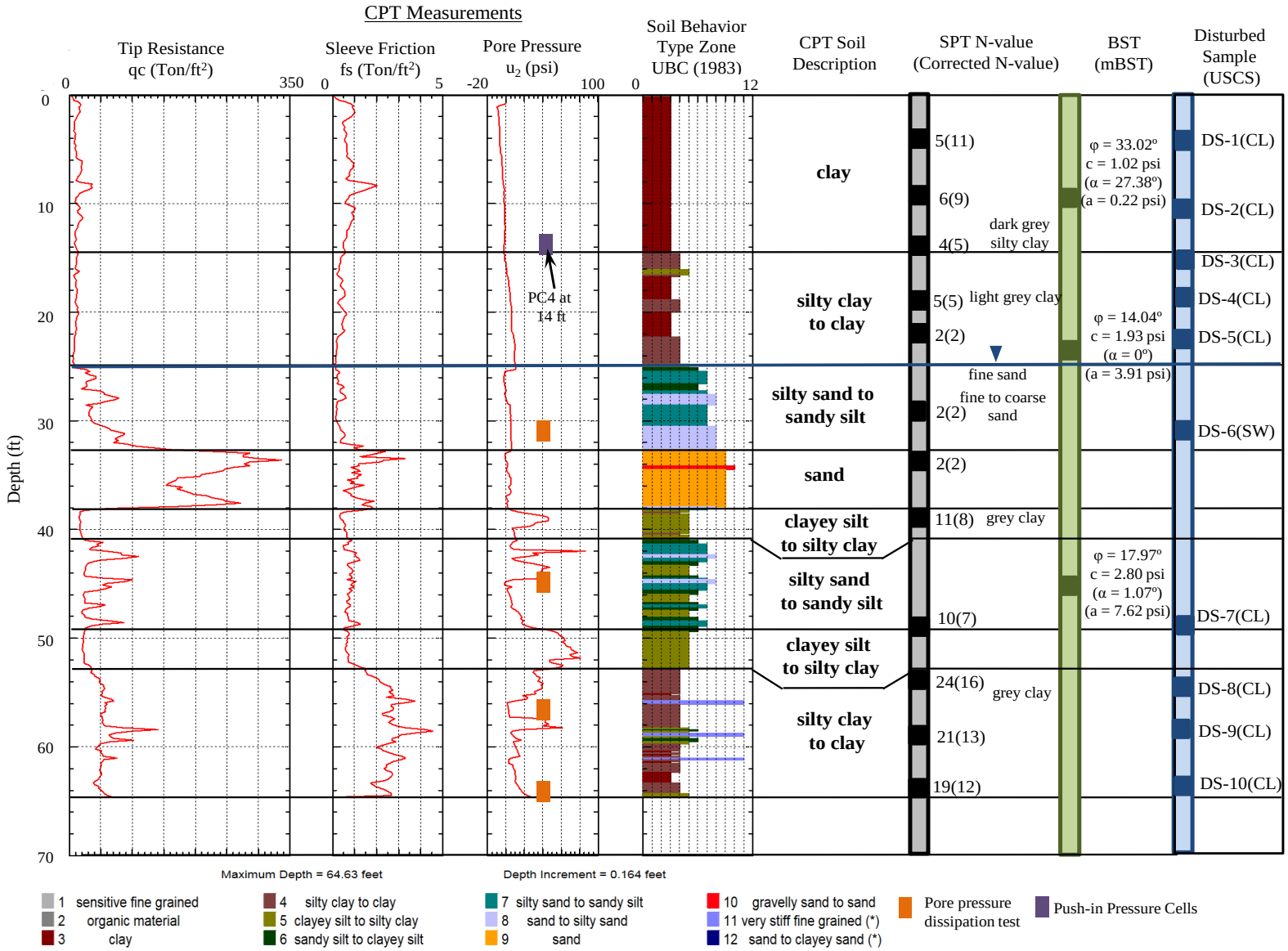

Figure B.1.8. In-situ soil investigations and soil profile for ISU8 at Poweshiek County

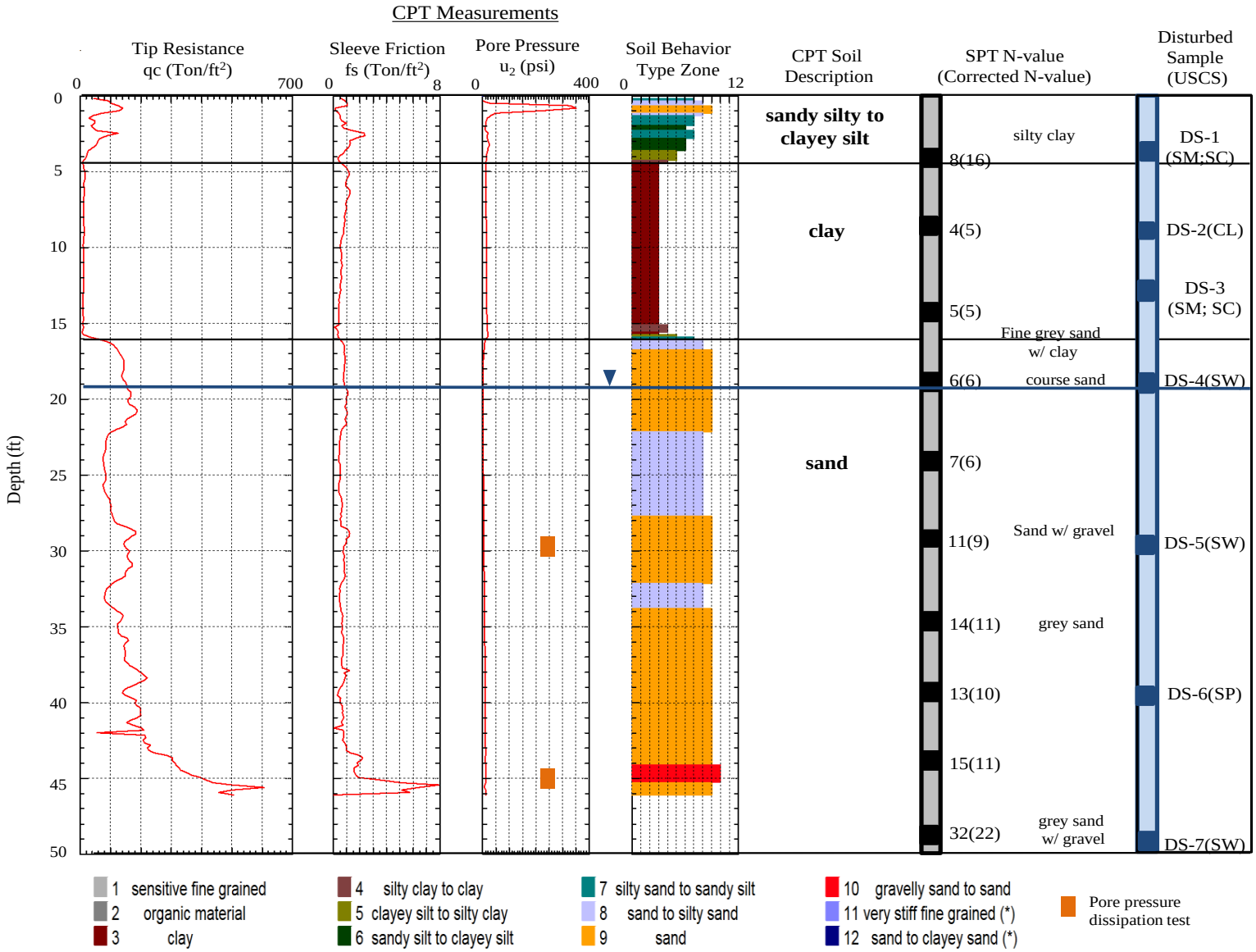

Figure B.1.9. In-situ soil investigations and soil profile for ISU9 at Des Moines County

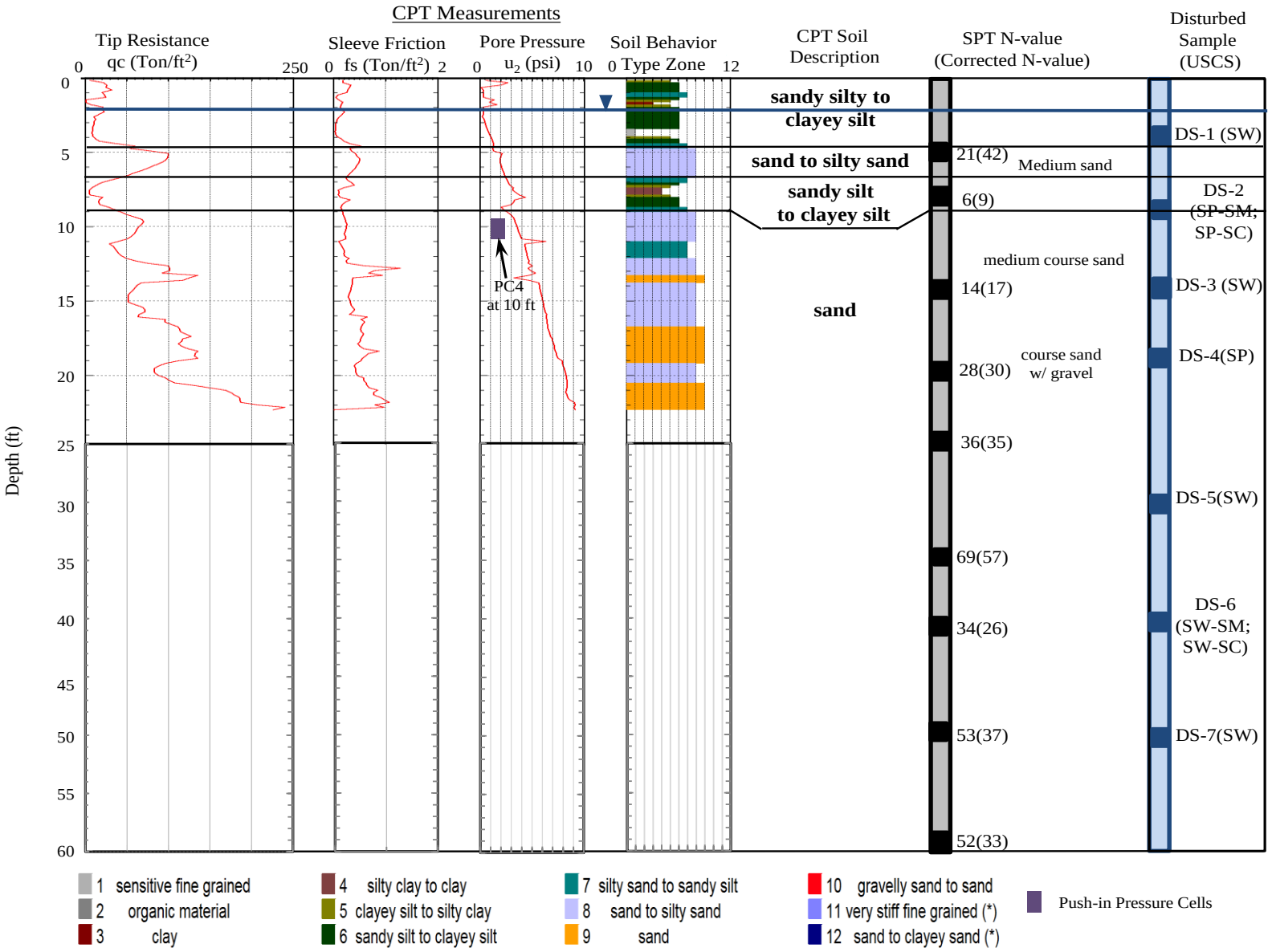

Figure B.1.10. In-situ soil investigations and soil profile for ISU10 at Cedar County

B.2. Estimated Soil Profiles and Properties Based on Cone Penetration Tests (CPT)

Table B.2.1. Summary of soil properties for ISU1 based on CPT

Soil Profiles	Depth (ft)	Soil Types	Average Effective Friction Angle, φ′ (degree)	Average Undrained Shear Strength, S_u (psi)	Over-consolidation Ratio (OCR)
Layer 1	0 to 4.43	Clay	31.93	5.63	-
Layer 2	4.43 to 9.19	Sensitive Fine Grained	30.09	7.19	7.99
Layer 3	9.19 to 15.42	Clay	33.23	19.39	12.74
Layer 4	15.42 to 18.86	Silty Sand to Sand	41.38	-	-
Layer 5	18.86 to 24.28	Sandy Silt to Clayey Silt	35.22	39.40	13.32
Layer 6	24.28 to 30.35	Sand to Silty Sand	42.18	-	-
Layer 7	30.35 to 32.97	Clayey Silt to silty Clay	37.12	66.20	17.06
Layer 8	32.97 to 33.79	Very Stiff Fine Grained Sand	36.77	-	-
Layer 9	33.79 to 35.43	Clay	37.74	110.07	26.24

Table B.2.2. Summary of soil properties for ISU2 based on CPT

Soil Profiles	Depth (ft)	Soil Types	Average Effective Friction Angle, φ′ (degree)	Average Undrained Shear Strength, S_u (psi)	Average Over-consolidation Ratio (OCR)
Layer 1	0 to 16	Clay	31.71	14.42	-
Layer 2	16 to 20	Clayey Silt to Silty Clay	28.51	11.31	7.52
Layer 3	20 to 36	Silty Clay to Clay	27.07	7.62	2.09
Layer 4	36 to 44	Clay	28.68	11.35	1.84
Layer 5	44 to 73	Clayey Silt to Silty Clay	27.04	18.10	6.50

Table B.2.3. Summary of soil properties for ISU3 based on CPT

Soil Profiles	Depth (ft)	Soil Types	Average Effective Friction Angle, φ′ (degree)	Average Undrained Shear Strength, S_u (psi)	Average Over-consolidation Ratio (OCR)
Layer 1	0 to 7.71	Clay	35.42	25.27	-
Layer 2	7.71 to 34	Clayey Silt to Silty Clay	32.76	16.55	5.94
Layer 3	34 to 41.5	Sandy Silt to Clayey Silt	34.36	14.95	3.19
Layer 4	41.5 to 45.11	Clayey Silt to Silty Clay	31.09	12.13	2.33
Layer 5	45.11 to 55.28	Clay	31.50	22.03	3.72
Layer 6	55.28 to 66.77	Clayey Silt to Silty Clay	29.09	23.09	2.74
Layer 7	66.77 to 69.88	Very Stiff Fine Grained	35.60	67.61	7.31

Table B.2.4. Summary of soil properties for ISU4 based on CPT

Soil Profiles	Depth (ft)	Soil Types	Average Effective Friction Angle, φ′ (degree)	Average Undrained Shear Strength, S_u (psi)	Average Over-consolidation Ratio (OCR)
Layer 1	0 to 7.71	Silty Clay to Clay	34.03	14.69	-
Layer 2	7.71 to 8.86	Silty Sand to Sandy Silt	34.59	-	-
Layer 3	8.86 to 12.96	Sensitive Fine Grained	25.41	4.09	2.15
Layer 4	12.96 to 19.85	Sandy Silt to Clayey Silt	30.68	12.27	5.48
Layer 5	19.85 to 21.16	Silty Sand to Sandy Silt	35.76	-	-
Layer 6	21.16 to 38.06	Clay	32.76	25.30	6.62
Layer 7	38.06 to 41.17	Silty Clay to Clay	30.97	18.14	3.76
Layer 8	41.17 to 50.36	Clayey Silt to Silty Clay	33.29	18.11	3.46

Table B.2.5. Summary of soil properties for ISU5 based on CPT

Soil Profiles	Depth (ft)	Soil Types	Average Effective Friction Angle, φ′ (degree)	Average Undrained Shear Strength, S_u (psi)	Average Over-consolidation Ratio (OCR)
Layer 1	0 to 25	Clay	31.08	13.28	5.60
Layer 2	25 to 29	Silty Clay to Clay	29.94	15.71	3.11
Layer 3	29 to 39	Clay	29.72	16.46	2.63
Layer 4	39 to 45	Silty Clay to Clay	32.09	30.61	3.92

Table B.2.6. Summary of soil properties for ISU6 and ISU7 based on CPT

Soil Profiles	Depth (ft)	Soil Types	Average Effective Friction Angle, φ′ (degree)	Average Undrained Shear Strength, S_u (psi)	Average Over-consolidation Ratio (OCR)
Layer 1	0 to 13.12	Clay	33.96	22.27	-
Layer 2	13.12 to 20.01	Sand to Silty Sand	38.28	-	-
Layer 3	20.01 to 29.36	Clay	28.82	10.27	3.33
Layer 4	29.36 to 30.51	Silty Sand to Sandy Silt	35.34	-	-
Layer 5	30.51 to 38.22	Silty Clay to Clay	29.86	14.15	3.05
Layer 6	38.22 to 50.85	Clayey Silt to Silty Clay	30.56	18.57	2.95
Layer 7	50.85 to 62.50	Clayey Silt to Silty Clay	33.63	41.68	5.98

Table B.2.7. Summary of soil properties for ISU8 based on CPT

Soil Profiles	Depth (ft)	Soil Types	Average Effective Friction Angle, φ′ (degree)	Average Undrained Shear Strength, S_u (psi)	Average Over-consolidation Ratio (OCR)
Layer 1	0 to 14.44	Clay	32.50	12.49	-
Layer 2	14.44 to 24.93	Silty Clay to Clay	28.15	8.43	2.69
Layer 3	24.93 to 32.48	Silty Sand to Sandy Silt	34.62	-	-
Layer 4	32.48 to 38.06	Sand	41.75	-	-
Layer 5	38.06 to 41.17	Clayey Silt to Silty Clay	29.90	16.60	3.18
Layer 6	41.17 to 49.21	Silty Sand to Sandy Silt	33.12	-	-
Layer 7	49.21 to 52.66	Clayey Silt to Silty Clay	30.41	18.94	3.11
Layer 8	52.66 to 64.47	Silty Clay to Clay	34.27	47.59	6.76

Table B.2.8. Summary of soil properties for ISU9 based on CPT

Soil Profiles	Depth (ft)	Soil Types	Average Effective Friction Angle, φ′ (degree)	Average Undrained Shear Strength, S_u (psi)	Average Over-consolidation Ratio (OCR)
Layer 1	0 to 4.27	Sandy Silt to Clayey Silt	46.19	392.44	-
Layer 2	4.27 to 15.91	Clay	30.97	71.59	6.90
Layer 3	15.91 to 45.93	Sand	40.21	-	-

Table B.2.9. Summary of soil properties for ISU10 based on CPT

Soil Profiles	Depth (ft)	Soil Types	Average Effective Friction Angle, φ′ (degree)	Average Undrained Shear Strength, S_u (psi)	Average Over-consolidation Ratio (OCR)
Layer 1	0 to 4.59	Sandy Silt to Clayey Silt	34.65	108.87	-
Layer 2	4.59 to 6.56	Sand to Silty Sand	41.30	-	-
Layer 3	6.56 to 8.86	Sandy Silt to Clayey Silt	32.89	115.15	16.66
Layer 4	8.86 to 22.15	Sand	39.61	-	-

B.3. Pore Water Pressure Measurements Using Cone Penetration Tests (CPT)

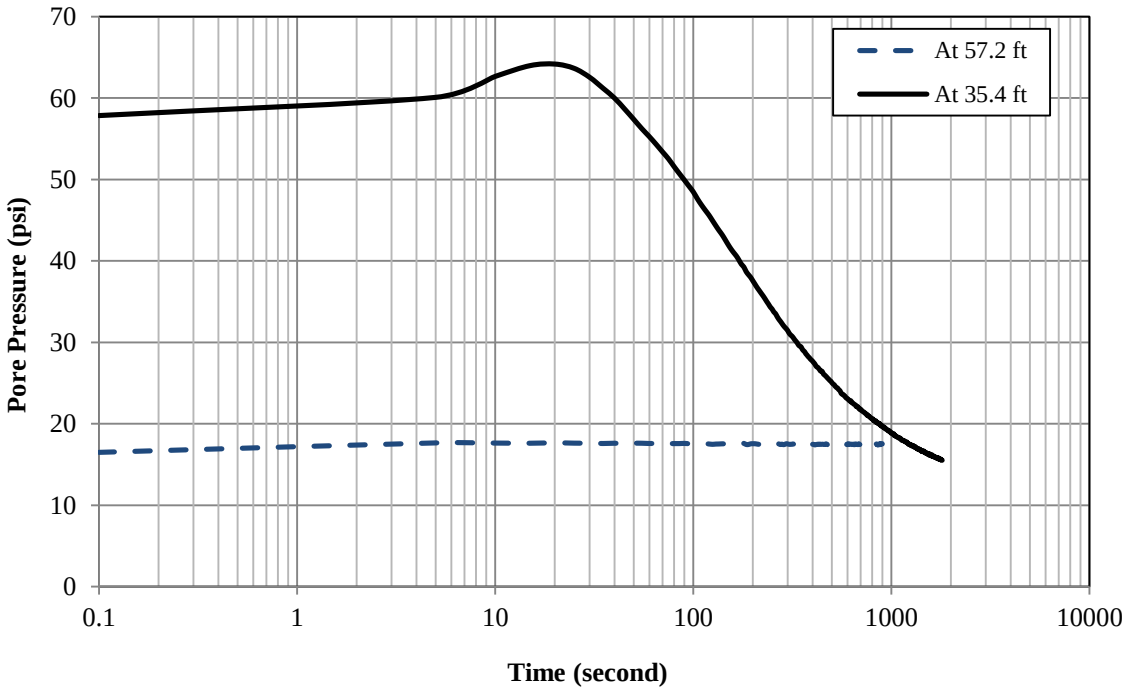

Figure B.3.1. CPT pore water pressure dissipation tests at ISU2 Mills County

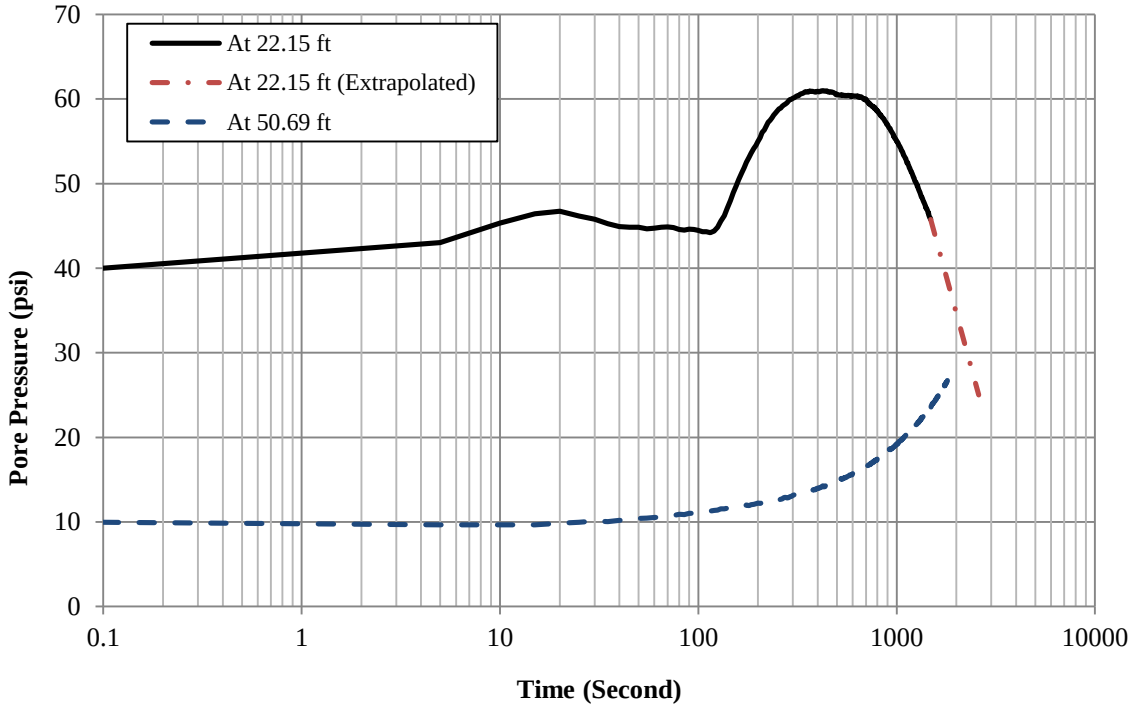

Figure B.3.2. CPT pore water pressure dissipation tests at ISU3 Polk County

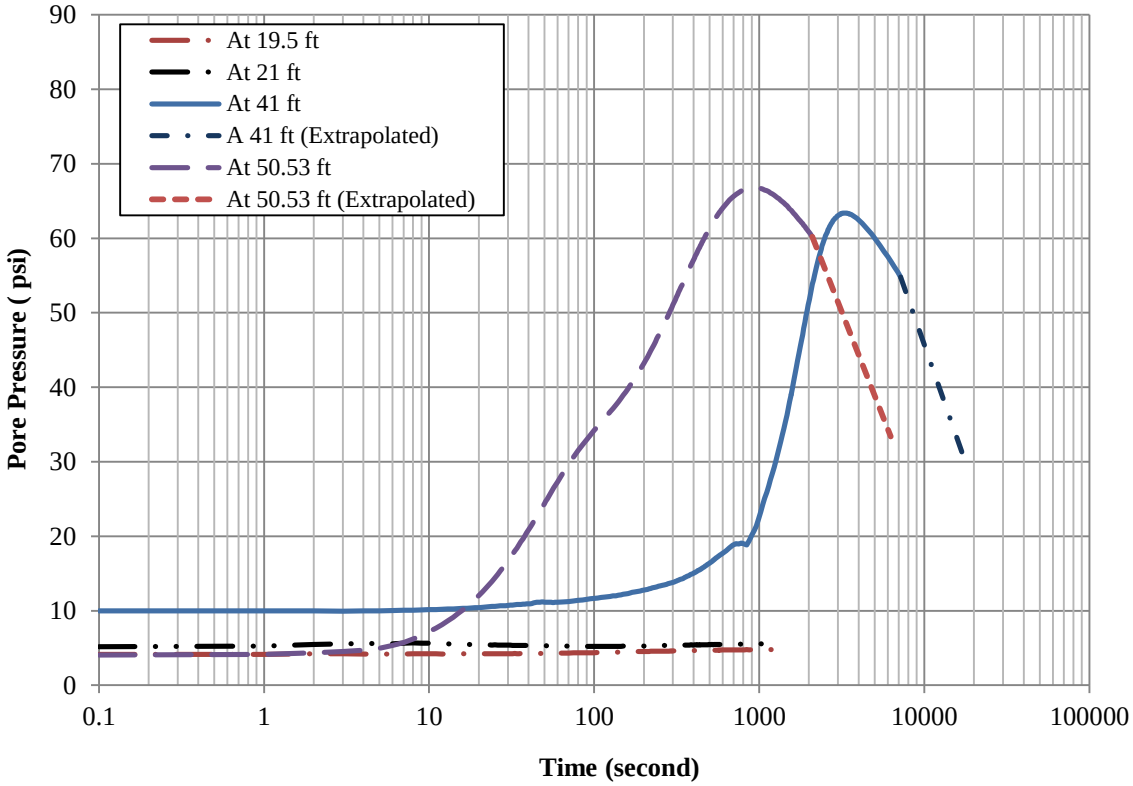

Figure B.3.3. CPT pore water pressure dissipation tests at ISU4 Jasper County

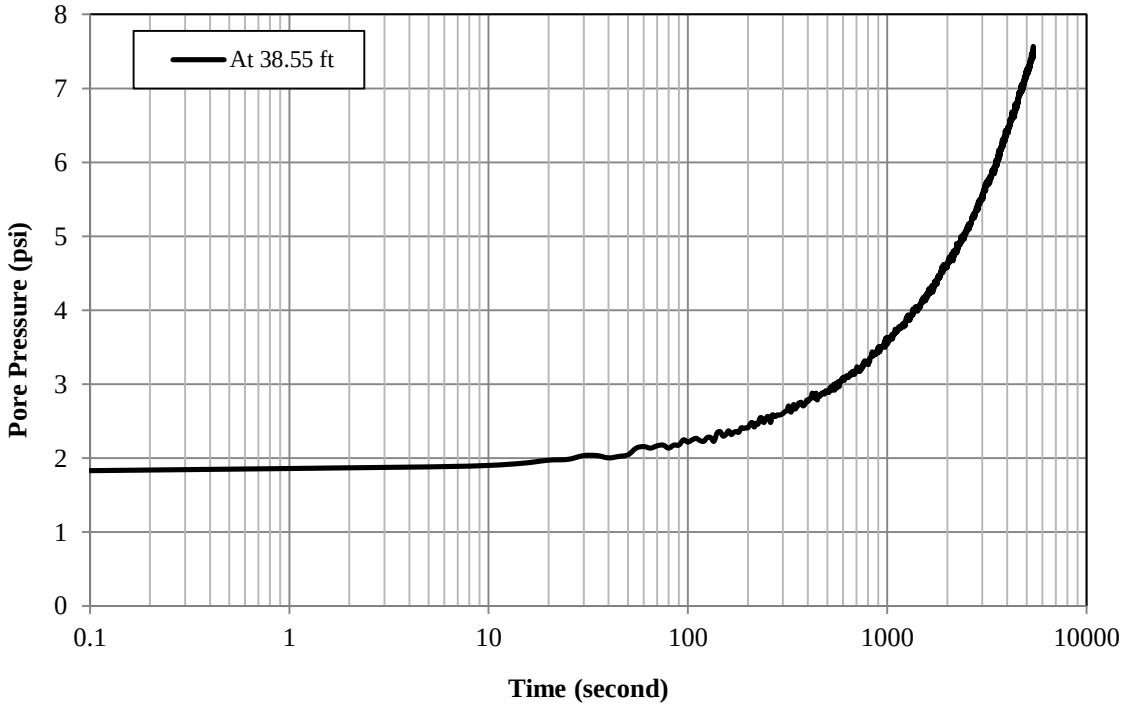

Figure B.3.4. CPT pore water pressure dissipation tests at ISU5 Clarke County

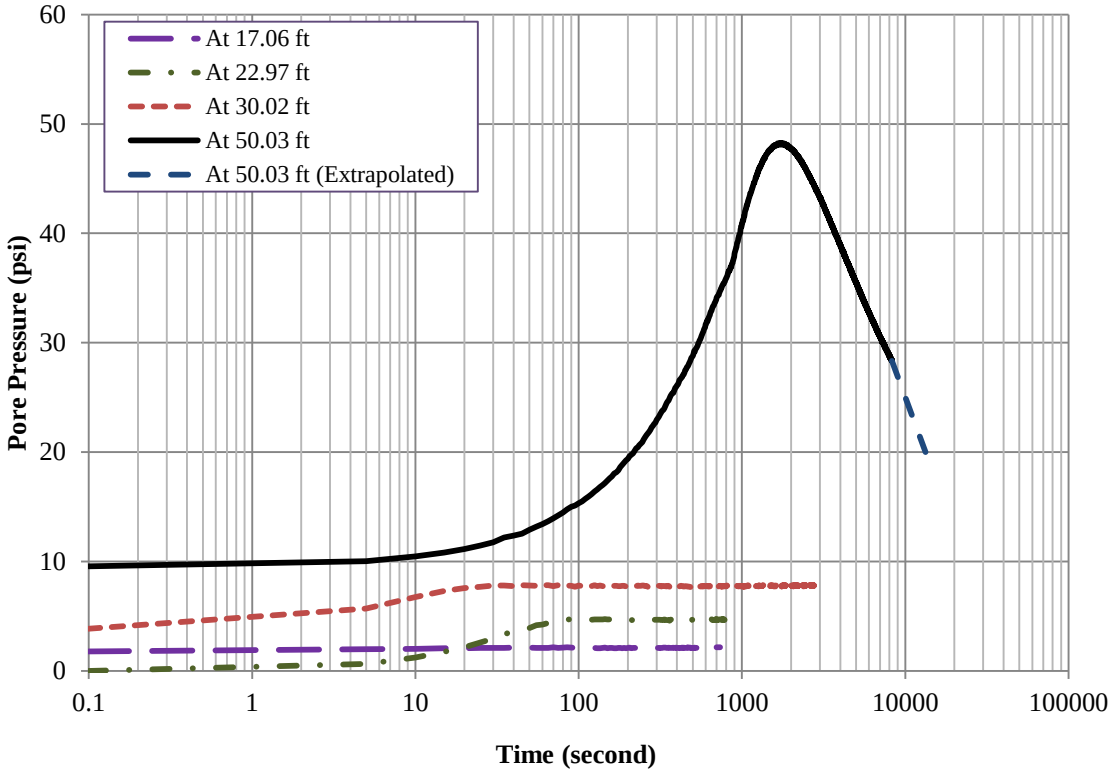

Figure B.3.5. CPT pore water pressure dissipation tests at ISU6 and ISU7 Buchanan County

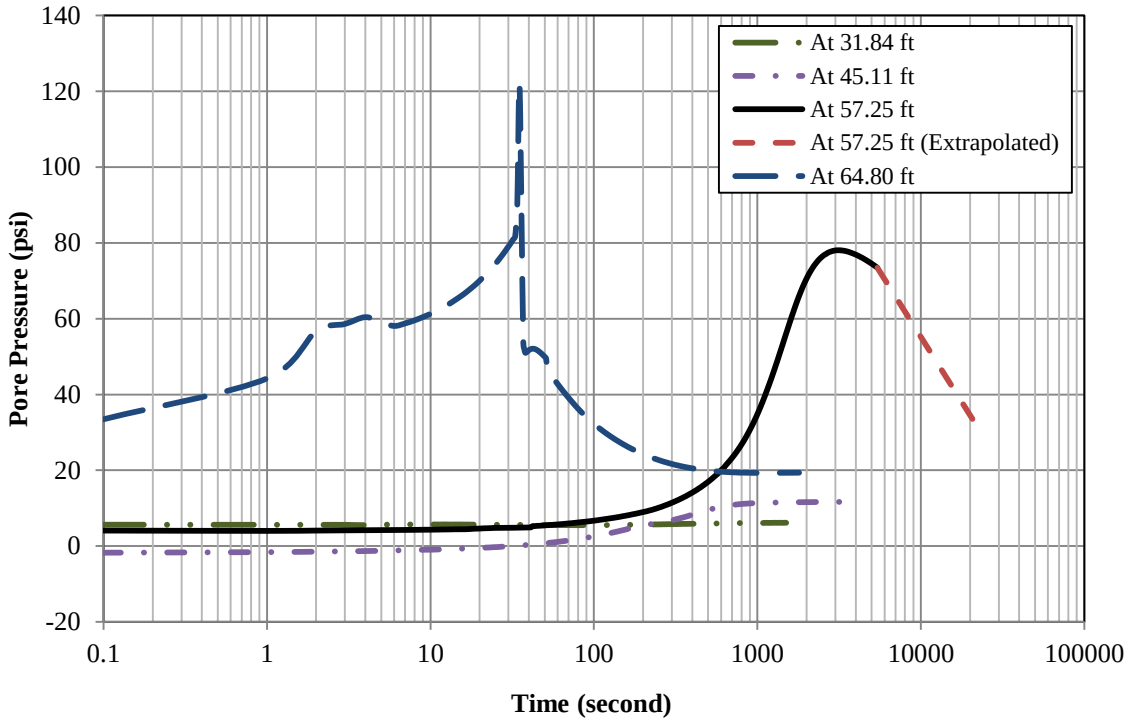

Figure B.3.6. CPT pore water pressure dissipation tests at ISU8 Poweshiek County

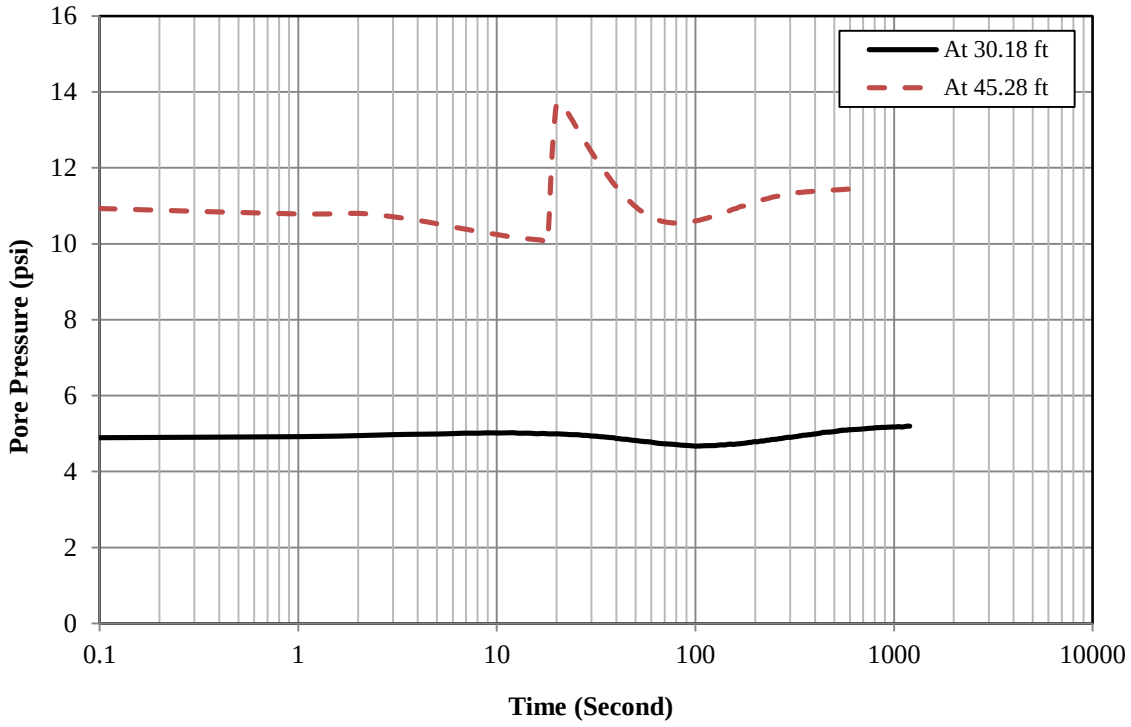

Figure B.3.7. CPT pore water pressure dissipation tests at ISU9 Des Moines County

B.4. Borehole Shear Test and modified Borehole Shear Test Results

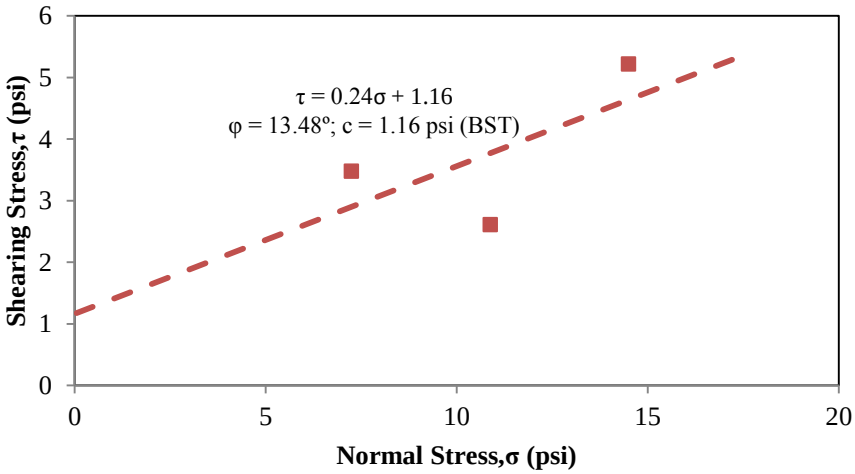

Figure B.4.1. ISU1 at 3-ft depth (BST)

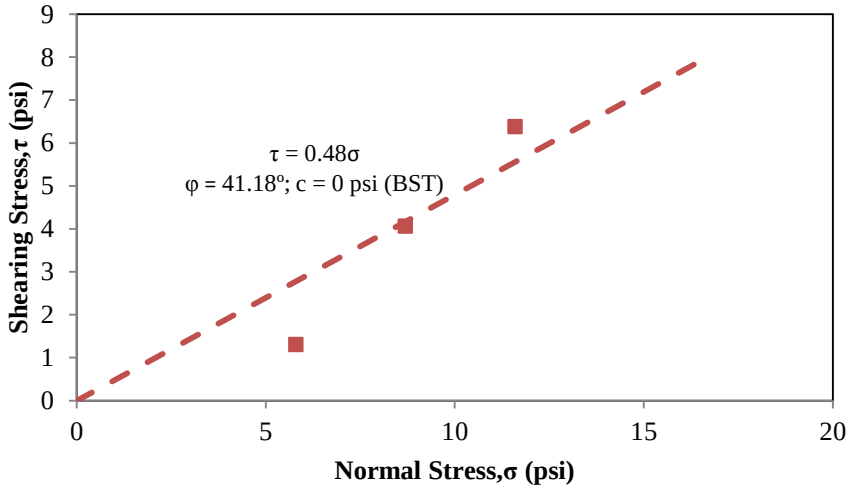

Figure B.4.2. ISU1 at 8-ft depth (BST)

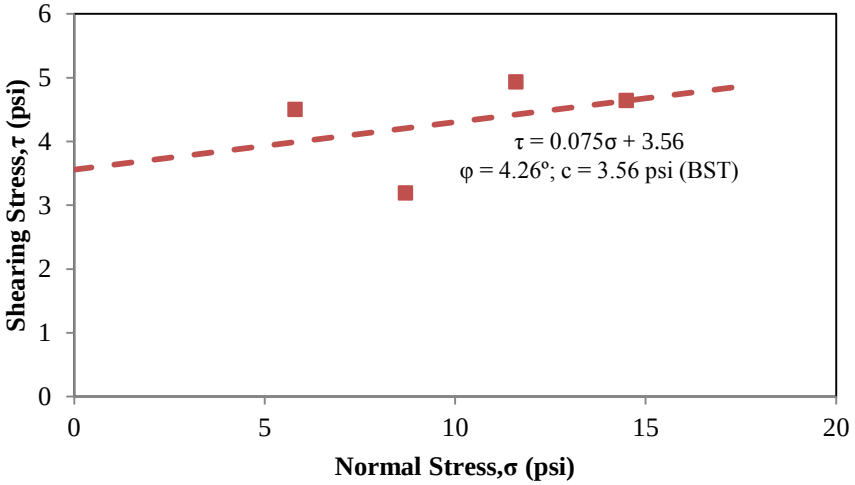

Figure B.4.3. ISU1 at 16-ft depth (BST)

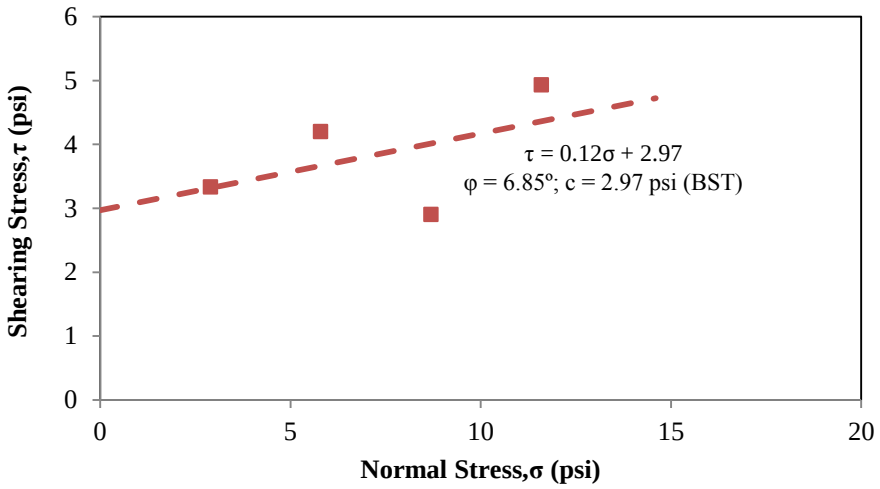

Figure B.4.4. ISU2 at 5-ft depth (BST)

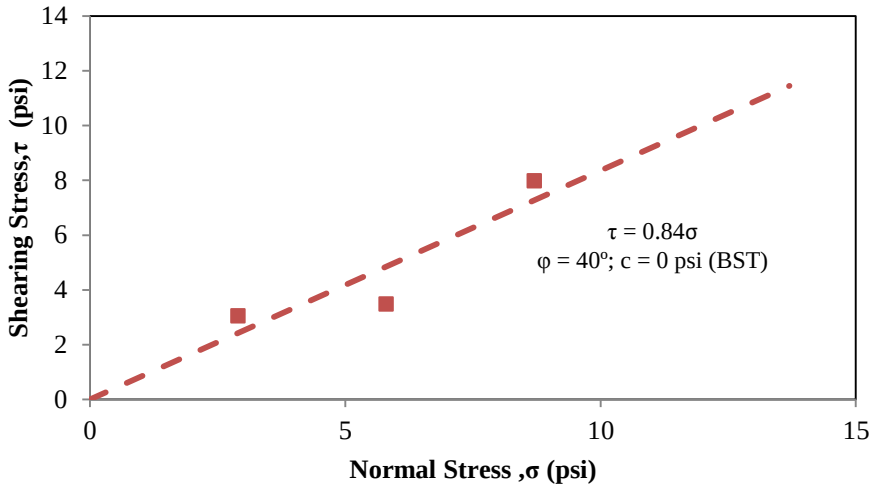

Figure B.4.5. ISU2 at 20-ft depth (BST)

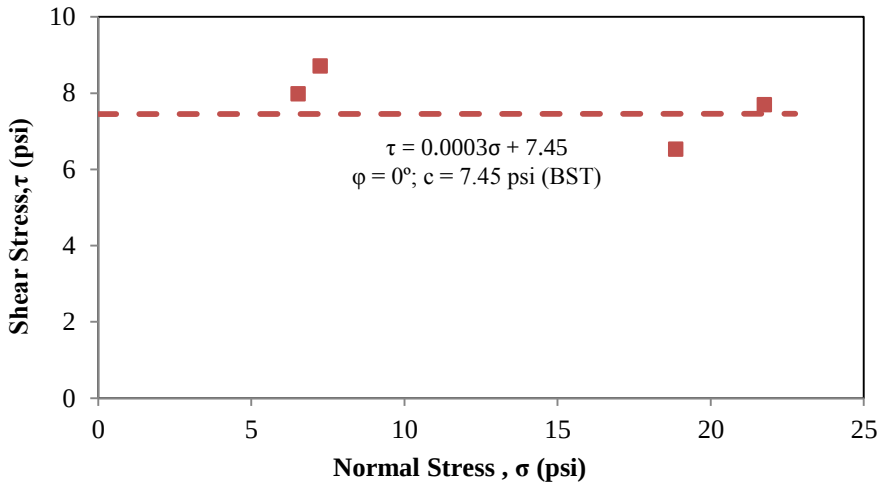

Figure B.4.6. ISU3 at 4-ft depth (BST)

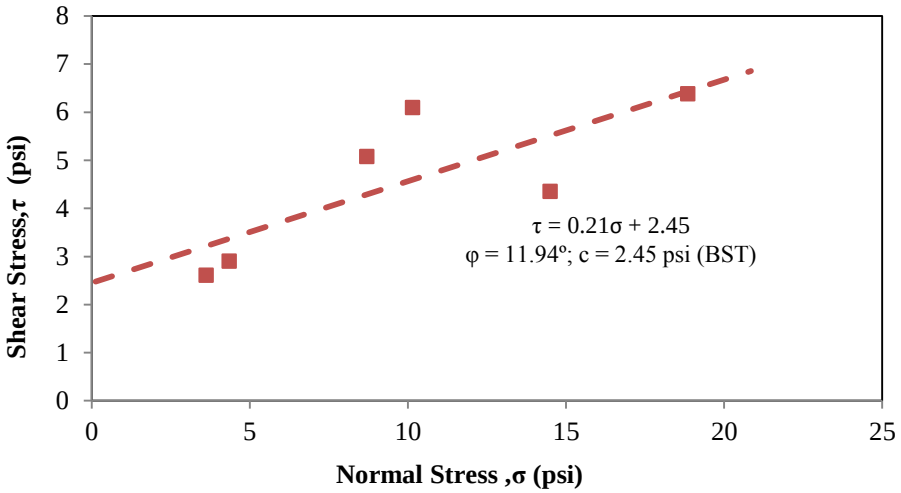

Figure B.4.7. ISU3 at 23-ft depth (BST)

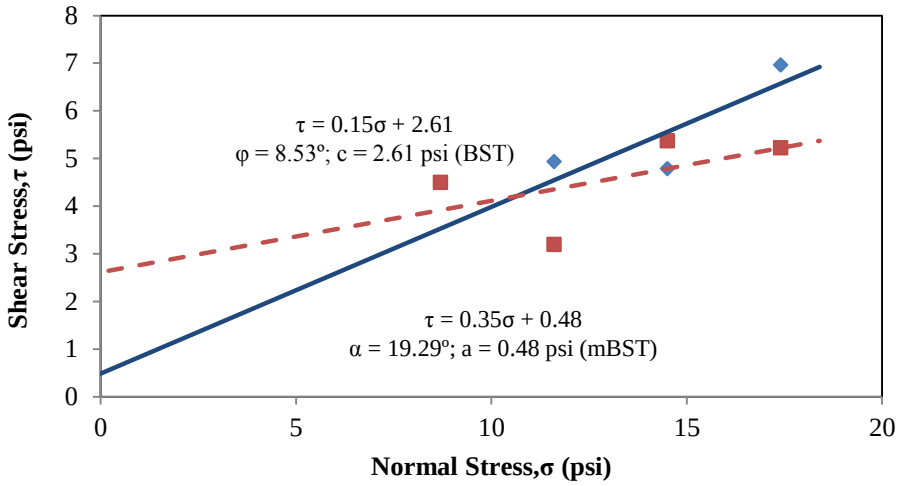

Figure B.4.8. ISU4 at 27-ft depth (BST & mBST)

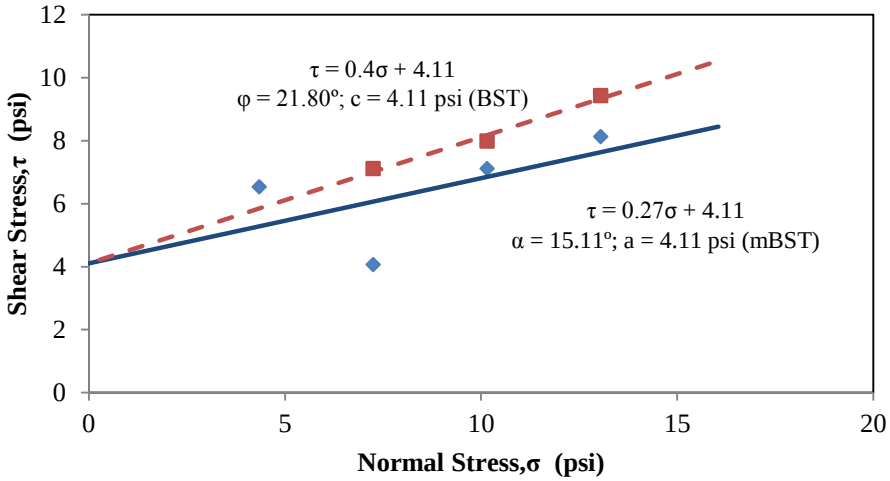

Figure B.4.9. ISU4 at 46-ft depth (BST & mBST)

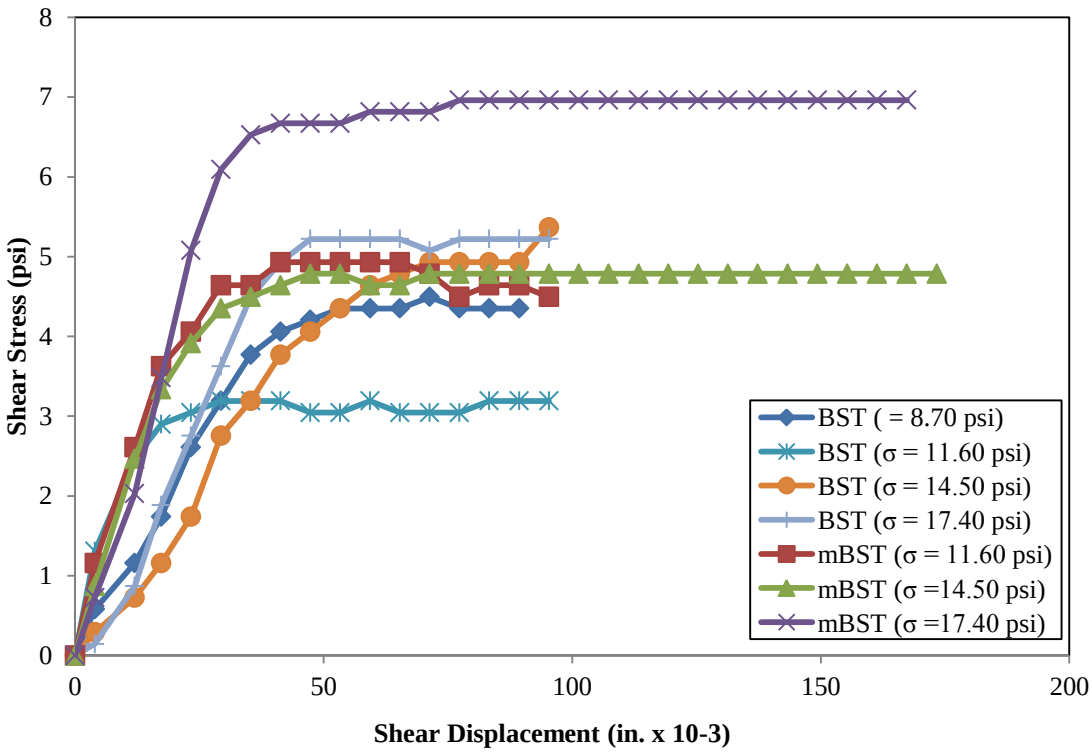

Figure B.4.10. BST and mBST generated shear stress-displacement relationships for ISU4 at 27-ft depth

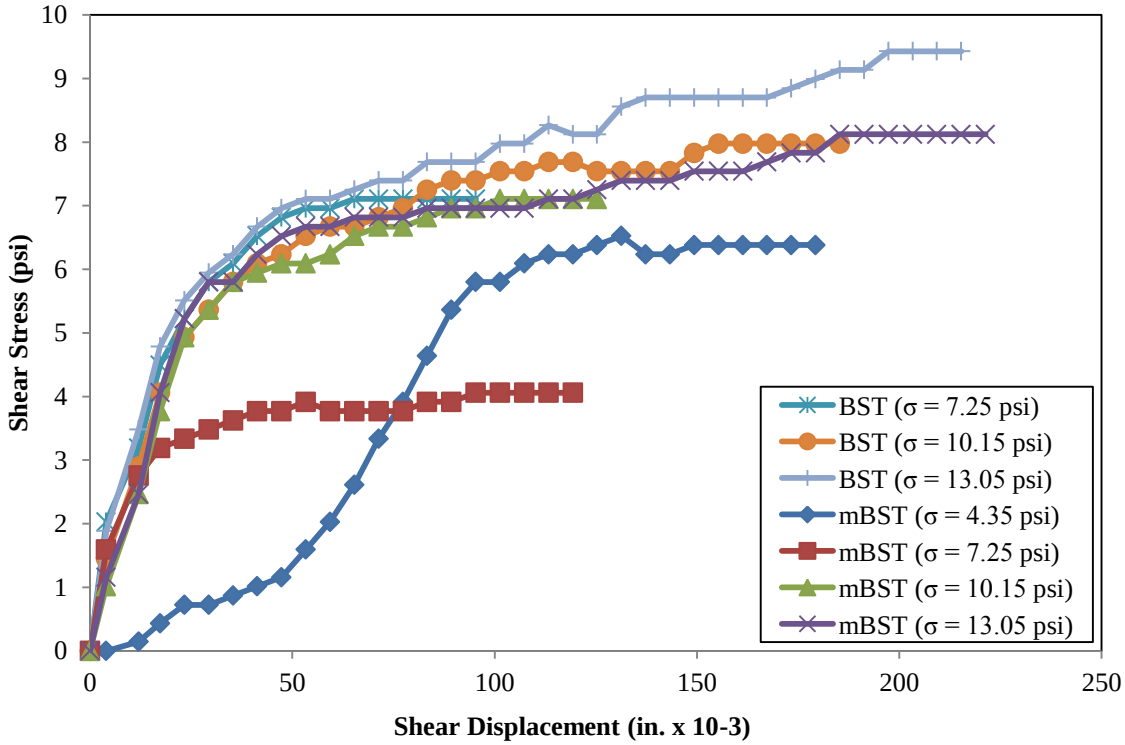

Figure B.4.11. BST and mBST generated shear stress-displacement relationships for ISU4 at 46-ft depth

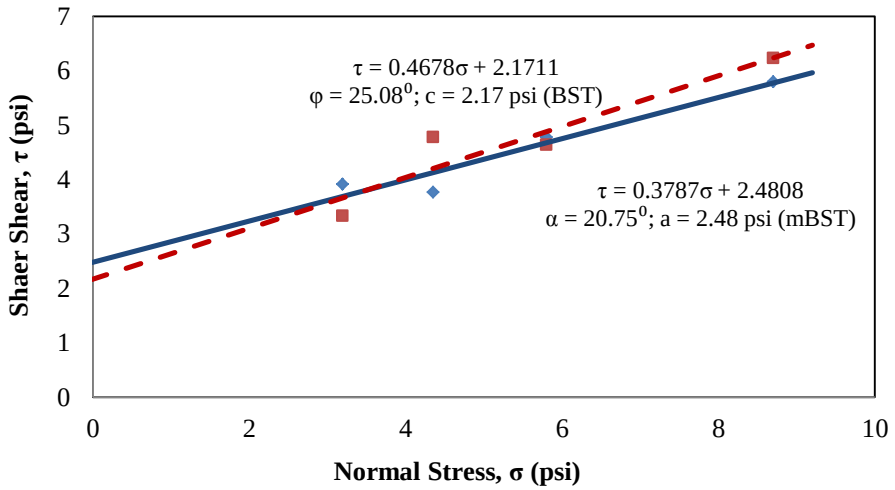

Figure B.4.12. ISU5 at 8.83-ft depth (BST & mBST)

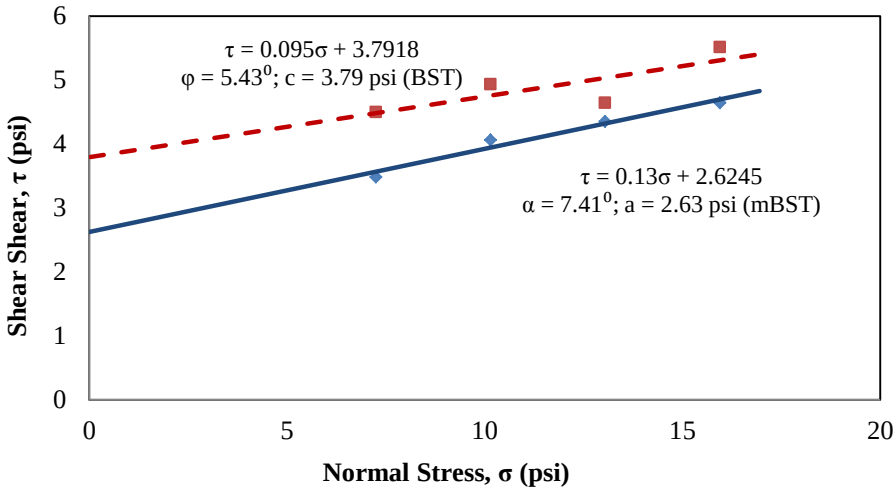

Figure B.4.13. ISU5 at 23.83-ft depth (BST & mBST)

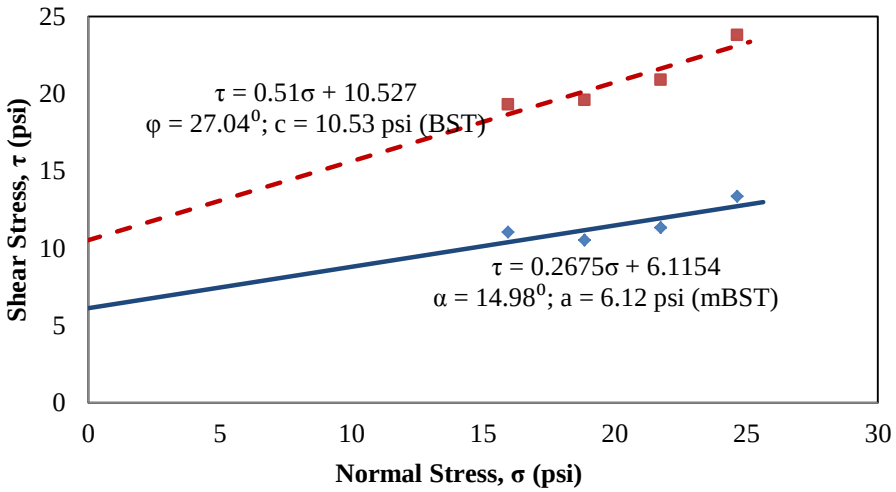

Figure B.4.14. ISU5 at 35.83-ft depth (BST & mBST)

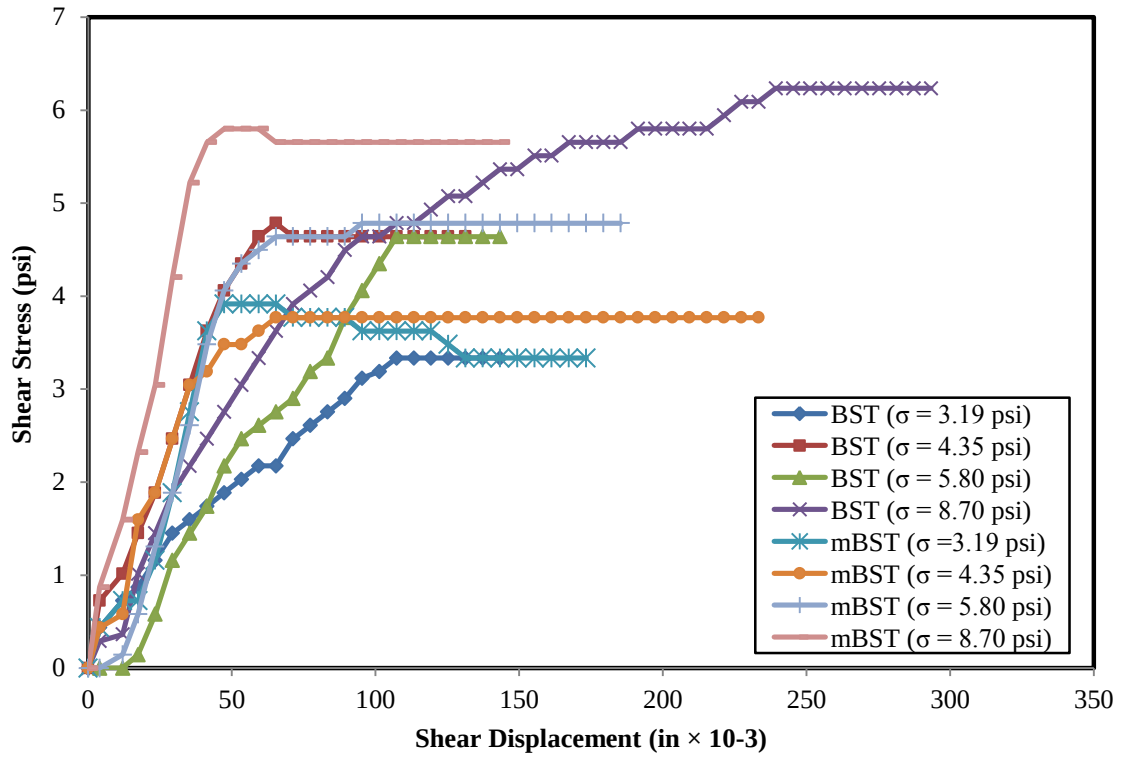

Figure B.4.15. BST and mBST generated shear stress-displacement relationships for ISU5 at 8.83-ft depth

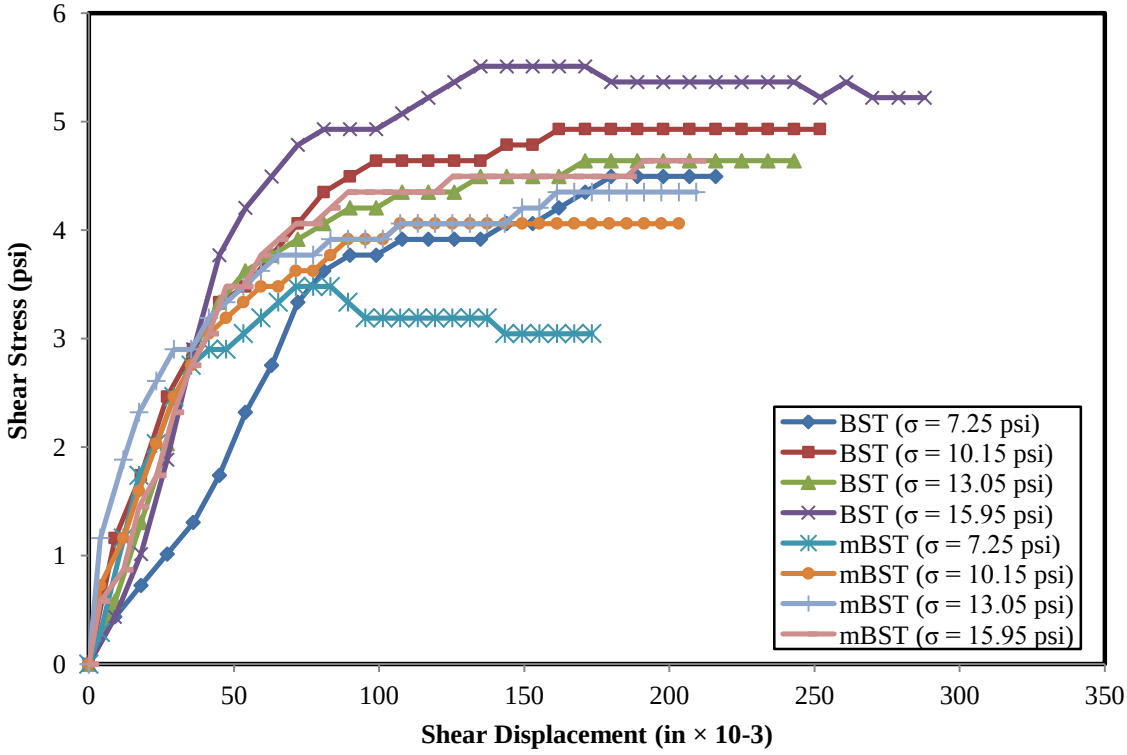

Figure B.4.16. BST and mBST generated shear stress-displacement relationships for ISU5 at 23.83-ft depth

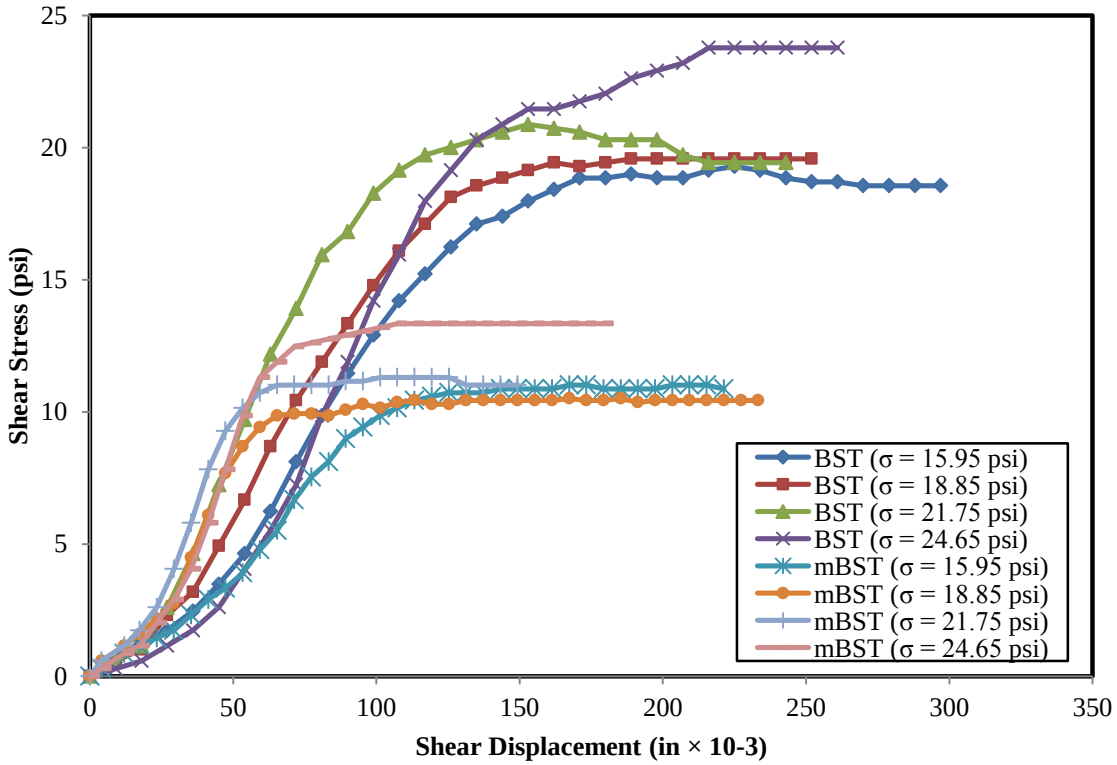

Figure B.4.17. BST and mBST generated shear stress-displacement relationships for ISU5 at 35.83-ft depth

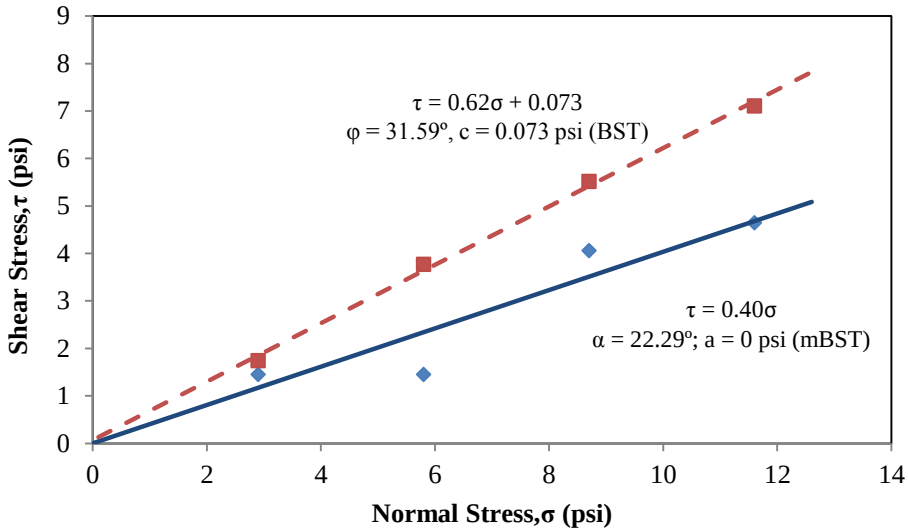

Figure B.4.18. ISU6 and ISU7 at 8.3-ft depth (BST & mBST)

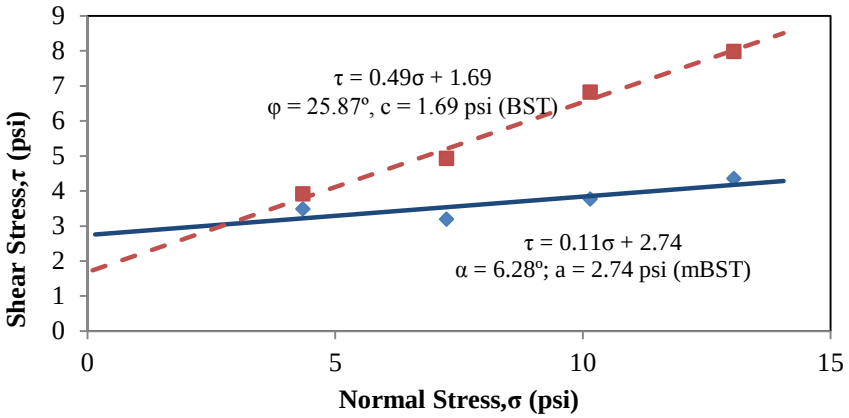

Figure B.4.19. ISU6 and ISU7 at 11.89-ft depth (BST & mBST)

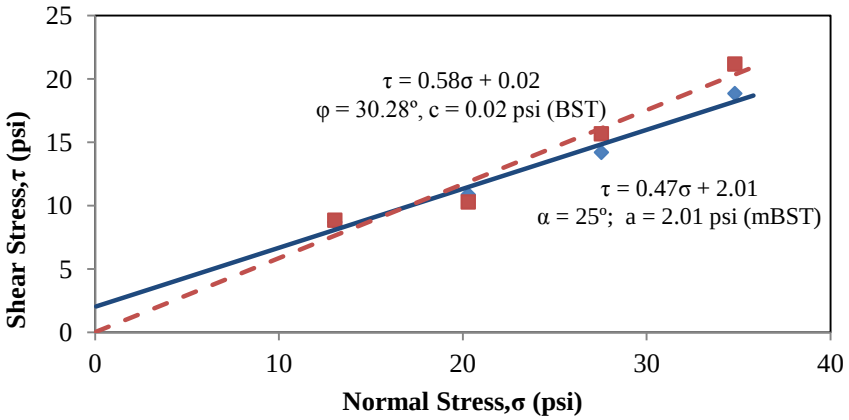

Figure B.4.20. ISU6 and ISU7 at 50.3-ft depth (BST & mBST)

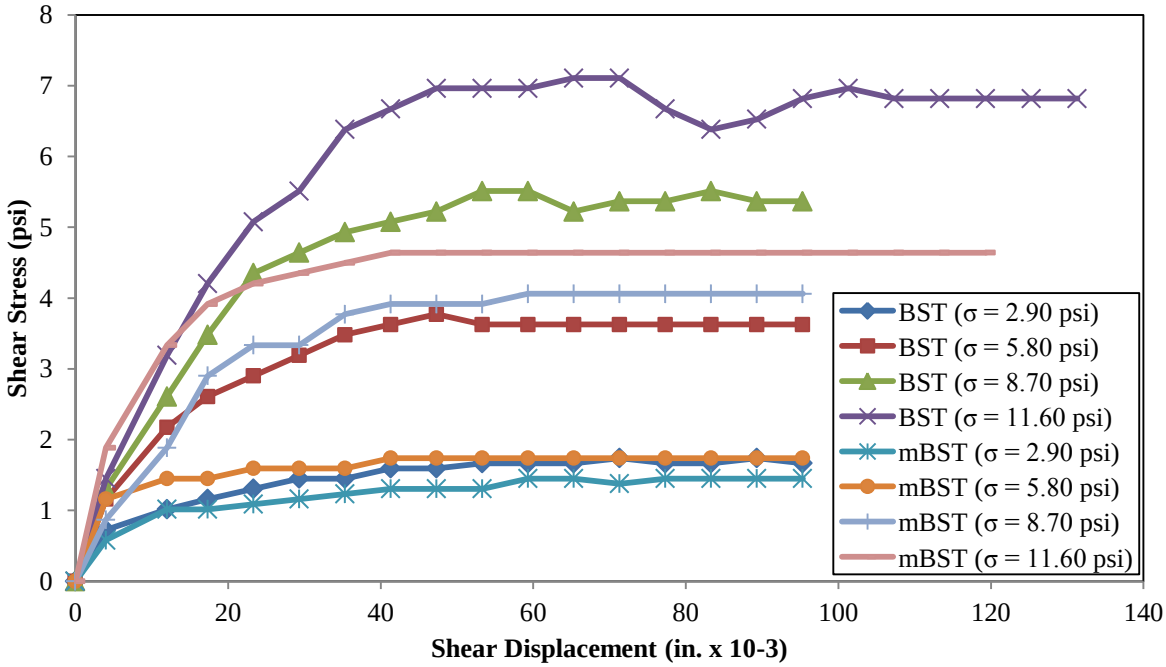

Figure B.4.21. BST and mBST generated shear stress-displacement relationships for ISU6 and ISU7 at 8.3-ft depth

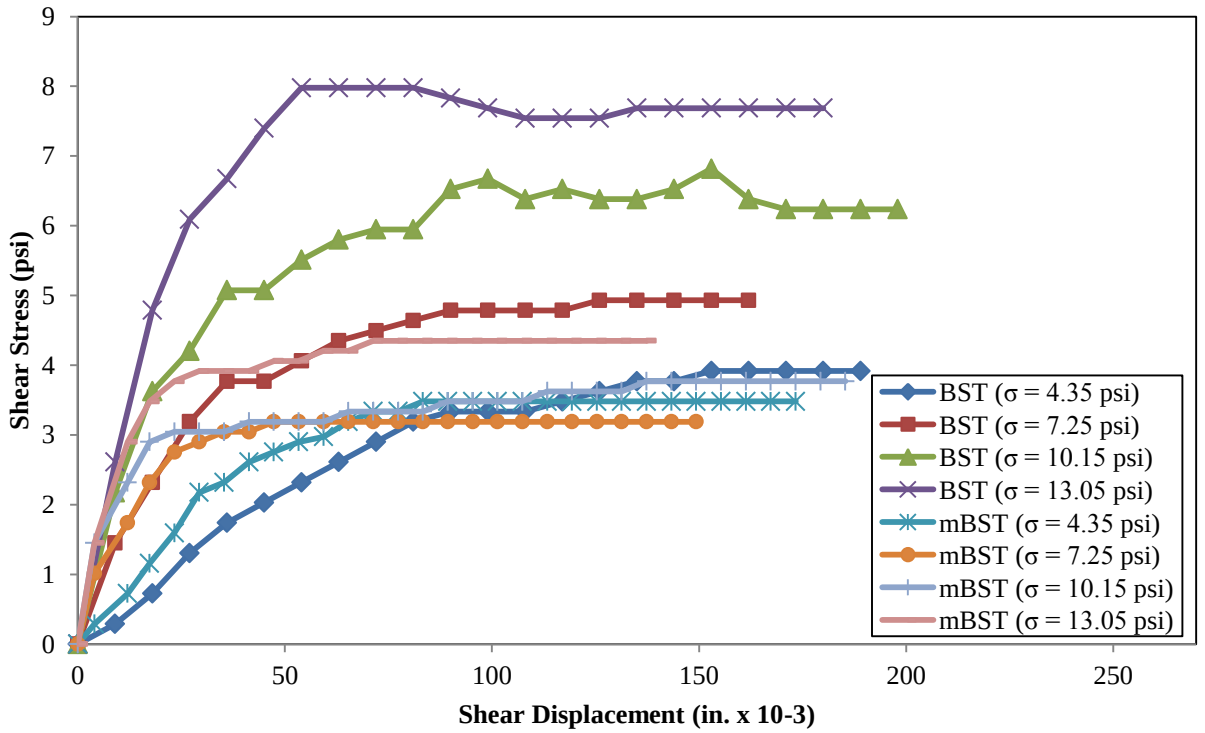

Figure B.4.22. BST and mBST generated shear stress-displacement relationships for ISU6 and ISU7 at 11.89-ft depth

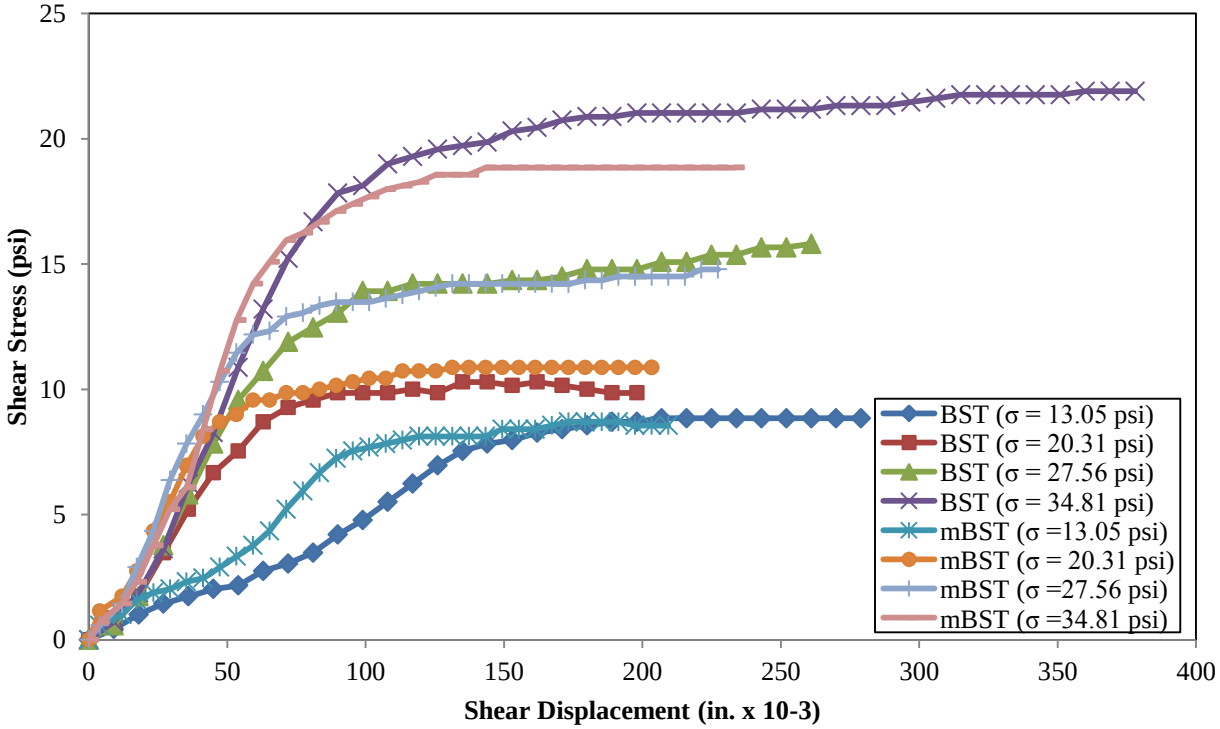

Figure B.4.23. BST and mBST generated shear stress-displacement relationships for ISU6 and ISU7 at 50.3-ft depth

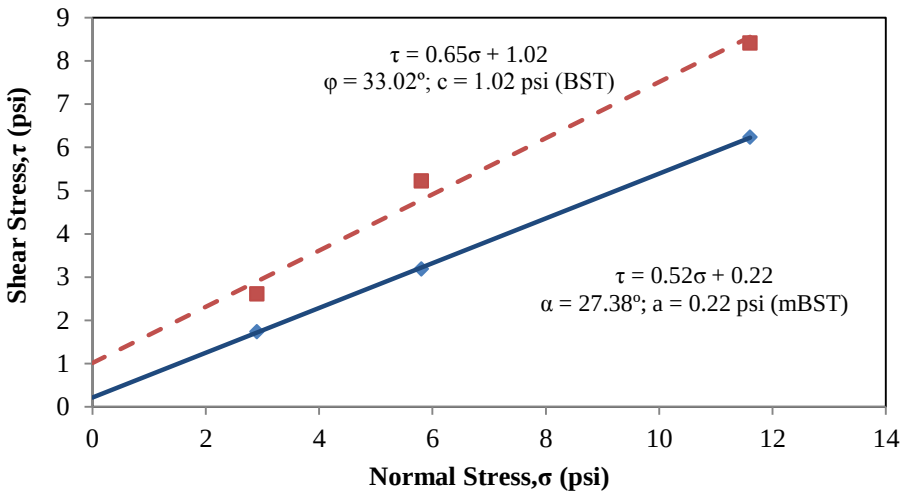

Figure B.4.24. ISU8 at 9-ft depth (BST & mBST)

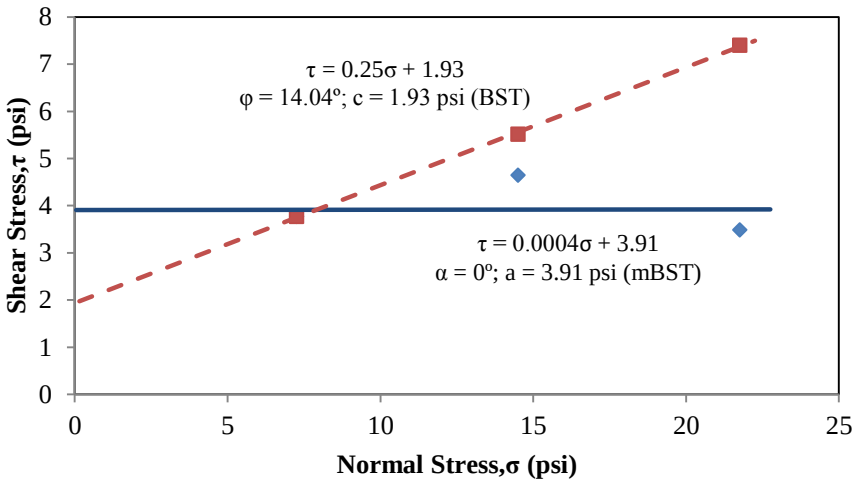

Figure B.4.25. ISU8 at 23-ft depth (BST & mBST)

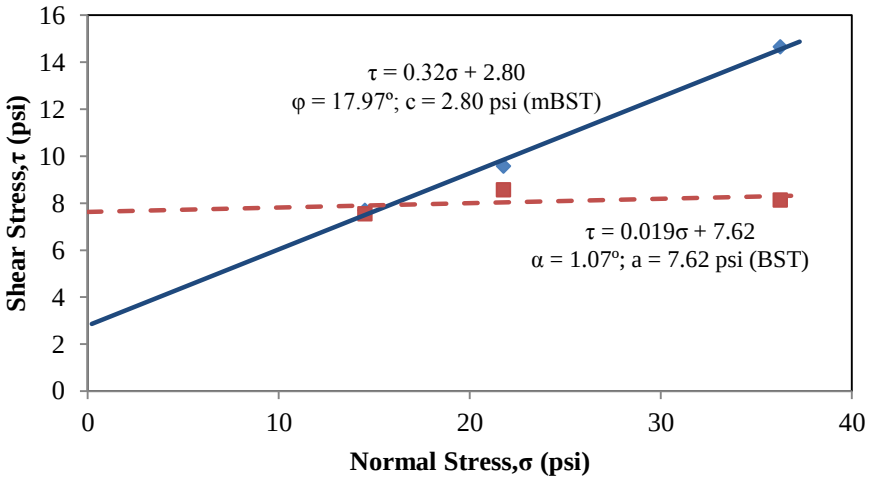

Figure B.4.26. ISU8 at 45-ft depth (BST & mBST)

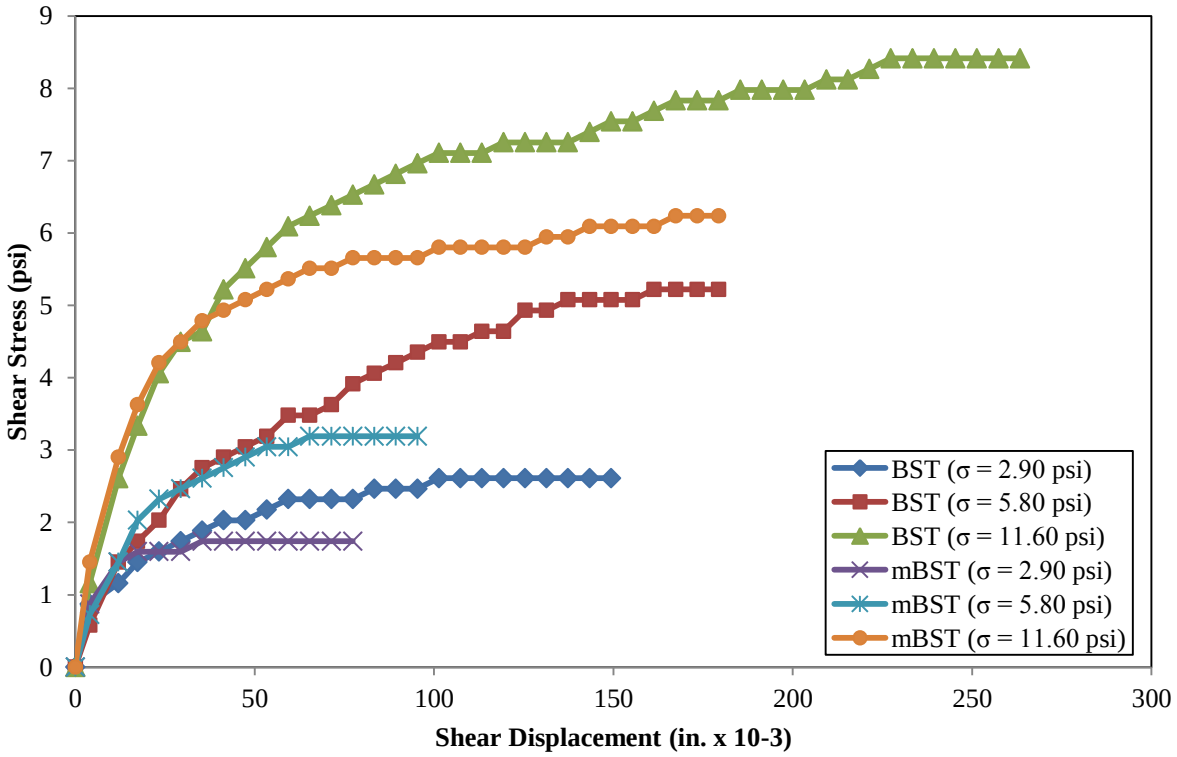

Figure B.4.27. BST and mBST generated shear stress-displacement relationships for ISU8 at 9-ft depth

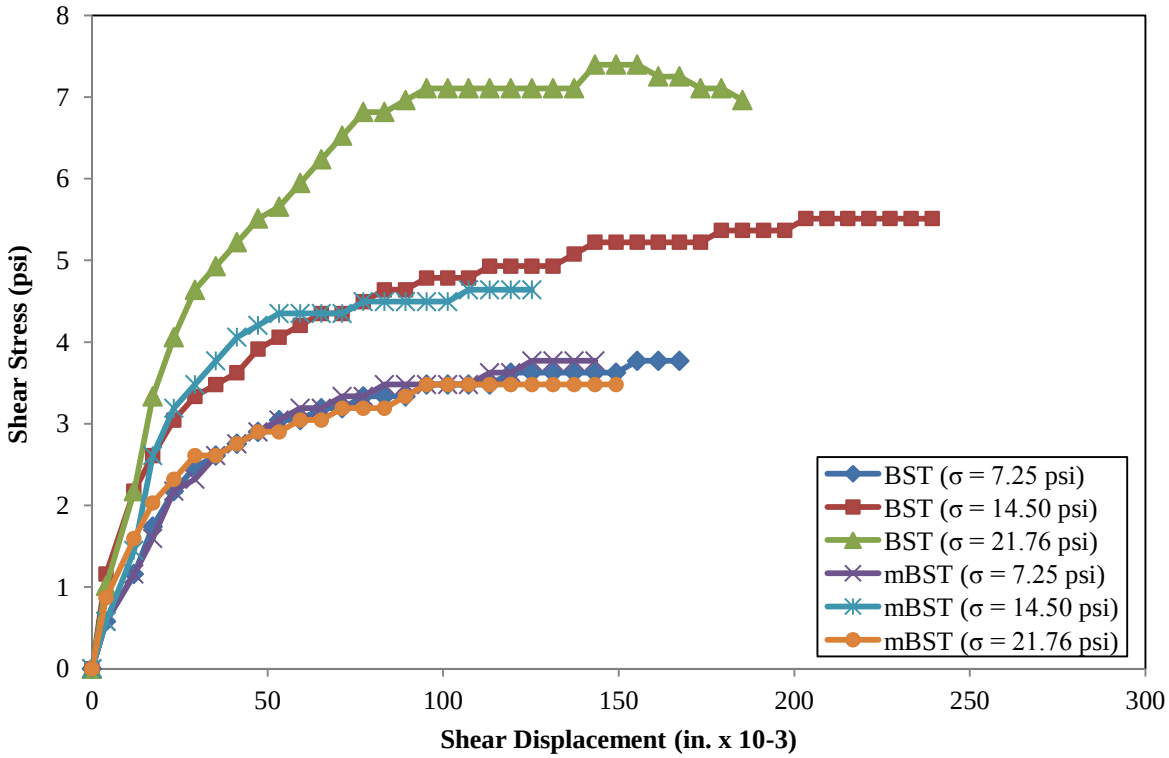

Figure B.4.28. BST and mBST generated shear stress-displacement relationships for ISU8 at 23-ft depth

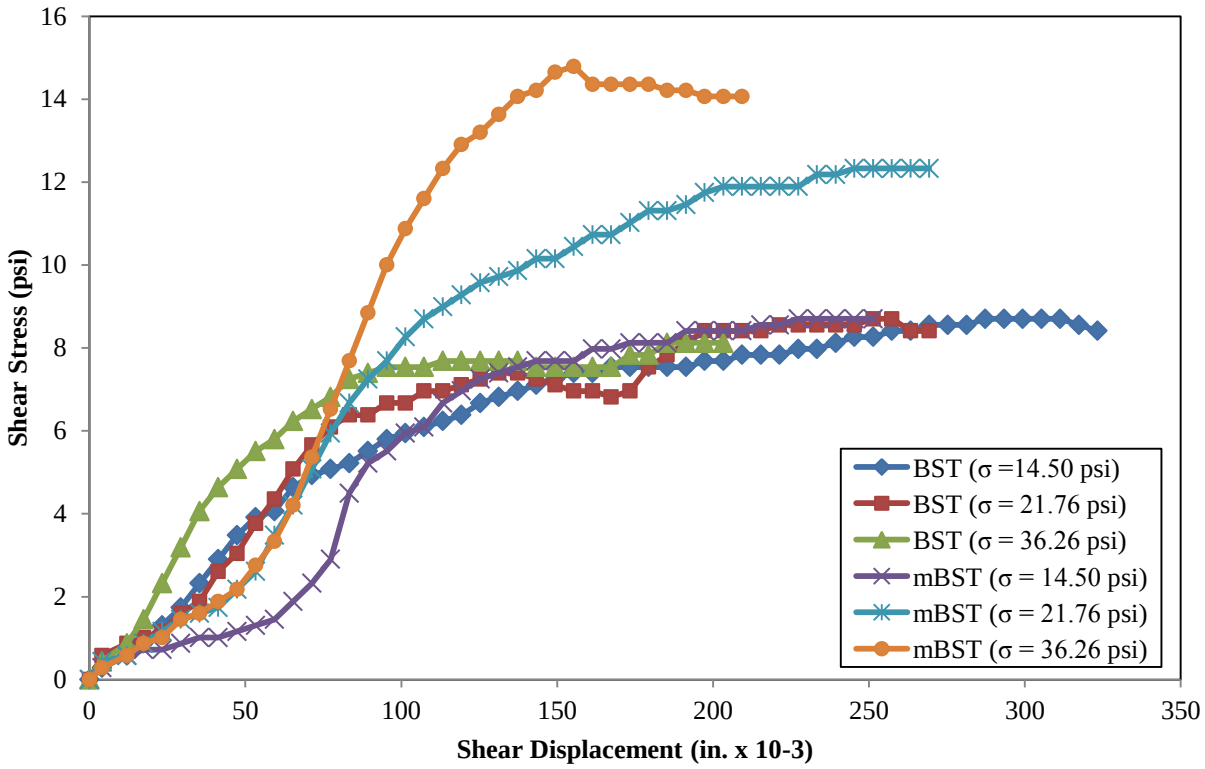

Figure B.4.29. BST and mBST generated shear stress-displacement relationships for ISU8 at 45-ft depth

B.5. Soil Classification and Properties Obtained from Gradation and Atterberg Limit Tests

Table B.5.1. Soil classification and properties for ISU1 from gradation and Atterberg limit tests

Disturbed Sample	Sample Depth (ft)	Soil Type (USCS)	D_{10} (in)	D_{30} (in)	D_{60} (in)	Liquid Limit, LL (%)	Plasticity Index, PI (%)	Moisture Content, ω (%)	Saturated Unit Weight, γ_{sat} (pcf)	Void Ratio, e
DS-1	0 to 2	ML	n/a	1.2E-4	7.8E-4	42.10	10.40	-	-	-
DS-2	6 to 7	CL	n/a	1.5E-4	8.4E-4	44.40	17.90	-	-	-
DS-3	14 to 15	CL	n/a	4.1E-4	2.8E-3	27.90	7.40	-	-	-
DS-4	15	CL	n/a	1E-4	2.8E-3	32.50	17.70	-	-	-
DS-5	21	CL	n/a	8.8E-5	5.8E-3	39.10	21.60	-	-	-

Table B.5.2. Soil classification and properties for ISU2 from gradation and Atterberg limit tests

Disturbed Sample	Sample Depth (ft)	Soil Type (USCS)	D_{10} (in)	D_{30} (in)	D_{60} (in)	Liquid Limit, LL (%)	Plasticity Index, PI (%)	Moisture Content, ω (%)	Saturated Unit Weight, γ_{sat} (pcf)	Void Ratio, e
DS-1	10	SC	n/a	4.8E-4	5.9E-3	28.67	13.39	-	-	-
DS-2	20	CL	n/a	1.7E-4	2.6E-3	43.74	25.04	30.00	121.01	0.81
DS-3	30	CL	n/a	2.7E-4	1.7E-3	43.16	19.21	12.49	141.73	0.34
DS-4	55	CL	n/a	3.3E-4	2.5E-3	47.54	28.40	9.58	146.68	0.26
DS-5	60	CL	n/a	4.7E-4	2.5E-3	45.54	24.72	10.71	144.69	0.29
DS-6	65	CL	n/a	1.8E-3	2.8E-3	28.75	7.81	13.31	140.44	0.36

Table B.5.3. Soil classification and properties for ISU3 from gradation and Atterberg limit tests

Disturbed Sample	Sample Depth (ft)	Soil Type (USCS)	D_{10} (in)	D_{30} (in)	D_{60} (in)	Liquid Limit, LL (%)	Plasticity Index, PI (%)	Moisture Content, ω (%)	Saturated Unit Weight, γ_{sat} (pcf)	Void Ratio, e
DS-1	2 to 4	CL	n/a	4.9E-4	2.7E-3	36.49	18.69	-	-	-
DS-2	15	SM	1.4E-4	7.3E-3	4E-2	19.39	-	23.03	127.81	0.62
DS-3	26	SM-SC	n/a	1.3E-3	1.3E-2	21.40	4.53	29.39	121.54	0.79
DS-4	35	CL	n/a	2.9E-4	2.4E-3	30.63	10.79	30.35	120.70	0.82
DS-5	50	CL	n/a	1.9E-4	1.5E-3	28.20	8.15	32.57	118.84	0.88
DS-6	60	CL	n/a	4.8E-4	4.2E-3	23.46	9.37	20.34	130.87	0.55
DS-7	65	SM	n/a	8.3E-4	8.2E-3	21.85	2.90	16.47	135.83	0.44

Table B.5.4. Soil classification and properties for ISU4 from gradation and Atterberg limit tests

Disturbed Sample	Sample Depth (ft)	Soil Type (USCS)	D_{10} (in)	D_{30} (in)	D_{60} (in)	Liquid Limit, LL (%)	Plasticity Index, PI (%)	Moisture Content, ω (%)	Saturated Unit Weight, γ_{sat} (pcf)	Void Ratio, e
DS-1	3.5 to 5	CL	n/a	6.5E-4	4.5E-3	29.32	11.41	25.36	125.37	0.68
DS-2	8.5 to 10	SW-SC	2.9E-3	8.7E-3	2.2E-2	29.32	-	17.18	134.86	0.46
DS-3	15	SM	3.7E-4	5.9E-3	2.4E-2	12.33	-	22.12	128.81	0.60
DS-4	18.5 to 20	SW	3.5E-3	1.7E-2	4.5E-2	-	-	15.46	137.24	0.42
DS-5	23.5 to 25	CL	n/a	2.4E-4	2.9E-3	27.49	13.46	12.65	141.48	0.34
DS-6	33 to 35	CL	n/a	1E-4	2.4E-3	38.68	22.70	16.86	135.30	0.46
DS-7	40	CL	n/a	3.3E-4	3.3E-3	29.38	16.70	15.75	136.83	0.43
DS-8	50	CL	n/a	3.3E-4	4.2E-3	25.98	13.19	15.09	137.77	0.41
DS-9	55	CL	n/a	4E-4	4E-3	25.33	13.06	13.12	140.74	0.35
DS-10	65	CL	n/a	3.3E-4	3.3E-3	29.63	15.76	14.73	138.29	0.40

Table B.5.5. Soil classification and properties for ISU5 from gradation and Atterberg limit tests

Disturbed Sample	Sample Depth (ft)	Soil Type (USCS)	D_{10} (in)	D_{30} (in)	D_{60} (in)	Liquid Limit, LL (%)	Plasticity Index, PI (%)	Moisture Content, ω (%)	Saturated Unit Weight, γ_{sat} (pcf)	Void Ratio, e
DS-1	3	SC	3.3E-5	8.1E-4	2.1E-2	26.31	11.27	20.39	130.82	0.55
DS-2	8 to 10	ML	9.0E-6	4.8E-4	2.7E-3	36.30	5.57	18.70	132.89	0.50
DS-3	10 to 12	CL	n/a	2.4E-4	2.6E-3	38.41	20.82	20.64	130.52	0.56
DS-4	16	CL	n/a	3.4E-4	2.7E-3	49.10	27.08	21.58	129.42	0.58
DS-5	28 to 30	CL	n/a	3.4E-4	2.8E-3	44.60	26.84	17.20	134.84	0.46
DS-6	37 to 38.5	CL	n/a	3.4E-4	2.7E-3	38.61	22.23	22.03	128.92	0.59
DS-7	38.5 to 40	SC	n/a	7.2E-4	6.4E-3	22.02	8.63	19.80	131.52	0.53
DS-8	43.5 to 45	CL	n/a	1.2E-4	2.6E-3	38.73	20.78	16.11	136.32	0.44
DS-9	48 to 50	CL	n/a	1E-4	2.4E-3	40.07	22.33	16.94	135.19	0.46

Table B.5.6. Soil classification and properties for ISU6 & ISU7 from gradation and Atterberg limit tests

Disturbed Sample	Sample Depth (ft)	Soil Type (USCS)	D_{10} (in)	D_{30} (in)	D_{60} (in)	Liquid Limit, LL (%)	Plasticity Index, PI (%)	Moisture Content, ω (%)	Saturated Unit Weight, γ_{sat} (pcf)	Void Ratio, e
DS-1	5	SC	9E-5	2.6E-3	1.8E-2	24.81	7.26	3.21	160.01	0.09
DS-2	14 to 15	SM	9E-5	2.8E-3	2.4E-2	18.16	3.97	25.16	125.56	0.68
DS-3	19.5	CL	n/a	4.2E-4	2.8E-3	24.81	10.90	28.67	122.19	0.77
DS-4	29 to 30	CL	n/a	6.3E-4	3.7E-3	25.28	10.60	18.99	132.52	0.51
DS-5	34 to 35	CL	n/a	4.7E-4	3.8E-3	24.37	11.99	16.87	135.28	0.46
DS-6	39 to 40	CL	n/a	4.6E-3	4.2E-3	26.72	13.15	8.15	149.35	0.22
DS-7	54 to 55	ML	n/a	3.7E-4	1.3E-3	30.98	7.43	20.15	131.10	0.54
DS-8	64 to 65	CL	n/a	4.8E-3	2.7E-3	24.43	9.64	13.54	140.09	0.37

Table B.5.7. Soil classification and properties for ISU8 from gradation and Atterberg limit tests

Disturbed Sample	Sample Depth (ft)	Soil Type (USCS)	D_{10} (in)	D_{30} (in)	D_{60} (in)	Liquid Limit, LL (%)	Plasticity Index, PI (%)	Moisture Content, ω (%)	Saturated Unit Weight, γ_{sat} (pcf)	Void Ratio, e
DS-1	3.5 to 5	CL	n/a	3.3E-4	2.3E-3	39.77	16.69	9.97	145.98	0.27
DS-2	10 to 11	CL	n/a	3.3E-4	2.3E-3	43.26	19.57	12.69	141.41	0.34
DS-3	15 to 16	CL	n/a	3.3E-4	2.4E-3	43.53	22.12	14.03	139.34	0.38
DS-4	18 to 19	CL	n/a	4.1E-4	2.4E-3	42.25	20.85	10.29	145.42	0.28
DS-5	21.5 to 23	CL	n/a	1.9E-4	8.7E-4	43.14	22.17	13.25	140.53	0.36
DS-6	30 31	SW	1.9E-3	1.4E-2	4.5E-2	-	-	10.73	144.65	0.29
DS-7	48.5 to 50	CL	n/a	3.3E-4	2.8E-3	34.14	17.45	7.63	150.36	0.21
DS-8	53.5 to 55	CL	n/a	6.3E-4	4.2E-3	34.14	17.45	3.09	160.31	0.08
DS-9	58.5 to 60	CL	5.5E-5	6.9E-4	5.2E-3	24.24	13.35	5.51	154.74	0.15
DS-10	63.5 to 65	CL	5E-5	5.5E-4	4.9E-3	23.29	10.20	5.23	155.35	0.14

Table B.5.8. Soil classification and properties for ISU9 from gradation and Atterberg limit tests

Disturbed Sample	Sample Depth (ft)	Soil Type (USCS)	D_{10} (in)	D_{30} (in)	D_{60} (in)	Liquid Limit, LL (%)	Plasticity Index, PI (%)	Moisture Content, ω (%)	Saturated Unit Weight, γ_{sat} (pcf)	Void Ratio, e
DS-1	3.5 to 5	SM; SC	9E-5	2.5E-3	9.8E-3	-	-	23.63	19.98	0.64
DS-2	8.5 to 10	CL	-	2.6E-3	2.8E-3	-	-	24.40	19.85	0.66
DS-3	13 to 15	SM; SC	5E-4	9.8E-3	3.3E-2	-	-	28.48	19.23	0.77
DS-4	18 to 20	SW	7.3E-3	2E-2	4.7E-2	-	-	18.26	20.97	0.49
DS-5	30	SW	7E-3	2.1E-2	5E-2	-	-	23.64	19.98	0.64
DS-6	40	SP	7E-3	1.6E-2	4E-2	-	-	28.40	19.24	0.77
DS-7	50	SW	6.7E-3	2.1E-2	5.2E-2	-	-	17.87	21.05	0.48
DS-8	55	SM; SC	1E-4	2.7E-3	2.2E-2	-	-	27	19.45	0.73
DS-9	60	SW	8.2E-3	2.3E-2	4.9E-2	-	-	17.94	21.04	0.48

Table B.5.9. Soil classification and properties for ISU10 from gradation and Atterberg limit tests

Disturbed Sample	Sample Depth (ft)	Soil Type (USCS)	D_{10} (in)	D_{30} (in)	D_{60} (in)	Liquid Limit, LL (%)	Plasticity Index, PI (%)	Moisture Content, ω (%)	Saturated Unit Weight, γ_{sat} (pcf)	Void Ratio, e
DS-1	3.5 to 5	SW	6E-3	2.3E-2	5.6E-2	-	-	14.64	138.43	0.40
DS-2	8.5 to 10	SP-SM SP-SC	4E-3	7.5E-3	1.5E-2	-	-	13.79	139.70	0.37
DS-3	13 to 15	SW	9.4E-3	3.3E-2	5.7E-2	-	-	15.00	137.90	0.41
DS-4	18 to 20	SP	1.8E-2	3.9E-2	5.9E-2	-	-	18.01	133.77	0.49
DS-5	30	SW	7.7E-3	2.7E-2	5.6E-2	-	-	10.37	145.28	0.28
DS-6	40	SW-SM SW-SC	6.3E-3	2.8E-2	5.8E-2	-	-	12.68	141.43	0.34
DS-7	50	SW	9.3E-3	3.4E-2	6E-2	-	-	6.59	152.46	0.18

B.6. Total Lateral Earth and Pore Water Pressure Measurements using Push-in Pressure Cells (PCs)

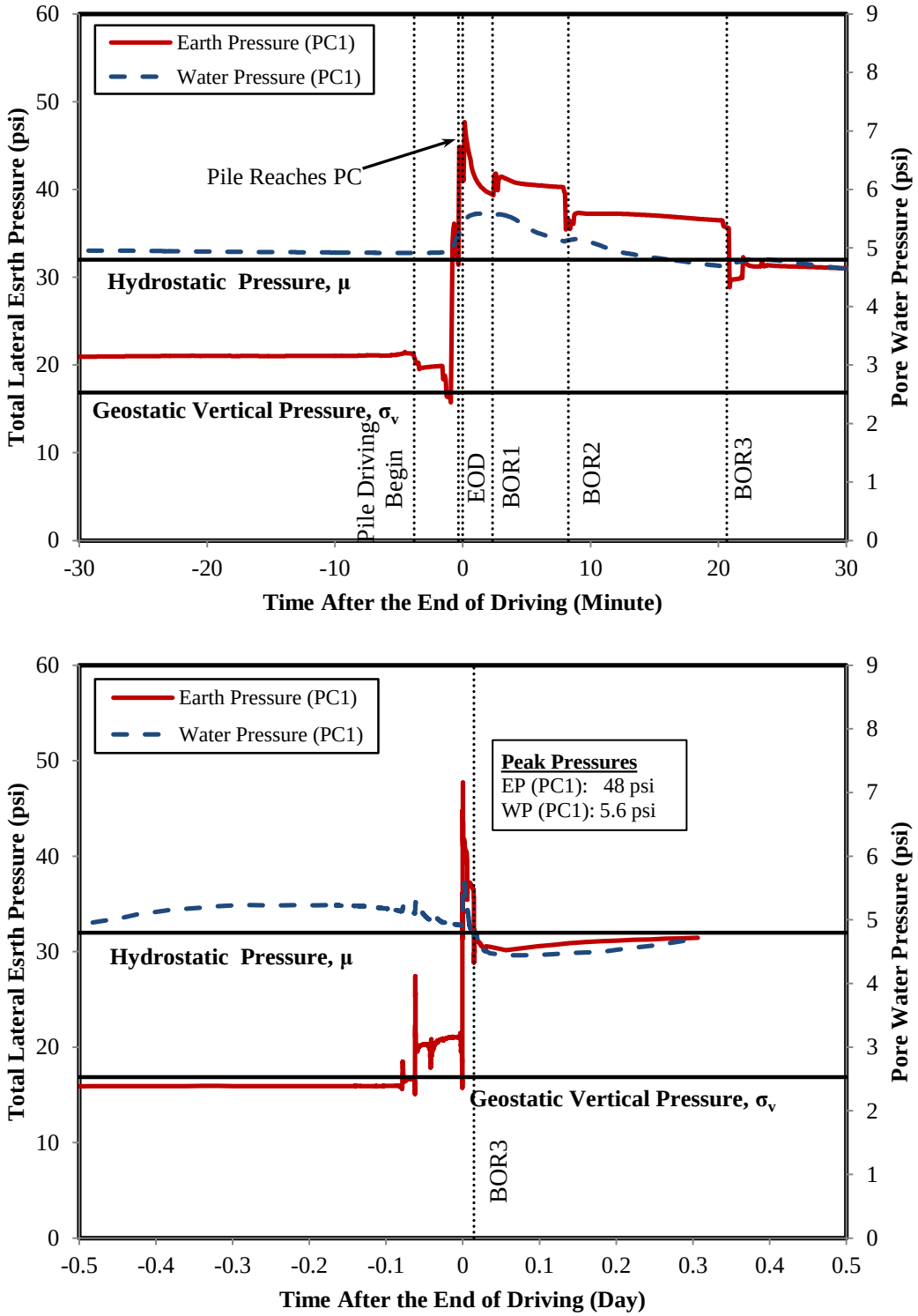

Figure B.6.1. Total lateral earth and pore water pressure measurements from PC1 at test pile ISU7

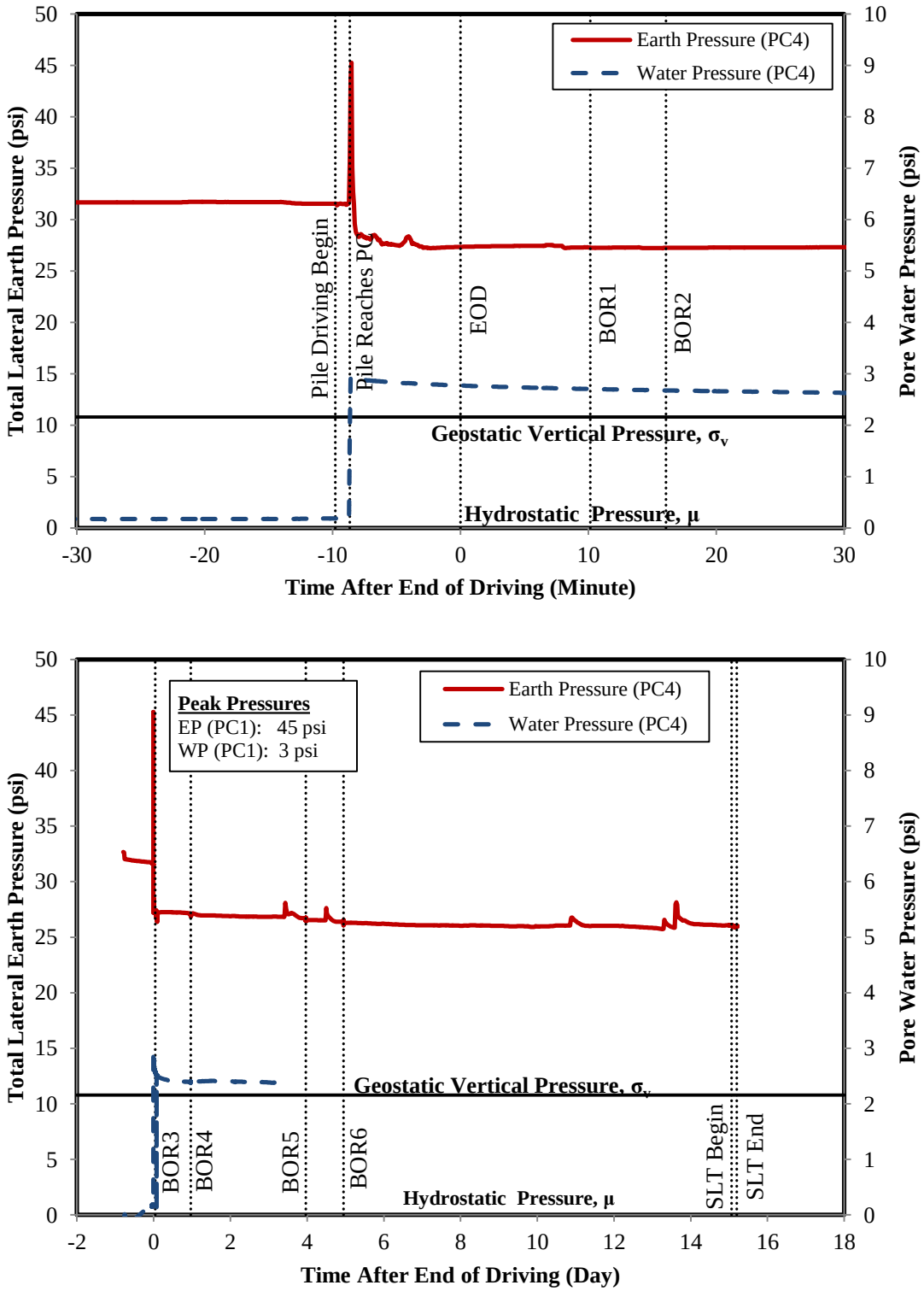

Figure B.6.2. Total lateral earth and pore water pressure measurements from PC4 at test pile ISU8

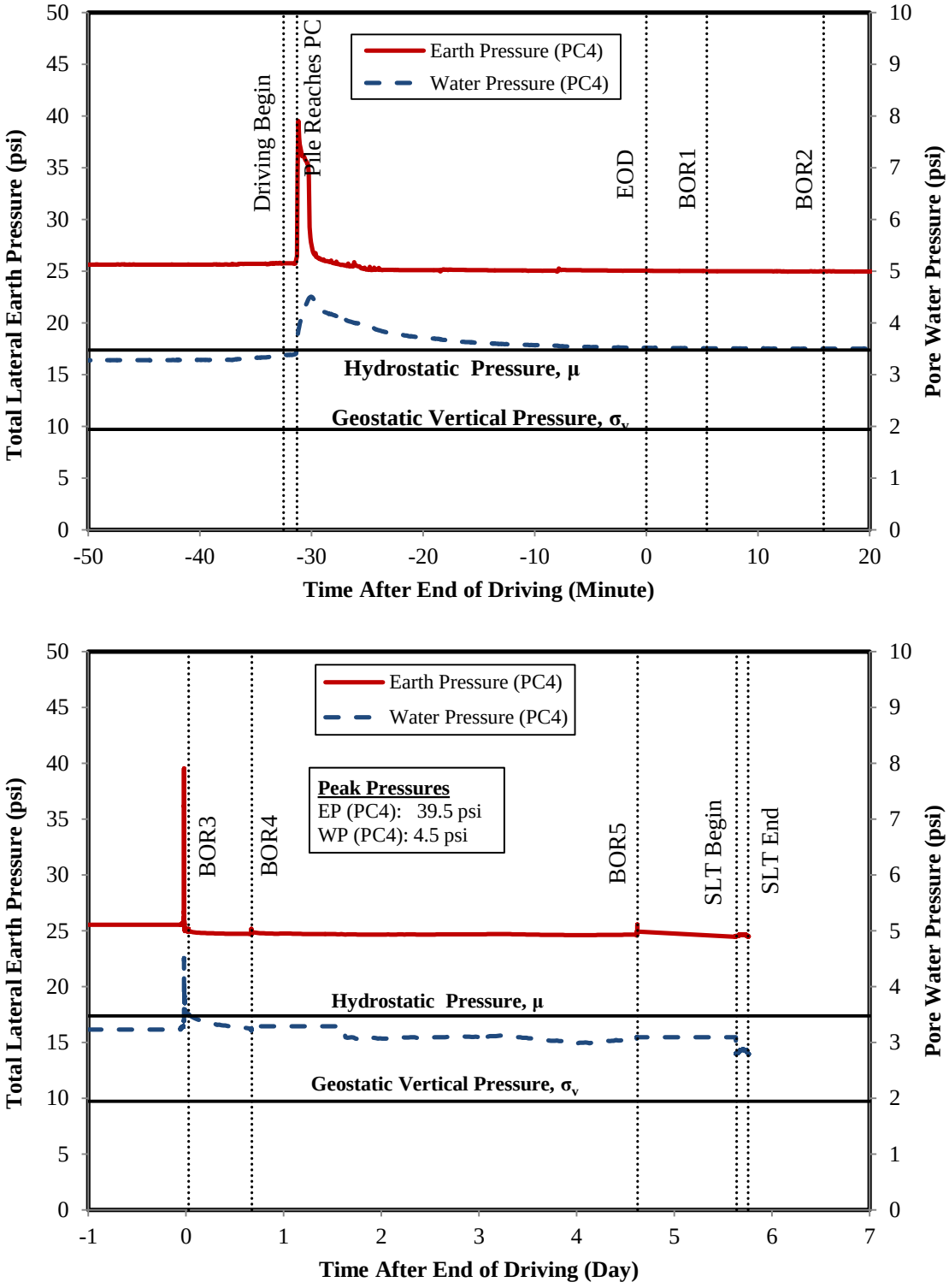

Figure B.6.3. Total lateral earth and pore water pressure measurements from PC4 at test pile ISU10

APPENDIX C: DETAILS OF FULL-SCALE PILE TESTS

C.1. Locations of Strain Gauges along Test Piles

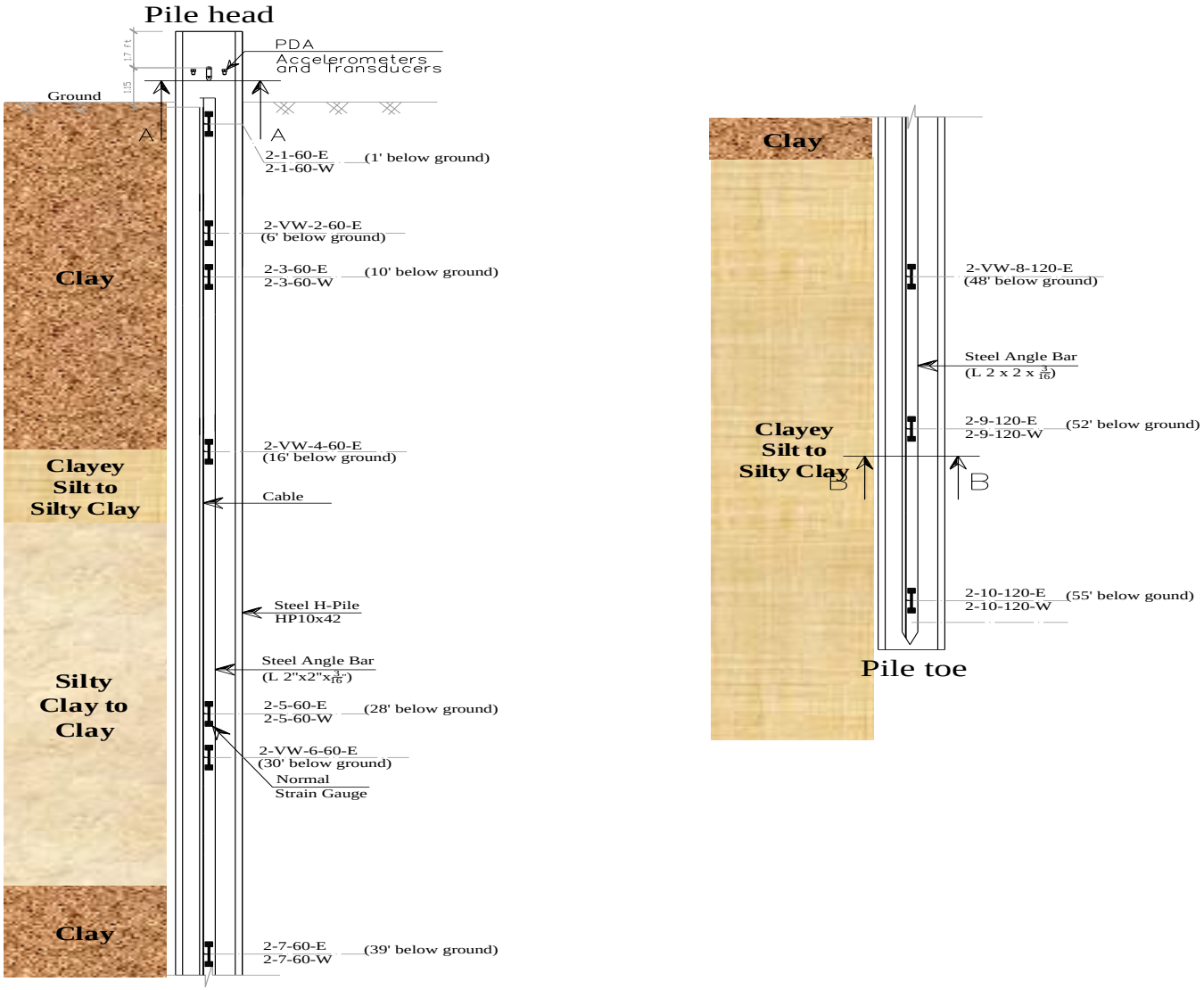

Figure C.1.1. Location of strain gauges along the ISU2 test pile at Mills County

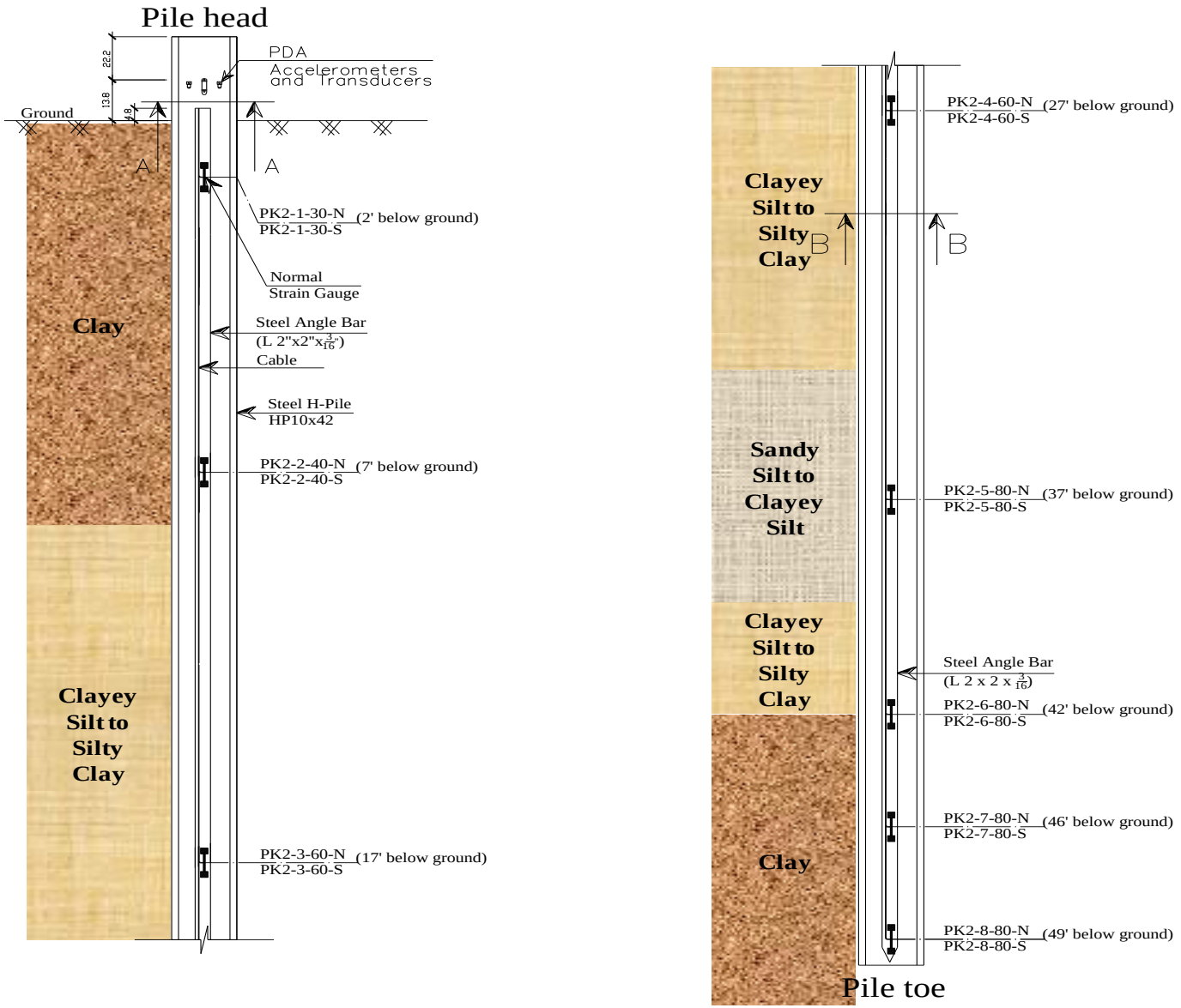

Figure C.1.2. Location of strain gauges along the ISU3 test pile at Polk County

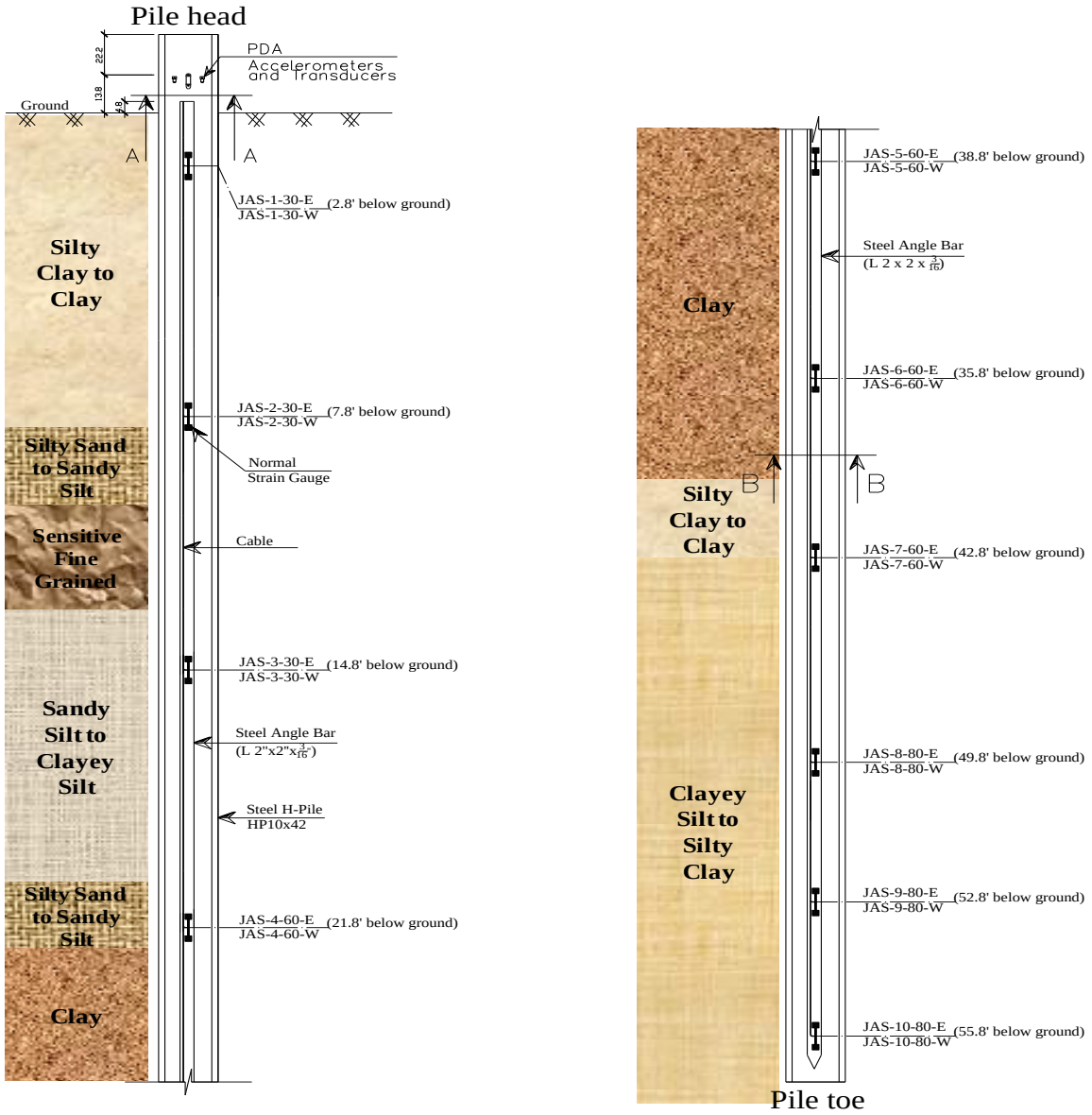

Figure C.1.3. Location of strain gauges along the ISU4 test pile at Jasper County

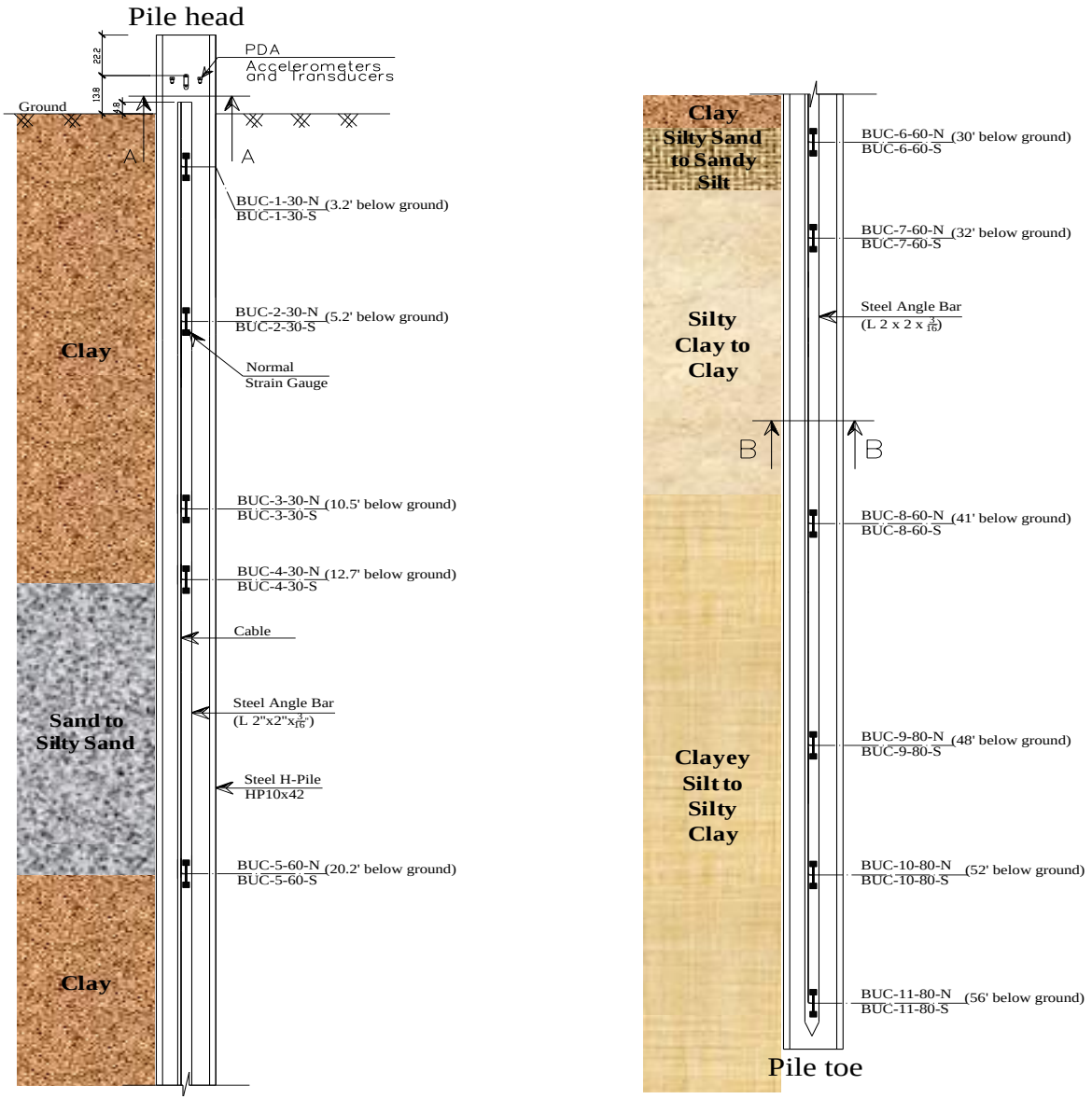

Figure C.1.4. Location of strain gauges along the ISU6 test pile at Buchanan County

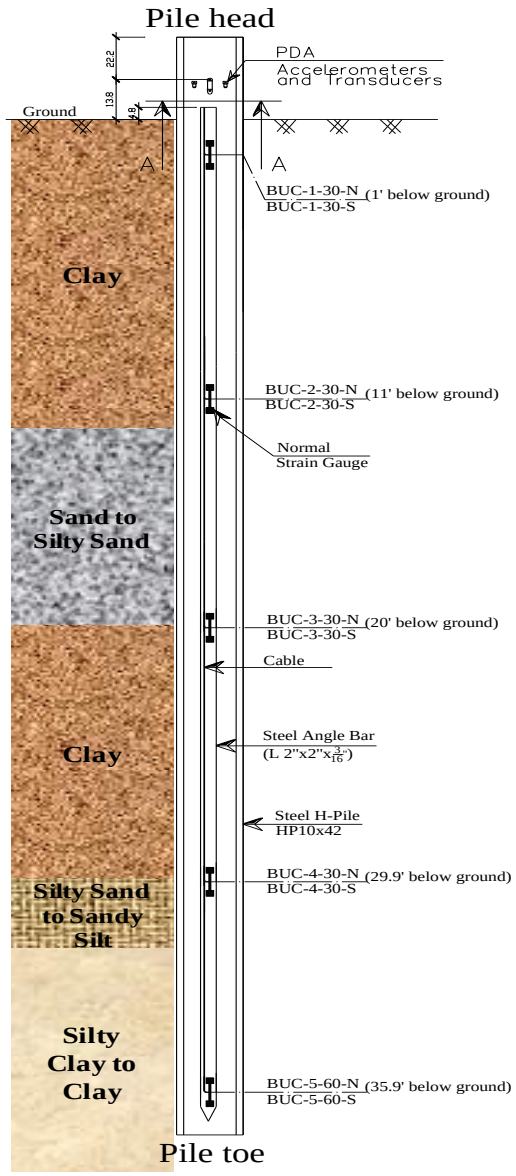

Figure C.1.5. Location of strain gauges along the ISU7 test pile at Buchanan County

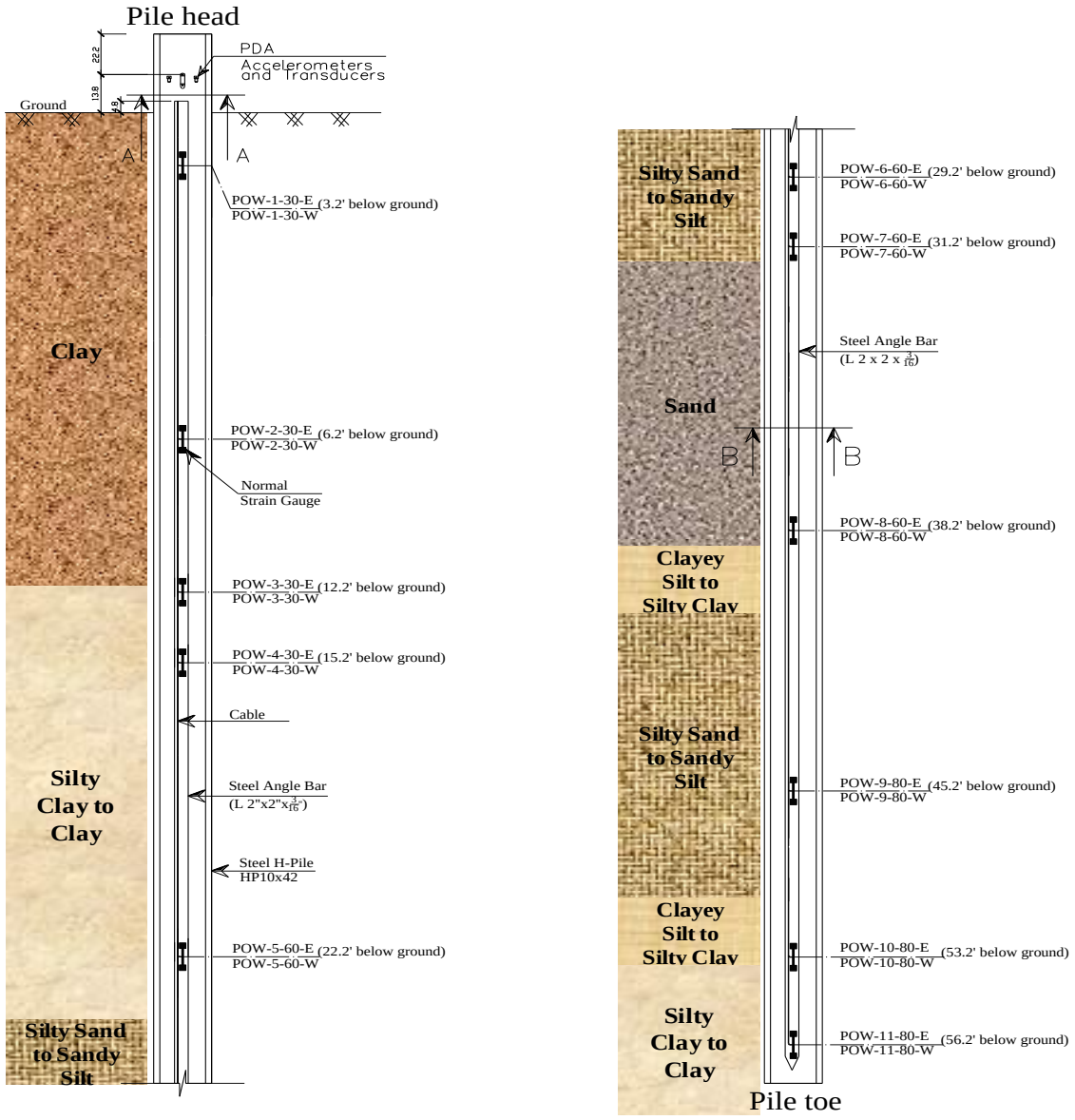

Figure C.1.6. Location of strain gauges along the ISU8 test pile at Poweshiek County

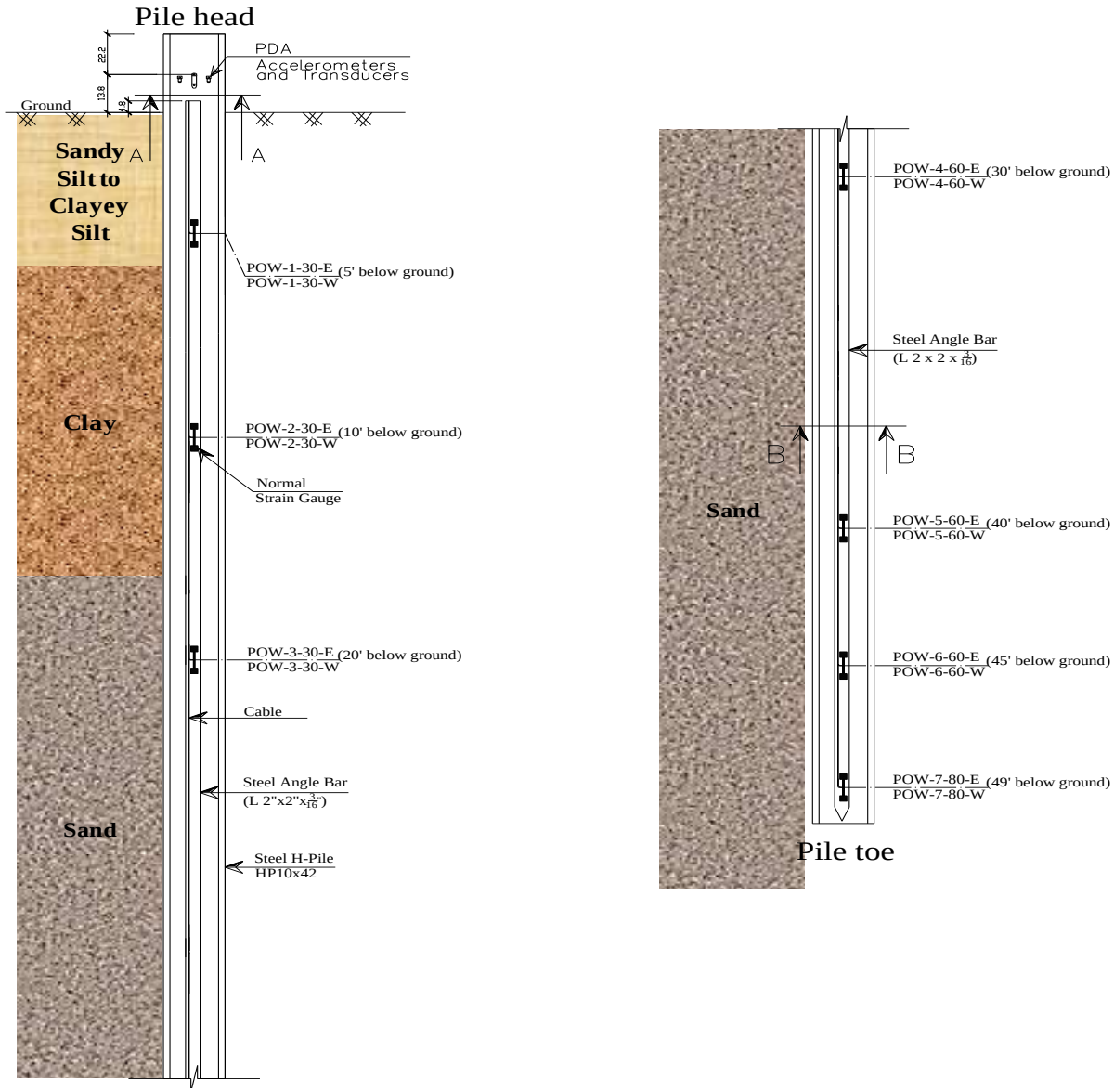

Figure C.1.7. Location of strain gauges along the ISU9 test pile at Des Moines County

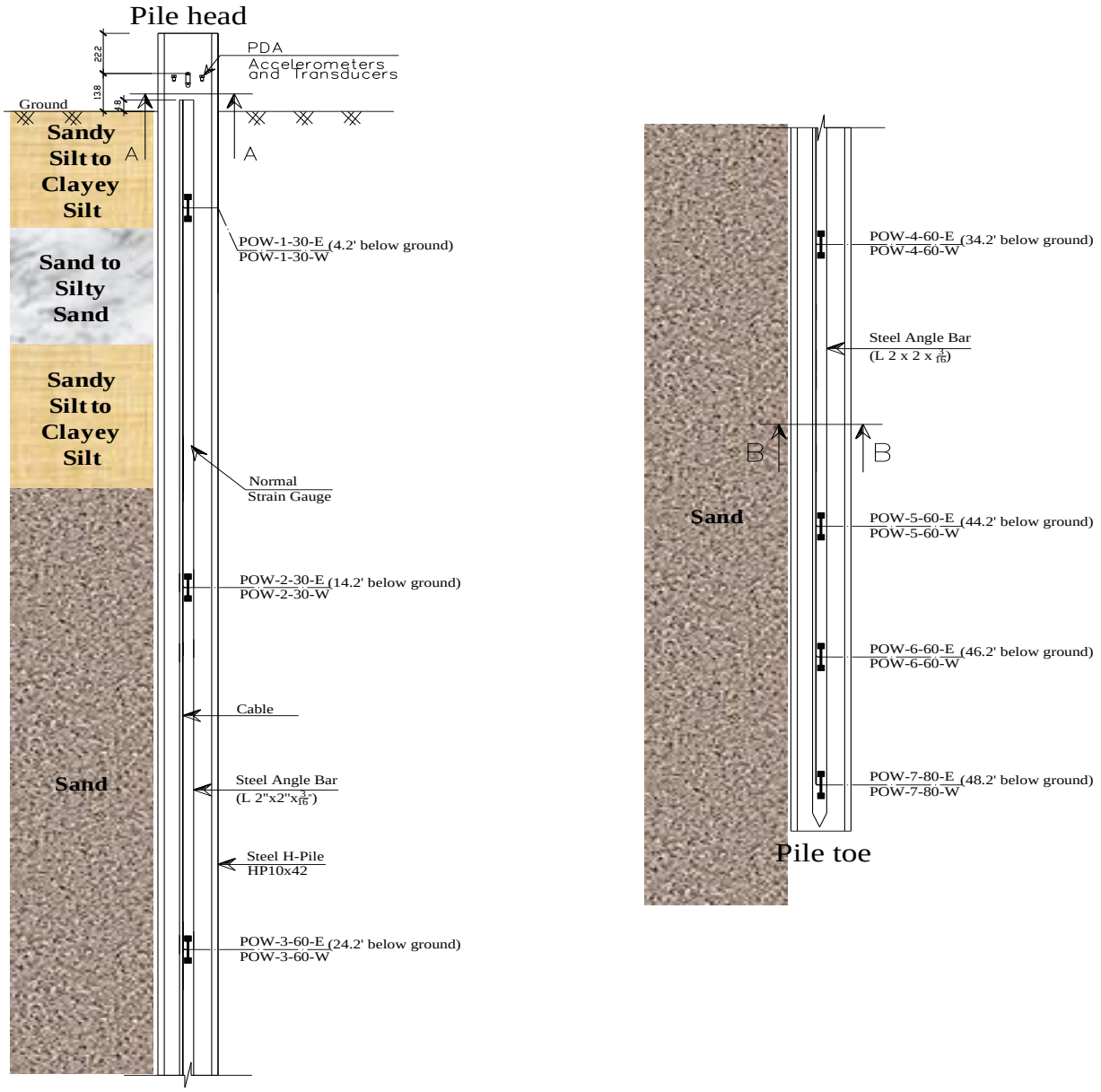

Figure C.1.8. Location of strain gauges along the ISU10 test pile at Cedar County

C.2. Pile Driving Analyzer (PDA) Measurements

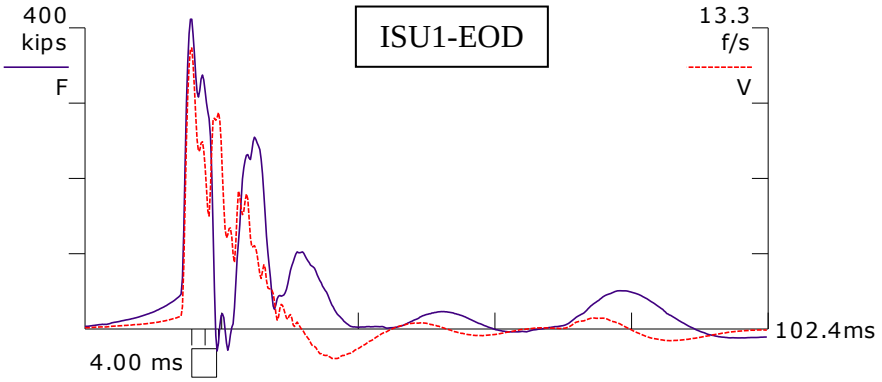

BN 174
12/18/2007 9:58:24 AM
RTL 239 kips
RSP 0 kips
RMX 141 kips
EMX 16.5 k-ft
ETR 38.9 (%)
STK 6.35 ft
CSX 24.5 ksi
TSX 1.7 ksi
BTA 100.0 (%)

LE 33.00 ft
AR 16.80 in^2
EM 30000 ksi
SP 0.492 k/ft3
WS 16807.9 f/s
EA/C 30.0 ksec/ft
LP 1.00 ft

Figure C.2.1. PDA force and velocity records for ISU1

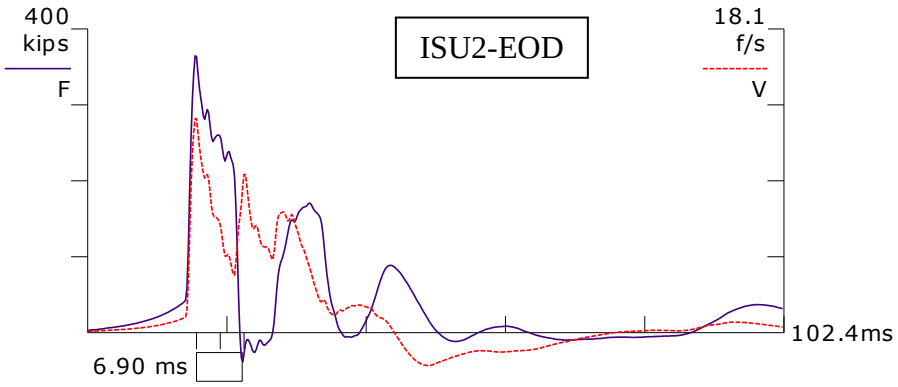

BN 1/236
7/14/2008 12:26:07 PM
RTL 205 kips
RSP 0 kips
RMX 105 kips
EMX 20.1 k-ft
ETR 46.5 (%)
STK 5.94 ft
CSX 29.4 ksi
TSX 4.0 ksi
BTA 100.0 (%)

LE 58.00 ft
AR 12.40 in^2
EM 30000 ksi
SP 0.492 k/ft3
WS 16807.9 f/s
EA/C 22.1 ksec/ft
LP 54.00 ft

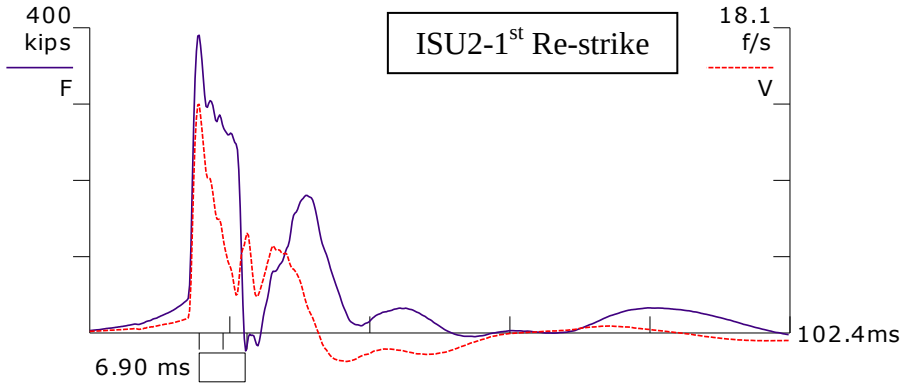

BN 6
7/14/2008 4:26:05 PM
RTL 271 kips
RSP 0 kips
RMX 148 kips
EMX 19.3 k-ft
ETR 44.5 (%)
STK 6.48 ft
CSX 31.5 ksi
TSX 1.9 ksi
BTA 100.0 (%)

LE 58.00 ft
AR 12.40 in^2
EM 30000 ksi
SP 0.492 k/ft3
WS 16807.9 f/s
EA/C 22.1 ksec/ft
LP 54.00 ft

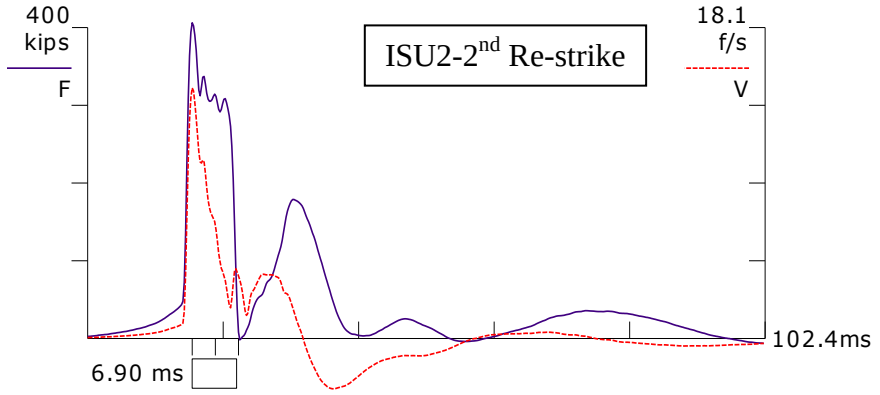

BN 5/4
7/15/2008 10:27:43 AM
RTL 328 kips
RSP 48 kips
RMX 162 kips
EMX 21.0 k-ft
ETR 48.5 (%)
STK 7.29 ft
CSX 32.8 ksi
TSX 0.4 ksi
BTA 100.0 (%)

LE 58.00 ft
AR 12.40 in^2
EM 30000 ksi
SP 0.492 k/ft3
WS 16807.9 f/s
EA/C 22.1 ksec/ft
LP 55.33 ft

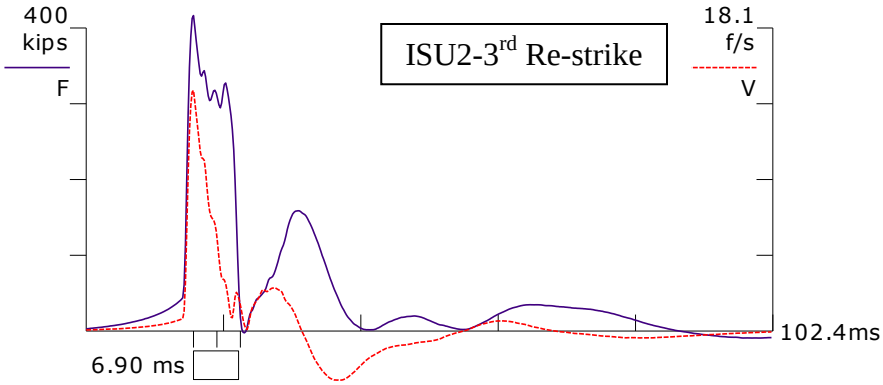

BN 6/5
7/17/2008 11:45:26 AM
RTL 359 kips
RSP 96 kips
RMX 146 kips
EMX 19.4 k-ft
ETR 45.0 (%)
STK 7.15 ft
CSX 33.6 ksi
TSX 0.5 ksi
BTA 100.0 (%)

LE 58.00 ft
AR 12.40 in^2
EM 30000 ksi
SP 0.492 k/ft3
WS 16807.9 f/s
EA/C 22.1 ksec/ft
LP 55.83 ft

Figure C.2.2. PDA force and velocity records for ISU2

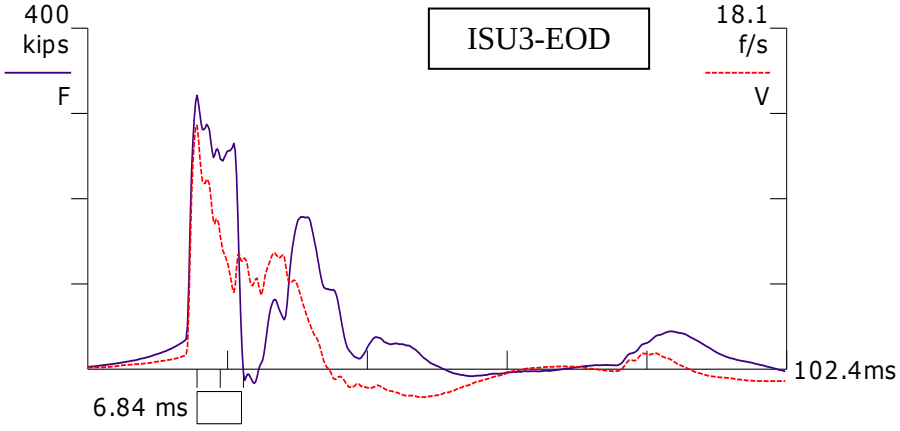

BN 273
1/7/2009 10:21:18 AM
RTL 237 kips
RSP 0 kips
RMX 120 kips
EMX 19.8 k-ft
ETR 46.6 (%)
STK 5.76 ft
CSX 25.9 ksi
TSX 1.1 ksi
BTA 100.0 (%)

LE 57.50 ft
AR 12.40 in^2
EM 30000 ksi
SP 0.492 k/ft3
WS 16807.9 f/s
EA/C 22.1 ksec/ft

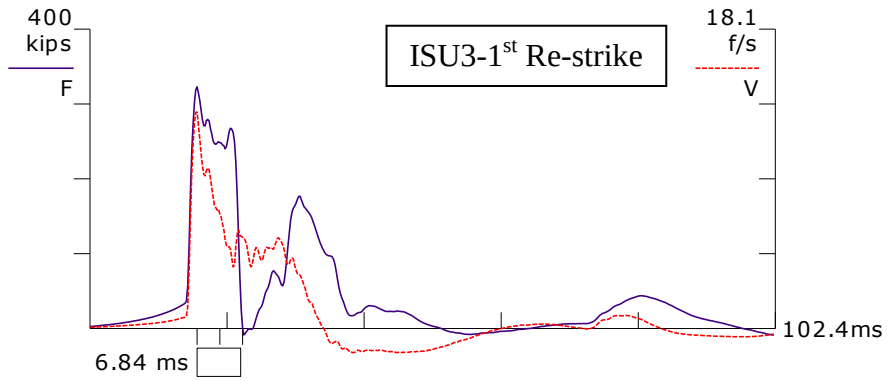

BN 4
1/7/2009 10:25:45 AM

RTL	245 kips
RSP	0 kips
RMX	117 kips
EMX	18.9 k-ft
ETR	44.5 (%)
STK	5.86 ft
CSX	26.0 ksi
TSX	1.2 ksi
BTA	100.0 (%)
LE	57.50 ft
AR	12.40 in^2
EM	30000 ksi
SP	0.492 k/ft3
WS	16807.9 f/s
EA/C	22.1 ksec/ft
LP	48.00 ft

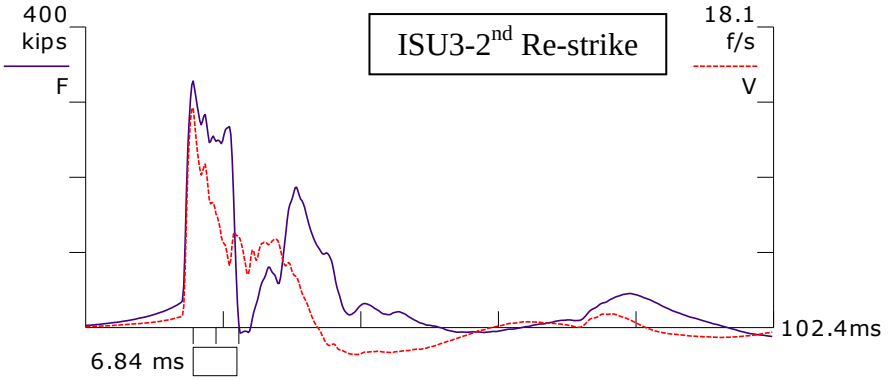

BN 4
1/7/2009 10:32:10 AM

RTL	251 kips
RSP	0 kips
RMX	123 kips
EMX	19.1 k-ft
ETR	45.0 (%)
STK	5.92 ft
CSX	26.5 ksi
TSX	0.9 ksi
BTA	100.0 (%)
LE	57.50 ft
AR	12.40 in^2
EM	30000 ksi
SP	0.492 k/ft3
WS	16807.9 f/s
EA/C	22.1 ksec/ft
LP	48.50 ft

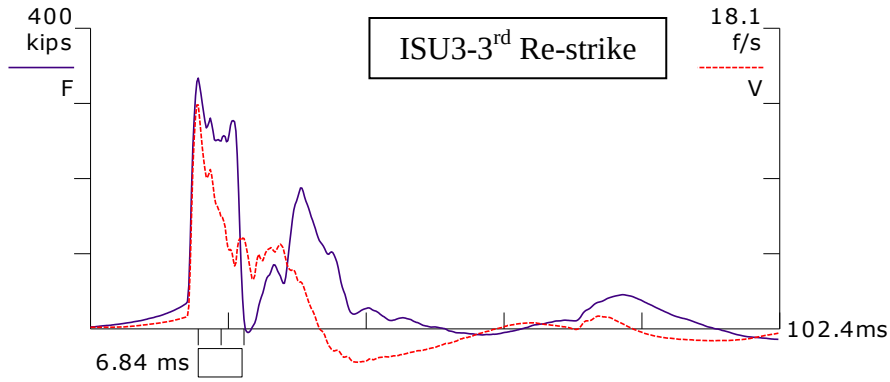

BN 5
1/7/2009 10:45:32 AM

RTL	262 kips
RSP	0 kips
RMX	128 kips
EMX	19.2 k-ft
ETR	45.3 (%)
STK	6.07 ft
CSX	26.9 ksi
TSX	0.0 ksi
BTA	100.0 (%)
LE	57.50 ft
AR	12.40 in^2
EM	30000 ksi
SP	0.492 k/ft3
WS	16807.9 f/s
EA/C	22.1 ksec/ft
LP	49.00 ft

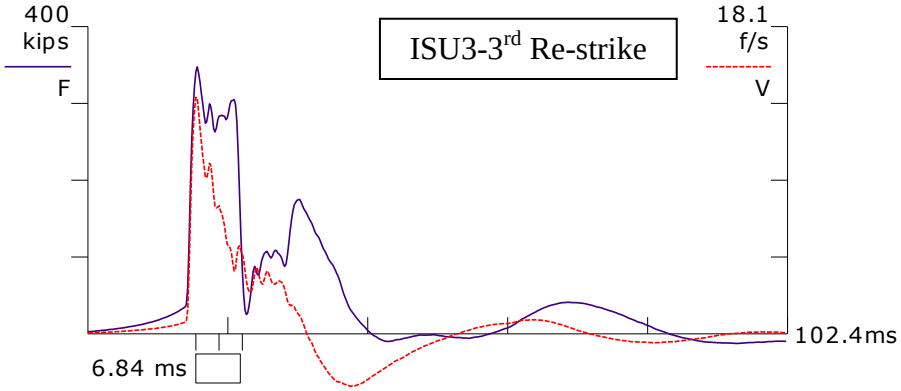

BN 2
1/8/2009 1:57:08 PM
RTL 314 kips
RSP 0 kips
RMX 157 kips
EMX 20.2 k-ft
ETR 47.6 (%)
STK 6.79 ft
CSX 28.0 ksi
TSX 1.6 ksi
BTA 100.0 (%)

LE 57.50 ft
AR 12.40 in^2
EM 30000 ksi
SP 0.492 k/ft3
WS 16807.9 f/s
EA/C 22.1 ksec/ft
LP 49.50 ft

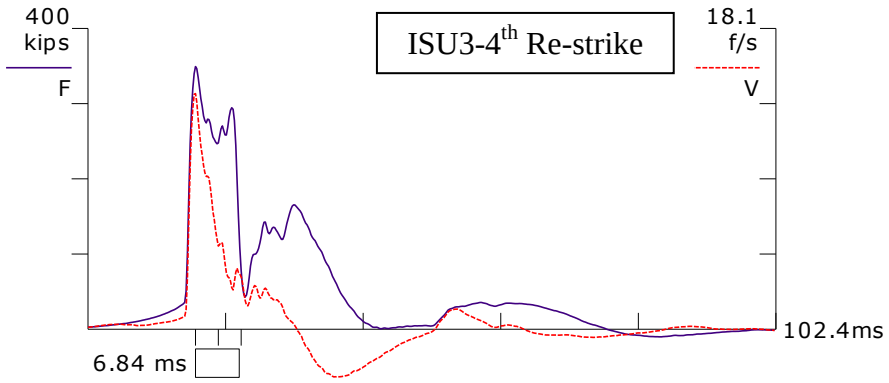

BN 8
1/9/2009 10:08:29 AM
RTL 336 kips
RSP 0 kips
RMX 163 kips
EMX 17.6 k-ft
ETR 41.5 (%)
STK 7.06 ft
CSX 28.2 ksi
TSX 0.9 ksi
BTA 100.0 (%)

LE 57.50 ft
AR 12.40 in^2
EM 30000 ksi
SP 0.492 k/ft3
WS 16807.9 f/s
EA/C 22.1 ksec/ft
LP 50.33 ft

Figure C.2.3. PDA force and velocity records for ISU3

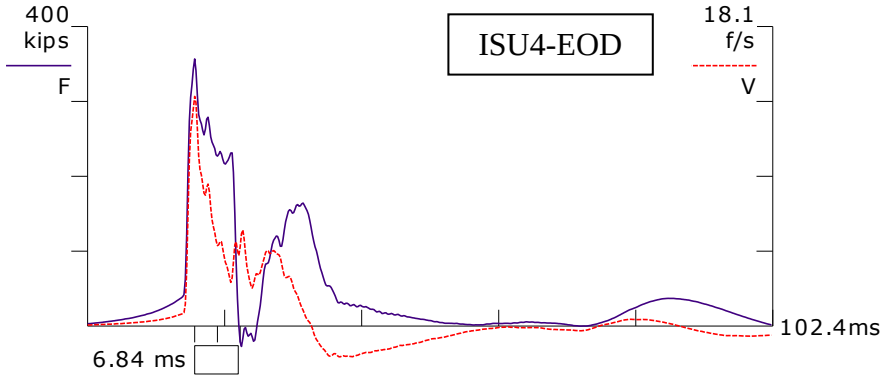

BN 231
4/22/2009 3:08:17 PM
RTL 268 kips
RSP 0 kips
RMX 143 kips
EMX 16.8 k-ft
ETR 38.7 (%)
STK 6.46 ft
CSX 28.8 ksi
TSX 2.7 ksi
BTA 100.0 (%)

LE 57.50 ft
AR 12.40 in^2
EM 30000 ksi
SP 0.492 k/ft3
WS 16807.9 f/s
EA/C 22.1 ksec/ft

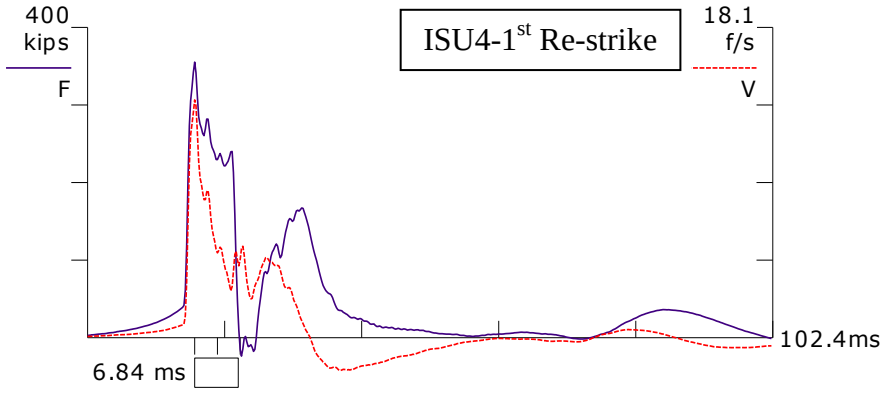

BN 5
4/22/2009 3:14:07 PM
RTL 273 kips
RSP 1 kips
RMX 144 kips
EMX 17.0 k-ft
ETR 39.3 (%)
STK 6.51 ft
CSX 28.7 ksi
TSX 2.1 ksi
BTA 100.0 (%)

LE 57.50 ft
AR 12.40 in^2
EM 30000 ksi
SP 0.492 k/ft3
WS 16807.9 f/s
EA/C 22.1 ksec/ft
LP 55.00 ft

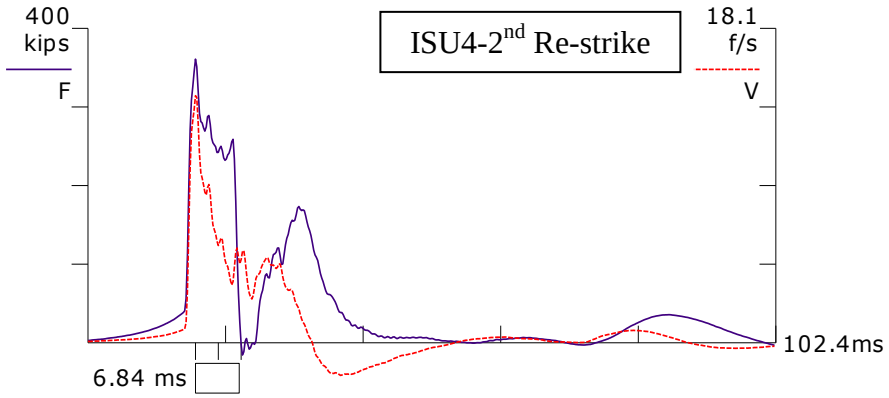

BN 3
4/22/2009 3:31:03 PM
RTL 284 kips
RSP 9 kips
RMX 143 kips
EMX 18.7 k-ft
ETR 43.2 (%)
STK 6.63 ft
CSX 29.1 ksi
TSX 1.3 ksi
BTA 100.0 (%)

LE 57.50 ft
AR 12.40 in^2
EM 30000 ksi
SP 0.492 k/ft3
WS 16807.9 f/s
EA/C 22.1 ksec/ft
LP 55.33 ft

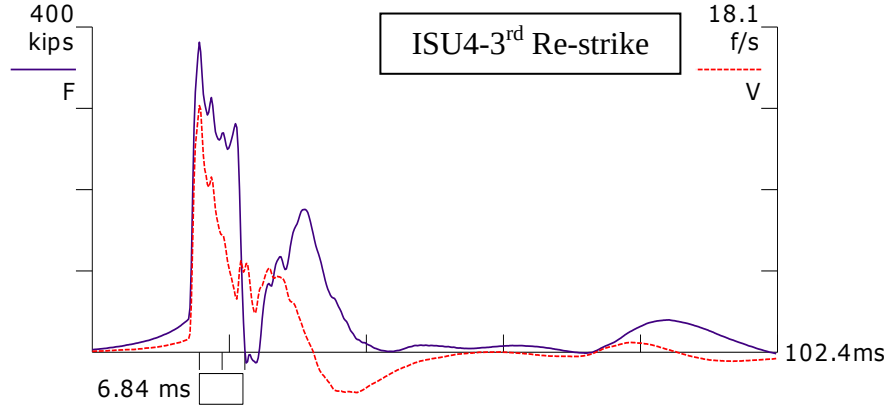

BN 3
4/22/2009 4:07:19 PM
RTL 293 kips
RSP 18 kips
RMX 154 kips
EMX 19.5 k-ft
ETR 45.0 (%)
STK 7.00 ft
CSX 30.7 ksi
TSX 1.1 ksi
BTA 100.0 (%)

LE 57.50 ft
AR 12.40 in^2
EM 30000 ksi
SP 0.492 k/ft3
WS 16807.9 f/s
EA/C 22.1 ksec/ft
LP 55.70 ft

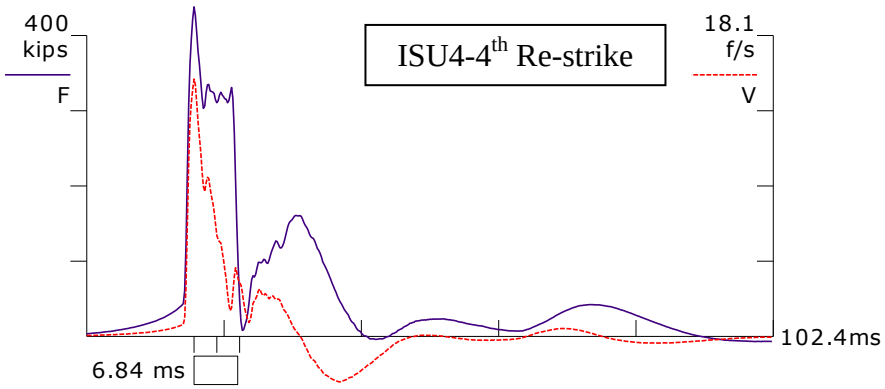

BN 3
4/23/2009 8:54:03 AM
RTL 379 kips
RSP 98 kips
RMX 161 kips
EMX 22.2 k-ft
ETR 51.4 (%)
STK 8.97 ft
CSX 35.3 ksi
TSX 1.1 ksi
BTA 100.0 (%)

LE 57.50 ft
AR 12.40 in^2
EM 30000 ksi
SP 0.492 k/ft3
WS 16807.9 f/s
EA/C 22.1 ksec/ft
LP 56.00 ft

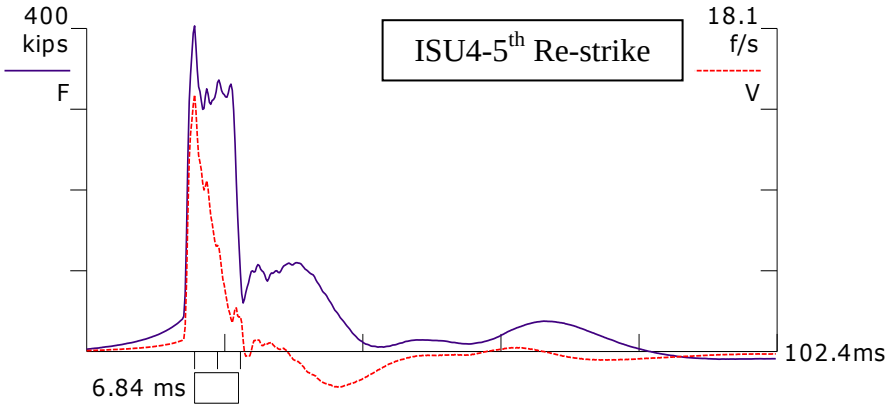

BN 6
4/24/2009 8:50:19 AM
RTL 387 kips
RSP 154 kips
RMX 162 kips
EMX 18.2 k-ft
ETR 42.1 (%)
STK 7.48 ft
CSX 32.5 ksi
TSX 0.1 ksi
BTA 100.0 (%)

LE 57.50 ft
AR 12.40 in^2
EM 30000 ksi
SP 0.492 k/ft3
WS 16807.9 f/s
EA/C 22.1 ksec/ft
LP 56.30 ft

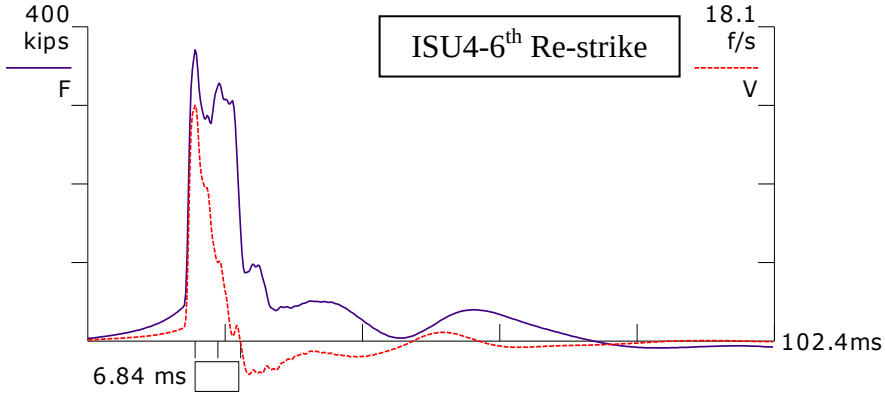

BN 11
4/27/2009 9:12:26 AM
RTL 407 kips
RSP 223 kips
RMX 223 kips
EMX 15.0 k-ft
ETR 34.8 (%)
STK 7.39 ft
CSX 29.9 ksi
TSX 1.0 ksi
BTA 100.0 (%)

LE 57.50 ft
AR 12.40 in^2
EM 30000 ksi
SP 0.492 k/ft3
WS 16807.9 f/s
EA/C 22.1 ksec/ft
LP 56.67 ft

Figure C.2.4. PDA force and velocity records for ISU4

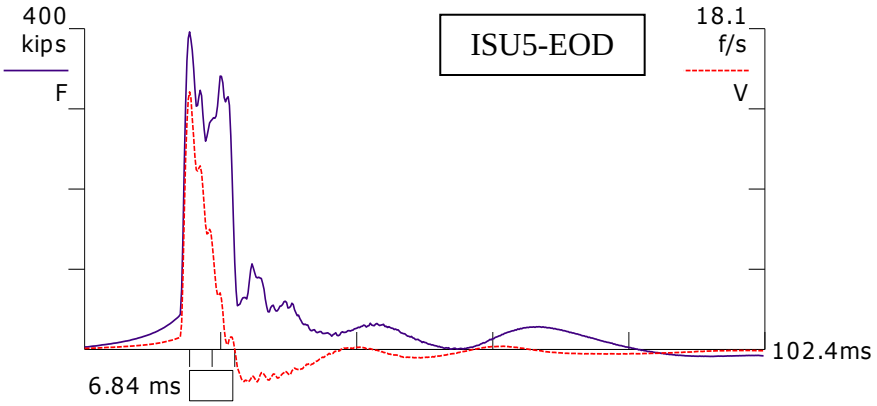

BN 603
5/19/2009 12:11:55 PM
RTL 413 kips
RSP 200 kips
RMX 200 kips
EMX 16.3 k-ft
ETR 40.5 (%)
STK 7.04 ft
CSX 31.9 ksi
TSX 1.0 ksi
BTA 100.0 (%)

LE 57.50 ft
AR 12.40 in^2
EM 30000 ksi
SP 0.492 k/ft3
WS 16807.9 f/s
EA/C 22.1 ksec/ft

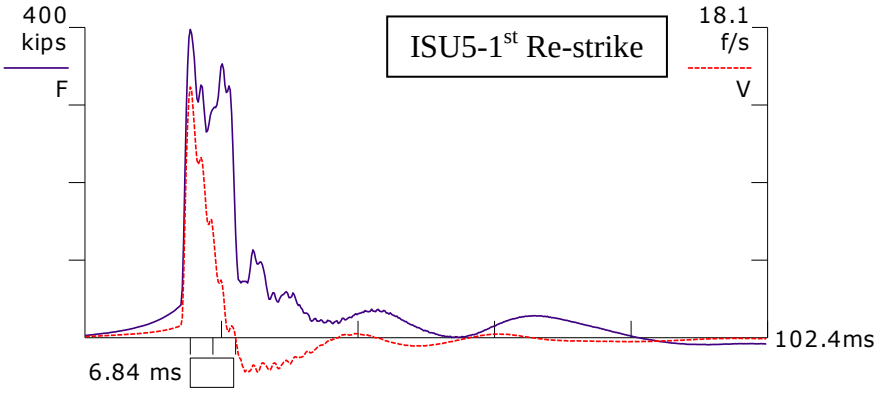

BN 6
5/19/2009 12:19:40 PM
RTL 428 kips
RSP 224 kips
RMX 224 kips
EMX 16.7 k-ft
ETR 41.6 (%)
STK 7.07 ft
CSX 32.0 ksi
TSX 1.0 ksi
BTA 100.0 (%)

LE 57.50 ft
AR 12.40 in^2
EM 30000 ksi
SP 0.492 k/ft3
WS 16807.9 f/s
EA/C 22.1 ksec/ft
LP 54.00 ft

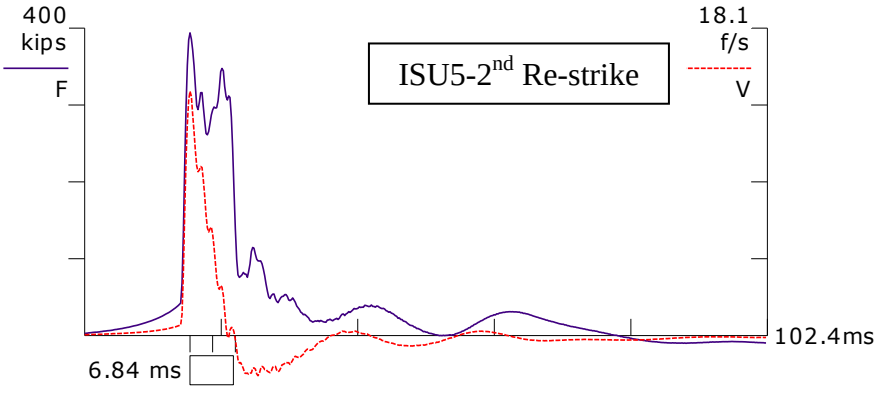

BN 6
5/19/2009 12:30:00 PM
RTL 428 kips
RSP 229 kips
RMX 229 kips
EMX 15.8 k-ft
ETR 39.2 (%)
STK 6.96 ft
CSX 31.8 ksi
TSX 1.1 ksi
BTA 100.0 (%)

LE 57.50 ft
AR 12.40 in^2
EM 30000 ksi
SP 0.492 k/ft3
WS 16807.9 f/s
EA/C 22.1 ksec/ft
LP 55.30 ft

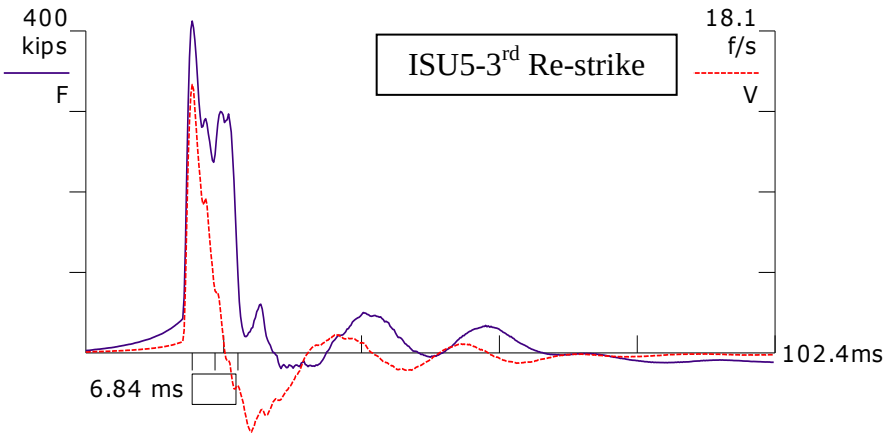

BN 12
5/19/2009 1:20:47 PM
RTL 442 kips
RSP 229 kips
RMX 229 kips
EMX 14.6 k-ft
ETR 36.4 (%)
STK 7.45 ft
CSX 33.3 ksi
TSX 4.1 ksi
BTA 100.0 (%)

LE 57.50 ft
AR 12.40 in^2
EM 30000 ksi
SP 0.492 k/ft3
WS 16807.9 f/s
EA/C 22.1 ksec/ft
LP 55.70 ft

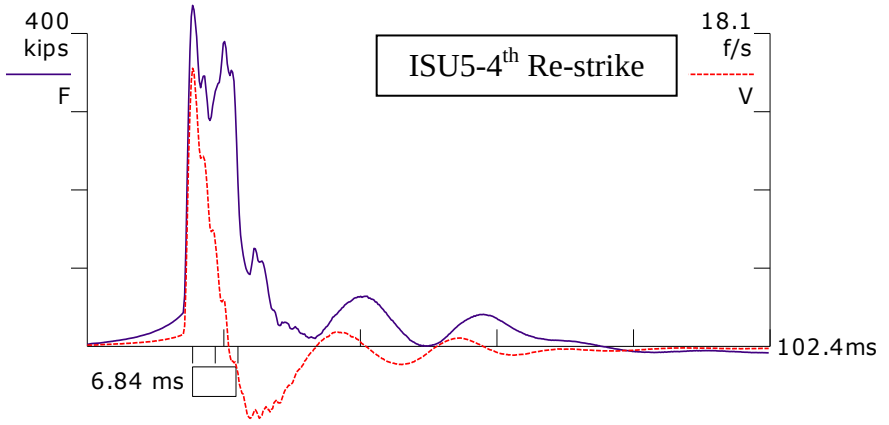

BN 6
5/20/2009 10:13:04 AM
RTL 518 kips
RSP 326 kips
RMX 326 kips
EMX 18.9 k-ft
ETR 46.9 (%)
STK 8.20 ft
CSX 35.2 ksi
TSX 1.5 ksi
BTA 100.0 (%)

LE 57.50 ft
AR 12.40 in^2
EM 30000 ksi
SP 0.492 k/ft3
WS 16807.9 f/s
EA/C 22.1 ksec/ft
LP 56.00 ft

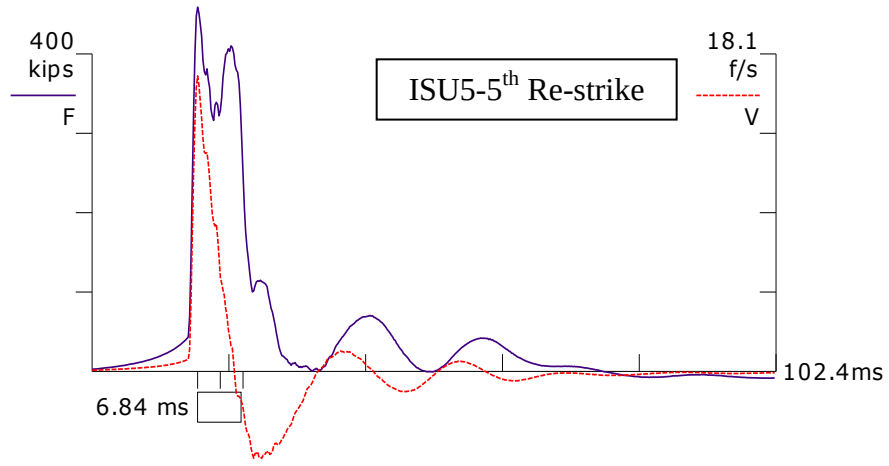

BN 7
5/22/2009 9:52:09 AM
RTL 563 kips
RSP 375 kips
RMX 375 kips
EMX 21.4 k-ft
ETR 53.1 (%)
STK 8.82 ft
CSX 37.0 ksi
TSX 2.8 ksi
BTA 100.0 (%)

LE 57.50 ft
AR 12.40 in^2
EM 30000 ksi
SP 0.492 k/ft3
WS 16807.9 f/s
EA/C 22.1 ksec/ft
LP 56.25 ft

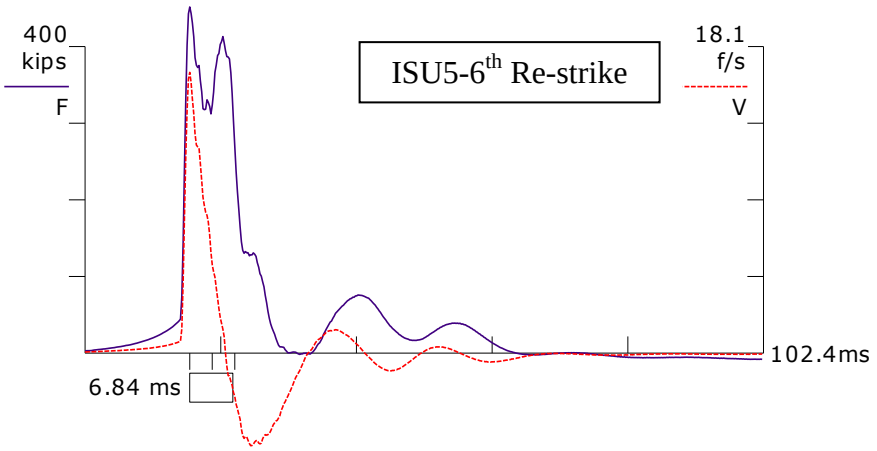

BN 19
5/27/2009 10:09:46 AM
RTL 572 kips
RSP 400 kips
RMX 400 kips
EMX 20.3 k-ft
ETR 50.6 (%)
STK 8.69 ft
CSX 36.4 ksi
TSX 3.3 ksi
BTA 100.0 (%)

LE 57.50 ft
AR 12.40 in^2
EM 30000 ksi
SP 0.492 k/ft3
WS 16807.9 f/s
EA/C 22.1 ksec/ft
LP 56.50 ft

Figure C.2.5. PDA force and velocity records for ISU5

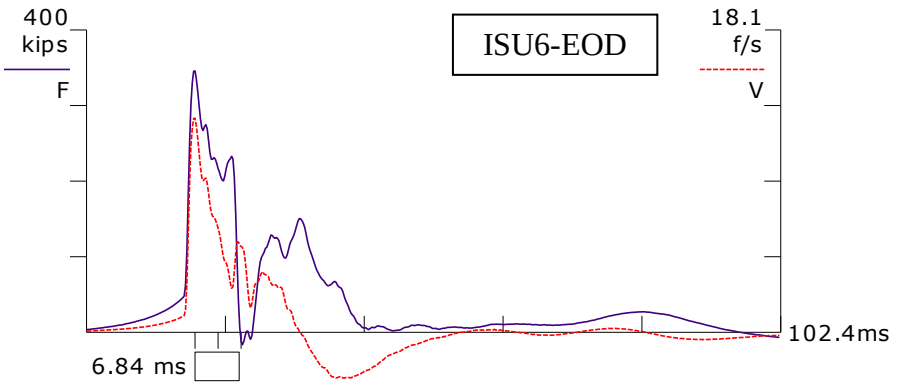

BN 268
6/9/2009 3:26:47 PM
RTL 252 kips
RSP 0 kips
RMX 146 kips
EMX 15.9 k-ft
ETR 36.9 (%)
STK 6.33 ft
CSX 27.9 ksi
TSX 1.3 ksi
BTA 100.0 (%)

LE 57.50 ft
AR 12.40 in^2
EM 30000 ksi
SP 0.492 k/ft3
WS 16807.9 f/s
EA/C 22.1 ksec/ft

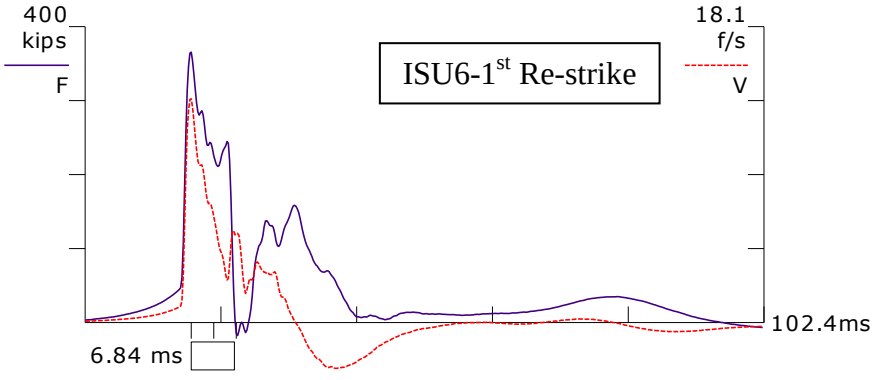

BN 3
6/9/2009 3:29:07 PM
RTL 267 kips
RSP 0 kips
RMX 151 kips
EMX 17.5 k-ft
ETR 40.4 (%)
STK 6.85 ft
CSX 29.5 ksi
TSX 1.4 ksi
BTA 100.0 (%)

LE 57.50 ft
AR 12.40 in^2
EM 30000 ksi
SP 0.492 k/ft3
WS 16807.9 f/s
EA/C 22.1 ksec/ft
LP 55.00 ft

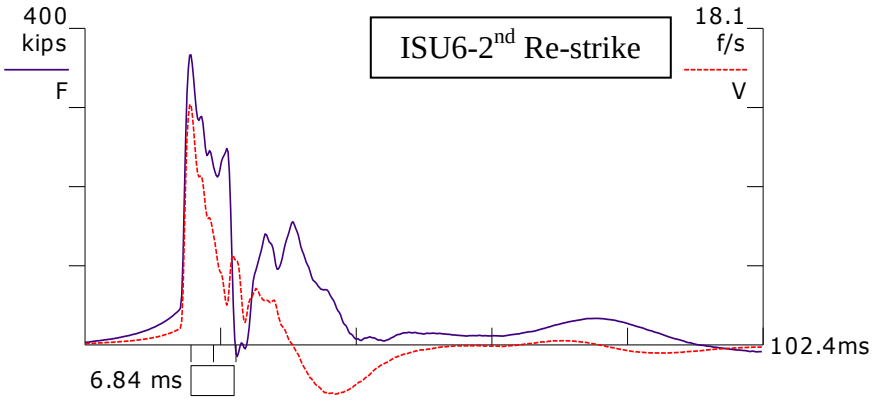

BN 4
6/9/2009 3:33:06 PM
RTL 276 kips
RSP 0 kips
RMX 149 kips
EMX 17.1 k-ft
ETR 39.5 (%)
STK 6.86 ft
CSX 29.6 ksi
TSX 1.2 ksi
BTA 100.0 (%)

LE 57.50 ft
AR 12.40 in^2
EM 30000 ksi
SP 0.492 k/ft3
WS 16807.9 f/s
EA/C 22.1 ksec/ft
LP 55.60 ft

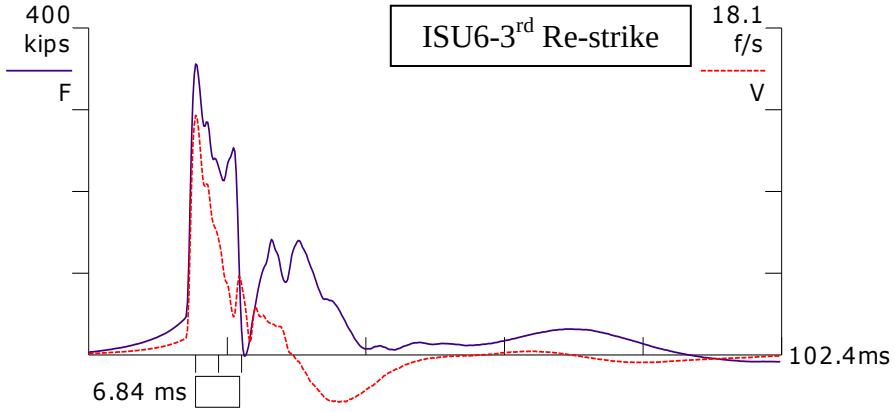

BN 4
6/9/2009 3:43:40 PM
RTL 297 kips
RSP 50 kips
RMX 145 kips
EMX 15.9 k-ft
ETR 36.7 (%)
STK 6.55 ft
CSX 28.7 ksi
TSX 0.6 ksi
BTA 100.0 (%)

LE 57.50 ft
AR 12.40 in^2
EM 30000 ksi
SP 0.492 k/ft3
WS 16807.9 f/s
EA/C 22.1 ksec/ft
LP 56.00 ft

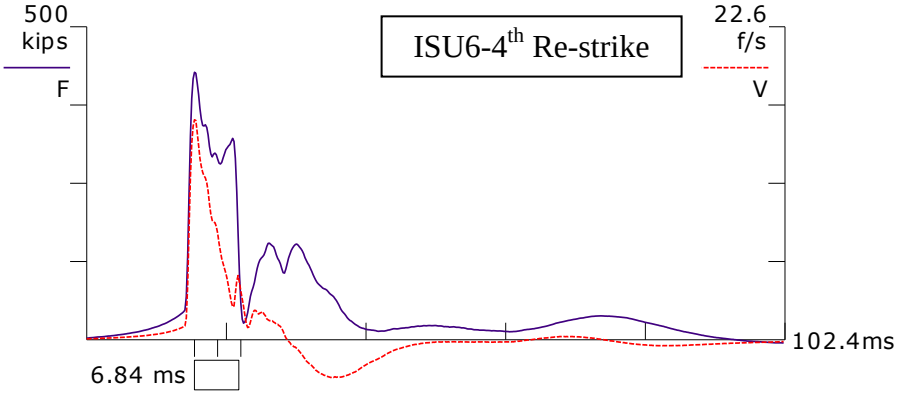

BN 4
6/9/2009 5:03:26 PM
RTL 380 kips
RSP 101 kips
RMX 167 kips
EMX 23.0 k-ft
ETR 53.2 (%)
STK 8.26 ft
CSX 34.5 ksi
TSX 0.0 ksi
BTA 100.0 (%)

LE 57.50 ft
AR 12.40 in^2
EM 30000 ksi
SP 0.492 k/ft3
WS 16807.9 f/s
EA/C 22.1 ksec/ft
LP 56.00 ft

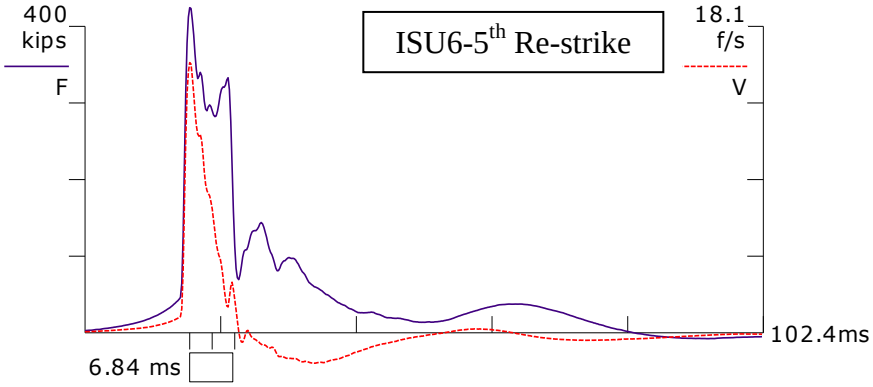

BN 5
6/10/2009 11:18:56 AM
RTL 423 kips
RSP 176 kips
RMX 195 kips
EMX 21.0 k-ft
ETR 48.6 (%)
STK 8.20 ft
CSX 34.2 ksi
TSX 1.0 ksi
BTA 100.0 (%)

LE 57.50 ft
AR 12.40 in^2
EM 30000 ksi
SP 0.492 k/ft3
WS 16807.9 f/s
EA/C 22.1 ksec/ft
LP 56.50 ft

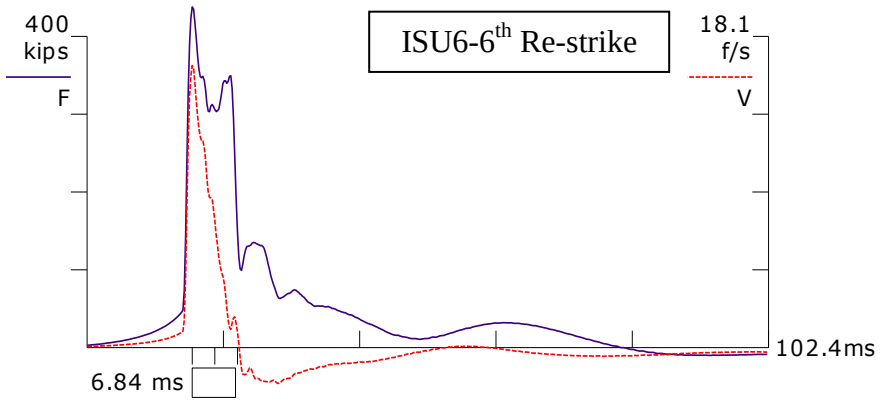

BN 5
6/12/2009 11:06:41 AM
RTL 465 kips
RSP 230 kips
RMX 231 kips
EMX 22.1 k-ft
ETR 51.1 (%)
STK 8.47 ft
CSX 35.3 ksi
TSX 1.2 ksi
BTA 100.0 (%)

LE 57.50 ft
AR 12.40 in^2
EM 30000 ksi
SP 0.492 k/ft3
WS 16807.9 f/s
EA/C 22.1 ksec/ft
LP 56.33 ft

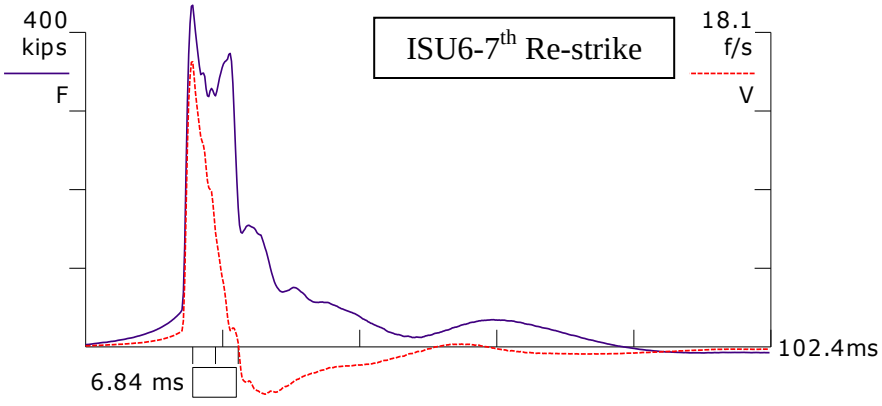

BN 5
6/16/2009 10:27:09 AM
RTL 485 kips
RSP 266 kips
RMX 266 kips
EMX 22.6 k-ft
ETR 52.2 (%)
STK 8.75 ft
CSX 35.0 ksi
TSX 1.0 ksi
BTA 100.0 (%)

LE 57.50 ft
AR 12.40 in^2
EM 30000 ksi
SP 0.492 k/ft3
WS 16807.9 f/s
EA/C 22.1 ksec/ft
LP 57.00 ft

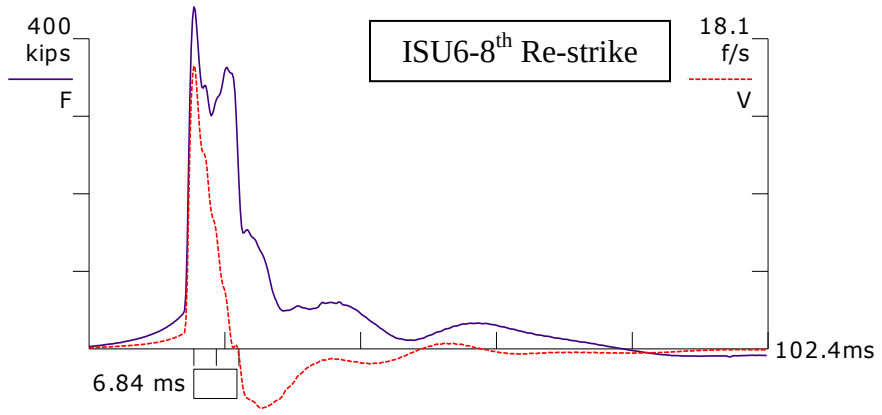

BN 4
6/19/2009 10:50:45 AM
RTL 514 kips
RSP 310 kips
RMX 310 kips
EMX 20.8 k-ft
ETR 48.0 (%)
STK 8.26 ft
CSX 35.6 ksi
TSX 1.2 ksi
BTA 100.0 (%)

LE 57.50 ft
AR 12.40 in^2
EM 30000 ksi
SP 0.492 k/ft3
WS 16807.9 f/s
EA/C 22.1 ksec/ft
LP 57.30 ft

Figure C.2.6. PDA force and velocity records for ISU6

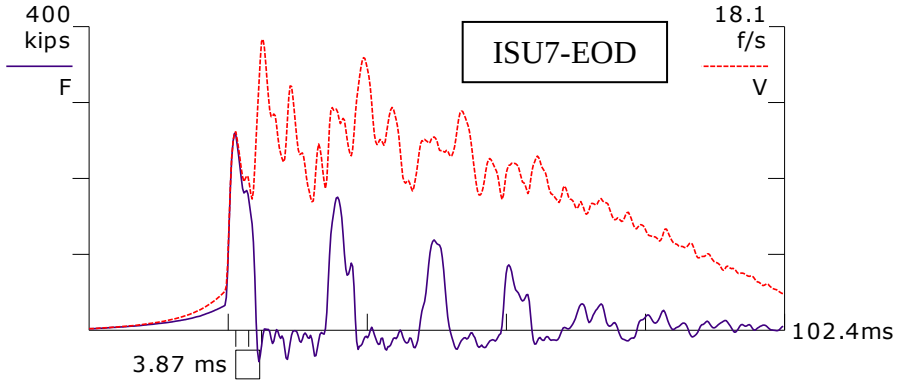

BN 10
6/9/2009 4:20:32 PM
RTL 59 kips
RSP 0 kips
RMX 0 kips
EMX 17.7 k-ft
ETR 41.0 (%)
STK 0.00 ft
CSX 20.9 ksi
TSX 5.6 ksi
BTA 100.0 (%)

LE 32.50 ft
AR 12.40 in^2
EM 30000 ksi
SP 0.492 k/ft3
WS 16807.9 f/s
EA/C 22.1 ksec/ft

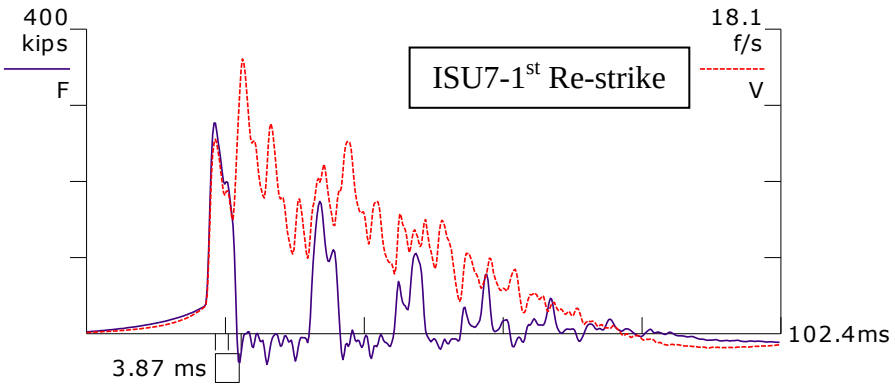

BN 2
6/9/2009 4:23:13 PM
RTL 80 kips
RSP 0 kips
RMX 0 kips
EMX 13.0 k-ft
ETR 30.0 (%)
STK 0.00 ft
CSX 22.3 ksi
TSX 5.3 ksi
BTA 100.0 (%)

LE 32.50 ft
AR 12.40 in^2
EM 30000 ksi
SP 0.492 k/ft3
WS 16807.9 f/s
EA/C 22.1 ksec/ft
LP 19.00 ft

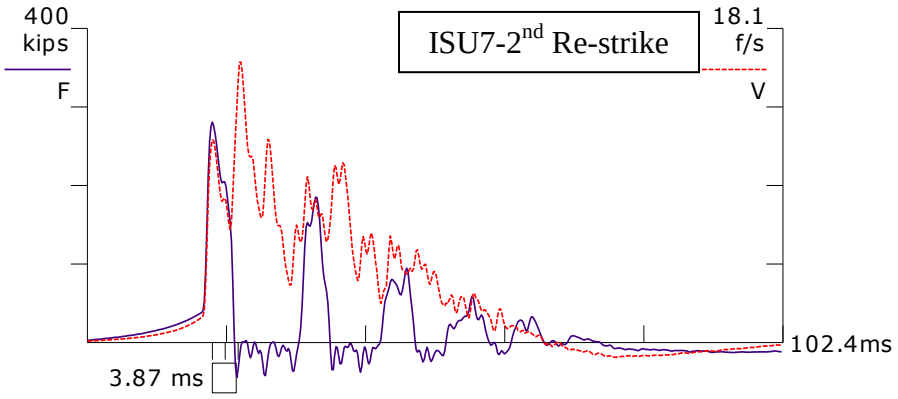

BN 3
6/9/2009 4:29:09 PM
RTL 86 kips
RSP 0 kips
RMX 11 kips
EMX 12.6 k-ft
ETR 29.2 (%)
STK 0.00 ft
CSX 22.6 ksi
TSX 5.7 ksi
BTA 100.0 (%)

LE 32.50 ft
AR 12.40 in^2
EM 30000 ksi
SP 0.492 k/ft3
WS 16807.9 f/s
EA/C 22.1 ksec/ft
LP 20.00 ft

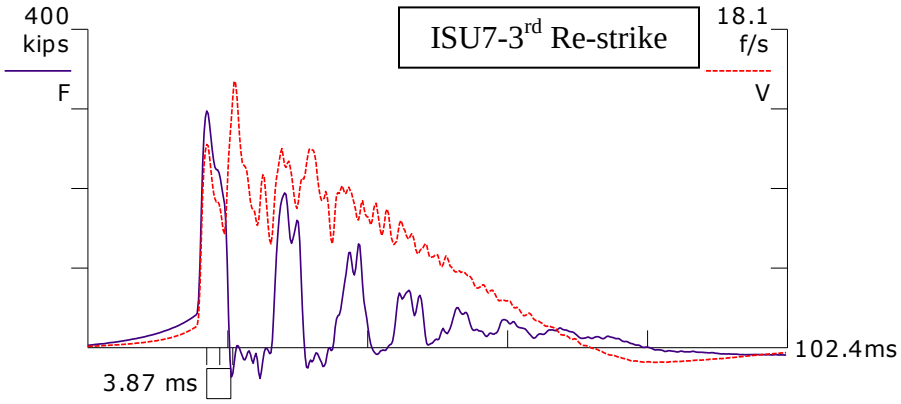

BN 4
6/9/2009 4:41:36 PM
RTL 103 kips
RSP 0 kips
RMX 6 kips
EMX 20.7 k-ft
ETR 47.9 (%)
STK 0.00 ft
CSX 24.0 ksi
TSX 4.2 ksi
BTA 100.0 (%)

LE 32.50 ft
AR 12.40 in^2
EM 30000 ksi
SP 0.492 k/ft3
WS 16807.9 f/s
EA/C 22.1 ksec/ft
LP 21.00 ft

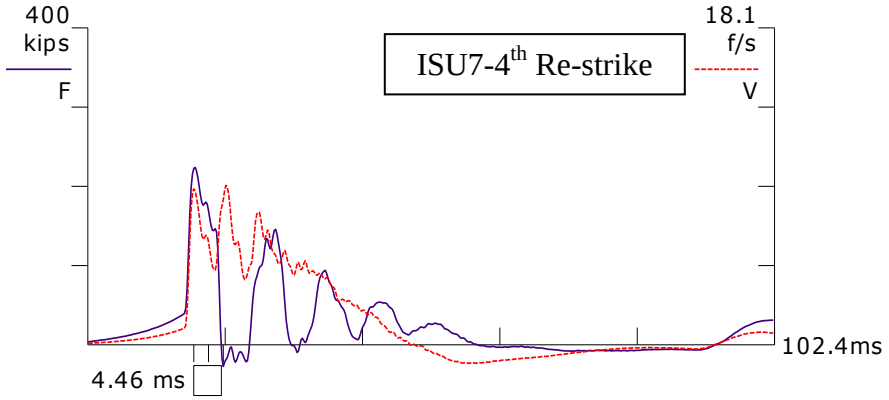

BN 9
6/10/2009 11:34:36 AM
RTL 104 kips
RSP 0 kips
RMX 31 kips
EMX 10.5 k-ft
ETR 24.4 (%)
STK 4.35 ft
CSX 18.1 ksi
TSX 2.6 ksi
BTA 100.0 (%)

LE 37.50 ft
AR 12.40 in^2
EM 30000 ksi
SP 0.492 k/ft3
WS 16807.9 f/s
EA/C 22.1 ksec/ft
LP 22.50 ft

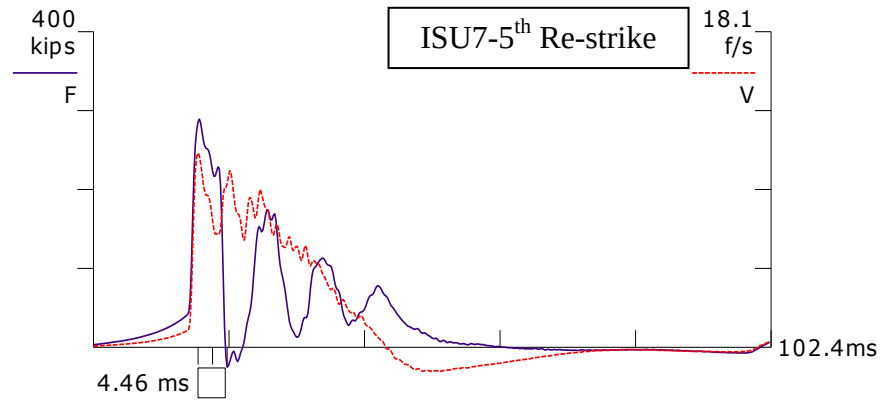

BN 5
6/12/2009 10:49:08 AM
RTL 150 kips
RSP 0 kips
RMX 66 kips
EMX 18.0 k-ft
ETR 41.7 (%)
STK 5.70 ft
CSX 23.3 ksi
TSX 2.4 ksi
BTA 100.0 (%)

LE 37.50 ft
AR 12.40 in^2
EM 30000 ksi
SP 0.492 k/ft3
WS 16807.9 f/s
EA/C 22.1 ksec/ft
LP 34.50 ft

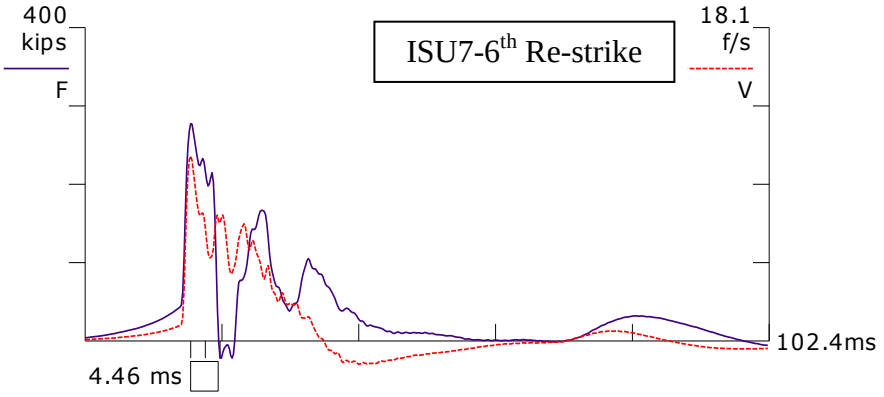

BN 6
6/16/2009 10:39:04 AM
RTL 170 kips
RSP 0 kips
RMX 86 kips
EMX 12.2 k-ft
ETR 28.3 (%)
STK 5.15 ft
CSX 22.4 ksi
TSX 2.1 ksi
BTA 100.0 (%)

LE 37.50 ft
AR 12.40 in^2
EM 30000 ksi
SP 0.492 k/ft3
WS 16807.9 f/s
EA/C 22.1 ksec/ft
LP 35.50 ft

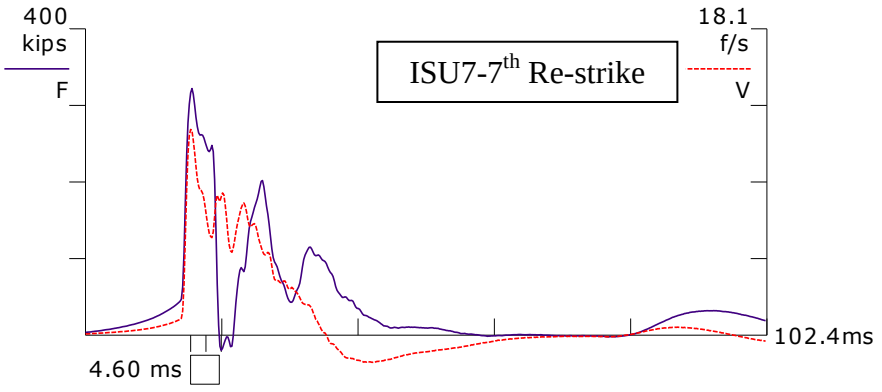

BN 8/7
6/19/2009 10:32:57 AM
RTL 192 kips
RSP 0 kips
RMX 93 kips
EMX 16.8 k-ft
ETR 38.8 (%)
STK 5.92 ft
CSX 26.0 ksi
TSX 1.7 ksi
BTA 100.0 (%)

LE 37.50 ft
AR 12.40 in^2
EM 30000 ksi
SP 0.492 k/ft3
WS 16807.9 f/s
EA/C 22.1 ksec/ft
LP 26.00 ft

Figure C.2.7. PDA force and velocity records for ISU7

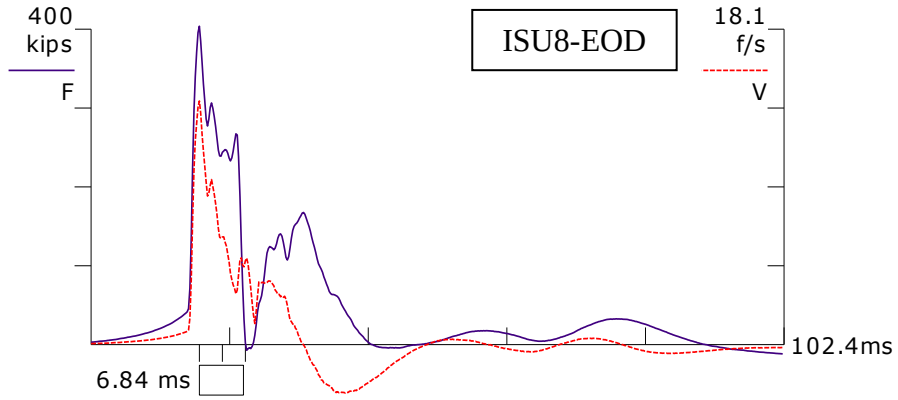

BN 336
8/6/2009 9:16:32 AM
RTL 304 kips
RSP 18 kips
RMX 164 kips
EMX 18.8 k-ft
ETR 43.6 (%)
STK 6.76 ft
CSX 32.6 ksi
TSX 1.6 ksi
BTA 100.0 (%)

LE 57.50 ft
AR 12.40 in^2
EM 30000 ksi
SP 0.492 k/ft3
WS 16807.9 f/s
EA/C 22.1 ksec/ft

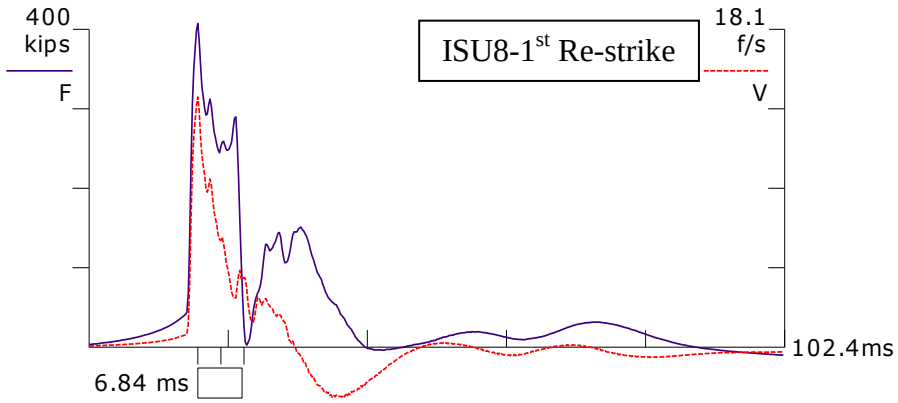

BN 6
8/6/2009 9:26:43 AM
RTL 330 kips
RSP 56 kips
RMX 161 kips
EMX 18.7 k-ft
ETR 43.2 (%)
STK 6.82 ft
CSX 32.9 ksi
TSX 1.6 ksi
BTA 100.0 (%)

LE 57.50 ft
AR 12.40 in^2
EM 30000 ksi
SP 0.492 k/ft3
WS 16807.9 f/s
EA/C 22.1 ksec/ft
LP 55.00 ft

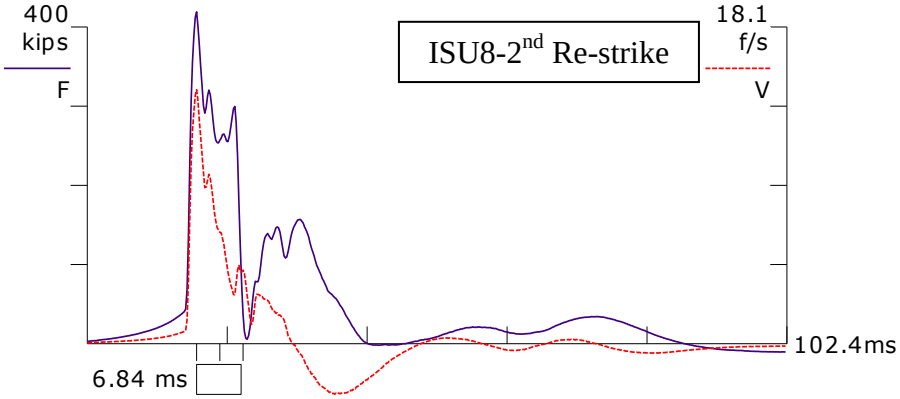

BN 4
8/6/2009 9:32:40 AM
RTL 342 kips
RSP 63 kips
RMX 169 kips
EMX 19.8 k-ft
ETR 45.8 (%)
STK 7.15 ft
CSX 33.8 ksi
TSX 1.5 ksi
BTA 100.0 (%)

LE 57.50 ft
AR 12.40 in^2
EM 30000 ksi
SP 0.492 k/ft3
WS 16807.9 f/s
EA/C 22.1 ksec/ft
LP 55.50 ft

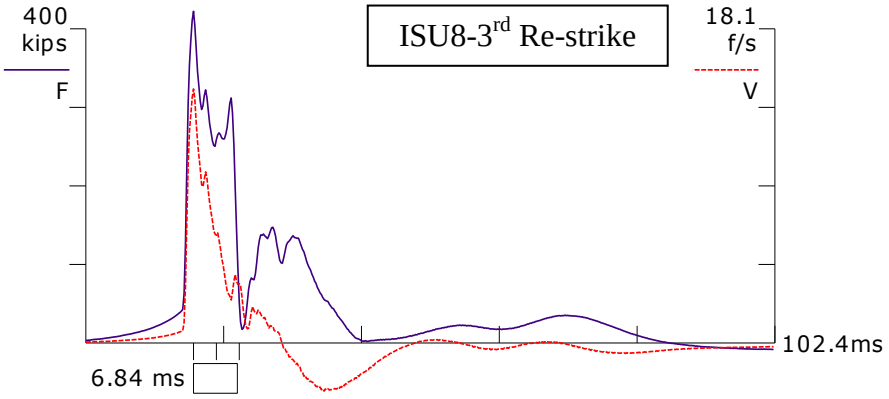

BN 4
8/6/2009 10:12:27 AM
RTL 361 kips
RSP 92 kips
RMX 161 kips
EMX 19.1 k-ft
ETR 44.2 (%)
STK 7.11 ft
CSX 34.1 ksi
TSX 1.1 ksi
BTA 100.0 (%)

LE 57.50 ft
AR 12.40 in^2
EM 30000 ksi
SP 0.492 k/ft3
WS 16807.9 f/s
EA/C 22.1 ksec/ft
LP 56.16 ft

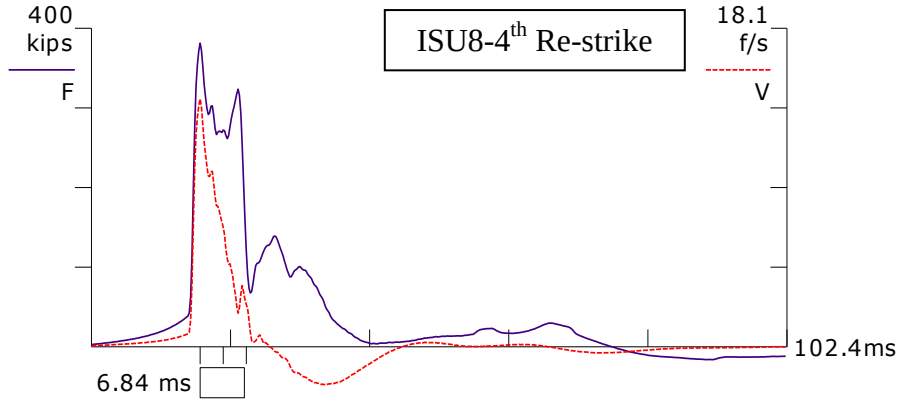

BN 5
8/7/2009 8:28:44 AM
RTL 380 kips
RSP 161 kips
RMX 180 kips
EMX 18.0 k-ft
ETR 41.7 (%)
STK 7.39 ft
CSX 30.8 ksi
TSX 0.6 ksi
BTA 100.0 (%)

LE 57.50 ft
AR 12.40 in^2
EM 30000 ksi
SP 0.492 k/ft3
WS 16807.9 f/s
EA/C 22.1 ksec/ft
LP 56.16 ft

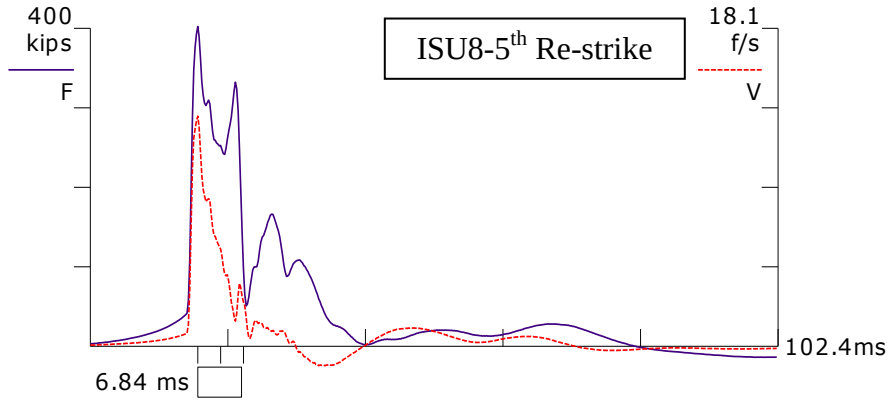

BN 4
8/10/2009 8:31:30 AM
RTL 367 kips
RSP 139 kips
RMX 177 kips
EMX 16.6 k-ft
ETR 38.3 (%)
STK 7.46 ft
CSX 32.4 ksi
TSX 1.4 ksi
BTA 100.0 (%)

LE 57.50 ft
AR 12.40 in^2
EM 30000 ksi
SP 0.492 k/ft3
WS 16807.9 f/s
EA/C 22.1 ksec/ft
LP 56.83 ft

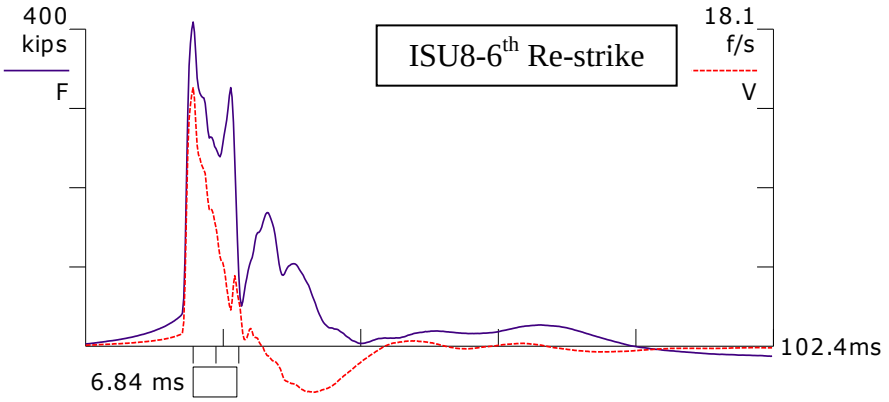

BN 5
8/11/2009 8:05:51 AM
RTL 384 kips
RSP 138 kips
RMX 208 kips
EMX 18.9 k-ft
ETR 43.8 (%)
STK 7.43 ft
CSX 33.0 ksi
TSX 0.5 ksi
BTA 100.0 (%)

LE 57.50 ft
AR 12.40 in^2
EM 30000 ksi
SP 0.492 k/ft3
WS 16807.9 f/s
EA/C 22.1 ksec/ft
LP 57.00 ft

Figure C.2.8. PDA force and velocity records for ISU8

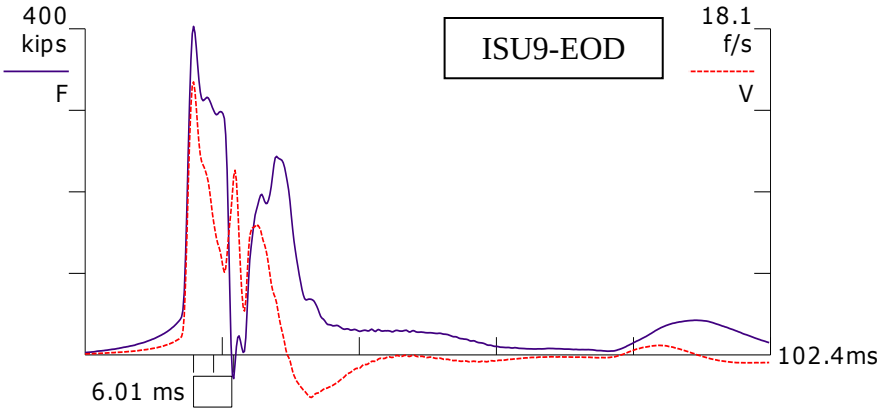

RTL 245 kips
RSP 146 kips
RMX 226 kips
EMX 24.1 k-ft
ETR 56.3 (%)
STK 8.28 ft
CSX 32.5 ksi
TSX 3.0 ksi
BTA 100.0 (%)

LE 50.50 ft
AR 12.40 in^2
EM 30000 ksi
SP 0.492 k/ft3
WS 16807.9 f/s
EA/C 22.1 ksec/ft
LP 47.00 ft

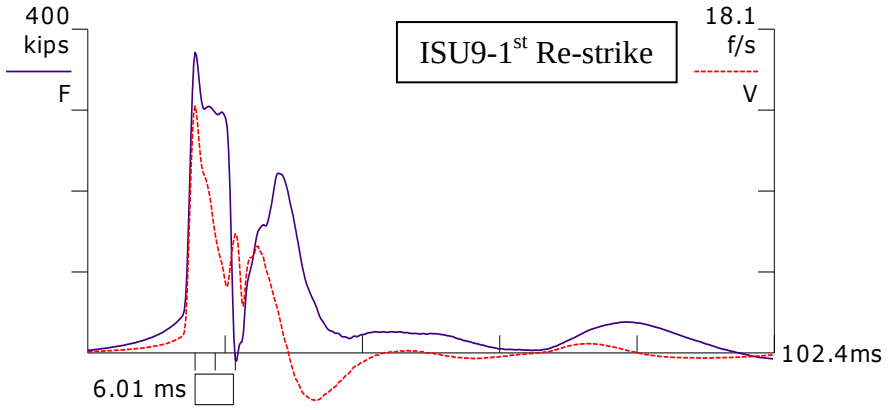

BN 5
1/18/2010 4:28:37 PM
RTL 260 kips
RSP 177 kips
RMX 217 kips
EMX 20.3 k-ft
ETR 47.3 (%)
STK 7.39 ft
CSX 30.0 ksi
TSX 0.8 ksi
BTA 100.0 (%)

LE 50.50 ft
AR 12.40 in^2
EM 30000 ksi
SP 0.492 k/ft3
WS 16807.9 f/s
EA/C 22.1 ksec/ft
LP 47.00 ft

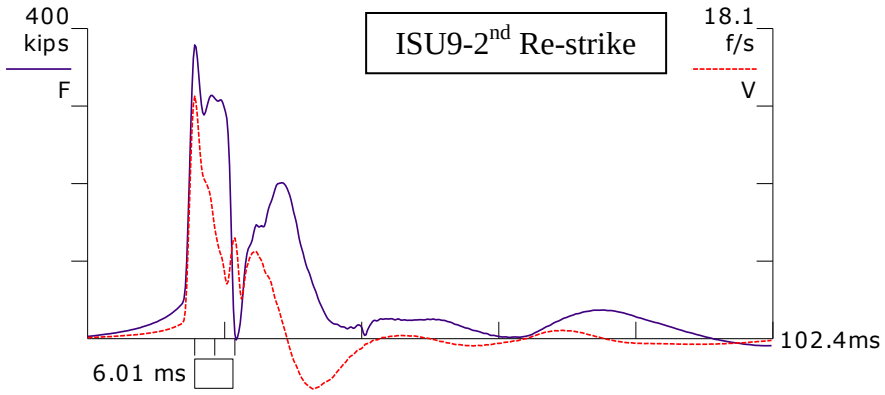

BN 4
1/18/2010 4:38:34 PM
RTL 284 kips
RSP 202 kips
RMX 215 kips
EMX 19.7 k-ft
ETR 45.9 (%)
STK 7.52 ft
CSX 30.6 ksi
TSX 5.7 ksi
BTA 100.0 (%)

LE 50.50 ft
AR 12.40 in^2
EM 30000 ksi
SP 0.492 k/ft3
WS 16807.9 f/s
EA/C 22.1 ksec/ft
LP 47.42 ft

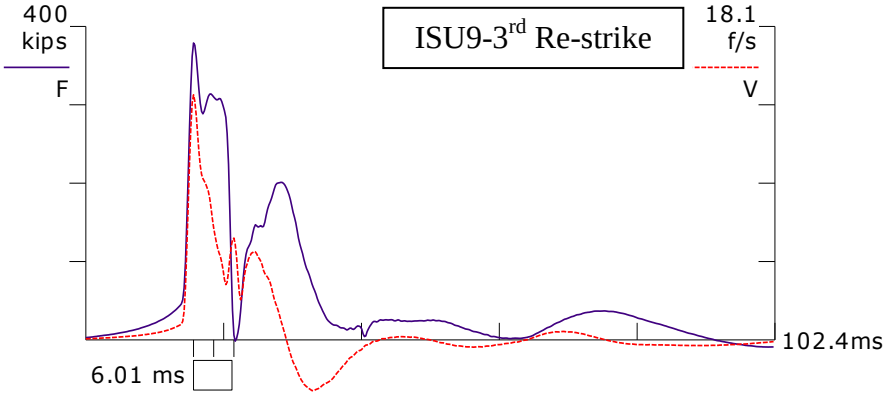

BN 4
1/18/2010 4:38:34 PM
RTL 284 kips
RSP 202 kips
RMX 215 kips
EMX 19.7 k-ft
ETR 45.9 (%)
STK 7.52 ft
CSX 30.6 ksi
TSX 5.7 ksi
BTA 100.0 (%)

LE 50.50 ft
AR 12.40 in^2
EM 30000 ksi
SP 0.492 k/ft3
WS 16807.9 f/s
EA/C 22.1 ksec/ft
LP 47.42 ft

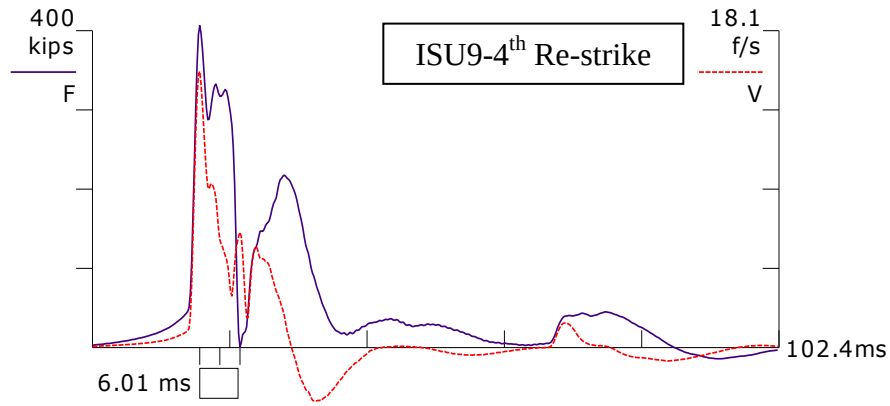

BN 4
1/19/2010 8:56:27 AM
RTL 305 kips
RSP 215 kips
RMX 227 kips
EMX 21.8 k-ft
ETR 50.9 (%)
STK 8.14 ft
CSX 32.8 ksi
TSX 0.0 ksi
BTA 100.0 (%)

LE 50.50 ft
AR 12.40 in^2
EM 30000 ksi
SP 0.492 k/ft3
WS 16807.9 f/s
EA/C 22.1 ksec/ft
LP 48.00 ft

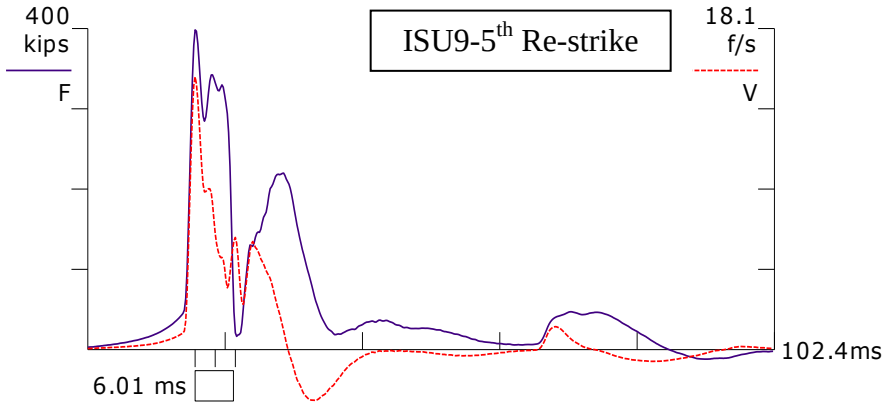

BN 5
1/21/2010 1:10:20 PM
RTL 310 kips
RSP 224 kips
RMX 229 kips
EMX 22.2 k-ft
ETR 51.9 (%)
STK 7.66 ft
CSX 32.1 ksi
TSX 0.0 ksi
BTA 100.0 (%)

LE 50.50 ft
AR 12.40 in^2
EM 30000 ksi
SP 0.492 k/ft3
WS 16807.9 f/s
EA/C 22.1 ksec/ft
LP 48.08 ft

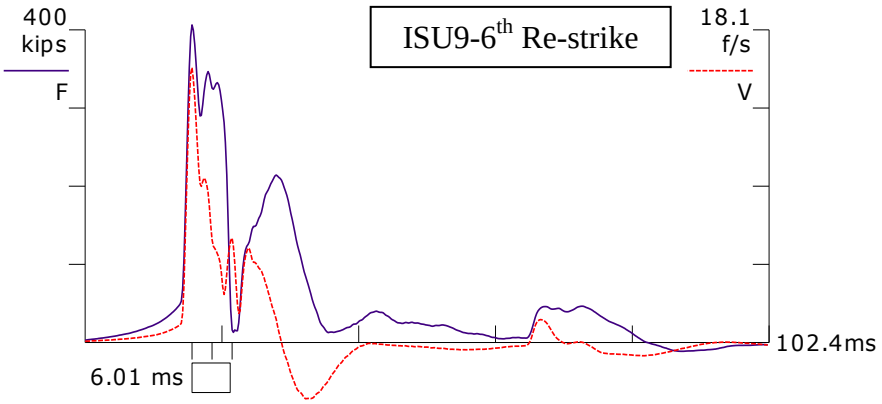

BN 11
1/28/2010 10:55:01 AM
RTL 320 kips
RSP 233 kips
RMX 233 kips
EMX 21.7 k-ft
ETR 50.6 (%)
STK 8.19 ft
CSX 32.8 ksi
TSX 0.2 ksi
BTA 100.0 (%)

LE 50.50 ft
AR 12.40 in^2
EM 30000 ksi
SP 0.492 k/ft3
WS 16807.9 f/s
EA/C 22.1 ksec/ft
LP 48.58 ft

Figure C.2.9. PDA force and velocity records for ISU9

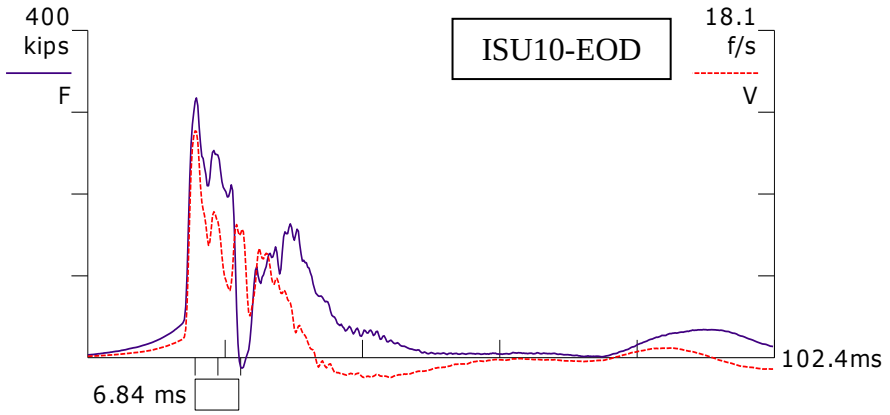

BN 320
3/31/2010 4:49:55 PM
RTL 213 kips
RSP 138 kips
RMX 158 kips
EMX 17.1 k-ft
ETR 39.9 (%)
STK 6.22 ft
CSX 25.6 ksi
TSX 1.2 ksi
BTA 100.0 (%)

LE 57.50 ft
AR 12.40 in^2
EM 30000 ksi
SP 0.492 k/ft3
WS 16807.9 f/s
EA/C 22.1 ksec/ft

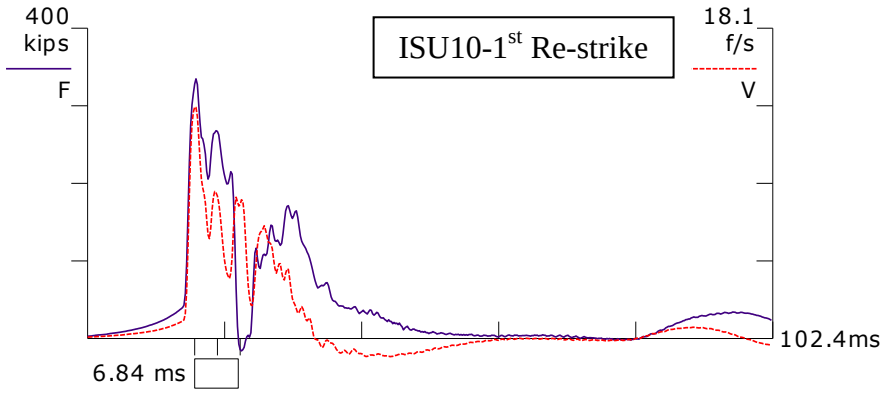

BN 3
3/31/2010 4:55:22 PM
RTL 220 kips
RSP 138 kips
RMX 160 kips
EMX 18.8 k-ft
ETR 43.9 (%)
STK 6.56 ft
CSX 27.0 ksi
TSX 1.5 ksi
BTA 100.0 (%)

LE 57.50 ft
AR 12.40 in^2
EM 30000 ksi
SP 0.492 k/ft3
WS 16807.9 f/s
EA/C 22.1 ksec/ft
LP 47.00 ft

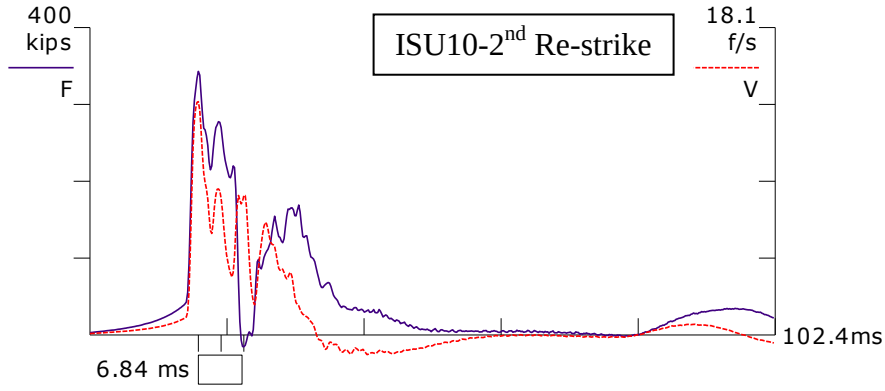

BN 3
3/31/2010 5:05:50 PM
RTL 225 kips
RSP 140 kips
RMX 163 kips
EMX 19.1 k-ft
ETR 44.7 (%)
STK 6.65 ft
CSX 27.7 ksi
TSX 1.5 ksi
BTA 100.0 (%)

LE 57.50 ft
AR 12.40 in^2
EM 30000 ksi
SP 0.492 k/ft3
WS 16807.9 f/s
EA/C 22.1 ksec/ft
LP 47.80 ft

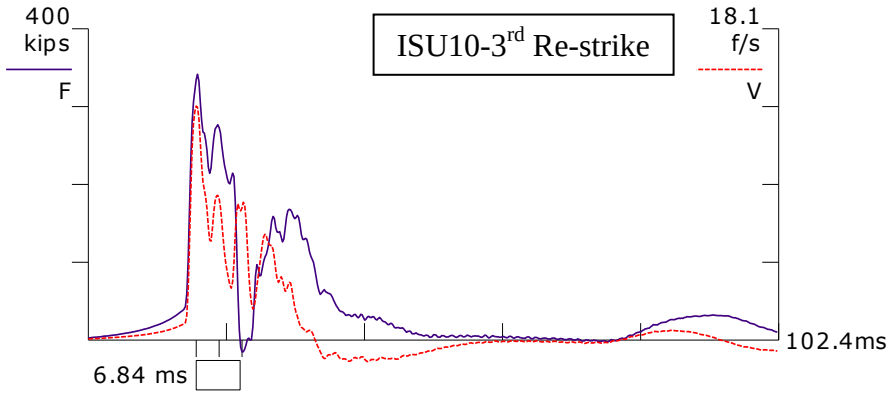

BN 3
3/31/2010 5:46:42 PM
RTL 225 kips
RSP 143 kips
RMX 166 kips
EMX 18.3 k-ft
ETR 42.7 (%)
STK 6.55 ft
CSX 27.5 ksi
TSX 1.5 ksi
BTA 100.0 (%)

LE 57.50 ft
AR 12.40 in^2
EM 30000 ksi
SP 0.492 k/ft3
WS 16807.9 f/s
EA/C 22.1 ksec/ft
LP 48.50 ft

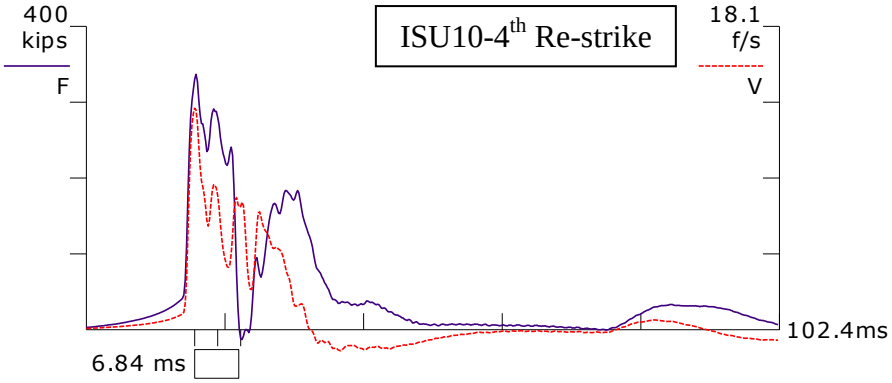

BN 4
4/1/2010 9:17:30 AM
RTL 224 kips
RSP 144 kips
RMX 170 kips
EMX 19.6 k-ft
ETR 45.7 (%)
STK 6.44 ft
CSX 27.2 ksi
TSX 1.2 ksi
BTA 100.0 (%)

LE 57.50 ft
AR 12.40 in^2
EM 30000 ksi
SP 0.492 k/ft3
WS 16807.9 f/s
EA/C 22.1 ksec/ft
LP 48.80 ft

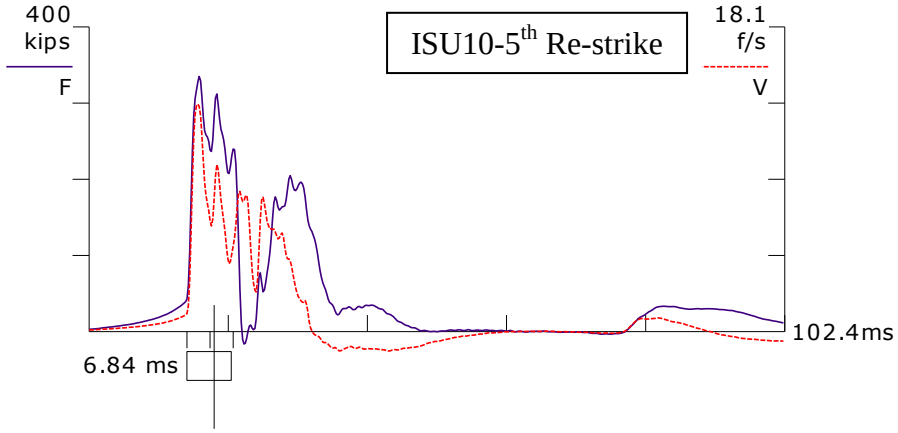

BN 4
4/5/2010 9:11:02 AM
RTL 219 kips
RSP 138 kips
RMX 175 kips
EMX 20.7 k-ft
ETR 48.3 (%)
STK 6.64 ft
CSX 27.0 ksi
TSX 1.7 ksi
BTA 89.0 (%)

LE 57.50 ft
AR 12.40 in^2
EM 30000 ksi
SP 0.492 k/ft3
WS 16807.9 f/s
EA/C 22.1 ksec/ft
LP 49.40 ft

Figure C.2.10. PDA force and velocity records for ISU10

C.3. Schematic Drawing and Configuration of the Vertical Static Load Tests

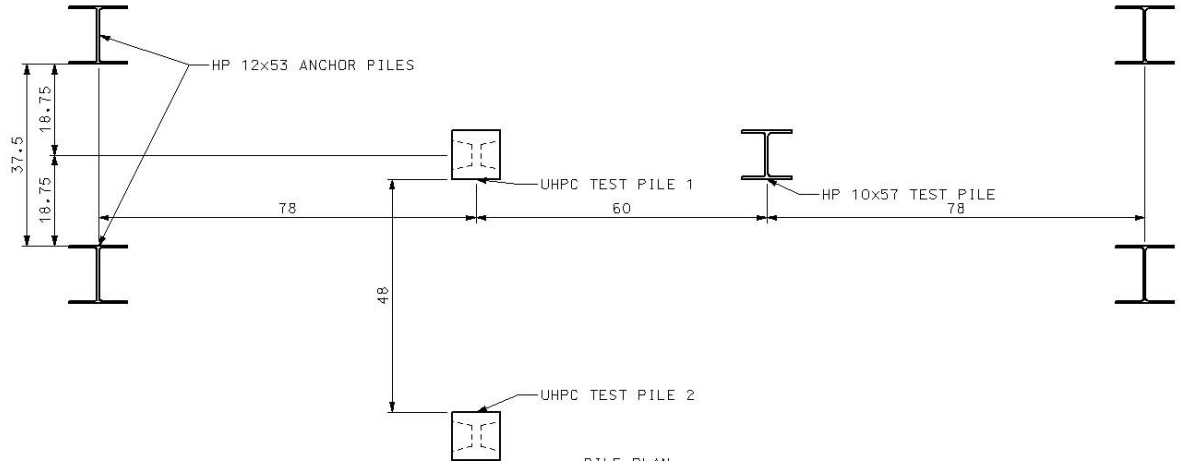

Figure C.3.1. Configuration of four anchor piles and a steel test pile for ISU1 at Mahaska County

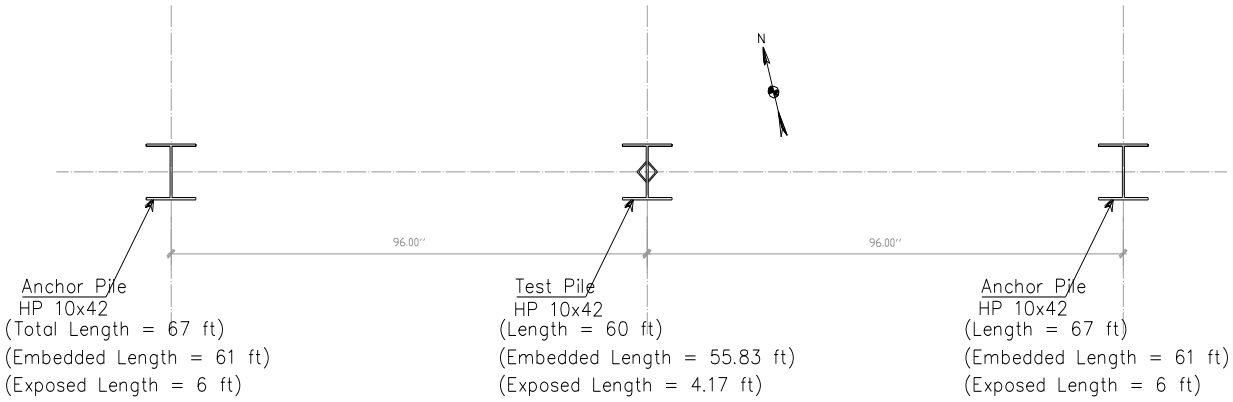

Figure C.3.2. Configuration of two anchor piles and a steel test pile for ISU2 at Mills County

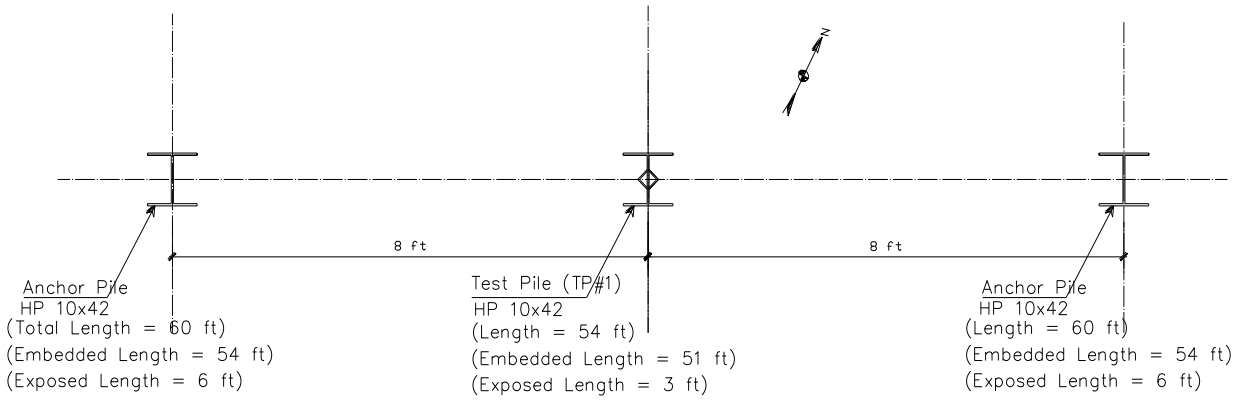

Figure C.3.3. Configuration of two anchor piles and a steel test pile for ISU3 at Polk County

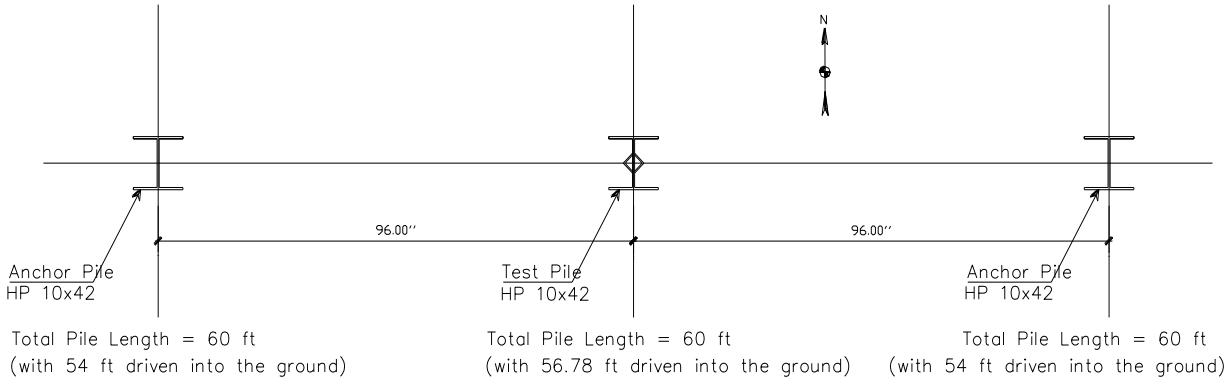

Figure C.3.4. Configuration of two anchor piles and a steel test pile for ISU4 at Jasper County

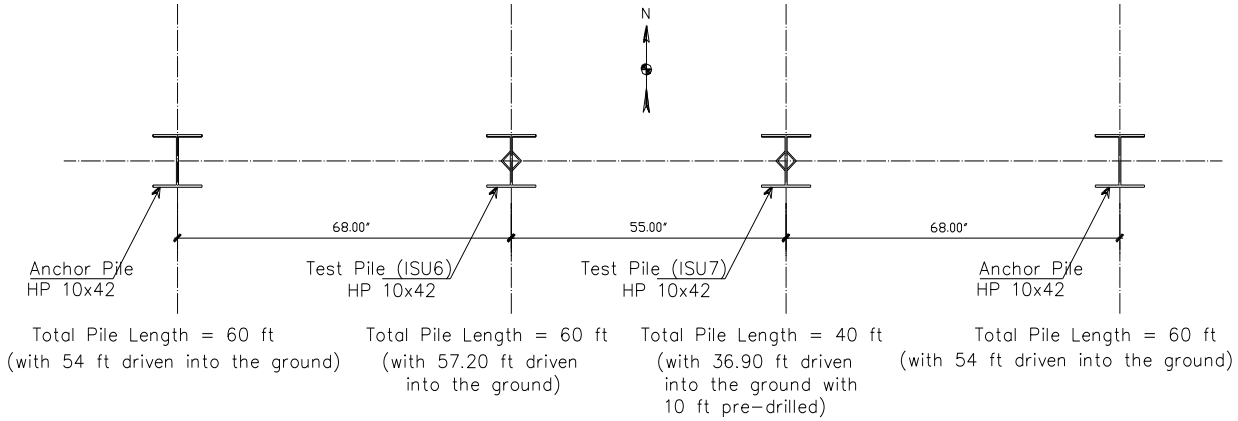

Figure C.3.5. Configuration of two anchor piles and two steel test piles for ISU6 and ISU7 at Buchanan County

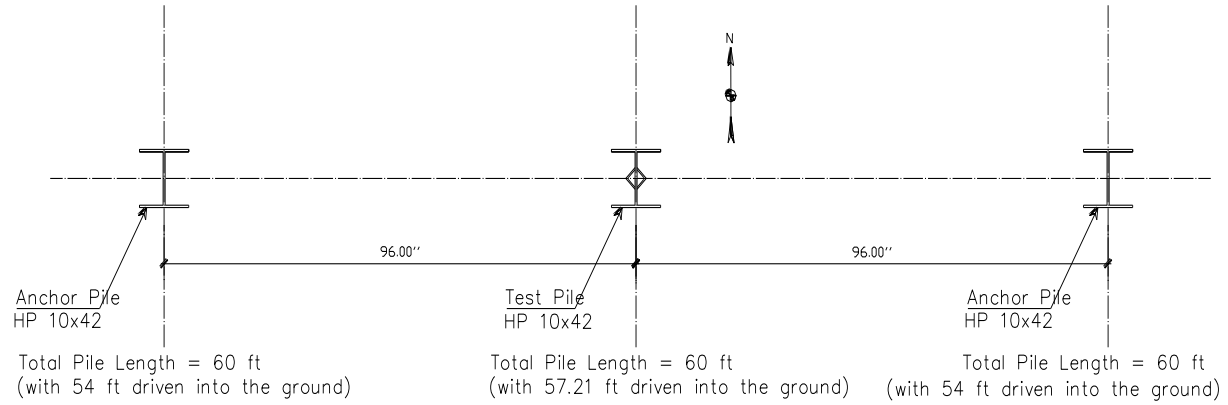

Figure C.3.6. Configuration of two anchor piles and a steel test pile for ISU8 at Poweshiek County

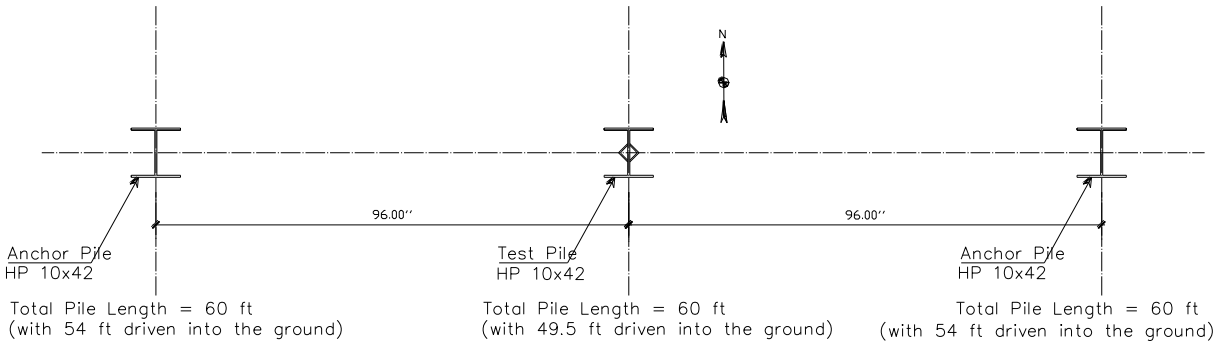

Figure C.3.7. Configuration of two anchor piles and a steel test pile for ISU9 at Des Moines County

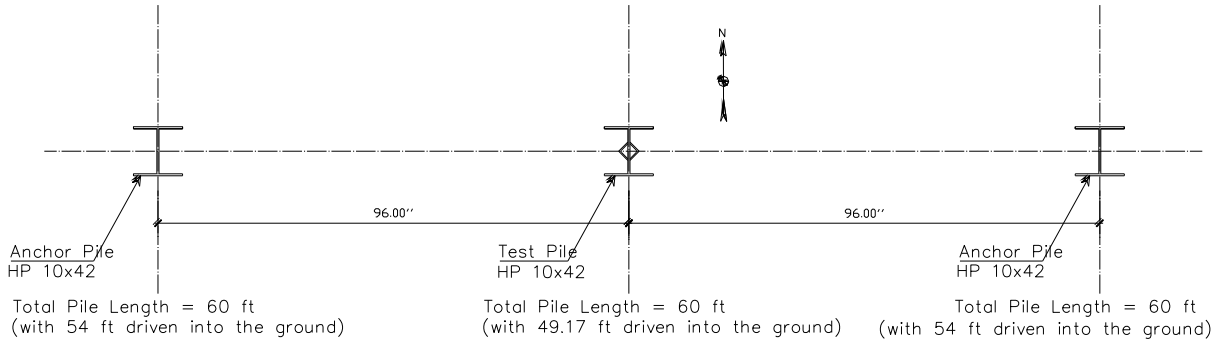

Figure C.3.8. Configuration of two anchor piles and a steel test pile for ISU10 at Cedar County

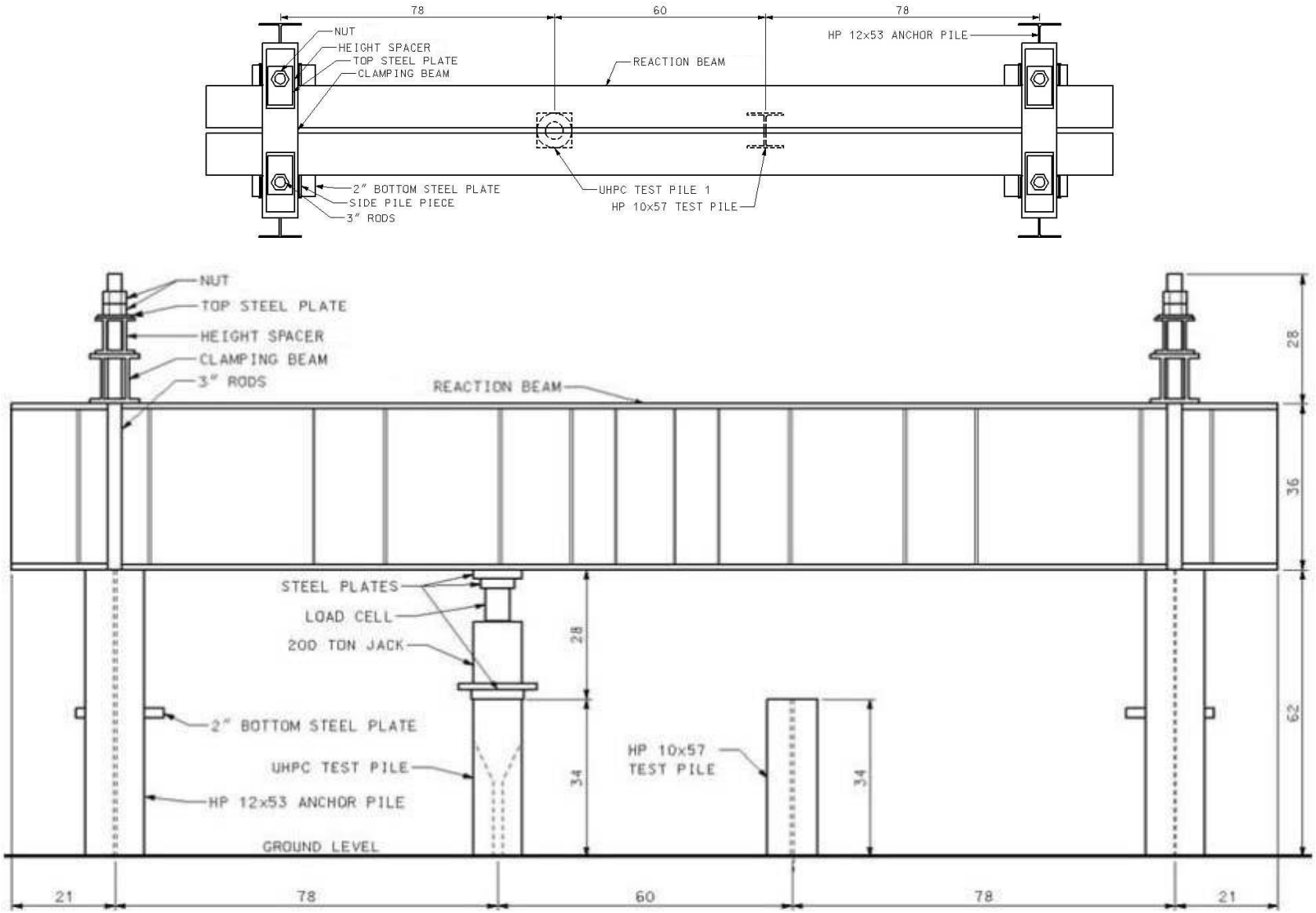

Figure C.3.9. Schematic drawing of vertical static load test for ISU1 at Mahaska County

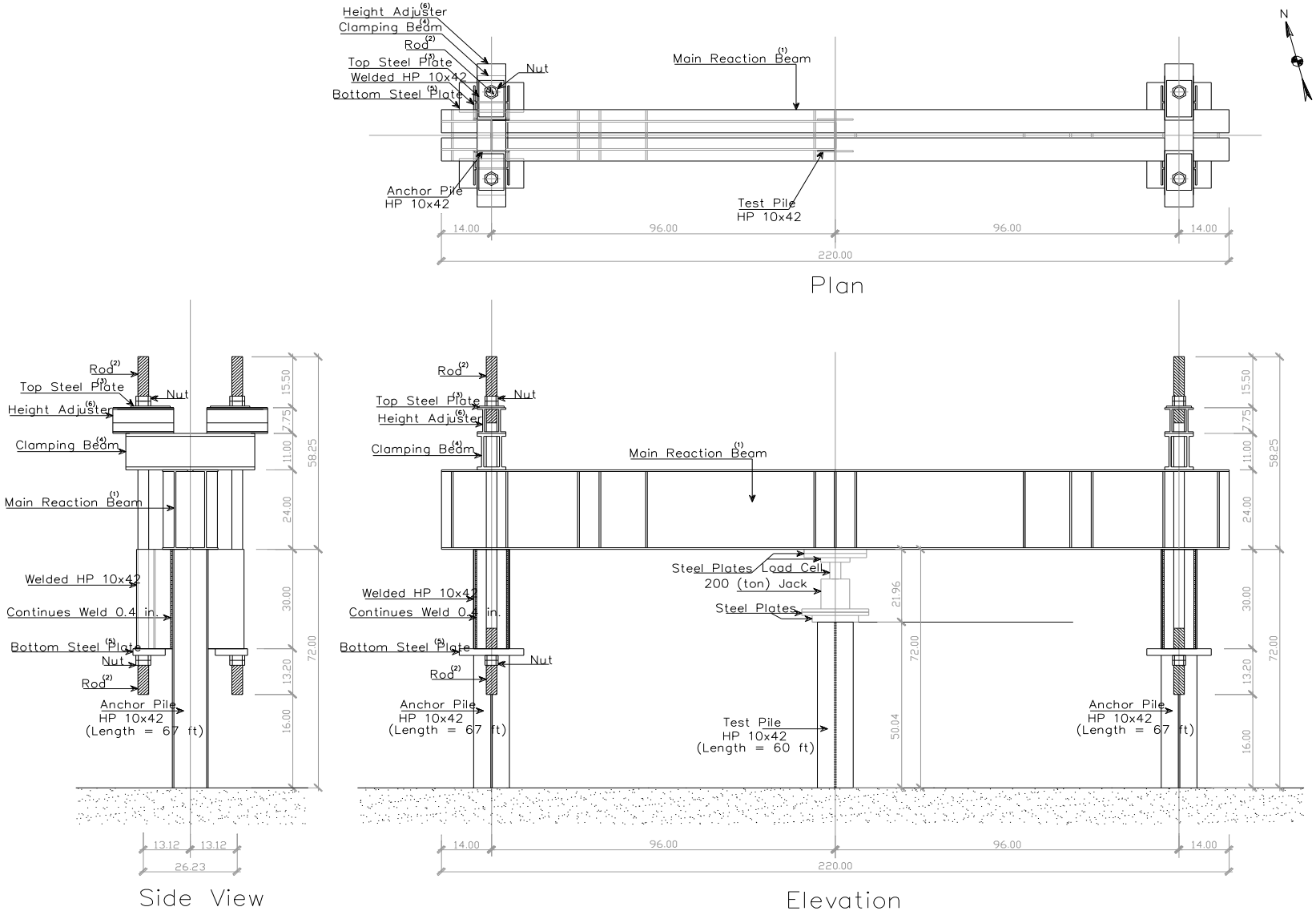

Figure C.3.10. Schematic drawing of vertical static load test for ISU2 at Mills County

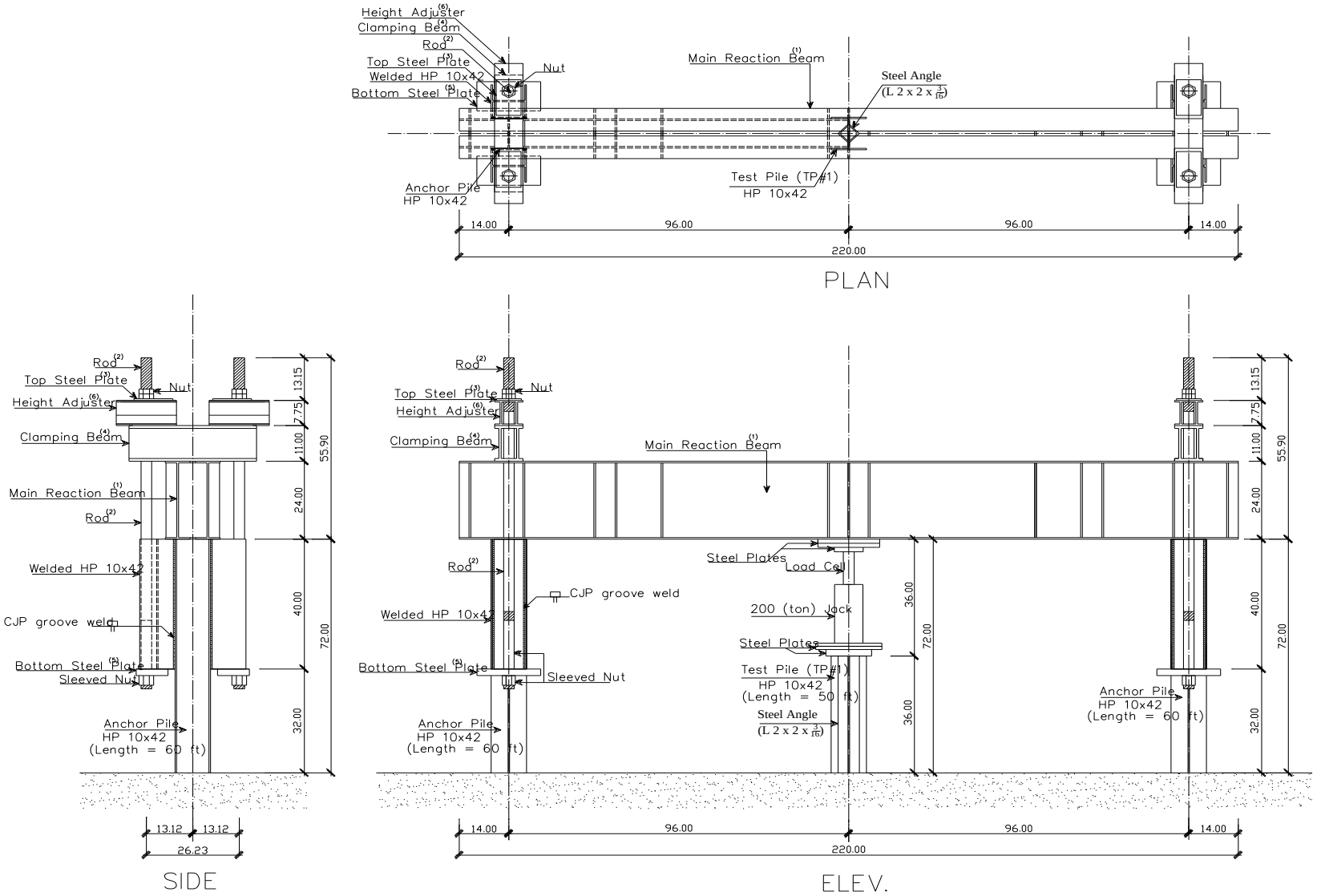

Figure C.3.11. Schematic drawing of vertical static load test for ISU3 at Polk County

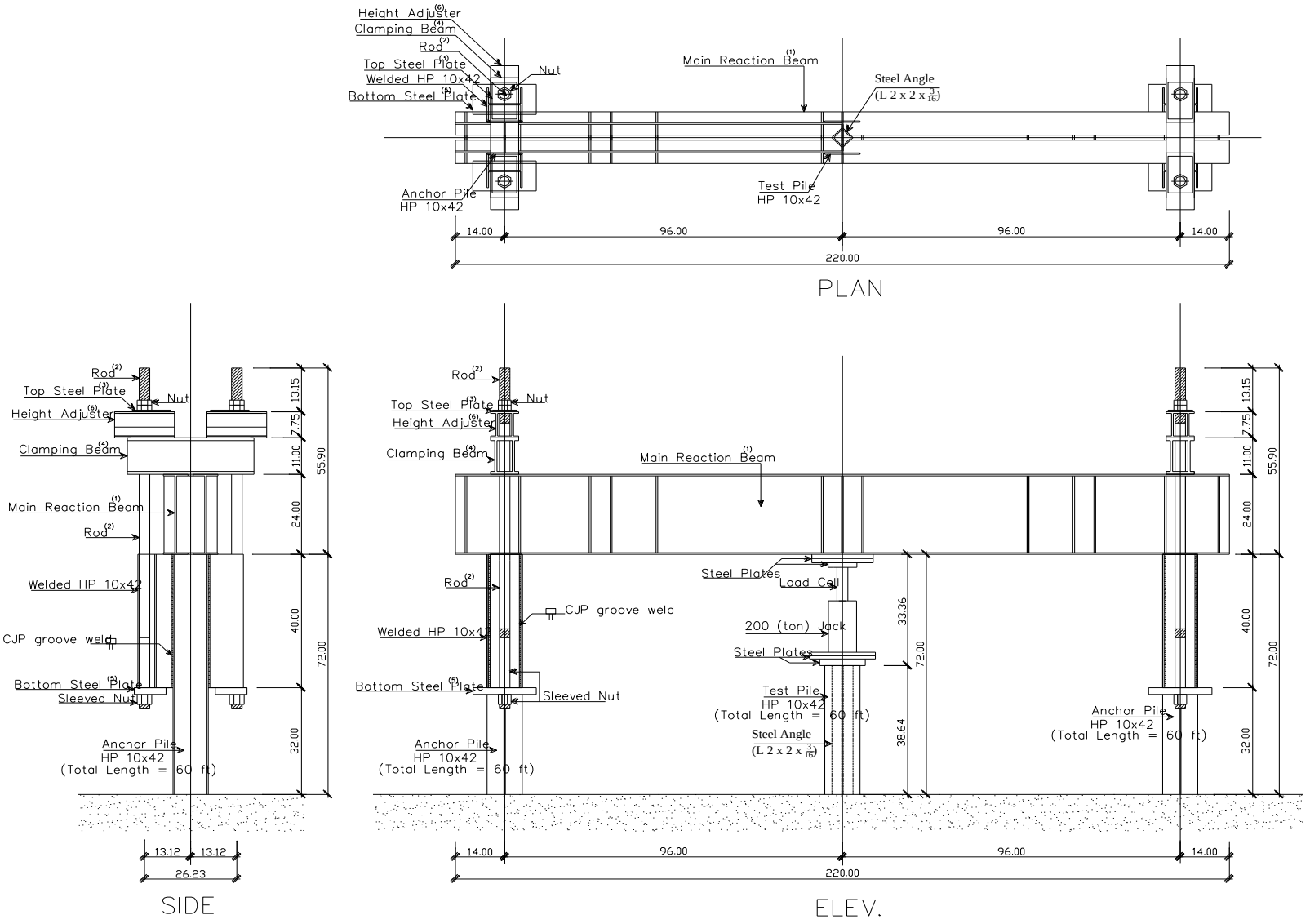

Figure C.3.12. Schematic drawing of vertical static load test for ISU4 at Jasper County

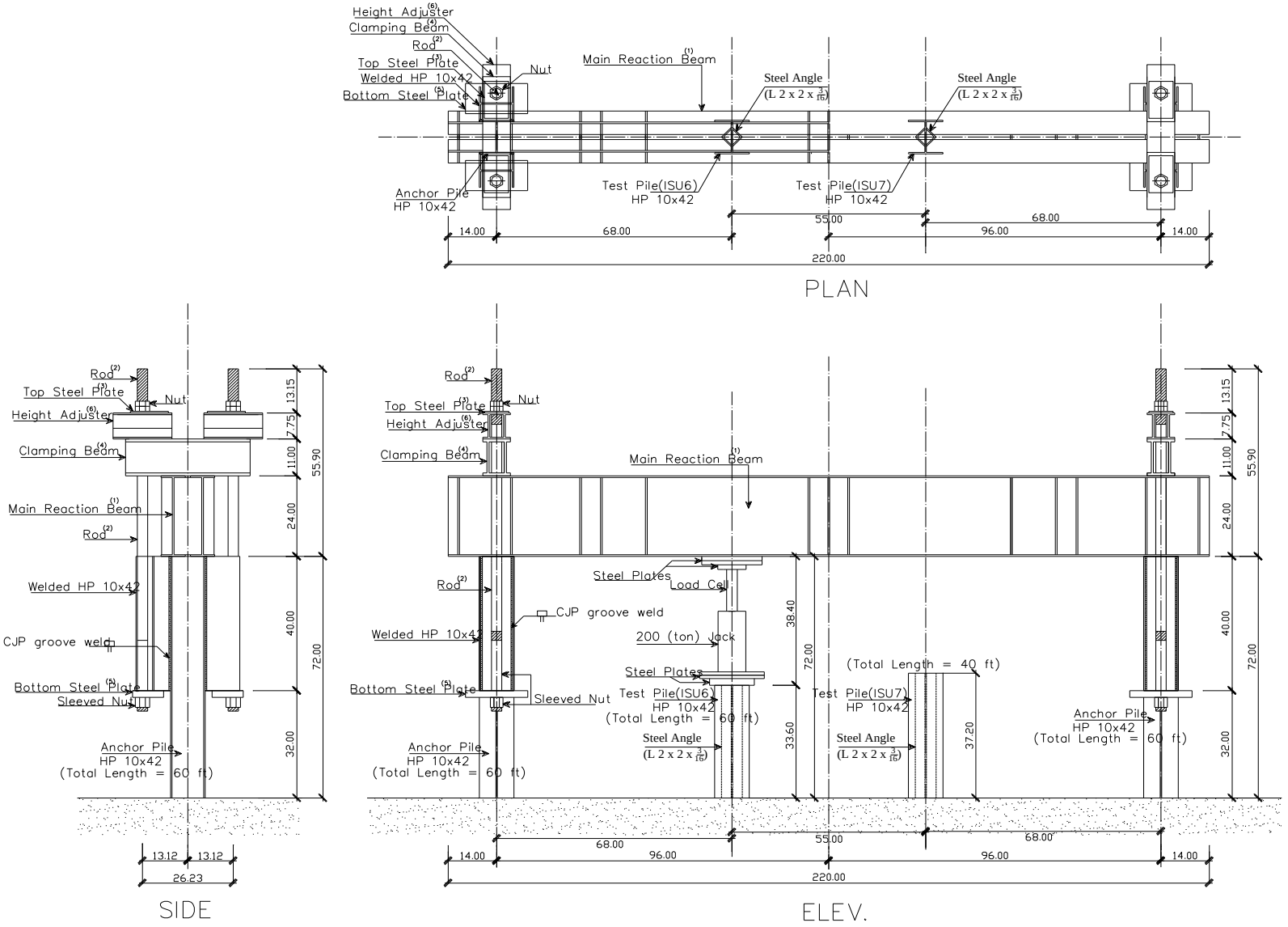

Figure C.3.13. Schematic drawing of vertical static load tests for ISU6 and ISU7 at Buchanan County

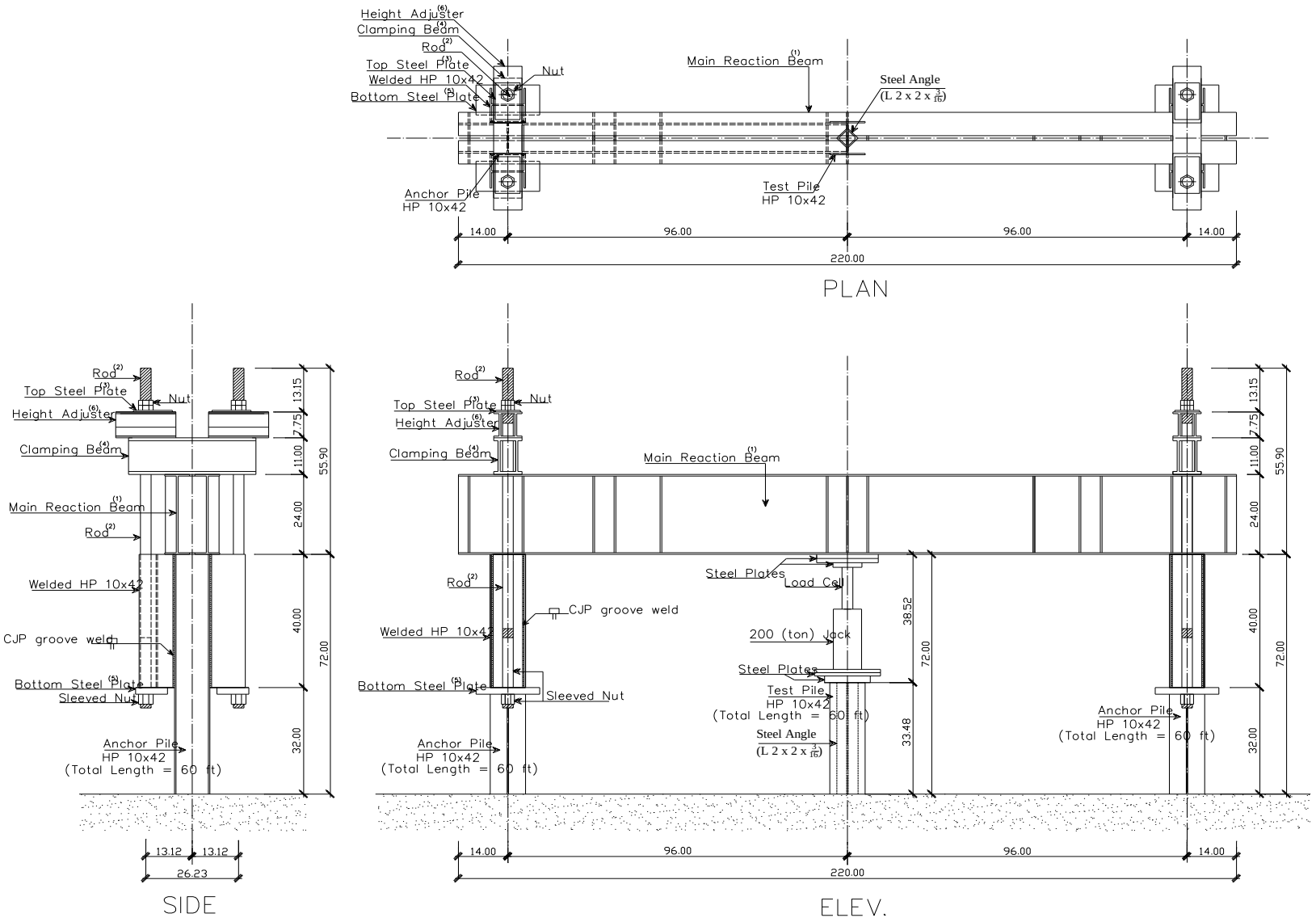

Figure C.3.14. Schematic drawing of vertical static load test for ISU8 at Poweshiek County

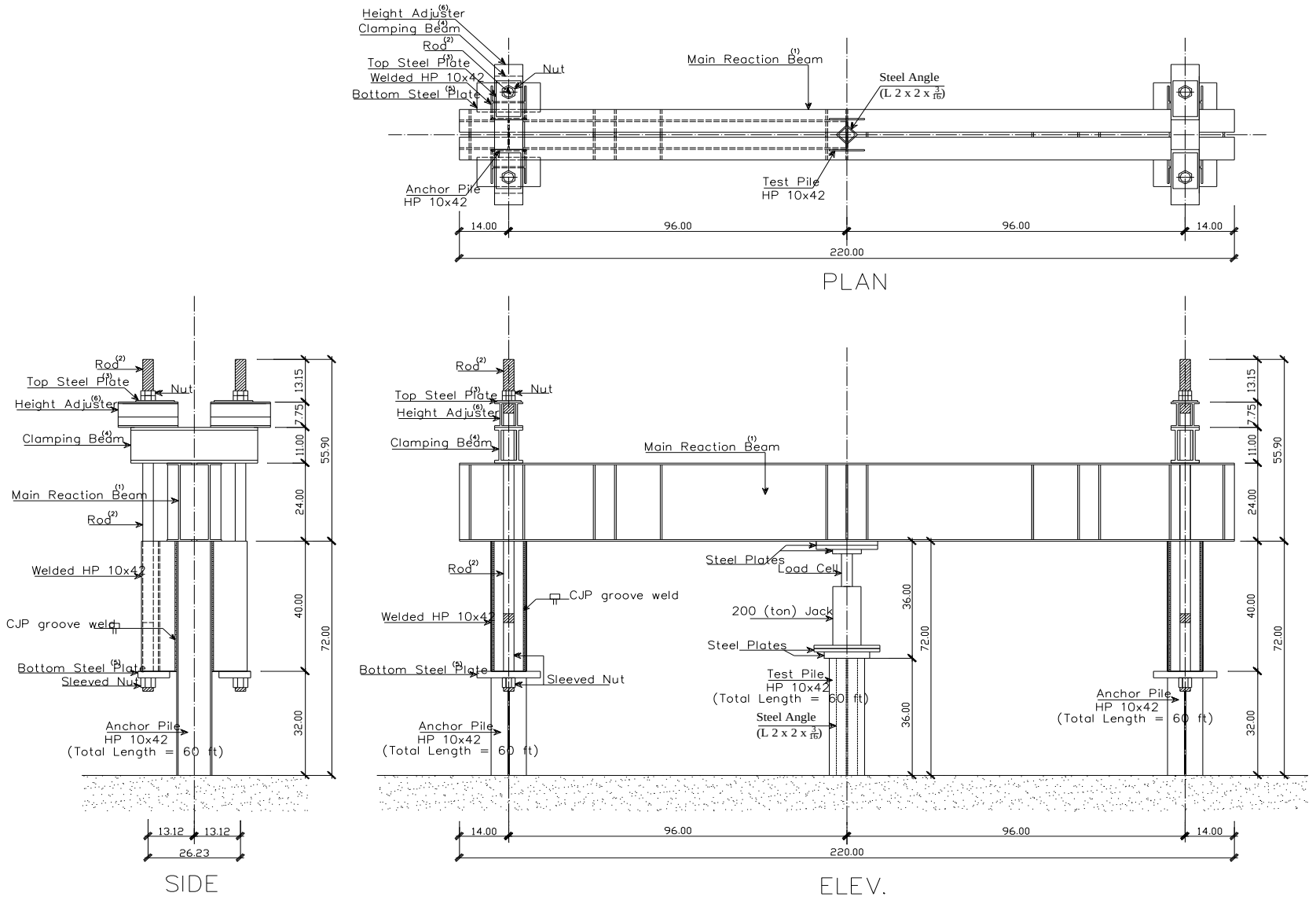

Figure C.3. 15. Schematic drawing of vertical static load tests for ISU9 and ISU10 at Des Moines County and Cedar County respectively

C.4. Static Load Test Load and Displacement

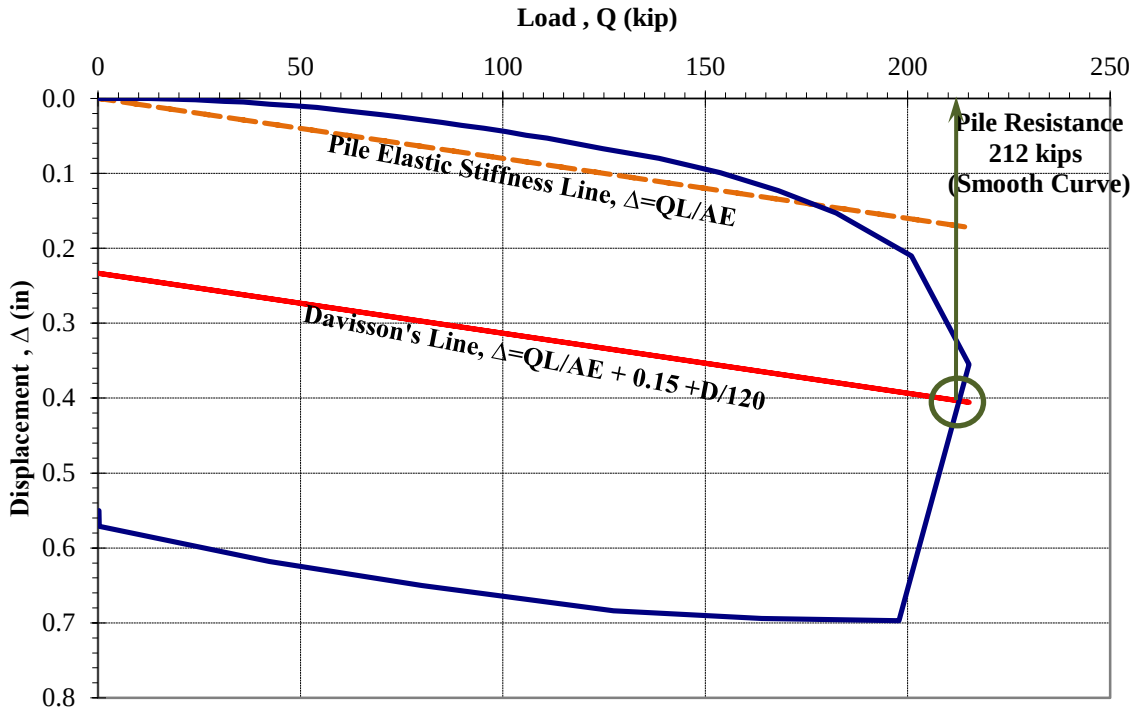

Figure C.4.1. A load-displacement curve and Davisson's criteria for ISU1 at Mahaska County

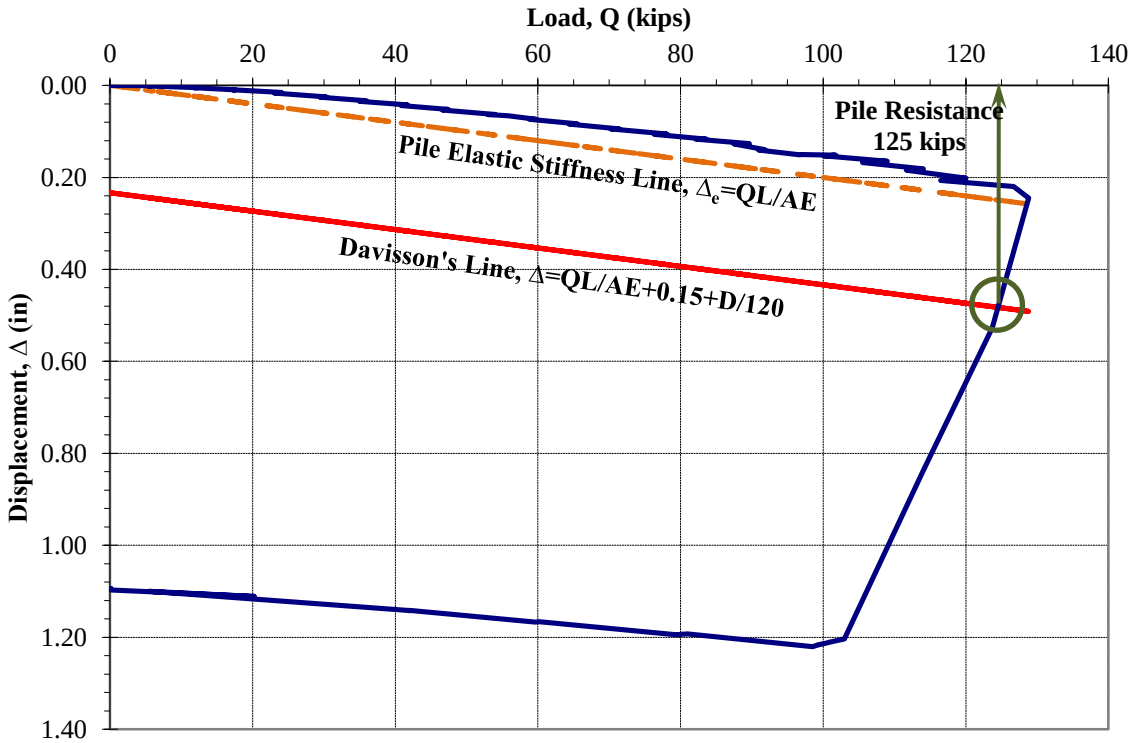

Figure C.4.2. A load-displacement curve and Davisson's criteria for ISU2 at Mills County

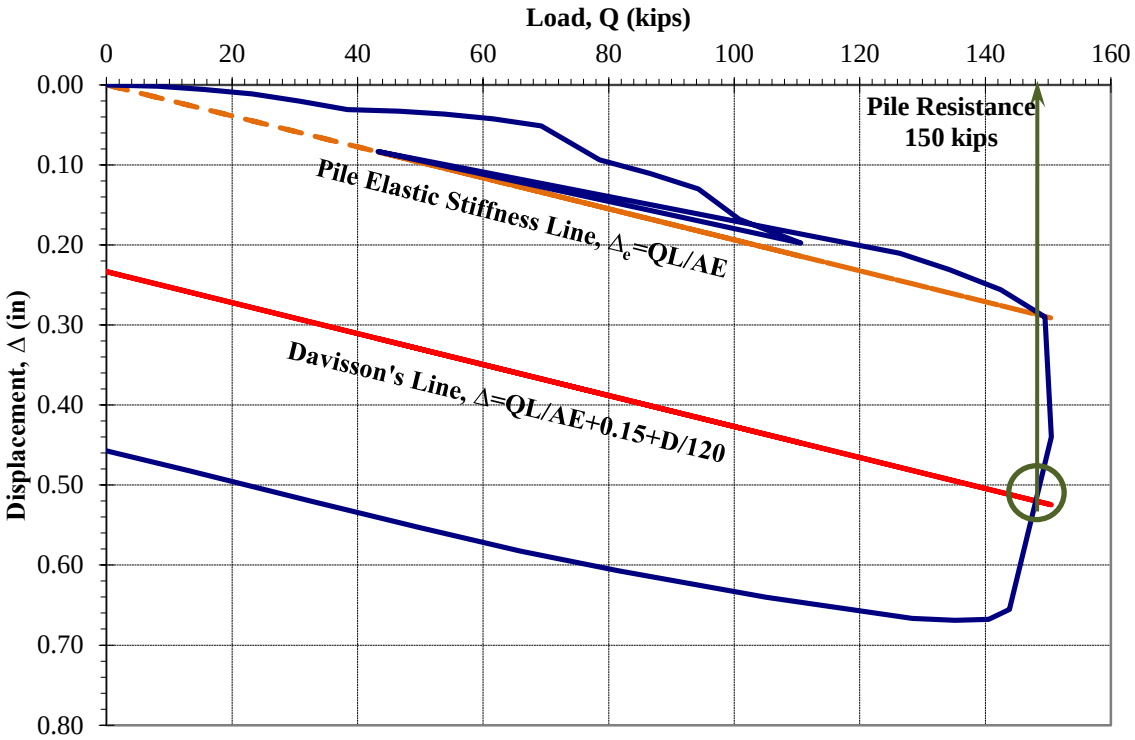

Figure C.4.3. A load-displacement curve and Davisson's criteria for ISU3 at Polk County

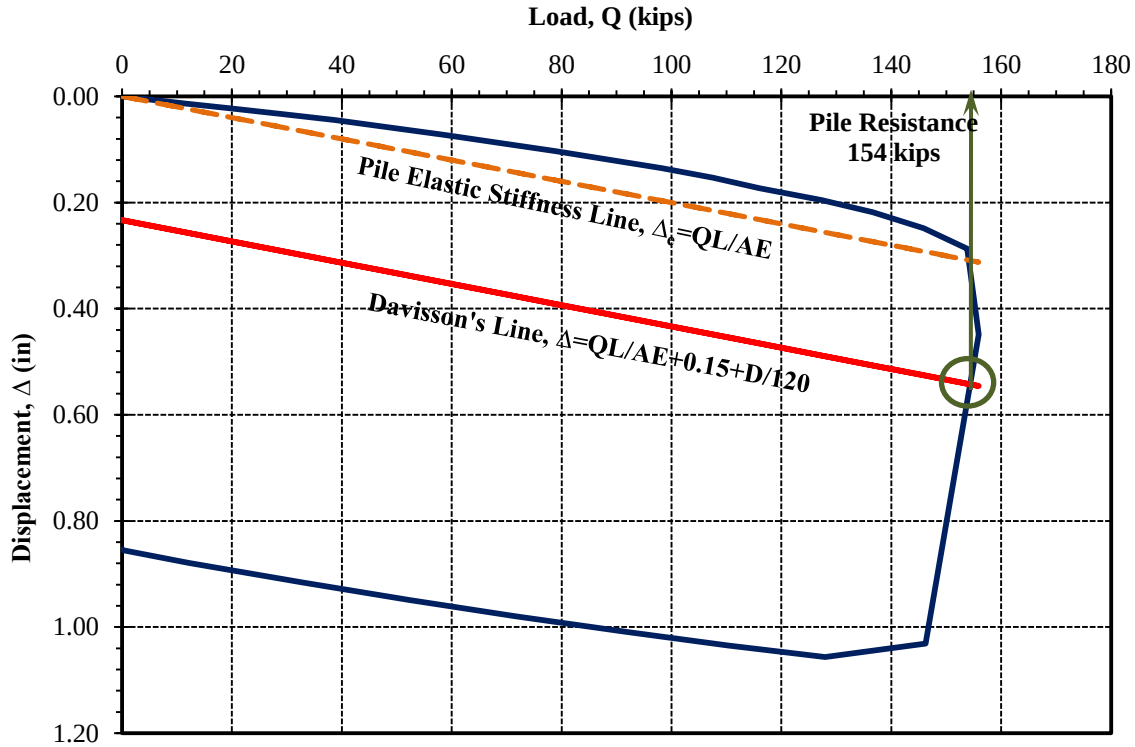

Figure C.4.4. A load-displacement curve and Davisson's criteria for ISU4 at Jasper County

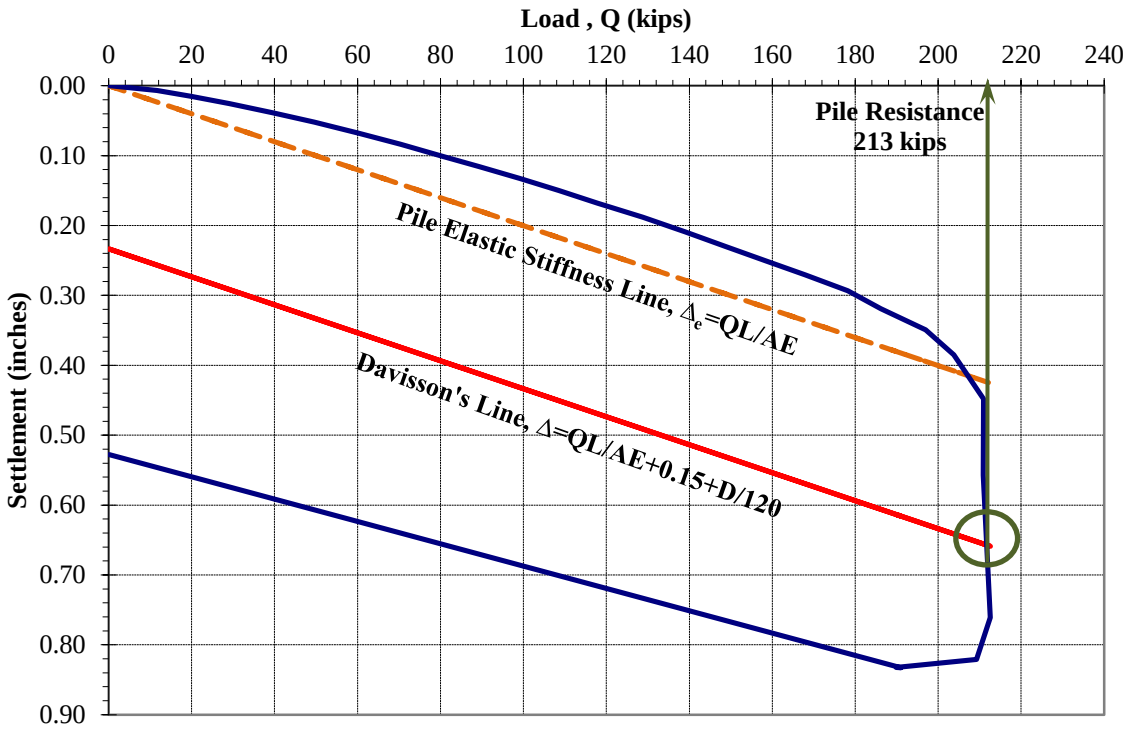

Figure C.4.5. A load-displacement curve and Davisson's criteria for ISU6 at Buchanan County

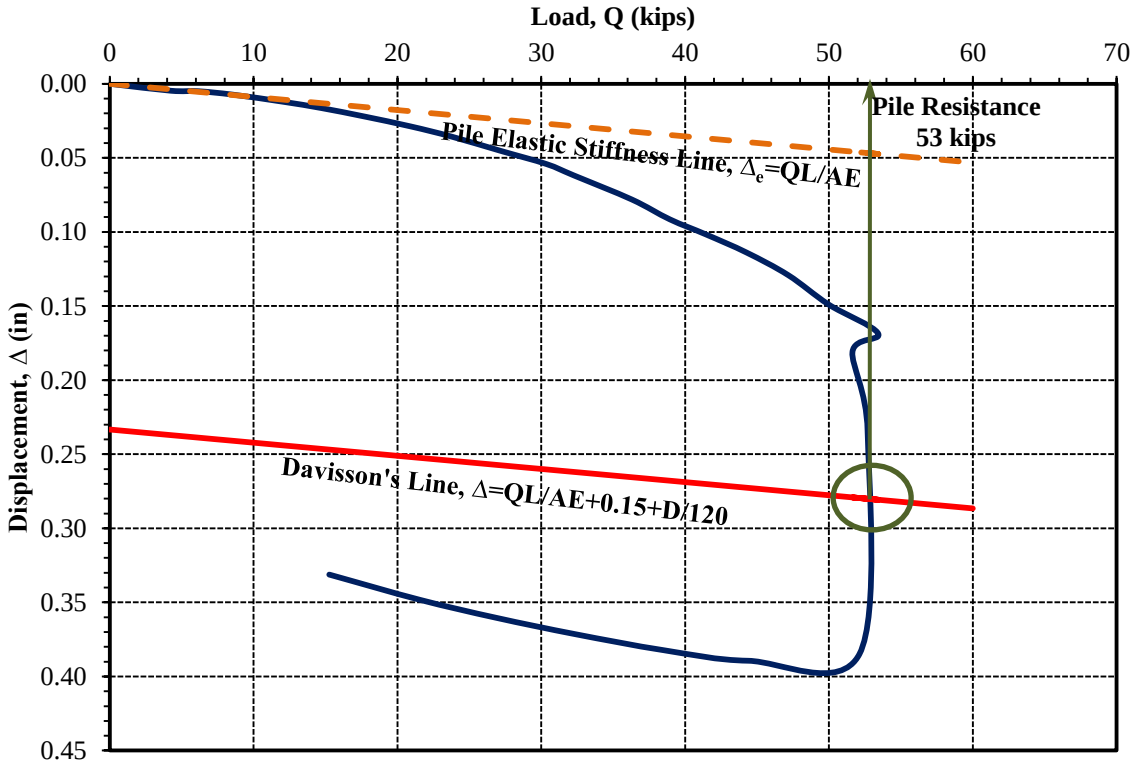

Figure C.4.6. A load-displacement curve and Davisson's criteria for ISU7 at Buchanan County

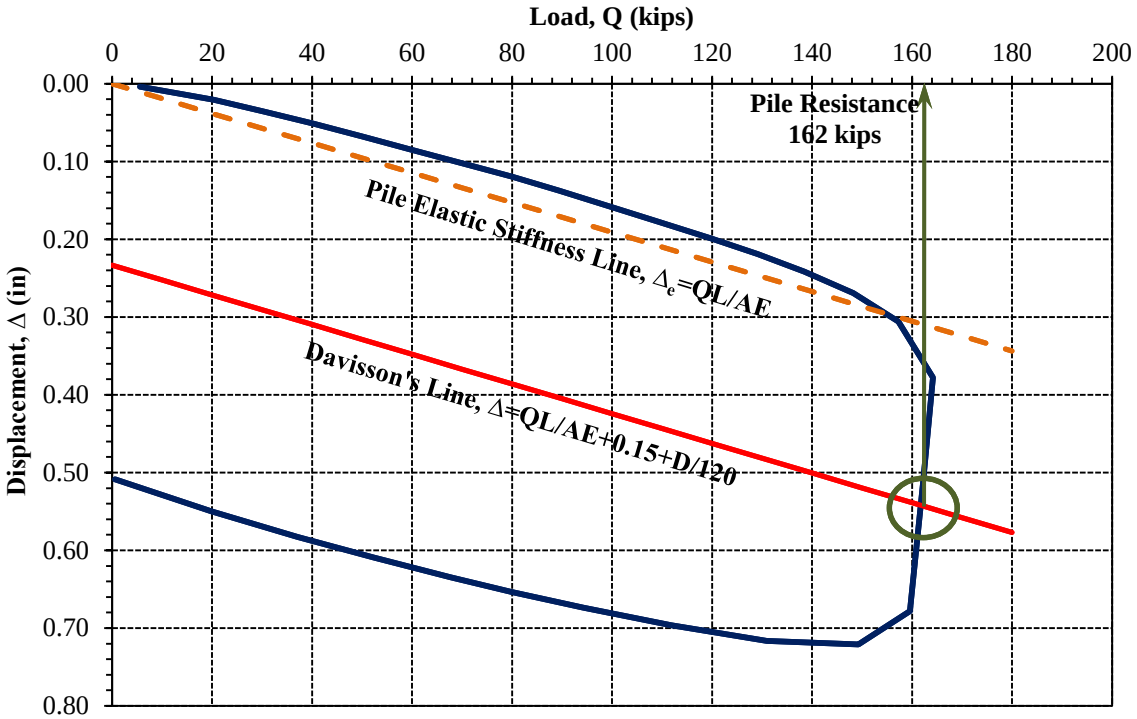

Figure C.4.7. A load-displacement curve and Davisson's criteria for ISU8 at Poweshiek County

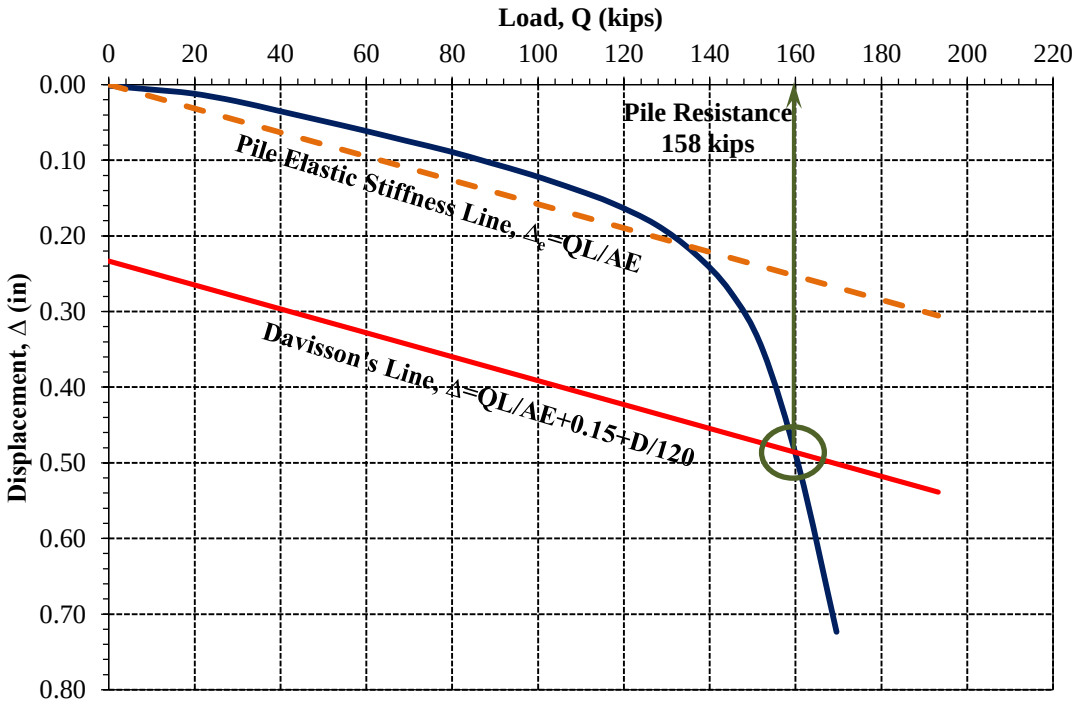

Figure C.4.8. A load-displacement curve and Davisson's criteria for ISU9 at Des Moines County

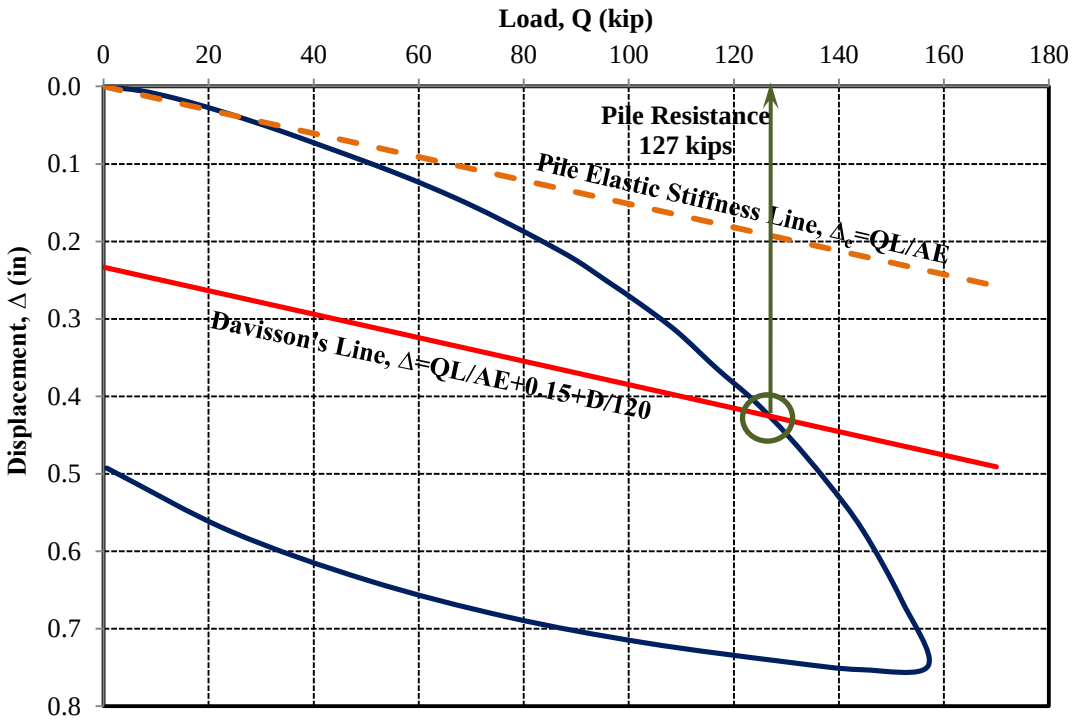

Figure C.4.9. A load-displacement curve and Davisson's criteria for ISU10 at Cedar County

APPENDIX D: DATA INTERPRETATION AND ANALYSIS

D.1. Static Load Test Pile Force Transferred Profiles

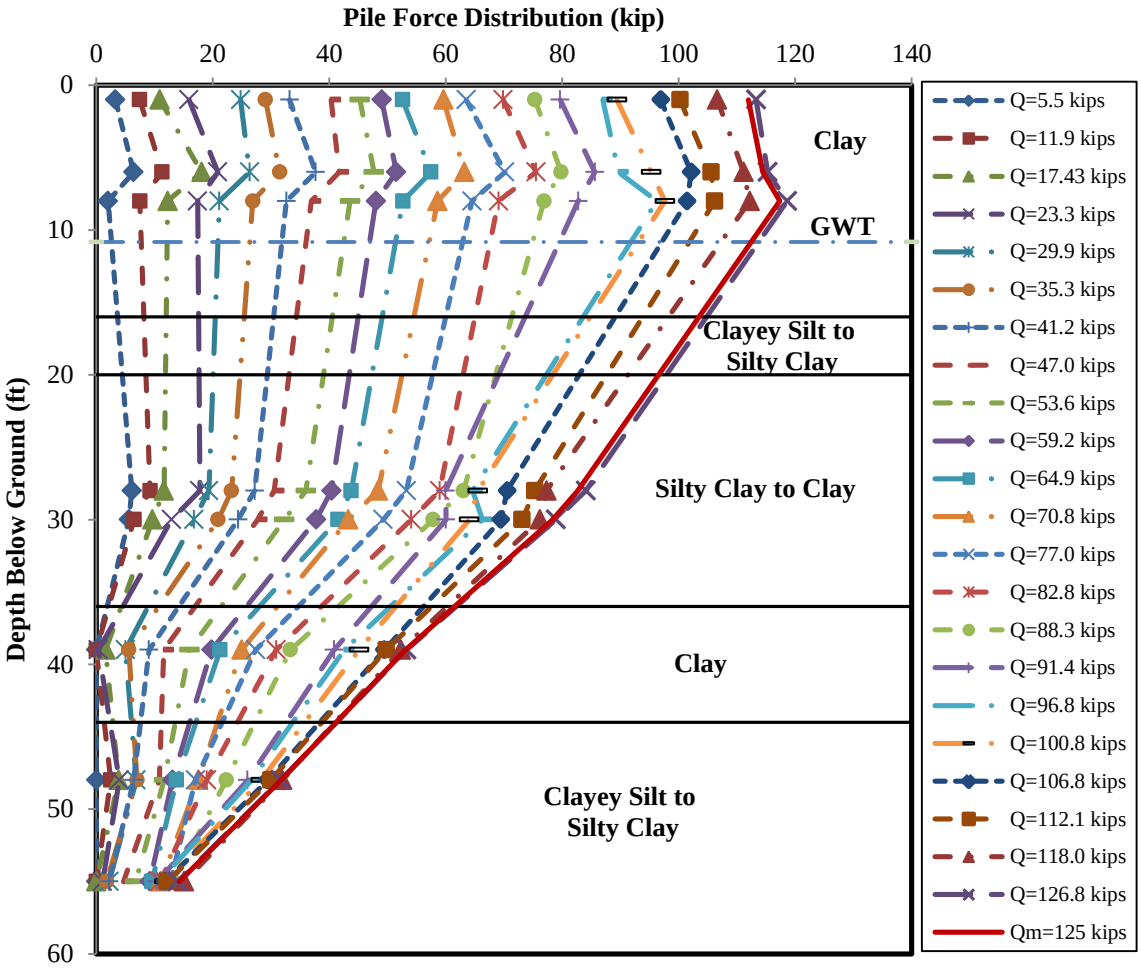

Figure D.1.1. Pile force distribution along the embedded pile length of the test pile ISU2

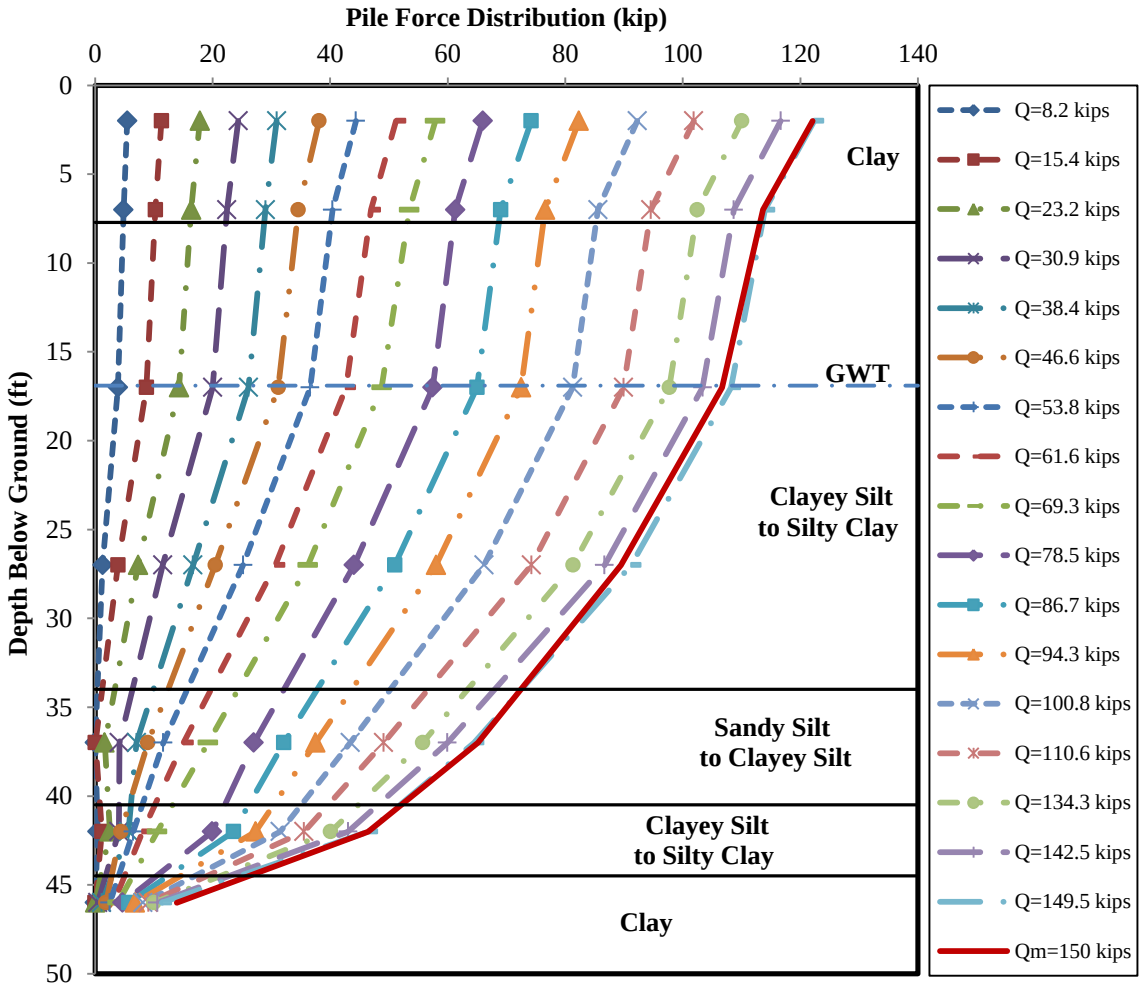

Figure D.1.2. Pile force distribution along the embedded pile length of the test pile ISU3

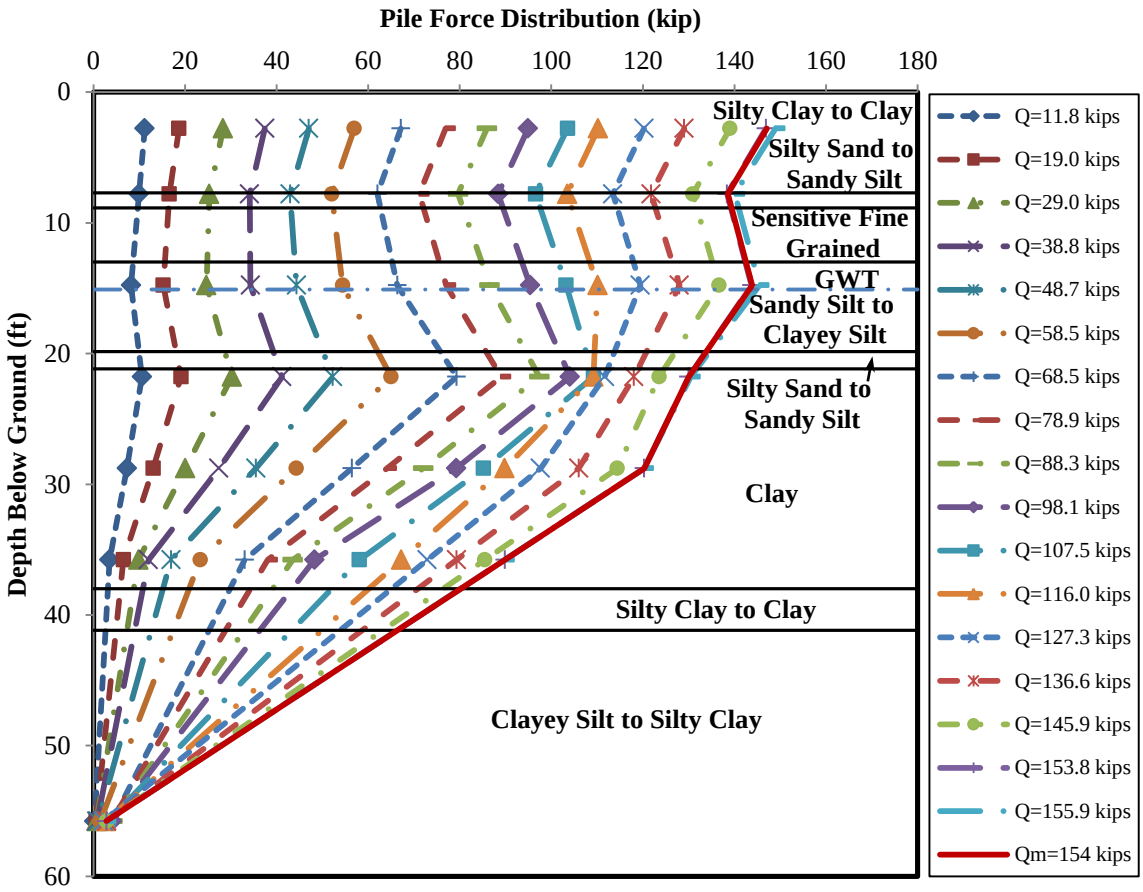

Figure D.1.3. Pile force distribution along the embedded pile length of the test pile ISU4

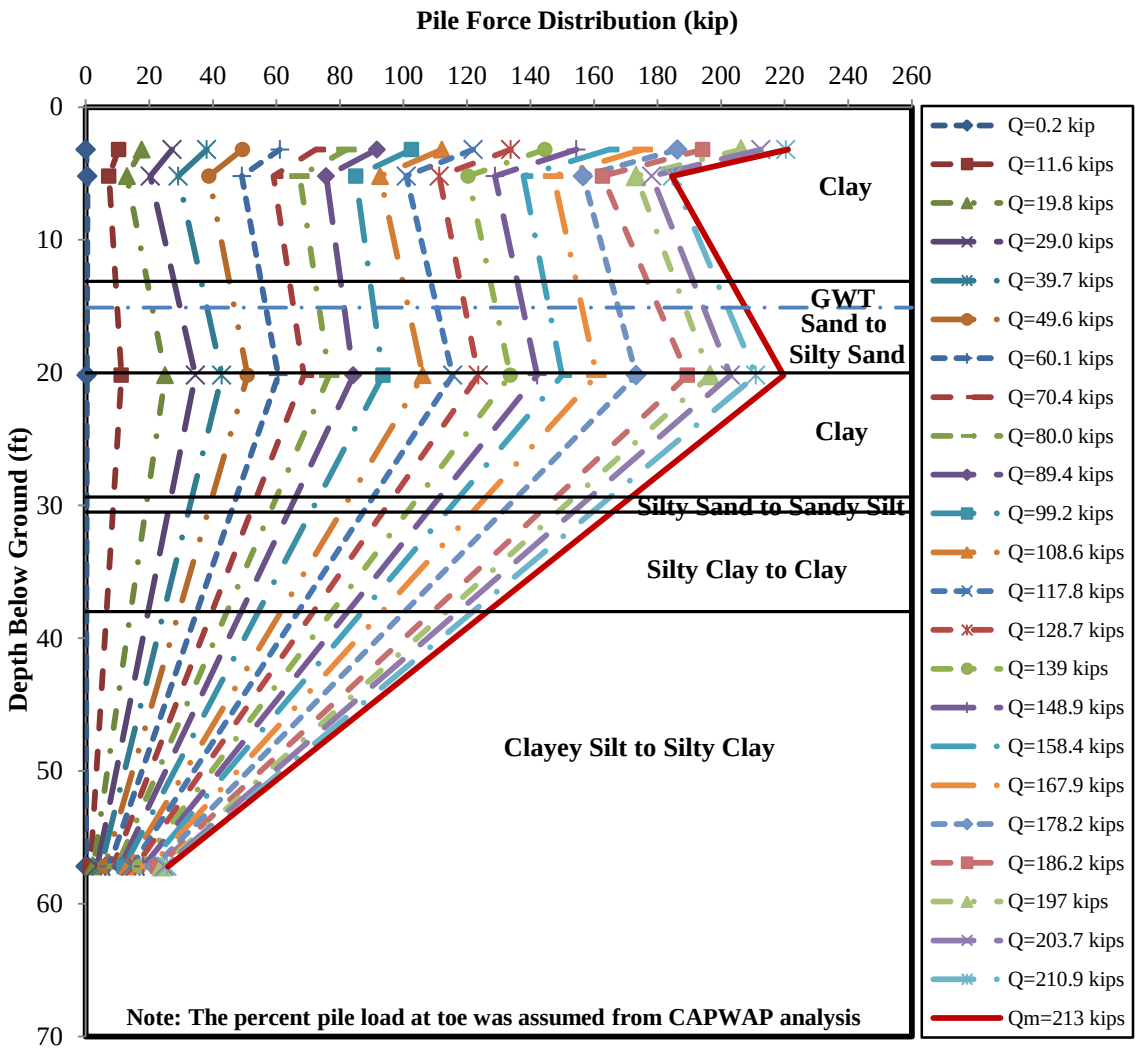

Figure D.1.4. Pile force distribution along the embedded pile length of the test pile ISU6

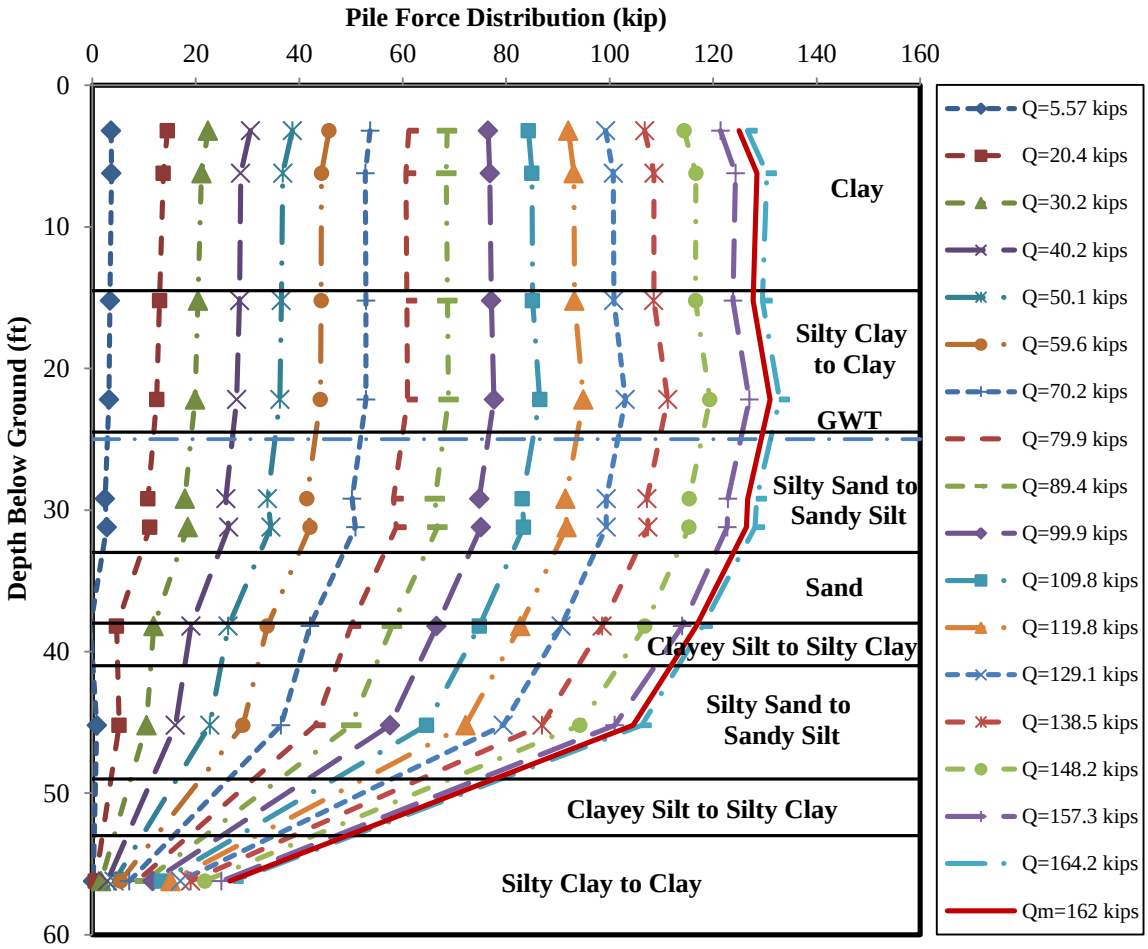

Figure D.1.5. Pile force distribution along the embedded pile length of the test pile ISU8

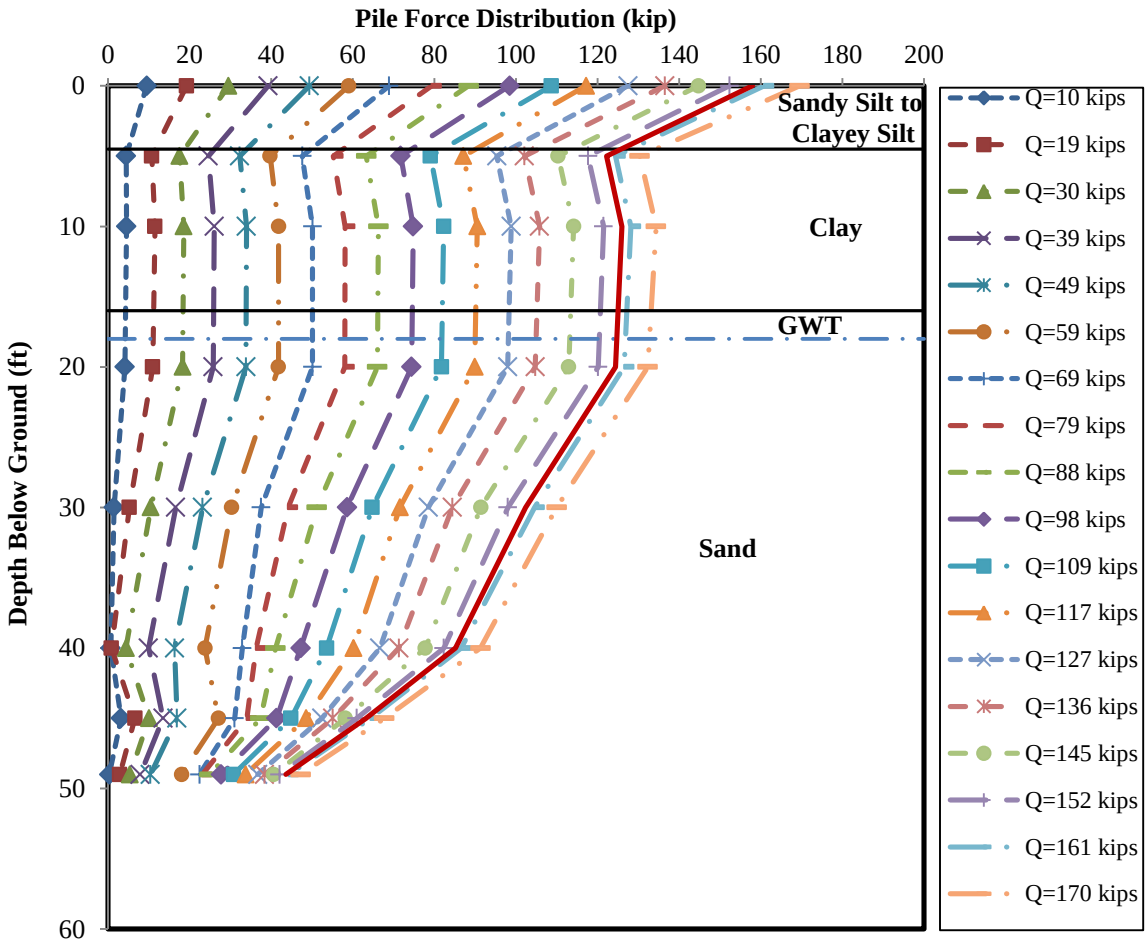

Figure D.1.6. Pile force distribution along the embedded pile length of the test pile ISU9

D.2. Shaft Resistance Distribution

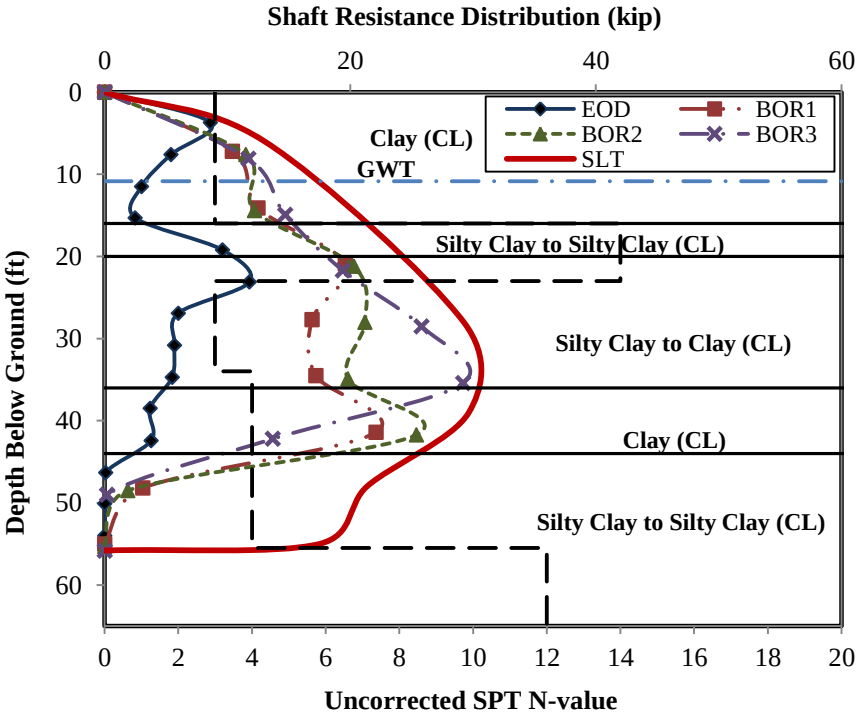

Figure D.2.1. SLT measured and CAPWAP estimated pile shaft resistance distributions for test pile ISU2

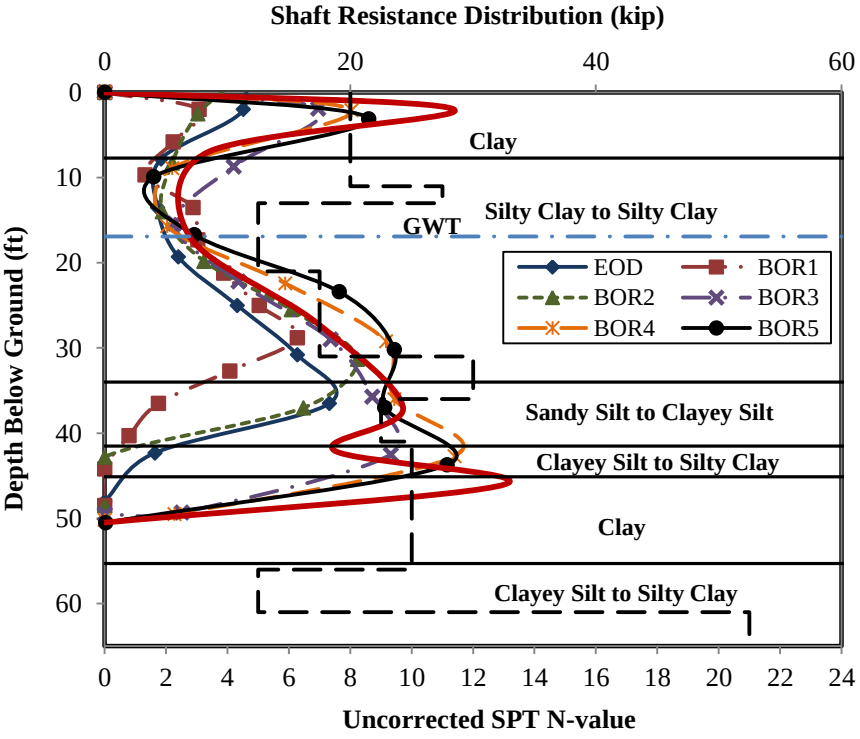

Figure D.2.2. SLT measured and CAPWAP estimated pile shaft resistance distributions for test pile ISU3

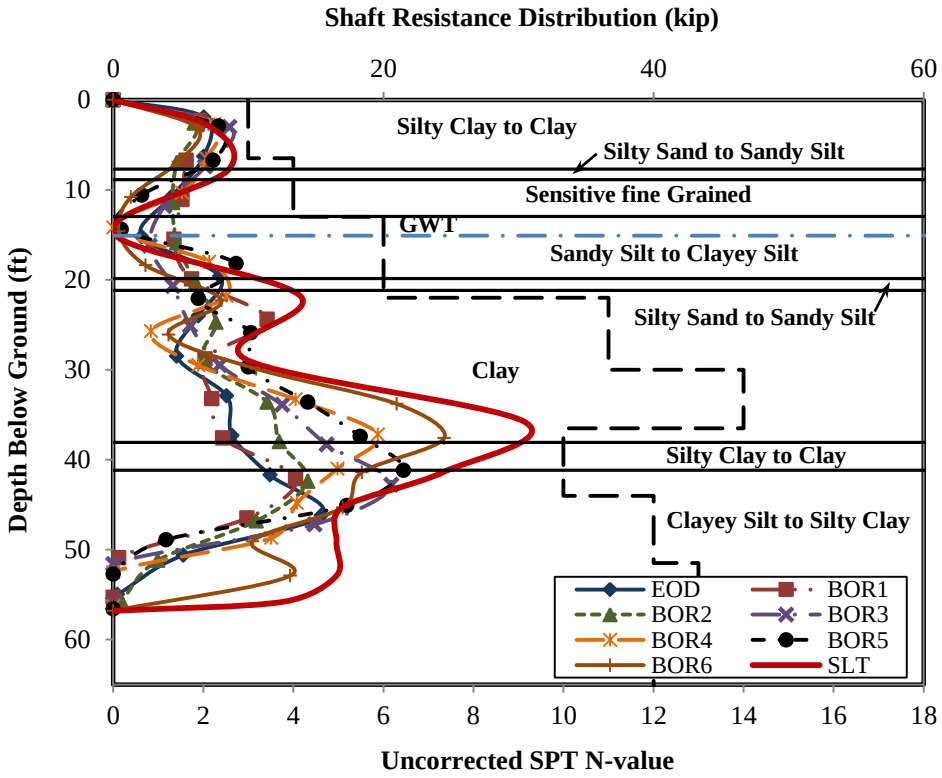

Figure D.2.3. SLT measured and CAPWAP estimated pile shaft resistance distributions for test pile ISU4

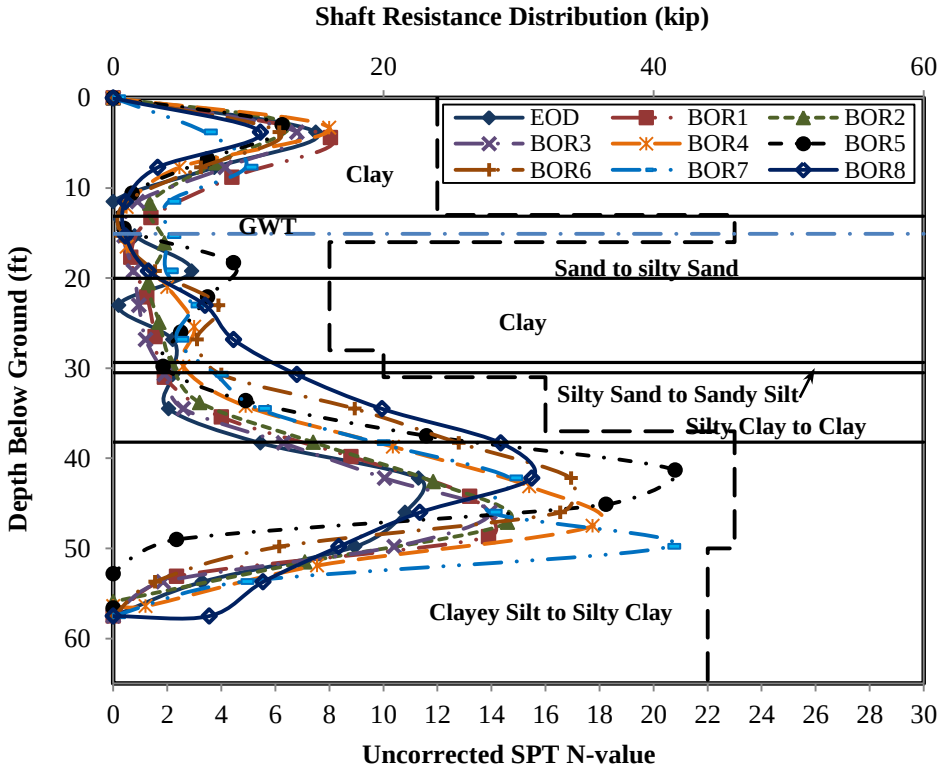

Figure D.2.4. CAPWAP estimated pile shaft resistance distributions for test pile ISU6

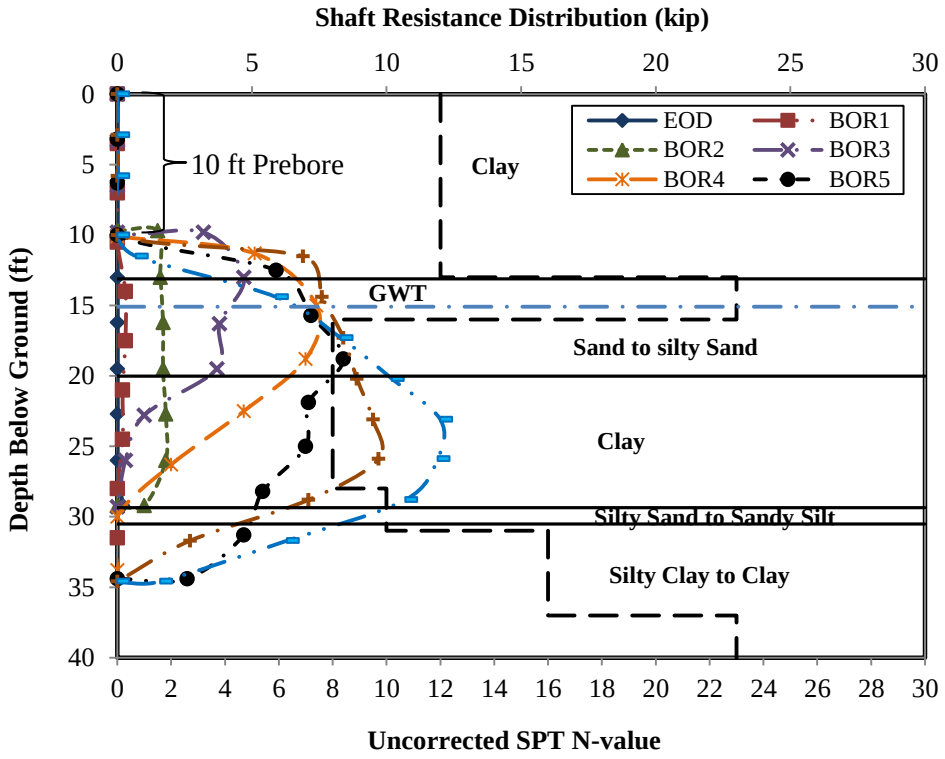

Figure D.2.5. CAPWAP estimated pile shaft resistance distributions for test pile ISU7

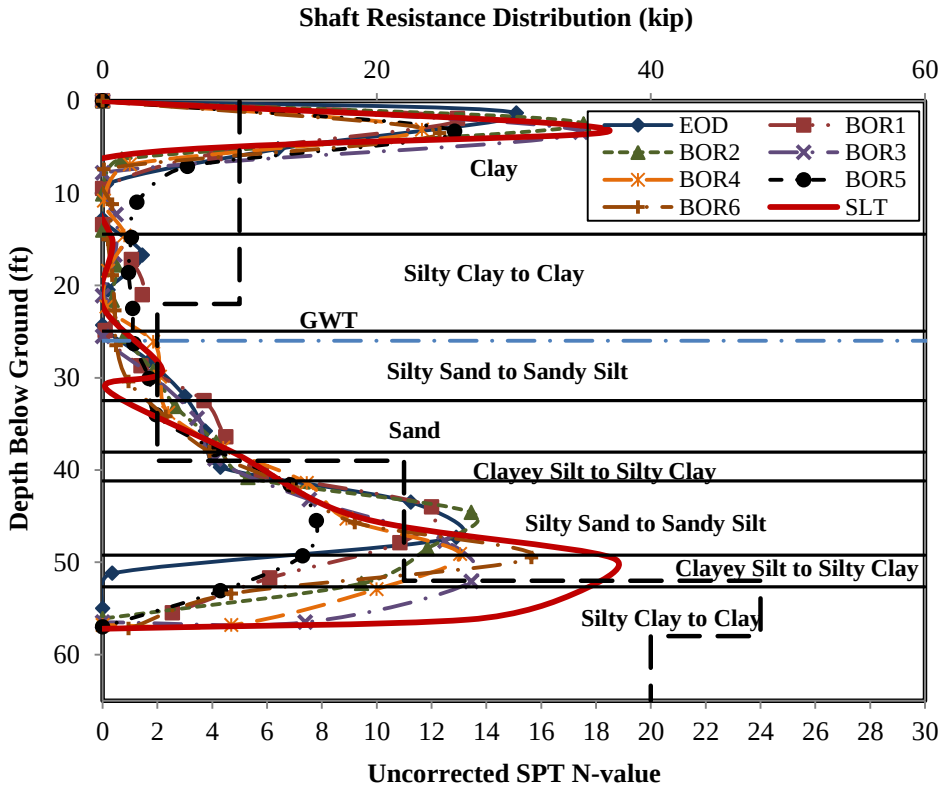

Figure D.2.6. SLT measured and CAPWAP estimated pile shaft resistance distributions for test pile ISU8

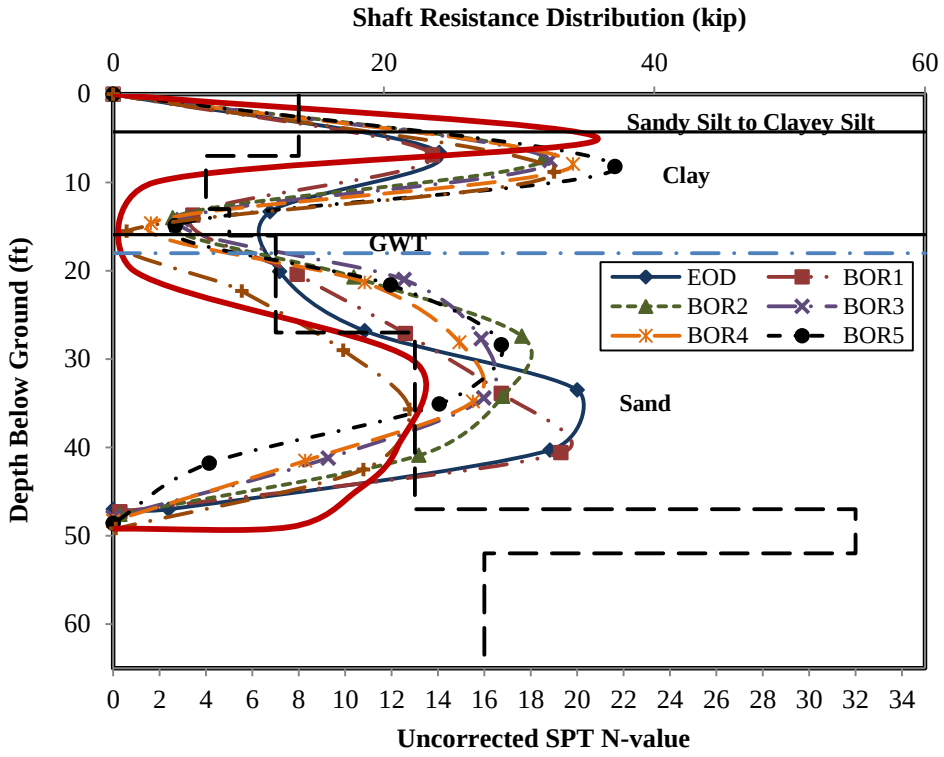

Figure D.2.7. SLT measured and CAPWAP estimated pile shaft resistance distributions for test pile ISU9

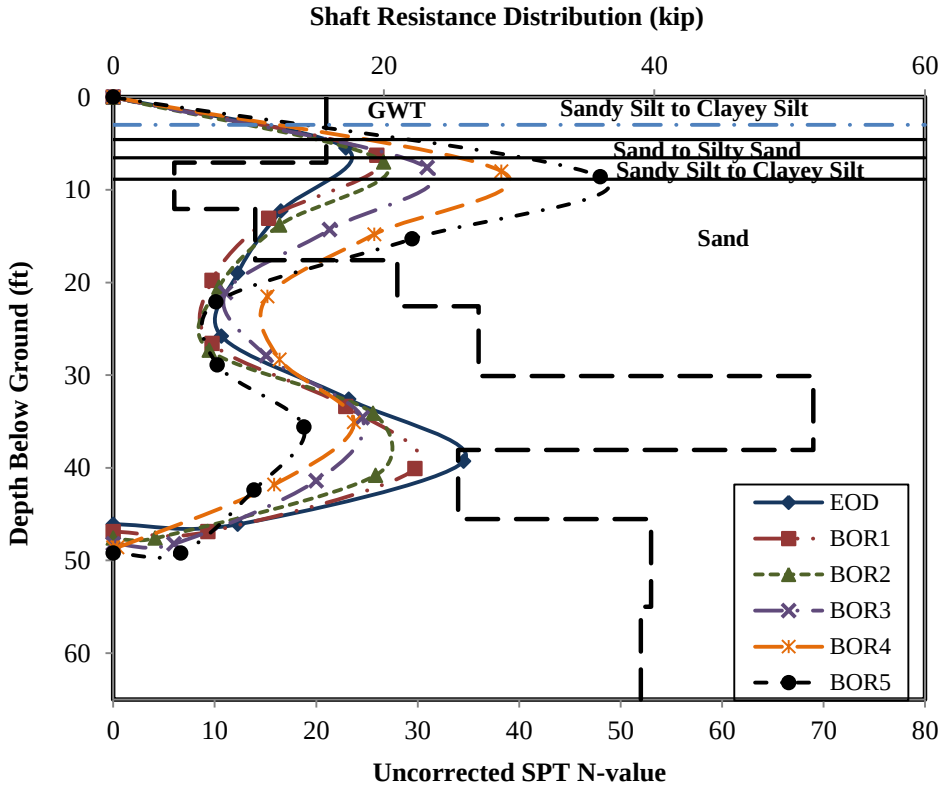

Figure D.2.8. CAPWAP estimated pile shaft resistance distributions for test pile ISU10

D.3. Pile Driving Resistance

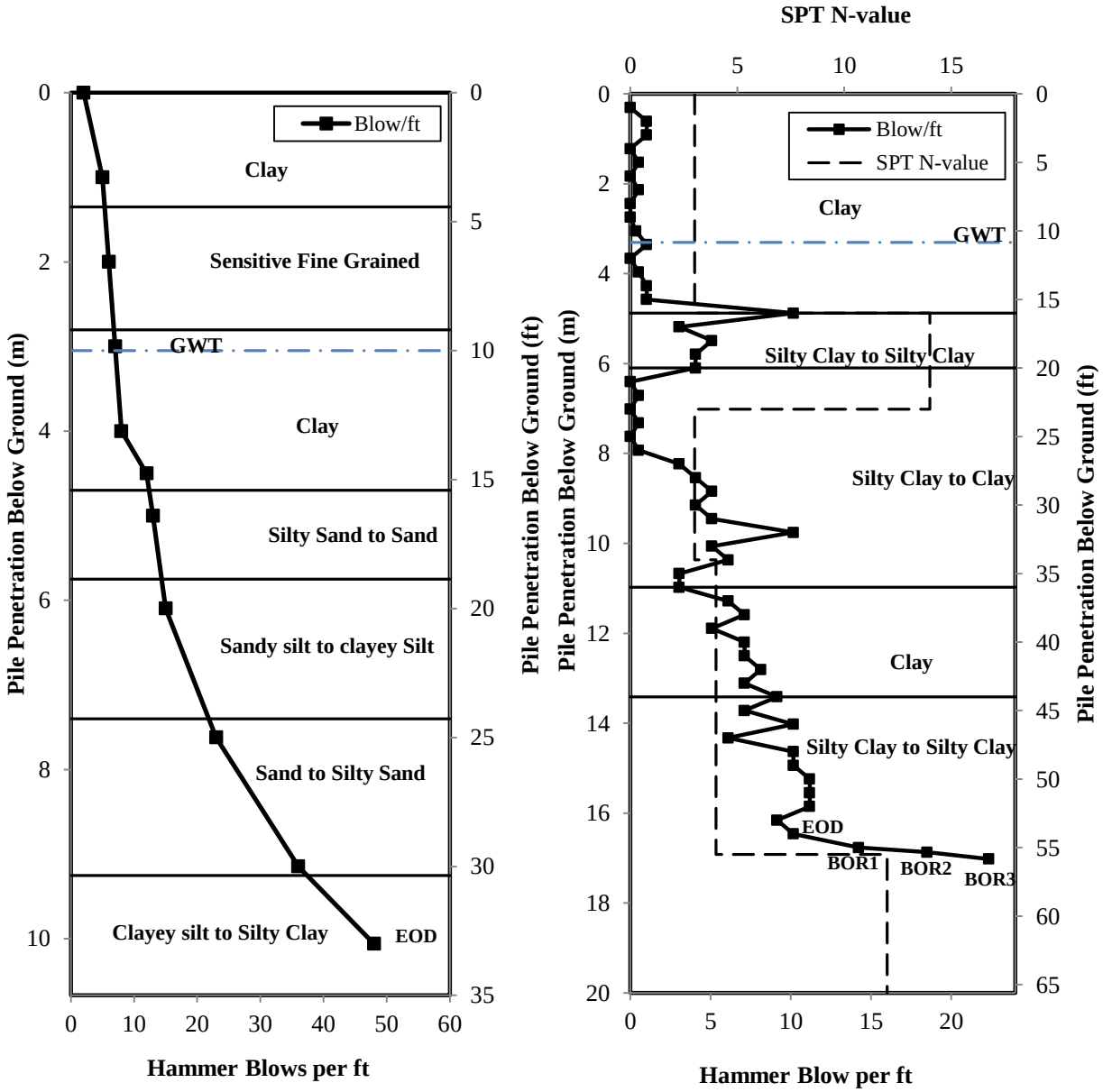

ISU1 (Mixed Profile) ISU2 (Clay Profile)

Figure D.3.1. Pile driving resistances for ISU1 and ISU2 in terms of hammer blow count

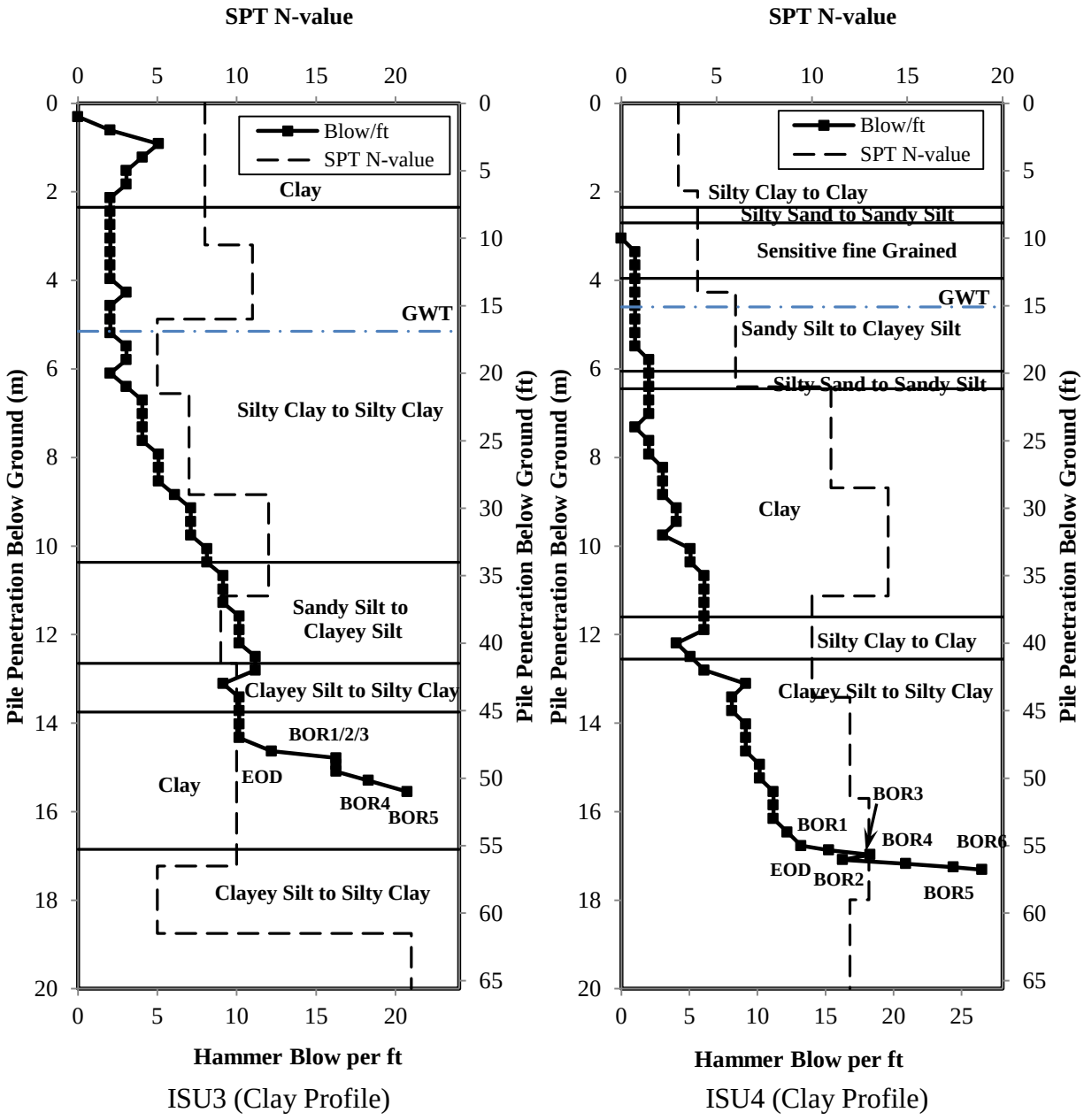

Figure D.3.2. Pile driving resistances for ISU3 and ISU4 in terms of hammer blow count

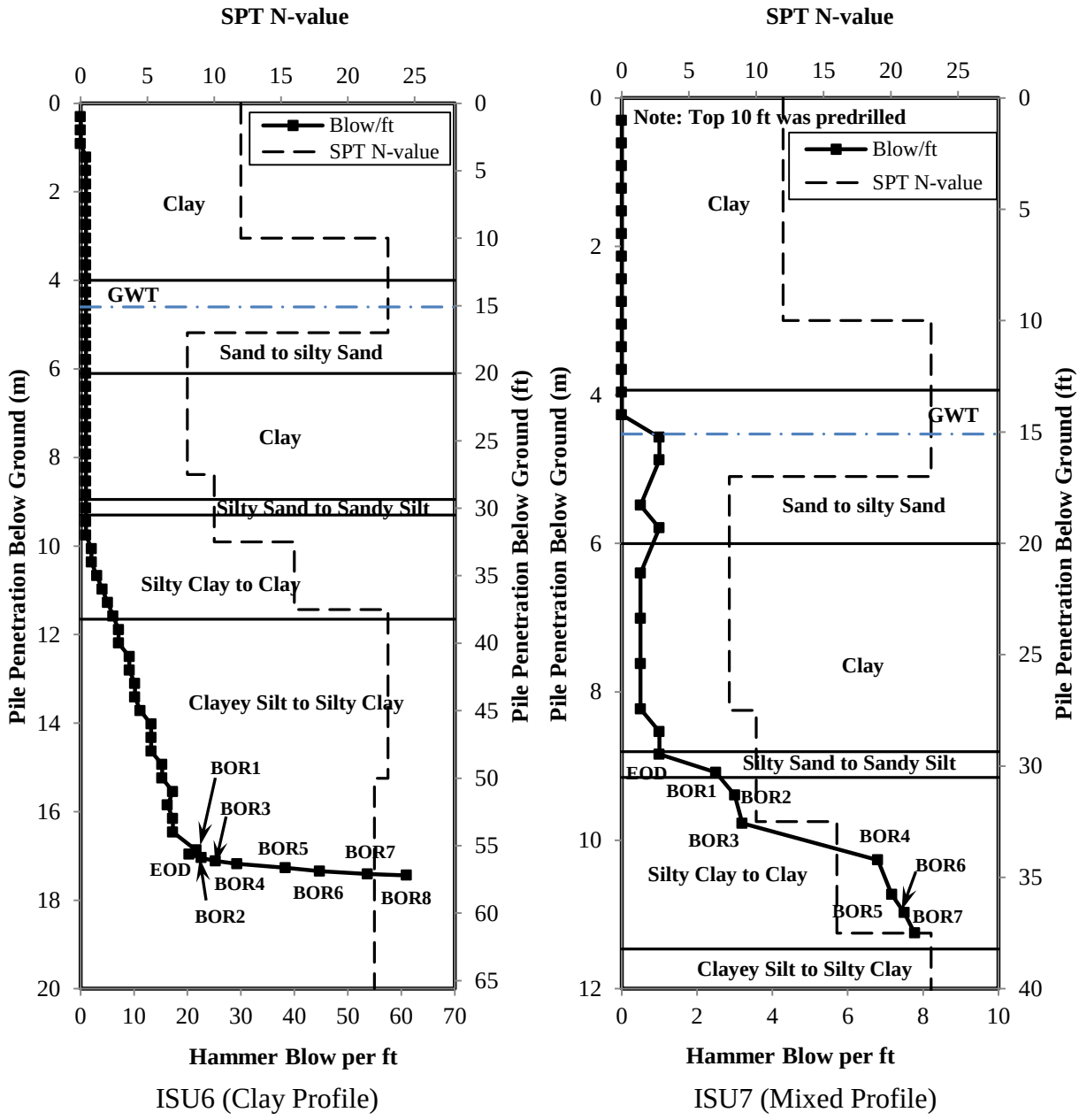

Figure D.3.3. Pile driving resistances for ISU6 and ISU7 in terms of hammer blow count

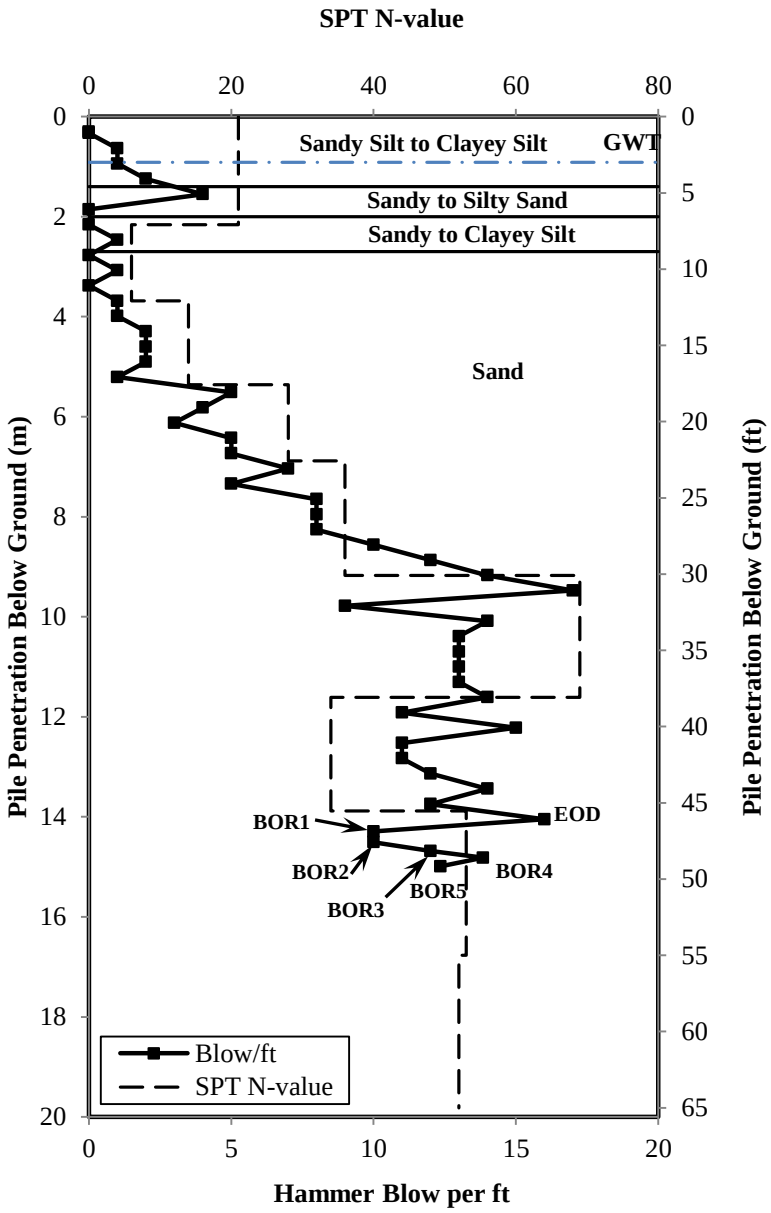

Figure D.3.4. Pile driving resistance for ISU10 (sand profile) in terms of hammer blow count

D.4. Relationship between Soil Properties and Pile Shaft Resistance Gain

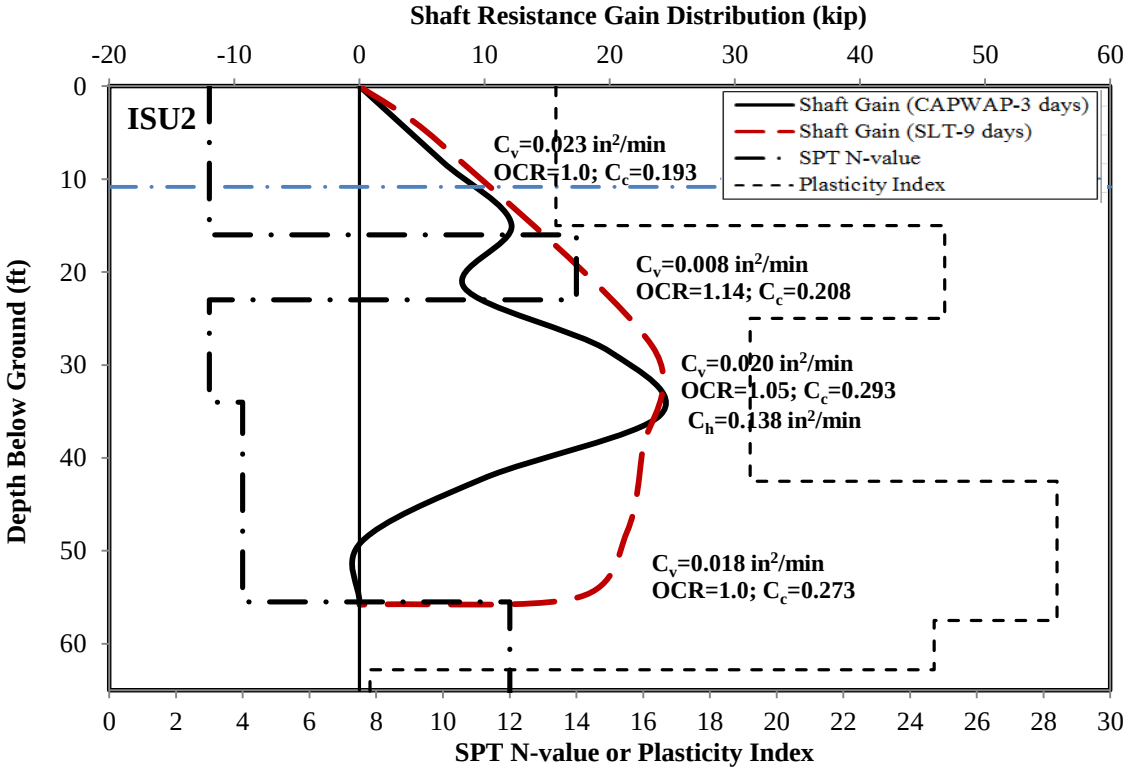

Figure D.4.1. Relationship between soil properties and shaft resistance gain for ISU2

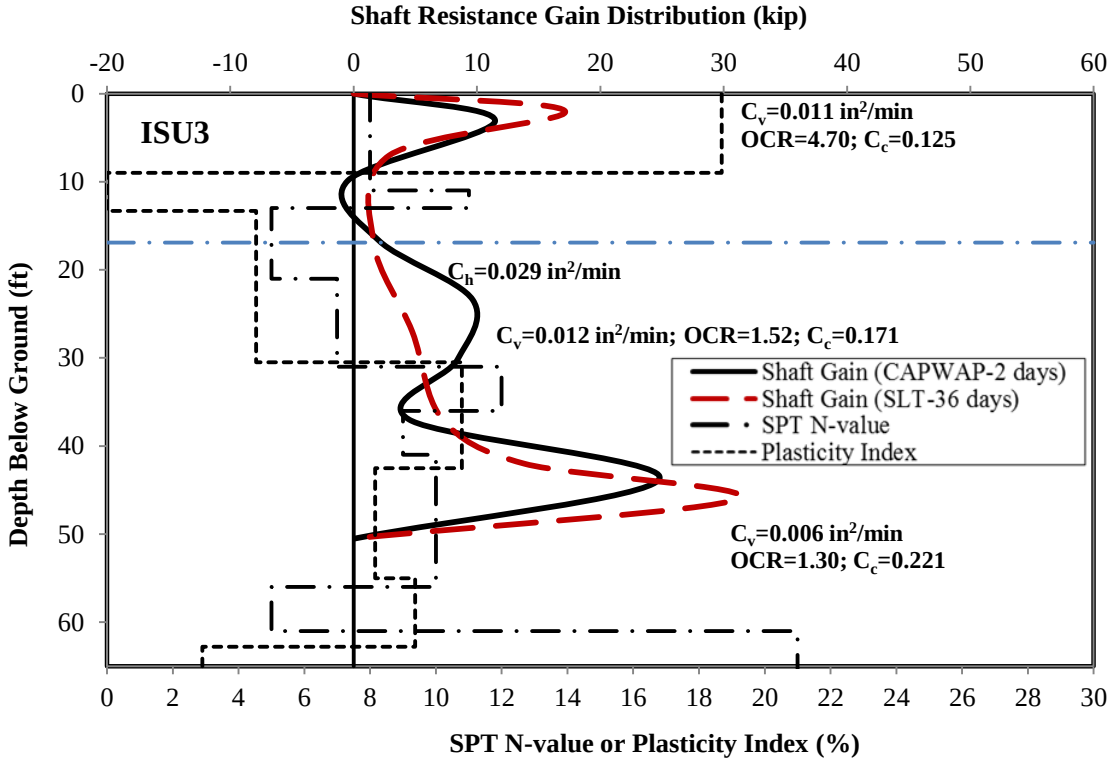

Figure D.4.2. Relationship between soil properties and shaft resistance gain for ISU3

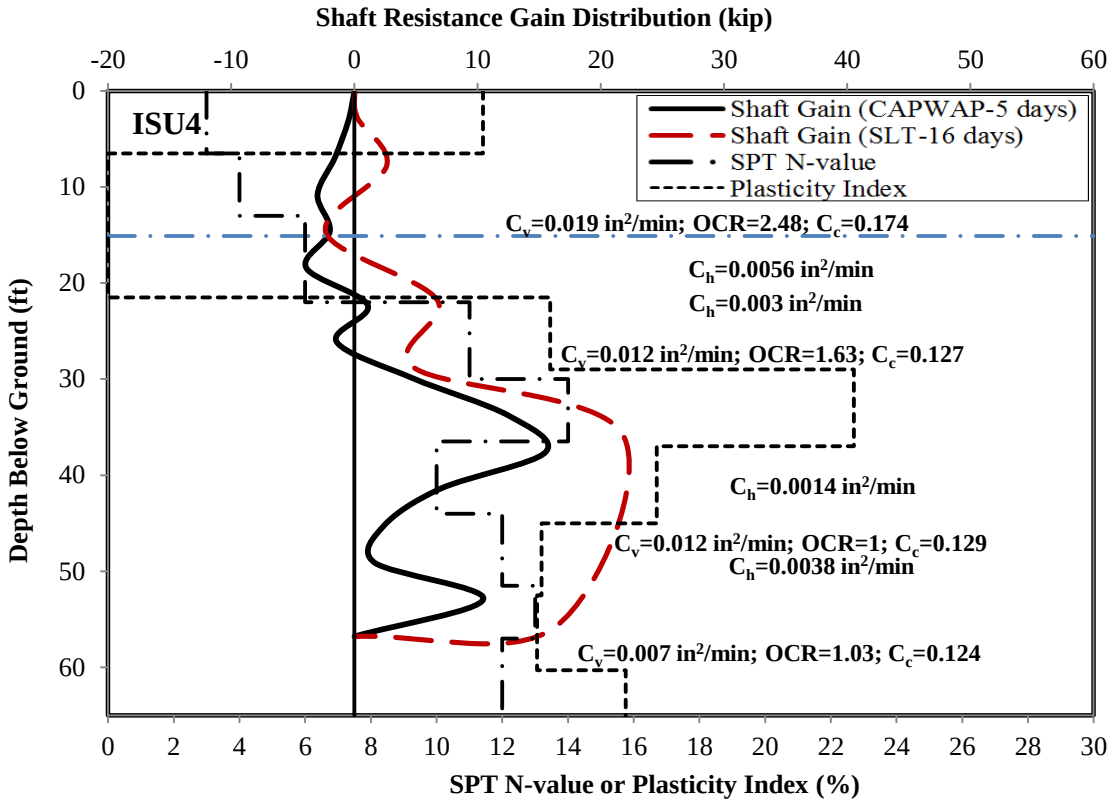

Figure D.4.3. Relationship between soil properties and shaft resistance gain for ISU4

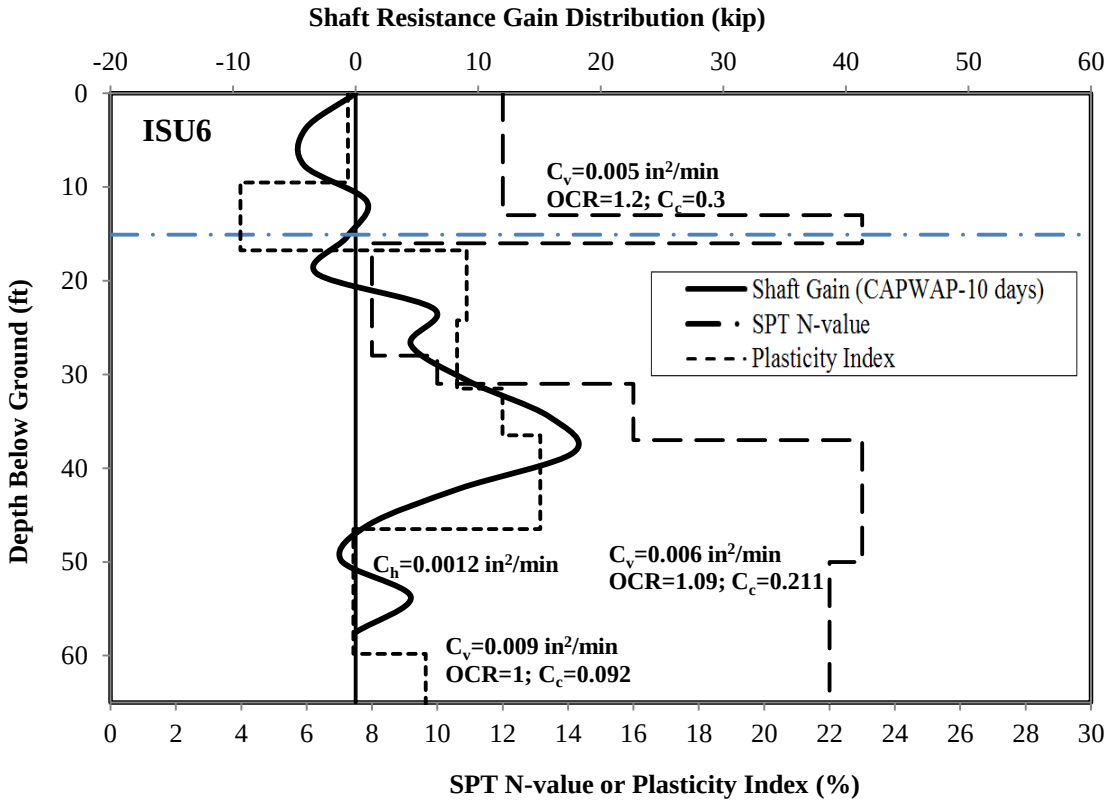

Figure D.4.4. Relationship between soil properties and shaft resistance gain for ISU6